Interaction between Orange Carotenoid Protein and mesoporous silica : from spectroscopic investigations to photoactive nanodevices

Silvia Leccese

Sorbonne Université

Ecole doctorale 397 Physique et Chimie des Matériaux

Laboratoire de Réactivité de Surface - LRS

Interactions between Orange Carotenoid Protein and mesoporous silica: from spectroscopic investigations to photoactive nanodevices

Par Silvia Leccese

Thèse de Doctorat de Chimie

Dirigée par Alberto Mezzetti et supervisée par Claude Jolivalt

Présentée et soutenue publiquement le 16 septembre 2022

Devant un jury composé de :

Mme Isabel DIAZ	Senior Researcher	Rapportrice
M. Michel SLIWA	Directeur de Recherche	Rapporteur
Mme Maguy JABER	Professeure	Examinatrice
M. Winfried LEIBL	Directeur de Recherche	Examinateur
Mme Claude JOLIVALT	Professeure	Co-superviseure
M. Alberto MEZZETTI	Maitre de Conférences	Directeur de thèse

To the pursuit of equilibrium in science,
that inspired me to find a balance in life.

Aknowledgments

I started this research project more than 3 years ago, within the framework of a Master internship, working in the Laboratoire de Reactivité de Surface (LRS). With great pleasure, it turned out to be my PhD research project.

I would like to address my deepest thank to Dr. Alberto Mezzetti, who gave me the chance to study in one of the most renowned universities in the world, always believing in me and in my capabilities. Thanks to his trust in my autonomy and independence, he gave me the possibility to evolve as a scientist and as a person. Despite the differences in how we approach new ideas as well as problems to solve, I can sincerely affirm that we found our equilibrium and we managed to move forward during this journey, always thinking positive.

I sincerely thank Prof. Claude Jolivalt for her upmost availability in letting me discover the world of mesoporous silica. I have really appreciated her scientific approach and rigorous perseverance in planning experiments and analysis. She taught me that, in science, it is necessary to define the goal, before outlining the path.

I would like to express my gratitude to Prof. Isabel Diaz and Dr. Michel Sliwa for accepting to review my thesis work as well as Prof. Maguy Jaber, and Dr. Winfried Leibl for kindly agreeing to be members of my thesis jury.

A warm-hearted appreciation to Diana Kirilovsky, who has been our mentor during this research work, throughout the peculiarities and the features of the Orange Carotenoid Protein. I would like to express my deep gratitude for having introduced me in her lab, at the CEA in Paris-Saclay, to learn how to produce OCP.

A special thank goes to Dr. Adjélé Wilson and Dr. Thomas Onfroy, without whom the experimental production of OCP and SBA-15 would not have been possible. A great thank goes also to all the technicians that helped me for the instrumental part and the analysis, notably Jean-Marc, Vincent, Saramblé, Dalila, Sandra and Mohamed.

I would like to express my appreciation to Hélène Pernot, Director of the LRS, for welcoming me and giving me the opportunity to work in this laboratory. Above all I must thank her kindness and empathy. The door of her office has always been opened for everyone and, in my

opinion, this is a great fortune for the lab. I would also like to thank Annie Mettendorff, Aurélien Chervalier, Sonia M'Barek and Hakima Si Bachir for their support in administrative tasks, and similarly all the permanent members of the LRS that gave us their advice or point of view on this project.

The greatest thank goes to all non-permanent members of the LRS, notably Master students, PhD students and Post-Doc that shared with me a piece of their life, both private and professional. Therefore, thanks to Ricardo, Hagop, Ola, Matthieu, Louis, Lise, Yacine, Corentin, Andrea, Giuseppe, Vincent, Albert, Ana, Brittany, Jihye, Yifan and all the others. I also need to thank them for having accepted to work in the dark when I was working in the lab with my photo-sensitive protein!

The warmest thank goes to my family in Italy, who supported me in each step despite the distance and to my partner, who has always "held my hand" during this journey.

In the end, I have to thank myself. I thought to quit the PhD a lot of times…to move forward during these years of pandemic was the hardest thing I've ever faced in my life but I'm so proud of myself for not having given up. I came out even stronger and more aware of myself.

Table of Contents

General Introduction

Photoreceptors are chemical structures, made of proteins and integrated into biological systems that are triggered by light. They use the information contained in the absorption of a photon to modulate biological activity in a wide range of organisms and plants. Orange Carotenoid Protein (OCP) is a water-soluble, blue-green light photoreceptor protein, involved in the photoprotection of cyanobacteria. It induces the thermal dissipation of excess solar energy counteracting oxidative stress and photodamage. OCP consists of two structural domains sharing a non-covalently linked antioxidant carotenoid as a cofactor. Blue light absorbed by the cofactor, induces photoactivation of OCP and its colour changes from orange to red.

SBA-15 (Santa Barbara Amorphous) has been chosen as inorganic support for OCP, aiming at the development of photochromic bio-compatible nanodevices. SBA-15 is a mesoporous silica matrix that has attracted much attention as host for immobilization of enzymes as well as drug delivery system. The structural parameters of SBA-15, such as the diameter of pores, can be modified by tuning parameters of its synthesis. In addition, the ability to modify the surface properties of these materials to match the physio-chemical properties of the target biomolecules, can provide higher protein loading. In this work we have immobilized OCP on different kinds of raw and surface-functionalized SBA-15 mesoporous silica nanoparticles and structurally characterized the obtained systems. SBA-15 matrices have demonstrated to be suitable supports for OCP, whose immobilization is strongly enhanced by illumination during the encapsulation step, showing that OCP photoactivation facilitates protein insertion in the matrix. OCP remains photoactive inside the mesoporous silica matrix, so that photochromic nanoparticles are obtained. Time-resolved FTIR difference spectroscopy studies strongly suggest that the photoactivation mechanism is the same as in solution. Furthermore, under appropriate conditions, OCP can also be released from SBA-15 nanoparticles.

Finally, we have developed photoactivable nanodevices with intensity-tuneable fluorescence based on OCP- and dye-loaded SBA-15 nanoparticles. More in details, we have immobilized fluorescent cyanine dyes or natural fluorescent antioxidant flavonols on SBA-15, in presence of OCP. Blue light illumination was found to provide reversible quenching of red or green fluorescence under green or violet illumination, respectively. SBA-15 acts not only as a biocompatible scaffold, but also as a protecting agent of the developed nanodevices against aging.

This thesis manuscript is composed of four chapters addressing objectives ranging from spectroscopic investigations on OCP photoactivation to more applied research topics. The materials & methods section is included in the experimental chapters (second, third and fourth one).

The first chapter is a literature review describing the most important photoreceptors present in nature with a special emphasis on Orange Carotenoid Protein photoreceptor, its original role and its peculiar photoactivation mechanism. In the first part, examples of photoreceptors and photoactive proteins, whose biological mechanisms is already known, are reported. Furthermore, their immobilization on mesoporous silica surfaces for applicative aims is shortly reviewed. In the second part, the peculiar properties of OCP are described. First, its biological role played in nature as photoprotective system for cyanobacteria. Then the attention is shifted to the current knowledge on its photoactivation mechanism, going through its structure and photo-physics. Finally, the proposed possibility of engineering its structure to modulate its spectroscopical properties, or its use as sensor for temperature and light or as antioxidant nanocarrier and delivery system is described.

The second chapter of this thesis deals with spectroscopic studies, notably UV-Visible and especially FTIR difference spectroscopy, involved to investigate the basis of the photoactivation mechanisms of OCP that is still to be clarified. This study is mainly focused on OCP binding echinenone or canthaxanthin as chromophore, aiming to pinpoint their similarities or differences in the framework of the photoactivation. A starting digression about the FTIR difference spectroscopy, usually involved in the study of photoactive proteins to obtain information on almost all the constituents of it, is presented and supported by details about experimental techniques as well as sample preparation methods. It is followed by a paragraph dealing with carotenoid IR band assignment. This represents a mandatory step for a deeper understanding of FTIR difference spectra (especially time-resolved FTIR difference spectra). Furthermore, the effect of the hydration state on the photo-activation of OCP has been investigated, revealing specific differences between OCP binding echinenone and OCP binding canthaxanthin. In fact, it was found that the latter (differently from the former) can be activated under strong dehydration conditions.

The third chapter is dedicated to the field of mesoporous silica and its interaction with OCP. Among the numerous mesoporous materials described in the literature for their ability to immobilize proteins, SBA-15 was chosen as inorganic support for OCP. The aim of this study was thus to immobilize OCP on a mesoporous SBA-15 to study the influence of structural and

textural features of SBA-15 on the chemical properties of OCP and to assess the photochromic behaviour of the immobilized protein and its stability in time, aiming to the development of photo-sensitive nano-devices. SBA-15 with two different pore sizes was synthesized and functionalized with covalently bound aminopropyl groups (SBA-15-NH_2) to modulate the interaction between SBA-15 and the protein and, consequently, the OCP immobilization yield by adsorption. SBA-15 matrices have been characterized by X-Ray Diffraction (XRD), Electron Microscopy (SEM/TEM), N_2 physisorption and Thermogravimetric analysis (TGA). The immobilization of OCP on these matrices and its photosensitivity have been followed by Visible spectroscopy in liquid and solid phase.

The last chapter of this manuscript is inspired to a work published by Andreoni *et al.* and focused on the development of a light-dependent tuneable energy-transfer between two dyes, using the spectral shift of the Visible absorption spectrum of OCP upon photoconversion. The idea of tuning the energy-transfer between fluorescent dyes, inspired us for the development of photoactivable nanodevices with variable fluorescence intensity, based on OCP- and dye-loaded nanoparticles of SBA-15. The photoconversion of OCP^O into OCP^R creates an overlap between the emission spectra of the fluorophores and the absorption spectrum of OCP^R, which is therefore able to partially quench the fluorescence of the fluorophores. The main application of this system could be in fluorescence imaging, a technique widely used in several fields, including biology. Nevertheless, mesoporous silica NPs are also a suitable vehicle for fluorescent molecules, and they have already been exploited in several applications. Among the several groups of organic fluorophores, cyanine molecules were chosen, as they are widely-used synthetic organic fluorescent dyes. Furthermore, the attention was also focused on some naturally occurring fluorescent flavonols (a sub-class of flavonoids). Beside their interesting emitting properties, flavonols are also powerful antioxidants. Therefore, nanoparticles with light-tuneable fluorescence intensity completely based on antioxidant molecules were obtained. The systems were analysed by photoluminescence and UV-Visible spectroscopy. The results also show that OCP can also serve as a photoprotective element in fluorescent nanoparticles, but also on light-harvesting systems based on SBA-15 mesoporous silica.

Finally, the thesis manuscript ends with general conclusions regarding the work performed during this PhD research project, with a look to future perspectives.

1. Introduction to photoactive proteins

1.1 Overview on photoreceptors and photoactive proteins

1.1.1 Receptors and photoreceptors

In nature, receptors are chemical structures, made of protein and integrated into biological systems, that receive and transduce signals. These signals are typically chemical messengers that bind to a receptor and cause some form of biological response in a cell[1]. Receptor proteins can be classified by their location: transmembrane receptors include ligand-gated ion channels and enzyme-linked hormone receptors[2]; intracellular receptors are found inside the cell and include cytoplasmic receptors and nuclear receptors. They can be complementary bound to a ligand, notably antigens, antibodies, hormones, neurotransmitters. When a ligand binds to a corresponding receptor, it activates or inhibits the biochemical pathway associated to the receptor[3].

Photoreceptors are receptors triggered by light. They use the information contained in the absorption of a photon to modulate biological activity in a wide range of organisms and plants[4]. They are photosensory proteins involved in photochemical processes that lead to the formation of a signal. They typically consist of a protein attached to a photopigment which reacts to light via-photoisomerization or photoreduction, thus initiating a change of the receptor protein which triggers a signal transduction cascade (see **Figure 1.1**)[5]. Indeed, photoreceptors covalently or non-covalently bind an organic chromophore which contains a conjugated π electron system, which usually derives from small-molecule metabolites or amino-acid side chains. Depending on the photochemistry of their chromophores, photoreceptors show different spectral properties covering the electromagnetic spectrum from UV to near-infrared wavelengths. To convert light signals into cellular signals, sensory photoreceptors need to perform two functions: first, a photosensor domain absorbs light; and second, an effector domain exerts biological activity (e.g., ion transport, protein conformational changes, catalysis). The signal transduction depends upon whether the photoreceptor is realized, notably as distinct proteins or distinct protein domains. In the absence of light, photoreceptors adopt their thermodynamically most stable, dark-adapted state. Upon light absorption, they undergo a photocycle, a series of photochemical reactions within the chromophore followed by structural and dynamic transitions within the surrounding protein scaffold (**Figure 1.1**)[5]. A question of general relevance in protein science is how the ultrafast, local structural changes of the active site during the initial photochemical event are converted into global conformational

changes in the receptor protein. The application of time-resolved techniques can reveal the sequence of molecular events leading to receptor activation[6].

The absolute light sensitivity of a photoreceptor is determined by its absorption cross section and its overall quantum yield for formation of the signalling state. After photon absorption, the initial photochemical reaction toward formation of the signalling state is very fast (picoseconds) to achieve high quantum yields and to minimize competing reactions. The initial reaction may be followed by slower changes (e.g., microseconds), which are faster than the timescale of most physiological responses. Therefore, the photochemical response of photoreceptors is not limiting. Furthermore, for some photoreceptor, it has been observed that mutations accelerate or decelerate the dark-recovery reaction[7,8].

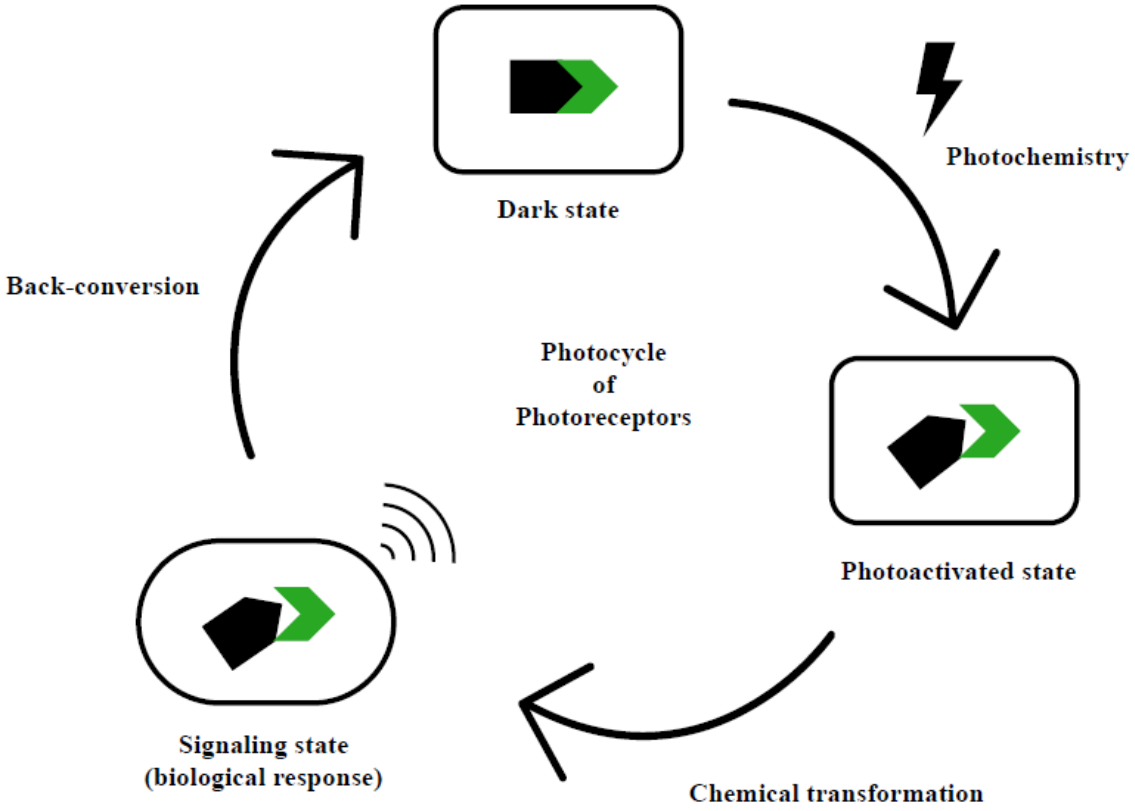

Figure 1.1 Operating scheme of photoreceptors. Photoexcitation of the photopigment leads to an electronically excited state. The photopigment returns to the electronic ground state with different conformation and/or oxidation state, which triggers subsequent structural changes, leading to the formation of the signalling state. The photoreceptor gives a signal to a subsequent component in a signal transduction chain, triggering a biological response. The photoreceptor back-converts to the dark state completing the cycle.

1.1.1.1 Photochemistry of photoreceptors

Several studies conducted on photosensory proteins have provided insights of the molecular mechanisms of six distinct types of photosensory modules: rhodopsin[9], phytochromes[4], cryptochromes[10], blue-light using flavin (BLUF) proteins[11], photoactive yellow proteins (PYPs) and light-oxygen-voltage (LOV) proteins[12]. Other photoreceptors are under study nowadays, notably the Orange Carotenoid Protein from cyanobacteria[13] (on which this thesis is focused), UVR8 (Ultraviolet Resistance locus 8) from plants and algae[14], cobalamin B12-dependent repressors from myxobacteria[15], and the UV receptor LITE-1 from *Caenorhabditis elegans* nematode[16].

The six, well known, photoreceptor proteins contain four distinct chromophores: retinal in the rhodopsin; bilin in the phytochromes; p-coumaric acid in PYP and flavin in LOV proteins, cryptochrome, and BLUF proteins. In general, three different mechanisms of photoactivation can occur: changes in hydrogen bonding due to a rotation or tautomerization of an active site, that drive conformational changes; C=C isomerization leading to proton transfer, which delete constrains in the conformation of the protein; a photochemistry event (as C=C isomerization or molecule photoreduction) creates a charge in the protein that drives conformational changes (see schematic representation in **Figure 1.2**). The molecular mechanisms involved in their photocycles are outlined below.

In the three available types of rhodopsin (from algae, microbes and animals)[9,17], the chromophore is a retinal molecule linked to a lysine side chain through a Schiff base, and the primary photochemical event is the photoisomerization of a C=C double bond in the retinal[18]. The structural changes that occur in both the retinal and the protein upon the formation of this first (red-shifted) photoproduct for rhodopsin are quite small[19]. These isomerization events occur within one picosecond with a quantum yield of ≥ 0.6[9]. In general, in the initial dark state of the protein, the Schiff base is protonated and the ultrafast retinal photoisomerization is followed by slower Schiff base deprotonation that occurs in 2 ms timescale. The proton is transferred to an amino acidic residue. This step is followed by the formation of an intermediate and by substantial protein conformational changes[20,21], leading to the formation of the active state of the protein[20]. The decay of this active state involves Schiff base re-protonation and small conformational changes that complete the photocycle.

Phytochrome photoreceptors exploit bilins (tetrapyrrole molecules) as chromophore. Upon photoexcitation, bilins initiate a complex set of dynamics that activate an output signal[22]. Variation in the bilin chromophore can involve changes in multiple dihedral angles, protonation state of the nitrogen atom in each of the four pyrrole rings, and hydrogen bonding of these groups. Furthermore, several different bilin chromophores have been identified[23]. In most of phytochromes, the ring of the bilin in the dark-adapted state occupies a Z conformation with respect to other rings. Photoexcitation of the dark state initiates an excited-state isomerization reaction, involving the ring that twists to generate a primary photoproduct with an E configuration[24,25]. The reaction occurs with a low quantum yield (<15%)[26] and on a picosecond timescale[27]. The photoactive state creation occurs via-intermediate states formation and extensive changes in the internal hydrogen-bonding network of the protein[28].

Photoactive Yellow Proteins (PYP) use the p-coumaric acid (pCA) as chromophore. The PYP photocycle is triggered by the trans-cis photoisomerization of the central C=C bond of the pCA chromophore. Several spectroscopy studies revealed that pCA isomerization in the early stage of PYP photocycle involves both double- and single-bond rotations that turn the carbonyl moiety of the chromophore[29]. This rotation does not affect the hydrogen bond between the phenolic oxygen of the pCA and the protonated side chain of the active site (a glutamic acid residue)[29,30]. Recent studies revealed that the excited state of the PYP protein turns immediately to the red-shifted photoproduct without the formation of an intermediate state[31]. A proton transfer event follows, notably regarding the deprotonation of Glu residue and the protonation of the pCA chromophore. The proton transfer event is followed by global protein conformational changes[30].

Light-Oxygen-Voltage (LOV) photoreceptor proteins have an oxidized flavin as chromophore. The covalent link between flavin and an adjacent cysteine residue, results in a photoactivated state[32,33]. Furthermore, LOV proteins are the only known photoreceptor in which photochemistry takes place from the triplet excited state[34]. With X-ray crystallography and FTIR spectroscopy, it was observed a rearrangement of the hydrogen-bond network of the flavin due to a rotation of a glutamine side chain[33,35]. This rearrangement takes place at the same time of the covalent link (flavin-cysteine) formation[36] and it sends the signal to the surface[37], causing the release of the C-terminal helix. Recently, the light-induced formation of a hydrogen bond between flavin and glutamine has been shown to be sufficient for conformational changes in a LOV protein mutant[38].

Flavin chromophore is also present in cryptochromes photoreceptors. After photoexcitation of the flavin, electron transfer from tryptophan to flavin occurs[39,40]. On the picosecond timescale, the charge of the tryptophan cation radical is transported toward the surface of the protein by a series of tryptophan residues (the so-called tryptophan triad)[41]. The role of the tryptophan triad can be considered to increase the distance of charge separation and to slow down the recombination reactions[42]. In cryptochromes, a proton transfer occurs from an aspartic acid residue close to flavin and this event destabilizes a β-sheet of the α/β subdomain within the sensory domain, leading to the conformational change of the C-terminal extension of the photoreceptor[43,44].

Last type of flavin-binding photoreceptors is BLUF (Blue-Light Using Flavin) proteins. After illumination, the flavin remains oxidized and only a small red shift (of about 10 nm) in the absorption spectrum is observed within hundreds of picoseconds[45]. The triggering events are hydrogen-bond rearrangements that weaken the bond strength of the two carbonyl moieties of flavin[46]. The primary changes leading to this rearrangement include the formation of a flavin radical by electron transfer and proton transfer from a tyrosine residue[47]. It was observed that the photoproduct of this rearrangement is a tautomerized glutamine residue, close to flavin[48,49]. Furthermore, FTIR spectroscopy revealed that a shift of a β strand of the protein could stabilize the reorganized hydrogen-bonding network[50].

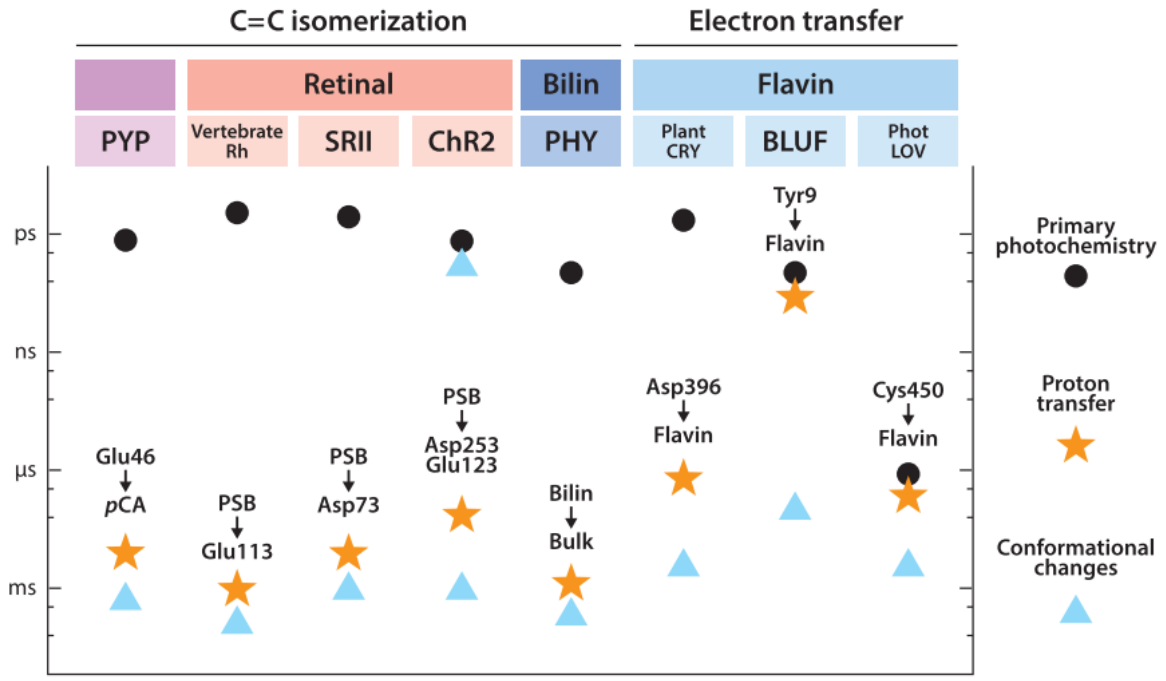

Figure 1.2 Schematic representation of key events in photoreceptor activation. The rates for the primary photochemical events (black circles), proton transfers involving the chromophore (orange stars), and large protein conformational changes for formation of the signalling state (blue triangles) in the sensory domains are indicated on a logarithmic timescale from picoseconds to milliseconds. Abbreviations: BLUF, blue-light using flavin; ChR2, channelrhodopsin-2; CRY, cryptochrome; LOV, light-oxygen-voltage; pCA, p-coumaric acid; Phot, phototropin, a LOV-containing plant photoreceptor; PHY, phytochrome; PSB, protonated Schiff base; PYP, photoactive yellow protein; Rh, rhodopsin; SRII, sensory rhodopsin II. Adapted from Kottke, Xie, Larsen, Hoff (2018) [6], reproduced with permission.

No results of photoreceptors encapsulated in mesoporous silica have been reported. Nevertheless, encapsulation of several other photoactive proteins, especially from photosynthesis, have been published.

1.1.2 Photosystems and photoactive proteins

Beside the photoreceptors, there is a vast scenery of pigments and photoactive proteins, including the light harvesting complexes and the photosynthetic reaction centres, acting respectively as key players in harvesting the light energy and in converting it into chemical energy. They are shortly reviewed in this paragraph.

Photosynthetic systems are possibly the most important photoactive systems present in nature because they make it possible to convert solar energy into chemical energy to synthesize organic molecules. The first step is the light harvesting, and this task is performed by light-harvesting complexes. Several kinds of light harvesting complexes exist in nature, from water soluble ones

(Peridinin Chlorophyll *a* Protein)[51] to membranes-embedded ones[52]. Of peculiar relevance in the framework of this thesis, are the light harvesting complexes of cyanobacteria, the phycobilisomes (PBS), which are described in paragraph 1.2.1.

The photochemical part of plants, green algae and cyanobacteria is carried out by two photosynthetic units: Photosystem I (PSI) and Photosystem II (PSII)[53]. PSII is a unique biological complex that can carry out the reaction of water oxidation, splitting water into oxygen and protons and generating a stream of high energy electrons towards the PSI. PSII is composed of two identical monomers, each one of them made up of 19 proteins. Each monomer contains 36 chlorophyll a, and 7 carotenoid molecules. PSI is an integral membrane pigment-protein complex that uses light energy to catalyse the transfer of electrons across the thylakoid membrane. Each monomer is composed by 12 subunits, binding special chlorophylls and Fe-S clusters. PSII absorbs red light while PSI absorbs far-red light. Although photosynthetic activity will be detected when the photosystems are exposed to either red or far-red light, the photosynthetic activity will be the greatest when plants are exposed to both wavelengths of light.

Among all photosynthetic organisms, there are purple bacteria that are considered to have the oldest and simplest photosynthetic apparatus. This apparatus is composed by light-harvesting complexes (e.g., LH1 and LH2). The first one (LH1, light-harvesting complex I) surrounds the reaction centre (RC), while the second one (LH2, light-harvesting complex II), sometimes called the "peripheral light-harvesting complex", has the aim to expand the light-harvesting capacity, both in terms of the area available and in the spectrum of wavelengths that can be used[54]. In purple bacteria, LH2 complex is composed by several identical subunits (normally between 8 and 10) and each subunit is made up of apoproteins and several pigments (e.g., bacteriochlorophylls and carotenoids). The pigments have the task of transporting their excitation energy to LH1 complex (and eventually to the reaction centre) to begin the photosynthetic process[54].

The real work of light harvesting, and energy transfer, is performed by the pigment molecules (mainly chlorophylls and carotenoids) that are scaffolded within the light-harvesting complexes. The main pigment in the reaction centres and photosynthetic complexes is the chlorophyll (Chl), a planar organic molecule derived from a pyrrole (**Figure 1.3**, A), playing a major role in light-harvesting complexes[55]. The most distributed chlorophyll in oxygenic photosynthetic organisms is Chl *a*, that usually occurs in reaction centres. Chl *a* presents two absorption bands, one in the blue region (around 430 nm) and other in the red region (around 650 nm). Light absorption in the first band lead to a second excited state (S2) that rapidly (in

femtoseconds) decay to the lowest excited state (S1). This state is involved in all energy transfer processes in photosynthesis[55]. Among the most diffused pigments in the nature, there are also carotenoids, produced in plants, algae, some bacteria (e.g., cyanobacteria) and fungi. They play different roles in nature, from light-harvesting in photosynthesis to antioxidation in nutrition and disease prevention[56]. Carotenoids are hydrophobic chromophore molecules derived from the isoprenoid metabolism and characterized by functionalized (or un-functionalized) end-rings associated with the double bond conjugated system (**Figure 1.3**, C). The conjugated π-electron system exhibits a strong absorption band in the range between 400 nm and 500 nm. This electronic transition occurs from the ground state (S0) to the second excited state (S2)[57]. Transitions to the lowest excited state (S1) are forbidden because of the symmetry of the carotenoid molecule[58]. Excited S2 state relaxes very fast (time scale of femtoseconds) to the S1 and from there to the ground state in a non-radiative way[59]. Nevertheless, both excited states (S2/S1) play an important role in photosynthesis. Indeed, carotenoid can absorb and transfer energy to chlorophylls in the major antenna complex of plants and green algae (e.g., Photosystem II)[60]. Moreover, in photosynthesis, carotenoids can act as scavengers of singlet-oxygen ($^1O_2$), a toxic molecule generated in stress conditions[61].

Another pigment involved in the light-harvesting antenna complex, in cyanobacteria and red algae, is the phycobilin, an open tetrapyrrole that absorbs light between 550 nm and 650 nm (**Figure 1.3**, B). In nature there are four types of phycobilins: phycocyanobilin (PBP), phycoerythrobilin (PEB), phycoerythrocyanin (PEC) and phycoviolobilin (PVB)[62].

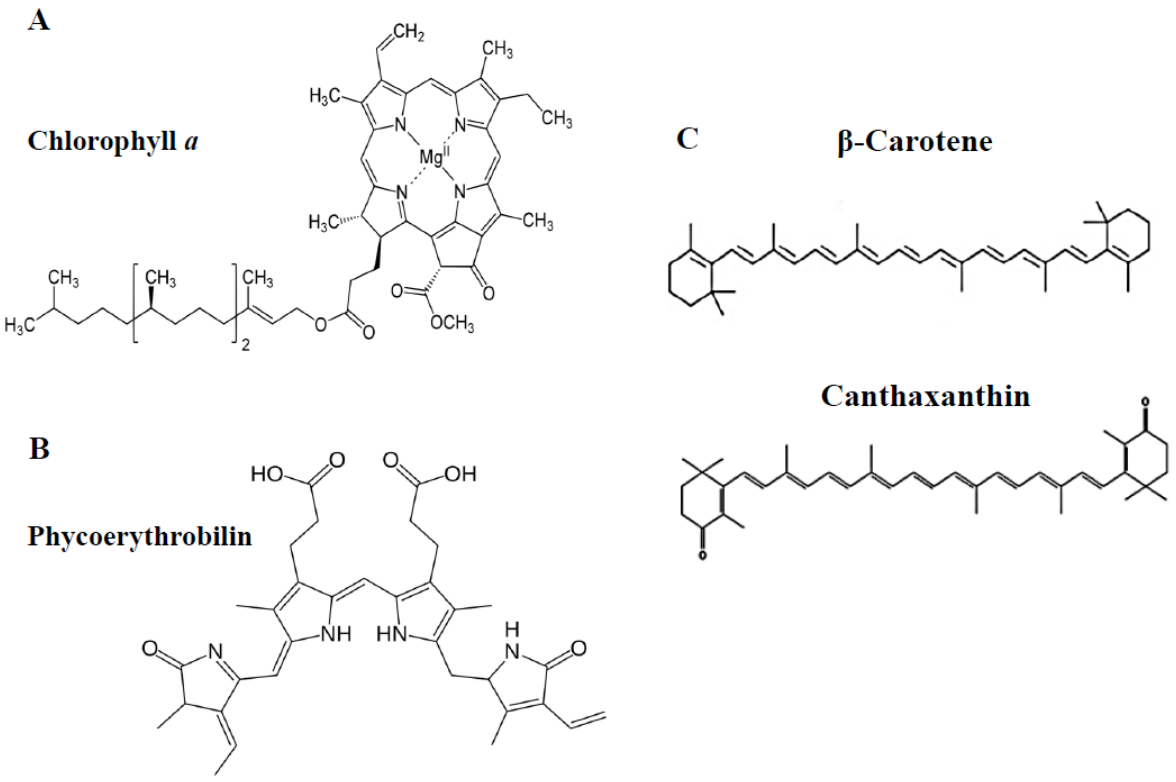

Figure 1.3 Chemical structure of (A) Chlorophyll *a*; (B) Phycoerythrobilin; (C) Carotenoids: β-carotene and canthaxanthin.

The photosynthetic reaction centre is externally characterized by the presence of phycobiliproteins, light transducing proteins that harvest and funnel ambient light into the photoreactive centre, to drive photosynthesis. The phycobiliproteins (phycoerythrin (PE), phycocyanin (PC), and allophycocyanin (APC)) are organized as disk-shaped macromolecular proteins with covalently attached phycobilins. They are placed in the phycobilisome (the light harvesting antennae of the photosystem II in cyanobacteria and algae), each with a region of maximum and relatively narrow wavelength of absorption in the visible spectrum[63]. Phycobiliproteins are able to efficiently absorb and transfer light energy at low intensity levels to chlorophyll, in order to perform photosynthesis[64]. The phycobiliproteins show interesting optical properties and are starting to be used as fluorescent markers in biochemical and biomedical research or as photosensitizers in anti-tumour research[65]. Moreover, they are promising candidates for signal transduction and biosensor-based applications[66].

Furthermore, outside the field of photoreceptors and of photosynthetic proteins, fluorescent proteins should be mentioned. Visible fluorescent proteins (VFPs) are genetically encoded fluorophores that are available in a wide variety of colours, spanning the whole visible spectrum. These probes have revolutionized cell-biology, allowing the visualization of

biological processes with high sensitivity and specificity in living cells, tissue, or even whole organs. The most important VFP is the genetically encoded green fluorescent protein (GFP)[67]. This protein contains a fluorophore that is synthesized within the protein itself, without the need for additional substrates for generating fluorescence. The GFP was firstly observed as a by-product after purification of the chemiluminescent protein aequorin from the jellyfish[68] but, in the following decades, GFPs were also discovered in several other light-emitting marine species. Later on, it was discovered that the GFP could be expressed and also become fluorescent in other organisms[69]. Furthermore, a large number of GFP-like proteins have been isolated, ranging in fluorescence from green to orange-red[70,71]. The general structure of these proteins is made up of α-helices and β-strands, with the chromophore placed almost exactly in the centre of the protein and is therefore buried inside the GFP protein. This protective shell effectively shields the chromophore from the environment. Although the precise sequence of events is still under debate[72], it is generally accepted that chromophore formation involves cyclization of a tripeptide (Ser, Tyr, and Gly residues) by nucleophilic attack of the amide nitrogen of Gly on the carbonyl of Ser[73]. The mature chromophore is formed upon oxidation of a C–C bond by molecular oxygen, causing the formation of a p-hydroxybenzylidene–imidazolidinone derivative with a large conjugated π-electron system. The most used GFP variant is the enhanced GFP (EGFP)[74].

1.1.3 Immobilization of photoactive proteins on silica nanoparticles

Nanobiotechnology, the material science involving the fabrication of materials with dimensions of 1-100 nm, is currently employed as a tool to explore several domains like imaging[75], sensing[76] and targeted drug delivery[77] among medical sciences, biology, chemistry, physics and engineering. Furthermore, there has been a recent shift towards generating surfaces that involve proteins in highly controlled patterns, preferably with nano-meter scale precision[78,79]. The engineering of biodevices and biomaterials is required to solve fundamental and applied problems related to complex interfaces, such as those existing between biological entities and artificial devices[80,81]. Recent advances in the field of nanotechnology have resulted in solid-state biosensors offering compatibility of inorganic materials with the chemical/biological agents, usually enzyme, antibody, or nucleic acid, thus enabling stable, direct, and reproducible screening and detection[76]. The immobilization of proteins on solid supports aims to maintain the integrity, native conformation, and biological function of protein itself (see **Figure 1.4**).

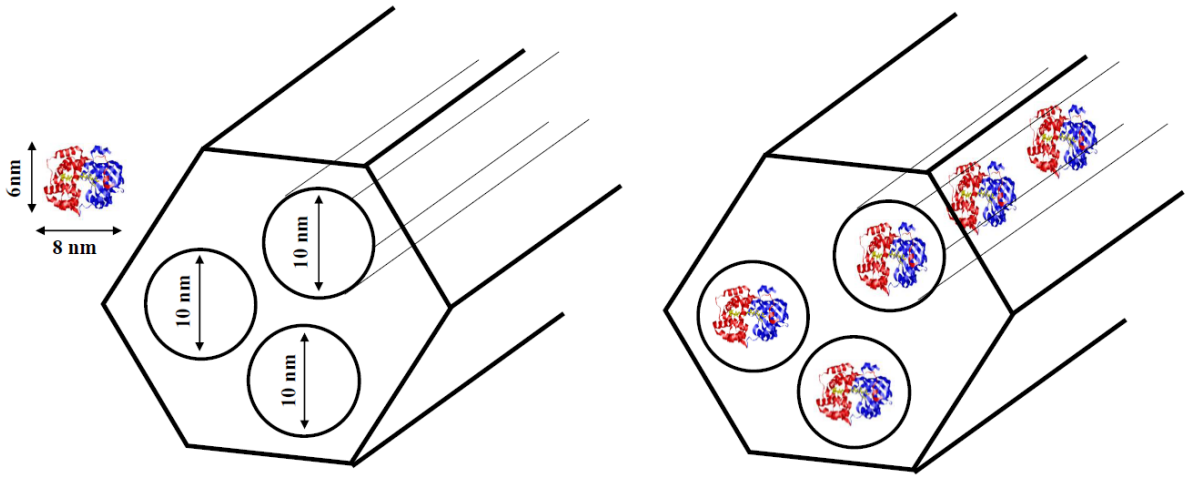

Figure 1.4 Schematic example of immobilization of a protein inside nanopores of mesoporous silica nanoparticles. (Left) bare structure of nano-structured hexagonal cylinders of silica nanoparticles and 2D dimensions of a protein. (Right) Protein immobilized inside the nanopores.

Photoreceptor- or photoactive-protein-loaded organic nanoparticles, such as liposomes, polymeric nanoparticles and dendrimers are commonly exploited for medical and ophthalmology applications. Nevertheless, inorganic nanoparticles have gained significant attention for their specific targeting, theragnostic properties and drug release. Nanotubes, nanoparticles, nanowires, and nano-porous materials for biocompatibility have been studied over the past decades.

The choice of photoreceptors for diagnostic imaging and photochromic biosensing represents an attractive opportunity because, in principle, it can make the visual interpretation of biological reactions or events, faster and clearer. However, no reports of photoreceptor proteins immobilized on mesoporous silica nanoparticles have been reported. Nevertheless, immobilization of other photoactive proteins or photosystems has been published and they are shortly reviewed below.

Noji *et al.*[82] reported the incorporation of the dimeric form of the photosystem II complex (PSII) into mesoporous silica SBA-15. The PSII, purified from a cyanobacterium (*Thermosynechococcus vulcanus*), had a molecular mass of 756 kDa and a size of 20 nm, while the SBA-15 used had a diameter of inner pores of 23 nm. The aim of their work was to realize a photosynthetic light-induced oxygen evolution system inside silica nanopores, extracting electrons from water and transferring them to an artificial organic mediator molecule in the external medium. The immobilization of PSII on SBA-15 was carried out by absorption of the photosynthetic complex solution on the matrix, under gentle stir and followed by Visible

spectroscopy. They managed to immobilize the PSII complex into SBA-15 and to realize a light-driven reduction of external organic compounds by electrons from water, suggesting the possible future construction of artificial photosynthetic systems[82].

Oda *et al.*[83] studied the adsorption of the photosynthetic light-harvesting-2 protein complex (LH2) isolated from a purple photosynthetic bacterium, on folded-sheet silica mesoporous material (FSM). The LH2 had a mass of 129 kDa and a molecular structure of 7.0 x 5.0 x 13 nm, while the FSM had an average internal pore diameter of 7.9 nm. The immobilization of LH2 on the FSM matrix was carried out by absorption; this stabilized the photosynthetic complex structure and increased stability of the structure at higher temperatures. Furthermore, silica nano-porous material provided a reaction environment suitable for the LH2. Indeed, the light-induced output of electrons from the LH2 to the electrode or to a redox dye in the outer medium was observed[84].

Besides the photosynthetic complexes, immobilization of the green fluorescent protein (GFP) on mesoporous silica matrices was reported[85]. More precisely, the enhanced green fluorescent proteins (EGFP, with a barrel-like structure and a dimension of 2.4 x 4.2 nm[86]) was chosen to be immobilized on several types of mesoporous silica: MCM-41, arrays of silica nanochannels (ASNCs) and SBA-15 (with larger pores compared to the previous). The surfaces were functionalized with aminopropyl moieties by grafting, to tune the surface charge and allow the electrostatic absorption of the protein. Structural and spectroscopical characterization of the system revealed that the structure of the EGFP was well-preserved upon immobilization and, furthermore, fluorescence lifetimes agreed with those of the free protein. The combination of nanomaterials and fluorescent or photochromic molecules opened new ways in areas at the interface between bioscience and nanotechnology, such as sensing and detection[85].

Recently a nanomaterial grafted with a protein shell, able to transport cytotoxic species and release them in response to light irradiation, has been discovered[87]. Mesoporous silica nanoparticles (MSN) were chosen as support and their surface was grafted with a light-sensitive cross-linker, to which a protein-shell was anchored. The protein shell, composed by avidin, streptavidin and biotinylated transferrin, was photosensitive and cleavable by light irradiation. Moreover, it acted as a targeting and a capping agent at the same time. Indeed, it was observed that this bio-compatible nanocarrier can enter tumoral cells (because of the presence of transferrin on the external surface), and once inside, upon light irradiation, it can release cytotoxic species aiming to the apoptosis of diseased cells[87].

However, there are other studies reporting the direct encapsulation of photoreceptors and photoactive proteins in sol-gel matrices. This is a transparent matrix that suggested the use of sol-gel-encapsulated photoactive proteins as optic biosensors. Already in 1995, a work was published about the entrapment of a mutant of the bacteriorhodopsin inside silica sol-gel[88]. The tetra-methoxy silane (TMOS) based sol-gel was mixed with the solution of the purified bacteriorhodopsin, mixed, dialyzed, and dried at 4°C. The photoreceptor was successfully encapsulated inside the sol-gel. However, the constraint of the sol-gel structure partially inactivated the rhodopsin, whose photo-activity decreased after storage at room temperature, probably because of the inhibition of molecular motion inside silica sol-gel.

Furthermore, silica sol-gel were used for the encapsulation of phycobiliproteins [89]. Phycobiliproteins were encapsulated inside a tetra-methoxy silane (TMOS) based sol-gel system. It was observed that the effects of sol-gel entrapment on the spectroscopic properties of three different phycobiliproteins were significantly different. Most of the proteins faced significant changes in conformation and aggregation state when entrapped in sol-gel matrices. Only phycoerythrin preserved its native structure after the encapsulation. Indeed, a thin film of sol-gel encapsulating phycoerythrin, was used to cover an optical surface, and resulted in strong fluorescence from the evanescent wave excitation of the protein, suggesting the potential of sol-gel-encapsulated phycobiliproteins for biosensor applications.

Although encapsulation within a silica sol-gel matrix necessarily modifies the functioning of the proteins, the native photo-activity can be retained therein. However, by switching from the sol-gel encapsulation to the immobilization on mesostructured silica nanoparticles (e.g., SBA-15), the native structure and therefore the activity of the photo-active protein can be even more retained. Indeed, the unique properties and utility of silica nanoparticles arise from a variety of attributes. First, nanopores and biomolecules (such as proteins) have similar size. Moreover, biomolecules encapsulated in silica usually retain their structural and functional properties, and they keep the response properties to chemical and physical external stimuli. They can sometimes exhibit enhanced activity in comparison to the soluble form. In addition, nano-porous silica offers a controllable surface topography at a nano-meter resolution in three dimensions, are optically transparent, exhibit good mechanical stability, are manufactured with different geometries and allows chemical surface modification[90]. Because of these advantages, and the normally good preservation of biological activity of the immobilized biomolecules, silica matrices have been largely used to immobilize proteins, nucleic acids and

even whole live cells for the development of biotechnological devices (bioreactors, biosensors, separation and photonic devices)[91–94] or for biomedical applications (biomaterials, biosensors and systems for production, screening and controlled delivery of bioactive compounds)[95,96]. Nevertheless, in this range of applications, light proves to be a powerful tool because it presents low toxicity, and its application can be spatially and temporally controlled by selecting the area and the exposure time.

Currently the most important application areas for bio-compatible nanoparticles in optical sensing are biomarker analysis, cancer diagnosis, diagnostic imaging, and immunoassays. An optic sensor uses an optical substrate to transmit excitation light to the sensing material, giving rise to an optic signal which depends only on the presence of the sensor in a particular area of a diagnostic device, and to transmit the signal back to the detector. For this purpose, the most used biomolecules are photoactive proteins or enzymes, which can support the formation of coloured products that can be detected by a change in colour, or products capable of emitting a fluorescent output. Moreover, dyes have been exploited in optical diagnostics, through colour changes or by emission of fluorescence, but they usually suffer from photobleaching. Therefore, immobilization of the dye in a mesoporous matrix can result in increased photostability[97].

In this way, the optical properties of the sensing element can be increased by directly immobilizing molecules (e.g., proteins, antibodies, enzymes) on the surface, as in the case of mesoporous silica nanoparticles.

Therefore, this work is specifically focused on the study of interactions between a photoreceptor protein (the Orange Carotenoid Protein) and mesoporous silica SBA-15, aiming to the development of photoactive bio-compatible nano-devices to be applied as optic sensors.

1.2 The Orange Carotenoid Protein

The Orange Carotenoid Protein (OCP) is a water-soluble, blue-green light photoactive protein, involved in the photoprotection of cyanobacteria[13]. Cyanobacteria are the first prokaryote appeared on earth to acquire the oxygenic photosynthetic ability. The existence of the cyanobacterial OCP was discovered in 1981[98] and firstly isolated from *Synechocystis* cyanobacteria in 1997[99]. The crystal structure of OCP was solved in 2003[100], its photoprotective function was reported in 2006[101] but the photoactivity of OCP was only elucidated in 2008[13]. Nowadays several families of OCP have been identified[102–104], different strains of cyanobacteria (*Synechocystic*, *Tolypothrix*), green algae (*Chlamydomonas reinhardtii*[105]) and even *E.coli* cells[106] have been used to express the different OCPs. Several homologous of this protein are under study, notably homologous of the OCP-NTD[107] and homologous of the OCP-CTD[108]. The peculiar properties of OCP are described in this chapter. First, its biological role played in nature as photoprotective system for cyanobacteria will be described. Then the attention will be shifted to the current knowledge on its photoactivation mechanism, going through its structure and photo-physics. Finally, the proposed possibility of engineering its structure to modulate its spectroscopical properties, or its use as sensor for temperature and light or as antioxidant nanocarrier and delivery system will be described.

1.2.1 Orange Carotenoid Protein: biological role

OCP is essential for the photoprotection mechanism in cyanobacteria, which are photosynthetic prokaryotes able to perform oxygenic photosynthesis[109]. The exposure of photosynthetic membranes to intense light can cause production of Reactive Oxygen Species (ROS). ROS are highly reactive molecules that can severely damage the structure and the function of the cells. Photosynthetic organisms have found several strategies to reduce the amount of photo-oxidative damage. One of them is to decrease the energy arriving to Photosystem II (PSII), the main source of ROS production by increasing thermal dissipation of excess energy at the level of the antennae. This thermal energy dissipation is accompanied by a non-photochemical quenching (NPQ) of chlorophyll fluorescence. In cyanobacteria, this mechanism differs from those existing in plants and algae. In fact, in cyanobacteria light is harvested by a peculiar antenna, the phycobilisome (PBS). The PBS is a huge extramembrane complex, mostly composed by phycobiliproteins binding blue and red pigments, the bilins. Strong light photoactivates the

OCP and the photoactive form of the protein is able to bind to the PBS and to quench its fluorescence[110]. This induces an increase of thermal dissipation of the excess energy absorbed by the PBS[101]. Thus, the role of OCP is, in binding the PBS, to induce a thermal dissipation of the excess of solar energy which in its absence would be directed to the photosynthetic reaction centres. In this way, OCP binding to PBS prevents formation of ROS[103,111].

OCP-related NPQ in cyanobacteria, takes place in the time range of seconds to few minutes and, more important, it is reversible under normal light conditions. *In vivo*, the reversibility of this reaction needs the presence of another proteins, the FRP (Fluorescence Recovery Protein)[112]. The FRP interacts with the active form of the OCP (OCP^R) and accelerates the recovery of the PBS fluorescence[103].

1.2.2 Orange Carotenoid Protein: structure

OCP is a 35 kDa protein, consisting of a unique long polypeptide chain of around 300 amino acids (the chain length depends on the type of OCP) organized into a globular conformation. The polypeptide chain is organized into two domains, respectively the N-terminal domain (NTD; residues 18-165) and the C-terminal domain (CTD; residues 190-317) bound by a flexible linker (approximately 25 residues) as shown in **Figure 1.5**[100,113]. The NTD is made up of α-helix bundles while the CTD has an α/β fold. The conformation of the dark protein is stabilized by interdomain interactions between the N-terminal extension (NTE) and the β-sheets of the CTD, but also includes a salt bridges between NTD and CTD residues, with the residues Arg155 and Glu244, that stabilize the interactions between the domains[100,114].

A hydrophobic pocket between the domains allows the embedding of a keto-carotenoid, non-covalently bound to OCP and only sparingly solvent accessible. This carotenoid, shared by the two domains, is also essential for the stability of the dark protein. The carotenoid molecule is composed by two β rings spanned by a conjugated carbon-carbon double bond chain. The keto terminus, called β1 ring, of the carotenoid is placed inside the CTD pocket and it is stabilized by H-bonds occurring between its carbonyl group and the side chain of two amino acids belonging to the CTD: Trp288 and Tyr201 (see **Figure 1.5**)[115]. The β2 ring is stabilized by π interactions with Tyr44 and Trp110 in the NTD[100,116].

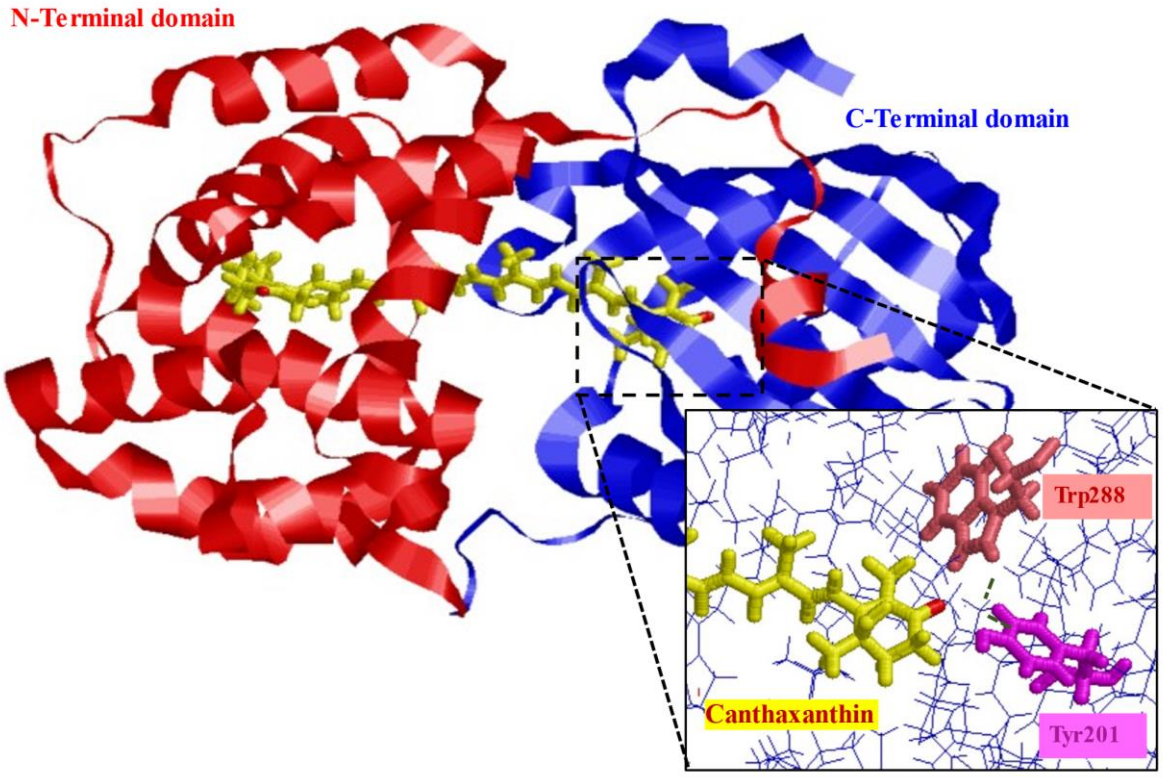

Figure 1.5 Crystal structure of OCP binding Canthaxanthin from cyanobacteria Synechocystis PCC 6803 (PDB 4xb5[117]). Canthaxanthin is depicted in yellow in the 3D view, with oxygen atoms in red. In the bottom, right corner, there is a zoom-in on interactions between the carbonyl group (Oxygen is drawn in red) of the carotenoid β1 ring and amino acids Tyr201 and Trp288 belonging to the C-terminal domain.

In all the published crystalline structures of OCP, the asymmetric unit contains a homodimer. Further experiments have suggested that the dimeric form of the OCP is present only at high protein concentrations[118,119]. Despite the presence of a dynamic monomer/dimer equilibrium of the OCP in solution[120], during photoactivation the OCP shifts the equilibrium to the monomeric form[118] although it can exist as a dimer or even a tetramer[121].

1.2.3 Orange Carotenoid Protein: photoactivation mechanism

The OCP-related photoprotection mechanism takes place through an activated form of OCP, called OCP red, which is produced upon photoactivation by strong blue light of the resting, dark-adapted state of OCP, called OCP orange. The exact mechanism of photoactivation of the OCP is still unknown in all its details, despite intensive research by several groups in the world in the last 10 years.

It is well established that, in darkness, OCP has an orange colour (hereafter referred as OCP^O) and its absorption spectrum shows a well resolved vibrational structure, typical of the carotenoid, with two maxima (474 nm and 496 nm) and a shoulder at 440 nm. The carotenoid acts as the sensor of light intensity. Indeed, absorption of a blue photon (450–500 nm) by the carotenoid, triggers large-scale structural modifications of OCP involving the whole protein backbone, so that OCP changes from the resting, dark-adapted orange state (OCP^O), to its so-called active red state (hereafter referred as OCP^R) that is meta-stable[13]. The spectrum of OCP^R is red-shifted and the vibrational structure is lost, with a single maximum (around 510 nm - 525 nm, depending on the carotenoid) (**Figure 1.6**)[13]. The photoconversion of OCP^O to the OCP^R has a very low quantum yield (around 0.2 %) and this ensures that only at high light intensities OCP^R is significantly accumulated[122,123]. This is a key-point of cyanobacteria photoprotection: OCP gets activated in large amounts to its active PBS-binding (and energy-dissipating) red form only under intense light. A work has been reported about the impact of the carotenoid type on the photo-activation rate and on the quantum yield. It has been showed that, the addition of a carbonyl in the structure of carotenoid (comparison between echinenone and the carbonyl-added canthaxanthin was carried out), results in increased photoactivation efficiency, reduced back-conversion, reduced binding to PBS and reduced energy-quenching activity[124].

OCP^O is not able to induce energy and fluorescence quenching at the level of PBS, while OCP^R binds to the PBS, inducing fluorescence and energy quenching of the light-harvesting antenna[125,126]. The rate of OCP^R accumulation strongly depends on light intensity[13] but it is not less temperature-dependent[127,128]. Photoconversion also depends on pH[116], high salt concentration[129] and Cu^+ presence[130]. However, OCP^R is not stable and, *in vitro*, its dark incubation leads to a spontaneous back-conversion to the OCP^O stable form. Differently from photoactivation, this back-conversion strongly depends on temperature[13]. Furthermore, the reactions of photoactivation and back-conversion can be affected by the presence of ions: kosmotropes (e.g., phosphate) inhibit the photoactivation while chaotropes (e.g., thiocyanate) stimulate activation of the protein in the dark[129].

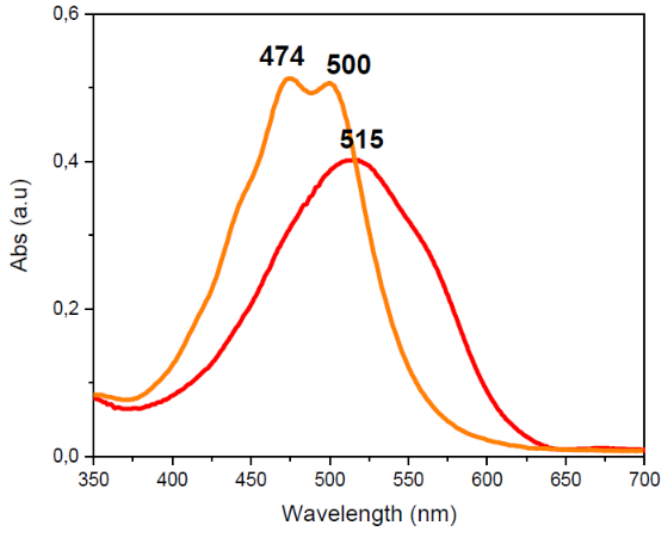

Figure 1.6 Visible spectra of OCP (binding Canthaxanthin) 0.3 mg/mL in water solution, before (orange line) and after (red line) photoactivation with blue light LED.

1.2.3.1 OCP photoactivation : conformational changes

The presence of a carbonyl group on the keto terminus of the carotenoid is essential for the photoactivity. Only OCPs carrying a ketocarotenoid, such as echinenone (ECN) or canthaxanthin (CAN), in addition to hydroxy-echinenone (hECN), are able to be photoactivated[131,132]. The crystal structure of OCP^O shows a bent conformation of the carotenoid, in an all-*trans* configuration. Moreover, spectroscopic studies confirm heterogeneity in OCP^O, suggesting two different positions in which the carotenoid could be accommodated[133,134]. Despite the lack of the crystal structure of OCP^R, crosslinking experiments have shown that, after blue-light exposition, OCP reaches a more elongated and open conformation[135], with the two NTD and CTD domains only connected by the linker[128,135]. In OCP^R the carotenoid remains in an all-*trans* configuration but it reaches a more planar conformation, suggested by the increase of its conjugation length[133,134]. This increase is confirmed by the red-shift of its Vis absorption spectrum and by the disappearance of the vibronic structure[13].

Upon photoconversion, all interactions between NTD and CTD are broken, including the salt-bridge (Glu244-Arg155) stabilizing the OCP^O conformation, allowing the domain separation[117,135,136]. The domains separation is caused by changes in the structure of OCP, notably the unfolding of the N-terminal helix (NTE)[119], a more elongated shape of the

protein[135] and a dimer-to-monomer transition[118]. During the reaction, the two H-bonds holding the carotenoid inside the CTD (occurring between residues Trp288 and Tyr201 and the carbonyl group of the β1 ring), break and the carotenoid moves 12 Å inside the NTD and, at the end, it turns to be only slightly solvent-exposed[117]. The longer conjugation length reached by the carotenoid was proposed to be related to different positions of the rings around a single C6–C7 (C6′–C7′) bond and to a less bent polyene chain[133,137]. Recently, it has been suggested that the breakage of these H-bonds between the carotenoid and OCP can be due to a structurally distorted, excited S* state of the carotenoid[123] even if a more recent work reported few weeks ago, questioned this thesis suggesting the existence of a S˜ state involved in the photo-activation mechanism leading to OCP^R [121]. It had been suggested that firstly the carotenoid migrates to the NTD, then the changes inside the NTD caused by the movement of the carotenoid into the NTD, weaken the interdomain interactions, both domains separate and, finally, the NTE dissociates[117,118,126,135,138,139]. At the same time, CTT dissociates from the CTD β-sheet and closes the CTD carotenoid tunnel after the translocation of the latter[140].

Substitution of the amino acids involved in the H-bonds (Trp288 and Tyr201) makes the protein red even in darkness, suggesting a key-role played by these two residues[116]. *In vitro*, mutants with substituted Trp288 and Tyr201 are in the red form even in darkness and able to quench PBS fluorescence with no need of photoactivation[139]. In vivo, these mutants are not able to quench the PBS and the reason of that is still a matter of question[139].

It should also be underlined that replacement of the keto-carotenoid (echinenone, hydroxy-echinenone, canthaxanthin) by a carotenoid lacking the keto group capable of accepting H-bonds from the two amino acidic residues (for example Zeaxanthin), makes OCP photo-inactive[131].

1.2.3.2 OCP photoactivation and back conversion

As already mentioned, only the OCP^R form is able to bind the PBS and to induce the NPQ[13,125]. For the PBS binding, a specific amino acid at the domain interface, Arg155, is essential[136]. Recently, new studies showed that other amino acids are essential for the PBS binding, notably all amino acids surrounding the carotenoid β1 ring in the OCP^R-NTD[141]. Furthermore, it was demonstrated that simple binding of OCP^R to PBS is not enough for its quenching and a structural rearrangement may be required to trigger the quenching

process[142]. The first structure of the OCP-PBS complex obtained by cryo-electron microscopy has been recently reported[143].

The separation of the domains upon photoactivation uncovers this amino acid making the protein able to bind to the PBS[117,125,126,136]. It was also shown that the isolated NTD can bind and quench the PBS[117,126]. The NTD can be therefore defined as the effector domain and the CTD as the regulator domain[126]. It was firstly observed that one single molecule of OCP^R interacting with the basal cylinders of PBS[125,127] is sufficient to quench almost all PBS fluorescence[144,145]. Later, Squire *et al*. discovered that two OCP molecules are required to completely quench the PBS[145] while the structure of the OCP-PBS complex resolved by cryo-EM revealed the presence of two OCP dimers attached to PBS, for an overall amount of four OCP molecules per PBS[143]. However, the exact mechanism of energy dissipation remains to be elucidated. Most probably, the carotenoid plays a direct role in the quenching via energy or charge transfer[138,146–148].

As previously stated, *in vitro* and in the dark, OCP^R back-converts to the orange stable form very quickly (the exact rate depending on temperature)[127]. *In vivo*, the recovery requires the presence of another protein, called Fluorescence Recovery Protein (FRP). FRP is an α-helix elongated protein that is stable as a dimer in solution[112,139]. FRP has two different activities: it is essential for the OCP^R-to-OCP^O conversion reaction and it promotes the detachment of OCP^R from PBS[149,150]. FRP is only able to interact with the OCP^R form[149] and it brings together NTD and CTD, stabilizing the intermediary state that facilitates the back-conversion[139]. FRP binds to the CTD of OCP^R as a dimer but then monomerizes[151,152]. In the absence of FRP, the cells remain in a quenched state, even in the dark[149,153]. Nevertheless, the activity of FRP is light independent[150]. *In vitro* experiments carried out adding FRP to OCP^R-PBS complex, accelerated the fluorescence recovery, indicating that FRP promotes the detachment of OCP from the phycobilisomes[125,150,151].

1.2.4 Carotenoids: Echinenone vs Canthaxanthin

Carotenoid plays a key-role in photoconversion and even if OCP could bind several types of carotenoid, only with three of them it preserves its photo-activity, notably with 3-hydroxy echinenone (hECN), echinenone (ECN) and canthaxanthin (CAN)[131,132]. Carotenoids are hydrophobic chromophore molecules derived from the isoprenoid metabolism and characterized by keto-group functionalized end-rings associated with the double bond

conjugated system. They enhance the efficiency of light-harvesting and electron transfer in photosynthetic apparatus protecting it against light-induced damage. They are in charge of defence mechanisms against oxidative stress[154] but their delivery to vulnerable cells is challenging due to their hydrophobic nature and susceptibility to degradation.

The biosynthesis of carotenoids has been described in several studies[155,156]. Animals and humans are not able to biosynthesize them, so they need to ingest these compounds from dietary sources[157]. For this reason they are used as food supplements, feed additives, drugs and cosmetics[157,158]. However, carotenoids from vegetal sources are low in bioavailability, whereas fat and lipid-based formulations may improve their bioavailability[159]. Some of them (e.g., canthaxanthin) are considered strong antitumor agents, playing the major role of inducing apoptosis of human cancer cells[160]. Canthaxanthin was isolated for the first time from a mushroom but it could also be found in algae and microalgae[161]. As lipophilic compound, it is added to animal feed to colour foods. Canthaxanthin is a powerful lipophilic antioxidant that scavenges reactive oxygen species and quenches singlet oxygen[162].

In *Synechocystis* cyanobacteria, the major carotenoids accumulated are β-carotene, hydroxy-carotenoids (zeaxanthin) and ketocarotenoids (echinenone and canthaxanthin[163]). Once produced the β-carotene, the biosynthesis of echinenone requires a ketolase enzyme (*crtO*) that attacks only one of the β-rings of β-carotene[164]. On the other side, the conversion of β-carotene into canthaxanthin is performed by the β-carotene ketolase enzyme (*crtW*). This enzyme introduces the keto-groups at the 4,4´-position to β-rings, that is missing in echinenone[164].

Regarding the OCP, the all-*trans* configuration of the carotenoid is maintained in both forms, orange and red, but in OCP^R it is more planar due to a rotation around the single C6–C7 bond of its conjugated double bonds chain[117,126,133] with an increased effective conjugation[13]. Recent studies propose an explanation of OCP photocycle as composed by a series of excited states, intermediary OCP forms and carotenoid conformations[165–167].

The OCP can bind 3′-hydroxyechinenone (3′-hECN), canthaxanthin (CAN) and echinenone (ECN) to carry out the photo-activity[131,132]. This thesis is focused on the study of two types of OCP, the one binding echinenone and the other one binding canthaxanthin, referred to as OCP(ECN) and OCP(CAN), respectively.

1.2.5 Orange Carotenoid Protein: applications

The dynamics of the photoconversion of the OCP have inspired several studies on the engineering of this protein. In 2017, Andreoni *et al.*[168] developed an antenna light system based on a DNA scaffold, on which two organic dyes had been genetically bound (notably two cyanines, Cy3 and Cy5) and a molecule of OCP assembled on it. It turned out to be a photoactive switch. Indeed, it was demonstrated that, in absence of the OCP, the green light (520 nm) absorbed by the Cy3 acceptor, is transferred to the Cy5 because of an energy transfer due to the spectral overlap between the Cy3 emission spectrum and the Cy5 excitation spectrum and, as a result, the Cy5 emits red light. When OCP is genetically encoded to the DNA scaffold and photoactivated, the green light absorbed by the Cy3 is quenched by OCP^O form, that turns into the OCP^R, switching off the energy transfer to Cy5 and therefore its fluorescence. This study has been used as starting point for the development of silica nanoparticles with tuneable fluorescence, detailed forward, in Chapter 4.

In 2019, Maksimov *et al.*[169] published a study about photoactive chimeras based on a genetically encoded OCP to be used as temperature sensor. In details, two photostable fluorescent proteins (notably GFP–Green Fluorescent Protein and RFP-Red Fluorescent Protein) have been genetically encoded to the OCP sequence in *E.coli* and then purified. Following the time-course of fluorescence intensity after photoactivation of the OCP, these two systems (RFP-OCP and OCP-GFP) showed to be suitable for temperature measurements in microenvironments because the temperature could affect the energy transfer between the proteins and, as a response, the fluorescence emission.

In 2022 a study was published by Piccinini *et al.*[170] regarding the use of the OCP as switch to control light response in *Aradopsis thaliana*. They developed a chloroplast-localized synthetic photo-switch based on OCP2, engineered to bind the NanoLuc luciferase protein and to be exploited as regulator upon light exposure, as carotenoid biosensor or to engineer microalgae aiming to express keto-carotenoids.

To enlarge the range of possibilities to produce carotenoid binding OCP proteins, in 2021 Pivato *et al.*[105] used the green algae *C. reinhardtii* as host for OCP2 holoproteins expression. These OCP proteins showed to be bound to different carotenoids from the ones usually present in cyanobacteria (which are ketocarotenoids), notably loroxanthin, neoxanthin or lutein. The proteins kept the photo-properties only in presence of ketocarotenoids.

Over the years, several patents have been registered. *In vivo* production of OCP was registered by Bourcier de Carbon in 2015[106]. Russian groups registered the use of OCP as sensor for defrosting of products in 2016[171] and the use of OCP as biosensor for determining intracellular temperature and viscosity in 2020[172]. In 2020 another group registered a patent about the use of blue-green algae for raw matter production[173].

1.2.5.1 OCP families and homologues of NTD and CTD domains

Bao *et al*. recently suggested the existence of three families of OCP: OCP1 (widely used to elucidate OCP mechanisms), OCP2 (that was found to have a faster accumulation of OCP^R and a faster back-conversion to OCP^O compared to OCP1) and OCPX[104]. It was first suggested that OCP2 and OCPX are ancestors of the family of OCP1[174], however it was then discovered that OCP1 and OCPX usually occur alone, while OCP2 generally coexists with OCP1 or OCPX[104,175]. From a structural point of view, OCPX and OCP1 have a tendance to dimerize at high concentrations[120,175] while, OCP2 remains monomeric even at high concentrations[104,175].

It was also discovered that cyanobacteria are able to express homologous of the OCP because they also have genes coding for it[100]. The homologous of the OCP-NTD are known as HCP (helical carotenoid proteins) or NTDH[107]. The homologous of the OCP-CTD, are classified as CTDH[108]. While HCPs are monomers, CTDHs are dimers, sharing one canthaxanthin molecule[108]. Among the nine different subclades of HCPs, the structure of HCP1 had been solved and found to be similar to NTD in structure and spectroscopic features[107,176]. The crystal structure of HCP2, found in nature in *Tolypothrix* cyanobacteria, was also solved[177]. Despite their structural similarities, the HCPs have different roles and regulation patterns: some of them are able to quench singlet oxygen, some others induce fluorescence quenching of the PBS[107,176,177]. Recently, CTDHs have been studied, showing that they are carotenoid proteins involved in carotenoid transfer to other proteins[178]. The secondary and tertiary structures of apo-CTDH (CTDH without carotenoid) and CTD of OCP^O are similar with the main difference of the position of CTT[140]. Normally, the CTT adopts an external position, while in apo-CTDH, CTT adopts an internal position. These results suggest that CTT changes its position depending on the presence or absence of the carotenoid[140]. Despite their role of singlet oxygen quenchers, CTDH are fundamentally carotenoid carriers from the membrane to HCPs (unable to take the carotenoid from the membrane) or to OCP[108,140].

In 2017 the possibility of carotenoid transfer between water-soluble proteins was discovered[179,180]. *E.coli* cells were used to express NTD and CTD in presence or absence of canthaxanthin. Incubating CAN-CTD (CTD binding canthaxanthin) with apo-NTD (NTD missing the carotenoid), photoactive OCP was produced[179]. Nevertheless, it was discovered that also some HCP clades, can transfer the carotenoid to a certain type of CTDH[181]. Further studies stated that the carotenoid transfer could be multidirectional, depending on the stability of interactions between partners[182].

Beside the use of OCP as potential sensor for light or temperature, the CTDH homolog of the OCP is under study for its properties of nanocarrier and antioxidant delivery. In 2018, Harris *et al.*[140] discovered the positive impact of the C-terminal tail of the CTDH on the carotenoid uptake as well as its delivery (notably to the HCPs) and this study was then confirmed two years later[183] using three-dimensional X-ray structures of CTDH and supported by molecular dynamics (MD) simulations. The mechanism of uptake and delivery of carotenoid can be generalized and extended to other systems[183]. These studies have been the precursors of the work published in 2020 by Maksimov *et al.*[184] suggesting the use of carotenoid-binding CTDH as nanocarrier for the delivery of the carotenoid to liposomes or mammalian cells, overcoming the issue of the low delivery of the antioxidant molecule. Indeed, due to their hydrophobicity, antioxidant molecules are susceptible to degradation and low uptake yield; this makes their delivery to membranes and cells very difficult. The demonstrated targeted delivery of carotenoids inside mammalian cells, makes the CTDH a suitable antioxidant nanocarrier reducing the oxidative stress. Insights about the mechanism of delivery are, for the time being, missing.

Despite the spread of delivery strategies based on liposomes, inclusion complexes and nanocarriers built in a controlled manner[184–186], the water-soluble carotenoid-binding OCP may provide the best opportunities for carotenoid transportation and targeted delivery[183].

1.2.6 OCP expression in *E.coli*

Recombinant OCP(ECN) and OCP(CAN) from *Synechocystis* were produced in *E. coli* according to the protocol reported by Bourcier de Carbon et al.[132], at the CEA in Paris-Saclay (for more details see Method: molecular biology for OCP expression). The production of holo-OCPs in *E.Coli* cells requires three plasmids, two of which are involved in the carotenoid

biosynthetic pathway and the third allows the expression of the gene coding for OCP (**Figure 1.7** shows OCP production in *E.coli*).

• The *pCDF-OCP* plasmid allowing expression of the gene encoding OCP under the control of an IPTG-inducible promoter as well as the streptomycin resistance gene (Sm).

• The plasmid *pAC-BETA* which contains the *crt* gene operon of *Erwinia herbicola* containing four genes: *crtB*, *crtE*, *crtI* and *crtY* under the control of the promoter constitutive of the *crtE* gene and coding for the enzymes necessary for the synthesis of β-carotene. It also carries a chloramphenicol resistance gene (Cm).

• The plasmid *pBAD–crtO* (or *crtW*) containing the *crtO* (or *crtW*) gene from *Synechocystis 6803* under the control of the arabinose-inducible promoter coding for a mono-ketolase which catalyses the conversion of β-carotene into ECN (or CAN) and a sequence coding for a resistance module to ampicillin (Amp).

The *E. Coli* bacteria (BL21-Gold (DE3)) are therefore transformed by these three plasmids at the same time and the cells of a transformed BL21 colony are then cultured for three days. Purification on Nichel-enriched column follows, the OCP-His-Tag is trapped on the column and then eluted. The OCP solution is dialyzed in TRIS and stored in TRIS-NaCl buffer.

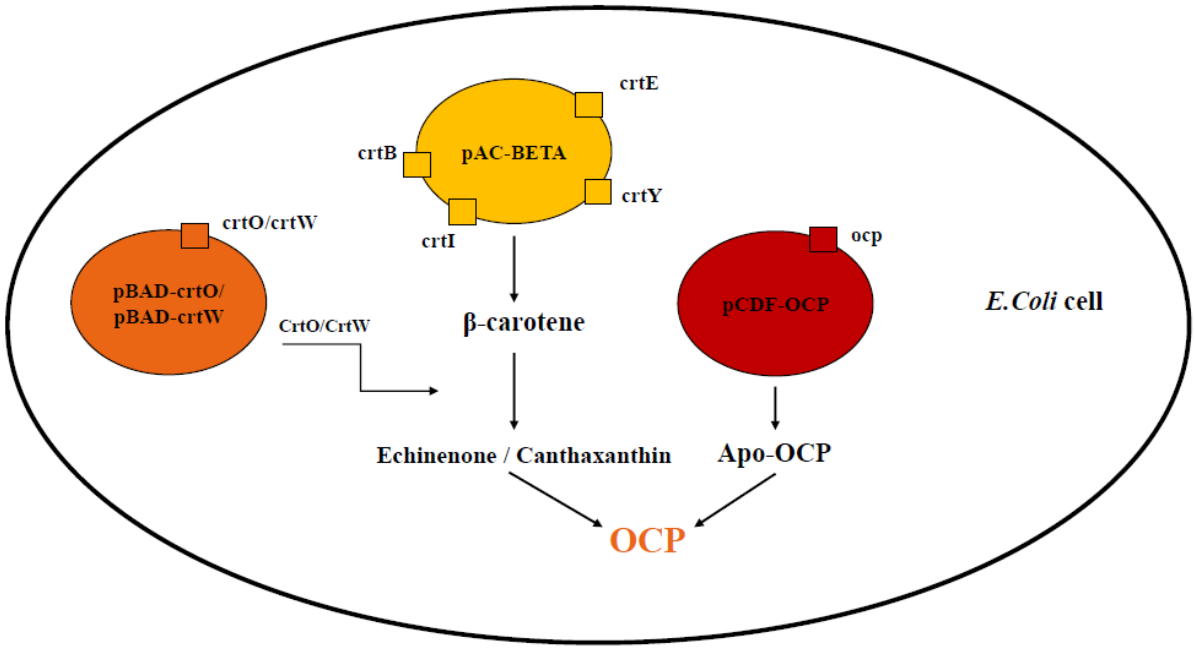

Figure 1.7 Schematic representation of OCP(ECN) or OCP(CAN) production in *E.coli*. *E.coli* producing OCP contains three plasmids: (orange) pBAD-crtO or pBAD-crtW, carries the crtO or crtW gene; (yellow) pAC-Beta carries the genes involved in β-carotene synthesis (crtB, crtE, crtI and crtY); CrtO or CrtW enzymes convert β-carotene in echinenone or canthaxantin, respectively; (red) pCDF-OCP carries the ocp gene.

1.3 Conclusion

Within the current photoreceptor scenario, the Orange Carotenoid Protein has been chosen to be investigated for its several interesting properties.

The Orange Carotenoid Protein was isolated for the first time in cyanobacteria in 1981[98], its structure was outlined in 2003[100] and in 2006 the biological role of OCP was identified[101]. Since then, the mechanism of photoactivation of the OCP has been deeply analysed and many of its aspects are known nowadays. Nevertheless, important questions remain opened. The fluorescence quenching mechanism is unclear, as like as the exact mechanism of photo-activation. The sequential steps occurring after the absorption of blue photons is still to be defined. In the same way the mechanism of back conversion needs to be elucidated. In addition, the crystalline structure of OCP^R has yet to be solved, even if, recently, the structure of the quenched OCP-PBS complex has been solved. Probably the lower stability of OCP makes the crystallization process difficult. Structural details of OCP^R form would be useful in the understanding of the photoactivation mechanism. This thesis gives support to the study of the mechanism of photoactivation and back-conversion of the OCP. The study is outlined in the following Chapter 2, and it is based on spectroscopic measurements, notably FT-IR difference spectroscopy and UV-Visible spectroscopy.

What makes this protein peculiar is its versatility. Several new families of OCP have been identified[104], furthermore different homologous are now well known (notably CTDHs and HCPs proteins)[187]. These homologues have been characterized *in vitro* but their role in cyanobacteria is still a matter of discussion. Understanding the role and mechanism of these carotenoid proteins is a new challenge for fundamental science, but it would also be the starting point for the development of several biotechnological applications. For example, the OCP engineered domains can be used to develop new photoactivable proteins, with different spectroscopical properties or optogenetic tools[188] while the CTDH can be used to develop new soluble carotenoid carriers[179,182].

In addition, the work performed for this thesis has demonstrated that the OCP can be immobilized on a solid mesoporous support (see Chapter 3), and it can be exploited for optical and photochromic applications (see Chapter 4). Indeed, the system would be used as optical sensor for temperature and pH local changes or as a photochromic switch to be employed in the development of bio-compatible photoactive nanoparticles with tuneable fluorescence with possible application in bio-imaging.

1.4 References

[1] P. Reyes, M.A. Ashraf, K.N. Brown, Physiology, Cellular Messengers, StatPearls Publishing, Treasure Island (FL), Universidad de Guadalajara, 2021. http://europepmc.org/abstract/MED/30844181.

[2] S. Rehman, M. Dimri, Biochemistry, G Protein Coupled Receptors, StatPearls Publishing, Treasure Island (FL), 2021. http://europepmc.org/abstract/MED/30085508.

[3] C.H. Heldin, B. Lu, R. Evans, J.S. Gutkind, Signals and receptors, Cold Spring Harb. Perspect. Biol. 8 (2016). https://doi.org/10.1101/cshperspect.a005900.

[4] A. Möglich, X. Yang, R.A. Ayers, K. Moffat, Structure and function of plant photoreceptors, Annu. Rev. Plant Biol. 61 (2010) 21–47. https://doi.org/10.1146/annurev-arplant-042809-112259.

[5] S. Kateriya, P. Hegemann, A. Hallmann, G. Kreimer, ALGAL SENSORY PHOTORECEPTORS Related papers, (n.d.).

[6] T. Kottke, A. Xie, D.S. Larsen, W.D. Hoff, Photoreceptors Take Charge: Emerging Principles for Light Sensing, Annu. Rev. Biophys. 47 (2018) 291–313. https://doi.org/10.1146/annurev-biophys-070317-033047.

[7] B.D. Zoltowski, B. Vaccaro, B.R. Crane, Mechanism-based tuning of a LOV domain photoreceptor, Nat. Chem. Biol. 5 (2009) 827–834. https://doi.org/10.1038/nchembio.210.

[8] X. Yang, E.A. Stojković, J. Kuk, K. Moffat, Crystal structure of the chromophore binding domain of an unusual bacteriophytochrome, RpBphP3, reveals residues that modulate photoconversion, Proc. Natl. Acad. Sci. U. S. A. 104 (2007) 12571–12576. https://doi.org/10.1073/pnas.0701737104.

[9] O.P. Ernst, D.T. Lodowski, M. Elstner, P. Hegemann, L.S. Brown, H. Kandori, Microbial and animal rhodopsins: Structures, functions, and molecular mechanisms, Chem. Rev. 114 (2014) 126–163. https://doi.org/10.1021/cr4003769.

[10] I. Chaves, R. Pokorny, M. Byrdin, N. Hoang, T. Ritz, K. Brettel, L.O. Essen, G.T.J. Van Der Horst, A. Batschauer, M. Ahmad, The cryptochromes: Blue light photoreceptors in plants and animals, Annu. Rev. Plant Biol. 62 (2011) 335–364. https://doi.org/10.1146/annurev-arplant-042110-103759.

[11] A. Losi, W. Gärtner, The evolution of flavin-binding photoreceptors: An ancient chromophore serving trendy blue-light sensors, Annu. Rev. Plant Biol. 63 (2012) 49–72. https://doi.org/10.1146/annurev-arplant-042811-105538.

[12] M.A. Van Der Horst, K.J. Hellingwerf, Photoreceptor Proteins, “Star Actors of Modern Times”: A Review of the Functional Dynamics in the Structure of Representative Members of Six Different Photoreceptor Families, Acc. Chem. Res. 37 (2004) 13–20. https://doi.org/10.1021/ar020219d.

[13] A. Wilson, C. Punginelli, A. Gall, C. Bonetti, M. Alexandre, J.M. Routaboul, C.A. Kerfeld, R. Van Grondelle, B. Robert, J.T.M. Kennis, D. Kirilovsky, A photoactive carotenoid protein acting as light intensity sensor, Proc. Natl. Acad. Sci. U. S. A. 105 (2008) 12075–12080. https://doi.org/10.1073/pnas.0804636105.

[14] R. Luca, F. Jean-Jacques, C. Catherine, F. Davide, O. Andrew, K. Eirini, B. Ralf, S. Eberhard, N. Ferenc, J.G. I., U. Roman, Perception of UV-B by the Arabidopsis UVR8 Protein, Science (80-.). 332 (2011) 103–106. https://doi.org/10.1126/science.1200660.

[15] J.M. Ortiz-Guerrero, M.C. Polanco, F.J. Murillo, S. Padmanabhan, M. Elías-Arnanz, Light-dependent gene regulation by a coenzyme B12-based photoreceptor, Proc. Natl. Acad. Sci. U. S. A. 108 (2011) 7565–7570. https://doi.org/10.1073/pnas.1018972108.

[16] J. Gong, Y. Yuan, A. Ward, L. Kang, B. Zhang, Z. Wu, J. Peng, Z. Feng, J. Liu, X.Z.S. Xu, The C. elegans Taste Receptor Homolog LITE-1 Is a Photoreceptor, Cell. 167 (2016) 1252-1263.e10. https://doi.org/10.1016/j.cell.2016.10.053.

[17] E.G. Govorunova, O.A. Sineshchekov, H. Li, J.L. Spudich, Microbial rhodopsins: Diversity, mechanisms, and optogenetic applications, Annu. Rev. Biochem. 86 (2017) 845–872. https://doi.org/10.1146/annurev-biochem-101910-144233.

[18] A. Terakita, T. Nagata, Functional properties of opsins and their contribution to light-sensing physiology., Zoolog. Sci. 31 (2014) 653–659. https://doi.org/10.2108/zs140094.

[19] H. Nakamichi, T. Okada, Crystallographic analysis of primary visual photochemistry, Angew. Chemie - Int. Ed. 45 (2006) 4270–4273. https://doi.org/10.1002/anie.200600595.

[20] S. Arnis, K.P. Hofmann, Two different forms of metarhodopsin II: Schiff base deprotonation precedes proton uptake and signaling state, Proc. Natl. Acad. Sci. U. S. A. 90 (1993) 7849–7853. https://doi.org/10.1073/pnas.90.16.7849.

[21] E. Zaitseva, M.F. Brown, R. Vogel, Sequential Rearrangement of Interhelical Networks Upon Rhodopsin Activation in Membranes: The Meta IIa Conformational Substate, J. Am. Chem. Soc. 132 (2010) 4815–4821. https://doi.org/10.1021/ja910317a.

[22] N.C. Rockwell, S.S. Martin, K. Feoktistova, J.C. Lagarias, Diverse two-cysteine photocycles in phytochromes and cyanobacteriochromes, Proc. Natl. Acad. Sci. U. S. A. 108 (2011) 11854–11859. https://doi.org/10.1073/pnas.1107844108.

[23] N.C. Rockwell, L. Shang, S.S. Martin, J.C. Lagarias, Distinct classes of red/far-red photochemistry within the phytochrome superfamily, Proc. Natl. Acad. Sci. U. S. A. 106 (2009) 6123–6127. https://doi.org/10.1073/pnas.0902370106.

[24] J. Dasgupta, R.R. Frontiera, K.C. Taylor, J.C. Lagarias, R.A. Mathies, Ultrafast excited-state isomerization in phytochrome revealed by femtosecond stimulated Raman spectroscopy, Proc. Natl. Acad. Sci. U. S. A. 106 (2009) 1784–1789. https://doi.org/10.1073/pnas.0812056106.

[25] K. Heyne, J. Herbst, D. Stehlik, B. Esteban, T. Lamparter, J. Hughes, R. Diller, Ultrafast dynamics of phytochrome from the cyanobacterium Synechocystis, reconstituted with phycocyanobilin and phycoerythrobilin, Biophys. J. 82 (2002) 1004–1016. https://doi.org/10.1016/S0006-3495(02)75460-X.

[26] J.M. Kelly, J.C. Lagarias, Photochemistry of 124-kilodalton Avena phytochrome under constant illumination in vitro, Biochemistry. 24 (1985) 6003–6010. https://doi.org/10.1021/bi00342a047.

[27] P.W. Kim, N.C. Rockwell, S.S. Martin, J.C. Lagarias, D.S. Larsen, Heterogeneous photodynamics of the Pfr state in the cyanobacterial phytochrome Cph1, Biochemistry. 53 (2014) 4601–4611. https://doi.org/10.1021/bi5005359.

[28] C. Song, G. Psakis, C. Lang, J. Mailliet, W. Gärtner, J. Hughes, J. Matysik, Two ground state isoforms and a chromophore D-ring photoflip triggering extensive intramolecular changes in a canonical phytochrome, Proc. Natl. Acad. Sci. U. S. A. 108 (2011) 3842–3847. https://doi.org/10.1073/pnas.1013377108.

[29] A. Xie, W.D. Hoff, A.R. Kroon, K.J. Hellingwerf, Glu46 donates a proton to the 4-hydroxycinnamate anion chromophore during the photocycle of photoactive yellow protein, Biochemistry. 35 (1996). https://doi.org/10.1021/bi9623035.

[30] A. Xie, L. Kelemen, J. Hendriks, B.J. White, K.J. Hellingwerf, W.D. Hoff, Formation of a new buried charge drives a large-amplitude protein quake in photoreceptor activation, Biochemistry. 40 (2001) 1510–1517. https://doi.org/10.1021/bi002449a.

[31] L.T. Mix, M. Hara, R. Rathod, M. Kumauchi, W.D. Hoff, D.S. Larsen, Noncanonical Photocycle Initiation Dynamics of the Photoactive Yellow Protein (PYP) Domain of the PYP-Phytochrome-Related (Ppr) Photoreceptor, J. Phys. Chem. Lett. 7 (2016) 5212–5218. https://doi.org/10.1021/acs.jpclett.6b02253.

[32] M. Salomon, J.M. Christie, E. Knieb, U. Lempert, W.R. Briggs, Photochemical and mutational analysis of the FMN-binding domains of the plant blue light receptor, phototropin, Biochemistry. 39 (2000) 9401–9410. https://doi.org/10.1021/bi000585+.

[33] S. Crosson, K. Moffat, Photoexcited structure of a plant photoreceptor domain reveals a light-driven molecular switch, Plant Cell. 14 (2002) 1067–1075. https://doi.org/10.1105/tpc.010475.

[34] T.E. Swartz, S.B. Corchnoy, J.M. Christie, J.W. Lewis, I. Szundi, W.R. Briggs, R.A. Bogomolni, The Photocycle of a Flavin-binding Domain of the Blue Light Photoreceptor Phototropin, J. Biol. Chem. 276 (2001) 36493–36500. https://doi.org/10.1074/jbc.M103114200.

[35] D. Nozaki, T. Iwata, T. Ishikawa, T. Todo, S. Tokutomi, H. Kandori, Role of Gln1029 in the photoactivation processes of the LOV2 domain in Adiantum phytochrome3, Biochemistry. 43 (2004) 8373–8379. https://doi.org/10.1021/bi0494727.

[36] A. Pfeifer, T. Majerus, K. Zikihara, D. Matsuoka, S. Tokutomi, J. Heberle, T. Kottke, Time-resolved fourier transform infrared study on photoadduct formation and secondary structural changes within the phototropin LOV domain, Biophys. J. 96 (2009) 1462–1470. https://doi.org/10.1016/j.bpj.2008.11.016.

[37] E. Peter, B. Dick, S.A. Baeurle, Mechanism of signal transduction of the LOV2-Jα photosensor from Avena sativa, Nat. Commun. 1 (2010). https://doi.org/10.1038/ncomms1121.

[38] E.F. Yee, R.P. Diensthuber, A.T. Vaidya, P.P. Borbat, C. Engelhard, J.H. Freed, R. Bittl, A. Möglich, B.R. Crane, Signal transduction in light-oxygen-voltage receptors lacking the adduct-forming cysteine residue, Nat. Commun. 6 (2015). https://doi.org/10.1038/ncomms10079.

[39] D. Immeln, A. Weigel, T. Kottke, J.L. Pérez Lustres, Primary Events in the Blue Light Sensor Plant Cryptochrome: Intraprotein Electron and Proton Transfer Revealed by Femtosecond Spectroscopy, J. Am. Chem. Soc. 134 (2012) 12536–12546. https://doi.org/10.1021/ja302121z.

[40] J. Brazard, A. Usman, F. Lacombat, C. Ley, M.M. Martin, P. Plaza, L. Mony, M. Heijde, G. Zabulon, C. Bowler, Spectro−Temporal Characterization of the Photoactivation Mechanism of Two New Oxidized Cryptochrome/Photolyase Photoreceptors, J. Am. Chem. Soc. 132 (2010) 4935–4945. https://doi.org/10.1021/ja1002372.

[41] B. Giovani, M. Byrdin, M. Ahmad, K. Brettel, Light-induced electron transfer in a cryptochrome blue-light photoreceptor, Nat. Struct. Biol. 10 (2003) 489–490. https://doi.org/10.1038/nsb933.

[42] C. Engelhard, X. Wang, D. Robles, J. Moldt, J. Moldt, A. Batschauer, R. Bitt, M. Ahmadb, Cellular metabolites enhance the light sensitivity of arabidopsis cryptochrome through alternate electron transfer pathwaysc, Plant Cell. 26 (2014) 4519–4531. https://doi.org/10.1105/tpc.114.129809.

[43] A. Hense, E. Herman, S. Oldemeyer, T. Kottke, Proton transfer to flavin stabilizes the signaling state of the blue light receptor plant cryptochrome, J. Biol. Chem. 290 (2015) 1743–1751. https://doi.org/10.1074/jbc.M114.606327.

[44] M. Kondoh, C. Shiraishi, P. Müller, M. Ahmad, K. Hitomi, E.D. Getzoff, M. Terazima, Light-Induced Conformational Changes in Full-Length Arabidopsis thaliana Cryptochrome, J. Mol. Biol. 413 (2011) 128–137. https://doi.org/https://doi.org/10.1016/j.jmb.2011.08.031.

[45] M. Gauden, S. Yeremenko, W. Laan, I.H.M. Van Stokkum, J.A. Ihalainen, R. Van Grondelle, K.J. Hellingwerf, J.T.M. Kennis, Photocycle of the flavin-binding photoreceptor AppA, a bacterial transcriptional antirepressor of photosynthesis genes, Biochemistry. 44 (2005) 3653–3662. https://doi.org/10.1021/bi047359a.

[46] S. Masuda, K. Hasegawa, A. Ishii, T.A. Ono, Light-Induced Structural Changes in a Putative Blue-Light Receptor with a Novel FAD Binding Fold Sensor of Blue-Light Using FAD (BLUF); Slr1694 of Synechocystis sp. PCC6803, Biochemistry. 43 (2004) 5304–5313. https://doi.org/10.1021/bi049836v.

[47] M. Gauden, I.H.M. Van Stokkum, J.M. Key, D.C. Lührs, R. Van Grondelle, P. Hegemann, J.T.M. Kennis, Hydrogen-bond switching through a radical pair mechanism in a flavin-binding photoreceptor, Proc. Natl. Acad. Sci. U. S. A. 103 (2006) 10895–10900. https://doi.org/10.1073/pnas.0600720103.

[48] A.L. Stelling, K.L. Ronayne, J. Nappa, P.J. Tonge, S.R. Meech, Ultrafast structural dynamics in BLUF domains: Transient infrared spectroscopy of AppA and its mutants, J. Am. Chem. Soc. 129 (2007) 15556–15564. https://doi.org/10.1021/ja074074n.

[49] T. Domratcheva, B.L. Grigorenko, I. Schlichting, A. V. Nemukhin, Molecular models predict light-induced glutamine tautomerization in BLUF photoreceptors, Biophys. J. 94 (2008) 3872–3879. https://doi.org/10.1529/biophysj.107.124172.

[50] J. Mehlhorn, T. Lindtner, F. Richter, K. Glaß, H. Steinocher, S. Beck, P. Hegemann, J.T.M. Kennis, T. Mathes, Light-Induced Rearrangement of the β5 Strand in the BLUF Photoreceptor SyPixD (Slr1694), J. Phys. Chem. Lett. 6 (2015) 4749–4753. https://doi.org/10.1021/acs.jpclett.5b02245.

[51] D. Carbonera, M. Valentin, R. Spezia, A. Mezzetti, The Unique Photophysical Properties of the Peridinin-Chlorophyll-a-Protein, Curr. Protein Pept. Sci. 15 (2014) 332–350. https://doi.org/10.2174/1389203715666140327111139.

[52] A.D. Grossman, Genetic networks controlling the initiation of sporulation and the development of genetic competence in Bacillus subtilis, Annu. Rev. Genet. 29 (1995) 477–508. https://doi.org/10.1146/annurev.ge.29.120195.002401.

[53] D.O. Hall, K. Rao, Photosynthesis, Cambridge University Press, 1999.

[54] D. Chandler, J. Hsin, J.C. Gumbart, Case Study : Light Harvesting Complex 2, Structure. (2011) 1–27.

[55] H. Scheer, An Overview of Chlorophylls and Bacteriochlorophylls: Biochemistry, Biophysics, Functions and Applications BT - Chlorophylls and Bacteriochlorophylls: Biochemistry, Biophysics, Functions and Applications, in: B. Grimm, R.J. Porra, W. Rüdiger, H. Scheer (Eds.), Springer Netherlands, Dordrecht, 2006: pp. 1–26.

https://doi.org/10.1007/1-4020-4516-6_1.

[56] A. Vershinin, Biological functions of carotenoids - Diversity and evolution, in: BioFactors, IOS Press, 1999: pp. 99–104. https://doi.org/10.1002/biof.5520100203.

[57] H. Hashimoto, C. Uragami, N. Yukihira, A.T. Gardiner, R.J. Cogdell, Understanding/unravelling carotenoid excited singlet states, J. R. Soc. Interface. 15 (2018). https://doi.org/10.1098/rsif.2018.0026.

[58] T. Polívka, J.L. Herek, D. Zigmantas, H.E. Åkerlund, V. Sundström, Direct observation of the (forbidden) S1 state in carotenoids, Proc. Natl. Acad. Sci. U. S. A. 96 (1999) 4914–4917. https://doi.org/10.1073/pnas.96.9.4914.

[59] T. Polívka, V. Sundström, Ultrafast dynamics of carotenoid excited states-from solution to natural and artificial systems, Chem. Rev. 104 (2004) 2021–2071. https://doi.org/10.1021/cr020674n.

[60] R. Croce, M.G. Müller, R. Bassi, A.R. Holzwarth, Carotenoid-to-chlorophyll energy transfer in recombinant major light-harvesting complex (LHCII) of higher plants. I. Femtosecond transient absorption measurements, Biophys. J. 80 (2001) 901–915. https://doi.org/10.1016/S0006-3495(01)76069-9.

[61] C.S. Foote, R.W. Denny, Chemistry of singlet oxygen. VII. Quenching by .beta.-carotene, J. Am. Chem. Soc. 90 (1968) 6233–6235. https://doi.org/10.1021/ja01024a061.

[62] S.B. Brown, J.D. Houghton, D.I. Vernon, New trends in photobiology biosynthesis of phycobilins. Formation of the chromophore of phytochrome, phycocyanin and phycoerythrin, J. Photochem. Photobiol. B Biol. 5 (1990) 3–23. https://doi.org/https://doi.org/10.1016/1011-1344(90)85002-E.

[63] K.E. Apt, J.L. Collier, A.R. Grossman, Evolution of the Phycobiliproteins, J. Mol. Biol. 248 (1995) 79–96. https://doi.org/https://doi.org/10.1006/jmbi.1995.0203.

[64] A.N. Glazer, Phycobiliproteins — a family of valuable, widely used fluorophores, J. Appl. Phycol. 6 (1994) 105–112. https://doi.org/10.1007/BF02186064.

[65] B. Fernández-Rojas, J. Hernández-Juárez, J. Pedraza-Chaverri, Nutraceutical properties of phycocyanin, J. Funct. Foods. 11 (2014) 375–392. https://doi.org/10.1016/j.jff.2014.10.011.

[66] W. Li, H.N. Su, Y. Pu, J. Chen, L.N. Liu, Q. Liu, S. Qin, Phycobiliproteins: Molecular structure, production, applications, and prospects, Biotechnol. Adv. 37 (2019) 340–353. https://doi.org/10.1016/j.biotechadv.2019.01.008.

[67] G.J. Kremers, J. Goedhart, Chapter 5 Visible fluorescent proteins for FRET, 1st ed., Elesvier B.V., 2009. https://doi.org/10.1016/S0075-7535(08)00005-3.

[68] O. SHIMOMURA, F.H. JOHNSON, Y. SAIGA, Extraction, purification and properties of aequorin, a bioluminescent, J. Cell. Comp. Physiol. 59 (1962) 223–239. https://doi.org/10.1002/jcp.1030590302.

[69] C. Martin, T. Yuan, E. Ghia, W.W. W., P.D. C., Green Fluorescent Protein as a Marker for Gene Expression, Science (80-.). 263 (1994) 802–805. https://doi.org/10.1126/science.8303295.

[70] N.G. Gurskaya, A.F. Fradkov, A. Terskikh, M. V. Matz, Y.A. Labas, V.I. Martynov, Y.G. Yanushevich, K.A. Lukyanov, S.A. Lukyanov, GFP-like chromoproteins as a source of far-red fluorescent proteins, FEBS Lett. 507 (2001) 16–20. https://doi.org/10.1016/S0014-5793(01)02930-1.

[71] M. V. Matz, K.A. Lukyanov, S.A. Lukyanov, Family of the green fluorescent protein: Journey to the end of the rainbow, BioEssays. 24 (2002) 953–959. https://doi.org/10.1002/bies.10154.

[72] D.P. Barondeau, C.J. Kassmann, J.A. Tainer, E.D. Getzoff, Understanding GFP chromophore biosynthesis: Controlling backbone cyclization and modifying post-translational chemistry, Biochemistry. 44 (2005) 1960–1970. https://doi.org/10.1021/bi0479205.

[73] B.G. Reid, G.C. Flynn, Chromophore formation in green fluorescent protein, Biochemistry. 36 (1997) 6786–6791. https://doi.org/10.1021/bi970281w.

[74] T.T. Yang, L. Cheng, S.R. Kain, Optimized codon usage and chromophore mutations provide enhanced sensitivity with the green fluorescent protein, Nucleic Acids Res. 24 (1996) 4592–4593. https://doi.org/10.1093/nar/24.22.4592.

[75] C.W.C. W., N. Shuming, Quantum Dot Bioconjugates for Ultrasensitive Nonisotopic Detection, Science (80-.). 281 (1998) 2016–2018. https://doi.org/10.1126/science.281.5385.2016.

[76] A. Vaseashta, D. Dimova-Malinovska, Nanostructured and nanoscale devices, sensors and detectors, Sci. Technol. Adv. Mater. 6 (2005) 312–318. https://doi.org/10.1016/j.stam.2005.02.018.

[77] L. Robert, Drugs on Target, Science (80-.). 293 (2001) 58–59. https://doi.org/10.1126/science.1063273.

[78] S.M. M., G.J. H., Exploring and Engineering the Cell Surface Interface, Science (80-.). 310 (2005) 1135–1138. https://doi.org/10.1126/science.1106587.

[79] C.M. Niemeyer, Functional devices from DNA and proteins, Nano Today. 2 (2007) 42–52. https://doi.org/10.1016/S1748-0132(07)70058-0.

[80] K. Blank, T. Mai, I. Gilbert, S. Schiffmann, J. Rankl, R. Zivin, C. Tackney, T. Nicolaus, K. Spinnler, F. Oesterhelt, M. Benoit, H. Clausen-Schaumann, H.E. Gaub, A force-based protein biochip, Proc. Natl. Acad. Sci. U. S. A. 100 (2003) 11356–11360. https://doi.org/10.1073/pnas.1934928100.

[81] N.J. Sniadecki, R.A. Desai, S.A. Ruiz, C.S. Chen, Nanotechnology for Cell–Substrate Interactions, Ann. Biomed. Eng. 34 (2006) 59–74. https://doi.org/10.1007/s10439-005-9006-3.

[82] T. Noji, C. Kamidaki, K. Kawakami, J.R. Shen, T. Kajino, Y. Fukushima, T. Sekitoh, S. Itoh, Photosynthetic oxygen evolution in mesoporous silica material: Adsorption of photosystem II reaction center complex into 23 nm nanopores in SBA, Langmuir. 27 (2011) 705–713. https://doi.org/10.1021/la1032916.

[83] I. Oda, K. Hirata, S. Watanabe, Y. Shibata, T. Kajino, Y. Fukushima, S. Iwai, S. Itoh, Function of membrane protein in silica nanopores: Incorporation of photosynthetic light-harvesting protein LH2 into FSM, J. Phys. Chem. B. 110 (2006) 1114–1120. https://doi.org/10.1021/jp0540860.

[84] I. Oda, M. Iwaki, D. Fujita, Y. Tsutsui, S. Ishizaka, M. Dewa, M. Nango, T. Kajino, Y. Fukushima, S. Itoh, Photosynthetic electron transfer from reaction center pigment-protein complex in silica nanopores, Langmuir. 26 (2010) 13399–13406. https://doi.org/10.1021/la101810v.

[85] Y. Ma, P. Rajendran, C. Blum, Y. Cesa, N. Gartmann, D. Brühwiler, V. Subramaniam, Microspectroscopic analysis of green fluorescent proteins infiltrated into mesoporous

silica nanochannels, J. Colloid Interface Sci. 356 (2011) 123–130. https://doi.org/10.1016/j.jcis.2010.12.082.

[86] O. Mats, C.A. B., K. Karen, G.L. A., T.R. Y., R.S. James, Crystal Structure of the Aequorea victoria Green Fluorescent Protein, Science (80-.). 273 (1996) 1392–1395. https://doi.org/10.1126/science.273.5280.1392.

[87] M. Martínez-Carmona, A. Baeza, M.A. Rodriguez-Milla, J. García-Castro, M. Vallet-Regí, Mesoporous silica nanoparticles grafted with a light-responsive protein shell for highly cytotoxic antitumoral therapy, J. Mater. Chem. B. 3 (2015) 5746–5752. https://doi.org/10.1039/c5tb00304k.

[88] H.H. Weetall, Retention of bacteriorhodopsin activity in dried sol-gel glass, Biosens. Bioelectron. 11 (1996) 327–333. https://doi.org/10.1016/0956-5663(96)88419-3.

[89] Z. Chen, D.L. Kaplan, K. Yang, J. Kumar, K.A. Marx, S.K. Tripathy, Phycobiliproteins encapsulated in sol-gel glass, J. Sol-Gel Sci. Technol. 7 (1996) 99–108. https://doi.org/10.1007/BF00401889.

[90] P.J. Calabretta, M.C. Chancellor, C. Torres, G.R. Abel, C. Niehaus, N.J. Birtwhistle, N.M. Khouderchah, G.H. Zemede, D.K. Eggers, Silica as a Matrix for Encapsulating Proteins: Surface Effects on Protein Structure Assessed by Circular Dichroism Spectroscopy, J. Funct. Biomater. 3 (2012) 514–527. https://doi.org/10.3390/jfb3030514.

[91] S. Bettati, B. Pioselli, B. Campanini, C. Viappiani, A. Mozzarelli, Protein-doped nanoporous silica gels, in: Encycl. Nanosci. Nanotechnol., American Scientific Publishers, 2004: pp. 81–103.

[92] L. Ronda, S. Bruno, B. Campanini, A. Mozzarelli, S. Abbruzzetti, C. Viappiani, A. Cupane, M. Levantino, S. Bettati, Immobilization of Proteins in Silica Gel: Biochemical and Biophysical Properties, Curr. Org. Chem. 19 (2015) 1653–1668. https://doi.org/10.2174/1385272819666150601211349.

[93] D. Avnir, O. Lev, J. Livage, Recent bio-applications of sol-gel materials, J. Mater. Chem. 16 (2006) 1013–1030. https://doi.org/10.1039/b512706h.

[94] L. Betancor, H.R. Luckarift, Bioinspired enzyme encapsulation for biocatalysis, Trends Biotechnol. 26 (2008) 566–572. https://doi.org/10.1016/j.tibtech.2008.06.009.

[95] T. Coradin, M. Boissière, J. Livage, Sol-gel chemistry in medicinal science, Curr. Med. Chem. 13 (2006) 99–108.

[96] X. Wang, N. Ben Ahmed, G. S Alvarez, M. V Tuttolomondo, C. Hélary, M. F Desimone, T. Coradin, Sol-gel encapsulation of biomolecules and cells for medicinal applications, Curr. Top. Med. Chem. 15 (2015) 223–244.

[97] K. Cui, X. Lu, J. Guan, Q. Lu, Z. Fei, P.J. Dyson, Formation and properties of self-assembly-driven fluorescent nanoparticle sensors, Chem. - A Eur. J. 19 (2013) 8550–8557. https://doi.org/10.1002/chem.201204349.

[98] T. Kay Holt, D.W. Krogmann, A carotenoid-protein from cyanobacteria, Biochim. Biophys. Acta - Bioenerg. 637 (1981) 408–414. https://doi.org/10.1016/0005-2728(81)90045-1.

[99] Y.P. Wu, D.W. Krogmann, The orange carotenoid protein of Synechocystis PCC 6803, Biochim. Biophys. Acta - Bioenerg. 1322 (1997) 1–7. https://doi.org/10.1016/S0005-2728(97)00067-4.

[100] C.A. Kerfeld, M.R. Sawaya, V. Brahmandam, D. Cascio, K.K. Ho, C.C. Trevithick-

Sutton, D.W. Krogmann, T.O. Yeates, The crystal structure of a cyanobacterial water-soluble carotenoid binding protein, Structure. 11 (2003) 55–65. https://doi.org/10.1016/S0969-2126(02)00936-X.

[101] A. Wilson, G. Ajlani, J.M. Verbavatz, I. Vass, C.A. Kerfeld, D. Kirilovsky, A soluble carotenoid protein involved in phycobilisome-related energy dissipation in cyanobacteria, Plant Cell. 18 (2006) 992–1007. https://doi.org/10.1105/tpc.105.040121.

[102] H. Bao, M.R. Melnicki, C.A. Kerfeld, Structure and functions of Orange Carotenoid Protein homologs in cyanobacteria, Curr. Opin. Plant Biol. 37 (2017) 1–9. https://doi.org/10.1016/j.pbi.2017.03.010.

[103] F. Muzzopappa, D. Kirilovsky, Changing Color for Photoprotection: The Orange Carotenoid Protein, Trends Plant Sci. 25 (2020) 92–104. https://doi.org/10.1016/j.tplants.2019.09.013.

[104] H. Bao, M.R. Melnicki, E.G. Pawlowski, M. Sutter, M. Agostoni, S. Lechno-Yossef, F. Cai, B.L. Montgomery, C.A. Kerfeld, Additional families of orange carotenoid proteins in the photoprotective system of cyanobacteria, Nat. Plants. 3 (2017). https://doi.org/10.1038/nplants.2017.89.

[105] M. Pivato, F. Perozeni, F. Licausi, S. Cazzaniga, M. Ballottari, Heterologous expression of cyanobacterial Orange Carotenoid Protein (OCP2) as a soluble carrier of ketocarotenoids in Chlamydomonas reinhardtii, Algal Res. 55 (2021) 102255. https://doi.org/10.1016/j.algal.2021.102255.

[106] C.B. De Carbon, A. Thurotte, A. Wilson, F. Perreau, Biosynthesis of soluble carotenoid holoproteins in Escherichia coli In Anabaena PCC 7120 In Synechocystis PCC 6803 In OCP producing E . coli, (n.d.) 1–11.

[107] M.R. Melnicki, R.L. Leverenz, M. Sutter, R. López-Igual, A. Wilson, E.G. Pawlowski, F. Perreau, D. Kirilovsky, C.A. Kerfeld, Structure, Diversity, and Evolution of a New Family of Soluble Carotenoid-Binding Proteins in Cyanobacteria, Mol. Plant. 9 (2016) 1379–1394. https://doi.org/10.1016/j.molp.2016.06.009.

[108] F. Muzzopappa, A. Wilson, V. Yogarajah, S. Cot, F. Perreau, C. Montigny, C.B. de Carbon, D. Kirilovsky, Paralogs of the C-terminal domain of the cyanobacterial orange carotenoid protein are carotenoid donors to helical carotenoid proteins, Plant Physiol. 175 (2017) 1283–1303. https://doi.org/10.1104/pp.17.01040.

[109] B.E. Schirrmeister, M. Gugger, P.C.J. Donoghue, Cyanobacteria and the Great Oxidation Event: Evidence from genes and fossils, Palaeontology. 58 (2015) 769–785. https://doi.org/10.1111/pala.12178.

[110] D. Jallet, A. Thurotte, R.L. Leverenz, F. Perreau, C.A. Kerfeld, D. Kirilovsky, Specificity of the cyanobacterial orange carotenoid protein: Influences of orange carotenoid protein and phycobilisome structures, Plant Physiol. 164 (2014) 790–804. https://doi.org/10.1104/pp.113.229997.

[111] D. Kirilovsky, C.A. Kerfeld, Cyanobacterial photoprotection by the orange carotenoid protein, Nat. Plants. 2 (2016) 16180. https://doi.org/10.1038/nplants.2016.180.

[112] M. Sutter, A. Wilson, R.L. Leverenz, R. Lopez-Igual, A. Thurotte, A.E. Salmeen, D. Kirilovsky, C.A. Kerfeld, Crystal structure of the FRP and identification of the active site for modulation of OCP-mediated photoprotection in cyanobacteria, Proc. Natl. Acad. Sci. U. S. A. 110 (2013) 10022–10027. https://doi.org/10.1073/pnas.1303673110.

[113] A. Wilson, J.N. Kinney, P.H. Zwart, C. Punginelli, S. D'Haene, F. Perreau, M.G.

Klein, D. Kirilovsky, C.A. Kerfeld, Structural determinants underlying photoprotection in the photoactive orange carotenoid protein of cyanobacteria, J. Biol. Chem. 285 (2010) 18364–18375. https://doi.org/10.1074/jbc.M110.115709.

[114] D. Kirilovsky, C.A. Kerfeld, The Orange Carotenoid Protein: a blue-green light photoactive protein, Cite This Photochem. Photobiol. Sci. 12 (2013) 1135. https://doi.org/10.1039/c3pp25406b.

[115] A. Wilson, J.N. Kinney, P.H. Zwart, C. Punginelli, S. D'Haene, F. Perreau, M.G. Klein, D. Kirilovsky, C.A. Kerfeld, Structural determinants underlying photoprotection in the photoactive orange carotenoid protein of cyanobacteria, J. Biol. Chem. 285 (2010) 18364–18375. https://doi.org/10.1074/jbc.M110.115709.

[116] A. Wilson, C. Punginelli, M. Couturier, F. Perreau, D. Kirilovsky, Essential role of two tyrosines and two tryptophans on the photoprotection activity of the Orange Carotenoid Protein, Biochim. Biophys. Acta - Bioenerg. 1807 (2011) 293–301. https://doi.org/10.1016/j.bbabio.2010.12.009.

[117] R.L. Leverenz, M. Sutter, A. Wilson, S. Gupta, A. Thurotte, C.B. De Carbon, C.J. Petzold, C. Ralston, F. Perreau, D. Kirilovsky, C.A. Kerfeld, A 12 Å carotenoid translocation in a photoswitch associated with cyanobacterial photoprotection, Science (80-.). 348 (2015) 1463–1466. https://doi.org/10.1126/science.aaa7234.

[118] H. Zhang, H. Liu, D.M. Niedzwiedzki, M. Prado, J. Jiang, M.L. Gross, R.E. Blankenship, Molecular mechanism of photoactivation and structural location of the cyanobacterial orange carotenoid protein, Biochemistry. 53 (2014) 13–19. https://doi.org/10.1021/bi401539w.

[119] H. Liu, H. Zhang, J.D. King, N.R. Wolf, M. Prado, M.L. Gross, R.E. Blankenship, Mass spectrometry footprinting reveals the structural rearrangements of cyanobacterial orange carotenoid protein upon light activation, Biochim. Biophys. Acta - Bioenerg. 1837 (2014) 1955–1963. https://doi.org/10.1016/j.bbabio.2014.09.004.

[120] Y. Lu, H. Liu, R.G. Saer, H. Zhang, C.M. Meyer, V.L. Li, L. Shi, J.D. King, M.L. Gross, R.E. Blankenship, Native mass spectrometry analysis of oligomerization states of fluorescence recovery protein and orange carotenoid protein: Two proteins involved in the cyanobacterial photoprotection cycle, Biochemistry. 56 (2017) 160–166. https://doi.org/10.1021/ACS.BIOCHEM.6B01094/SUPPL_FILE/BI6B01094_SI_001.PDF.

[121] E. Andreeva, S. Nizinski, A. Wilson, M. Levantino, E. De Zitter, R. Munro, F. Muzzopappa, A. Thureau, N. Zala, G. Burdzinski, M. Sliwa, D. Kirilovsky, G. Schirò, J.-P. Colletier, Oligomerization processes limit photoactivation and recovery of the Orange Carotenoid Protein, (2022). https://doi.org/10.1101/2022.02.04.479168.

[122] F. Muzzopappa, D. Kirilovsky, The Orange Carotenoid Protein and the Regulation of Energy Transfer in Cyanobacteria, Elsevier Ltd., 2020. https://doi.org/10.1016/b978-0-12-809633-8.21536-7.

[123] P.E. Konold, I.H.M. Van Stokkum, F. Muzzopappa, A. Wilson, M.L. Groot, D. Kirilovsky, J.T.M. Kennis, Photoactivation Mechanism, Timing of Protein Secondary Structure Dynamics and Carotenoid Translocation in the Orange Carotenoid Protein, J. Am. Chem. Soc. 141 (2019) 520–530. https://doi.org/10.1021/jacs.8b11373.

[124] A. Wilson, E.A. Andreeva, S.J. Nizinski, L. Talbot, E. Hartmann, I. Schlichting, G. Burdzinski, M. Sliwa, D. Kirilovsky, J.-P. Colletier, Structure-function-dynamics relationships in the peculiar Planktothrix PCC7805 OCP1:

impact of his-tagging and carotenoid type, BioRxiv. (2022) 2022.01.04.474796. https://doi.org/10.1101/2022.01.04.474796.

[125] M. Gwizdala, A. Wilson, D. Kirilovsky, In vitro reconstitution of the cyanobacterial photoprotective mechanism mediated by the orange carotenoid protein in synechocystis PCC 6803, Plant Cell. 23 (2011) 2631–2643. https://doi.org/10.1105/tpc.111.086884.

[126] R.L. Leverenz, D. Jallet, M. De Li, R.A. Mathies, D. Kirilovsky, C.A. Kerfeld, Structural and functionalmodularity of the orange carotenoid protein: Distinct roles for the N- and C-terminal domains in cyanobacterial photoprotection, Plant Cell. 26 (2014) 426–437. https://doi.org/10.1105/tpc.113.118588.

[127] D. Jallet, A. Thurotte, R.L. Leverenz, F. Perreau, C.A. Kerfeld, D. Kirilovsky, Specificity of the cyanobacterial orange carotenoid protein: Influences of orange carotenoid protein and phycobilisome structures, Plant Physiol. 164 (2014) 790–804. https://doi.org/10.1104/pp.113.229997.

[128] E.G. Maksimov, E.A. Shirshin, N.N. Sluchanko, D. V. Zlenko, E.Y. Parshina, G. V. Tsoraev, K.E. Klementiev, G.S. Budylin, F.J. Schmitt, T. Friedrich, V. V. Fadeev, V.Z. Paschenko, A.B. Rubin, The Signaling State of Orange Carotenoid Protein, Biophys. J. 109 (2015) 595–607. https://doi.org/10.1016/j.bpj.2015.06.052.

[129] J.D. King, H. Liu, G. He, G.S. Orf, R.E. Blankenship, Chemical activation of the cyanobacterial orange carotenoid protein, FEBS Lett. 588 (2014) 4561–4565. https://doi.org/10.1016/j.febslet.2014.10.024.

[130] H. Liu, Y. Lu, B. Wolf, R. Saer, J.D. King, R.E. Blankenship, Photoactivation and relaxation studies on the cyanobacterial orange carotenoid protein in the presence of copper ion, Photosynth. Res. 135 (2018) 143–147. https://doi.org/10.1007/s11120-017-0363-1.

[131] C. Punginelli, A. Wilson, J.M. Routaboul, D. Kirilovsky, Influence of zeaxanthin and echinenone binding on the activity of the Orange Carotenoid Protein, Biochim. Biophys. Acta - Bioenerg. 1787 (2009) 280–288. https://doi.org/10.1016/j.bbabio.2009.01.011.

[132] C.B. De Carbon, A. Thurotte, A. Wilson, F. Perreau, D. Kirilovsky, Biosynthesis of soluble carotenoid holoproteins in Escherichia coli, Sci. Rep. 5 (2015) 1–8. https://doi.org/10.1038/srep09085.

[133] E. Kish, M.M.M. Pinto, D. Kirilovsky, R. Spezia, B. Robert, Echinenone vibrational properties: From solvents to the orange carotenoid protein, Biochim. Biophys. Acta - Bioenerg. 1847 (2015) 1044–1054. https://doi.org/10.1016/j.bbabio.2015.05.010.

[134] V. Šlouf, V. Kuznetsova, M. Fuciman, C.B. de Carbon, A. Wilson, D. Kirilovsky, T. Polívka, Ultrafast spectroscopy tracks carotenoid configurations in the orange and red carotenoid proteins from cyanobacteria, Photosynth. Res. 131 (2017) 105–117. https://doi.org/10.1007/s11120-016-0302-6.

[135] S. Gupta, M. Guttman, R.L. Leverenz, K. Zhumadilova, E.G. Pawlowski, C.J. Petzold, K.K. Lee, C.Y. Ralston, C.A. Kerfeld, Local and global structural drivers for the photoactivation of the orange carotenoid protein, Proc. Natl. Acad. Sci. U. S. A. 112 (2015) E5567–E5574. https://doi.org/10.1073/pnas.1512240112.

[136] A. Wilson, M. Gwizdala, A. Mezzetti, M. Alexandre, C.A. Kerfeld, D. Kirilovsky, The essential role of the N-terminal domain of the orange carotenoid protein in cyanobacterial photoprotection: Importance of a positive charge for phycobilisome binding, Plant Cell. 24 (2012) 1972–1983. https://doi.org/10.1105/tpc.112.096909.

[137] V.U. Chukhutsina, J. Baxter, A. Fadini, R.M. Morgan, M.A. Pope, K. Maghlaoui, C. Orr, A. Wagner, J.J. van Thor, Light activation of Orange Carotenoid Protein reveals initial C8'-C7' double bond trans/cis photoisomerization, BioRxiv. (2022) 2022.01.17.475858. https://doi.org/10.1101/2022.01.17.475858.

[138] E.G. Maksimov, F.J. Schmitt, E.A. Shirshin, M.D. Svirin, I. V. Elanskaya, T. Friedrich, V. V. Fadeev, V.Z. Paschenko, A.B. Rubin, The time course of non-photochemical quenching in phycobilisomes of Synechocystis sp. PCC6803 as revealed by picosecond time-resolved fluorimetry, Biochim. Biophys. Acta - Bioenerg. 1837 (2014) 1540–1547. https://doi.org/10.1016/j.bbabio.2014.01.010.

[139] N.N. Sluchanko, K.E. Klementiev, E.A. Shirshin, G. V. Tsoraev, T. Friedrich, E.G. Maksimov, The purple Trp288Ala mutant of Synechocystis OCP persistently quenches phycobilisome fluorescence and tightly interacts with FRP, Biochim. Biophys. Acta - Bioenerg. 1858 (2017) 1–11. https://doi.org/10.1016/j.bbabio.2016.10.005.

[140] D. Harris, A. Wilson, F. Muzzopappa, N.N. Sluchanko, T. Friedrich, E.G. Maksimov, D. Kirilovsky, N. Adir, Structural rearrangements in the C-terminal domain homolog of Orange Carotenoid Protein are crucial for carotenoid transfer, Commun. Biol. 1 (2018). https://doi.org/10.1038/s42003-018-0132-5.

[141] A. Wilson, F. Muzzopappa, D. Kirilovsky, Elucidation of the essential amino acids involved in the binding of the cyanobacterial Orange Carotenoid Protein to the phycobilisome, Biochim. Biophys. Acta - Bioenerg. 1863 (2022). https://doi.org/10.1016/j.bbabio.2021.148504.

[142] W. Lou, D.M. Niedzwiedzki, R.J. Jiang, R.E. Blankenship, H. Liu, Binding of red form of Orange Carotenoid Protein (OCP) to phycobilisome is not sufficient for quenching, Biochim. Biophys. Acta - Bioenerg. 1861 (2020). https://doi.org/10.1016/j.bbabio.2020.148155.

[143] M.A. Dominguez-Martin, P. V Sauer, M. Sutter, H. Kirst, D. Bina, B.J. Greber, E. Nogales, T. Polívka, C.A. Kerfeld, Structure of the Quenched Cyanobacterial OCP-Phycobilisome Complex, BioRxiv. (2021) 2021.11.15.468719. https://doi.org/10.1101/2021.11.15.468719.

[144] M. Gwizdala, J.L. Botha, A. Wilson, D. Kirilovsky, R. Van Grondelle, T.P.J. Krüger, Switching an Individual Phycobilisome off and on, J. Phys. Chem. Lett. 9 (2018) 2426–2432. https://doi.org/10.1021/acs.jpclett.8b00767.

[145] A.H. Squires, P.D. Dahlberg, H. Liu, N.C.M. Magdaong, R.E. Blankenship, W.E. Moerner, Single-molecule trapping and spectroscopy reveals photophysical heterogeneity of phycobilisomes quenched by Orange Carotenoid Protein, Nat. Commun. 10 (2019). https://doi.org/10.1038/s41467-019-09084-2.

[146] L. Tian, I.H.M. Van Stokkum, R.B.M. Koehorst, A. Jongerius, D. Kirilovsky, H. Van Amerongen, Site, rate, and mechanism of photoprotective quenching in cyanobacteria, J. Am. Chem. Soc. 133 (2011) 18304–18311. https://doi.org/10.1021/ja206414m.

[147] R. Berera, I.H.M. Van Stokkum, M. Gwizdala, A. Wilson, D. Kirilovsky, R. Van Grondelle, The photophysics of the orange carotenoid protein, a light-powered molecular switch, J. Phys. Chem. B. 116 (2012) 2568–2574. https://doi.org/10.1021/jp2108329.

[148] T. Polívka, P. Chábera, C.A. Kerfeld, Carotenoid-protein interaction alters the S1 energy of hydroxyechinenone in the Orange Carotenoid Protein, Biochim. Biophys. Acta - Bioenerg. 1827 (2013) 248–254. https://doi.org/10.1016/j.bbabio.2012.10.005.

[149] C. Boulay, A. Wilson, S. D'Haene, D. Kirilovsky, Identification of a protein required for recovery of full antenna capacity in OCP-related photoprotective mechanism in cyanobacteria, Proc. Natl. Acad. Sci. U. S. A. 107 (2010) 11620–11625. https://doi.org/10.1073/pnas.1002912107.

[150] A. Thurotte, C. Bourcier de Carbon, A. Wilson, L. Talbot, S. Cot, R. López-Igual, D. Kirilovsky, The cyanobacterial Fluorescence Recovery Protein has two distinct activities: Orange Carotenoid Protein amino acids involved in FRP interaction, Biochim. Biophys. Acta - Bioenerg. 1858 (2017) 308–317. https://doi.org/10.1016/j.bbabio.2017.02.003.

[151] N.N. Sluchanko, Y.B. Slonimskiy, E.A. Shirshin, M. Moldenhauer, T. Friedrich, E.G. Maksimov, OCP–FRP protein complex topologies suggest a mechanism for controlling high light tolerance in cyanobacteria, Nat. Commun. 9 (2018) 1–15. https://doi.org/10.1038/s41467-018-06195-0.

[152] Y.B. Slonimskiy, E.G. Maksimov, E.P. Lukashev, M. Moldenhauer, C.M. Jeffries, D.I. Svergun, T. Friedrich, N.N. Sluchanko, Functional interaction of low-homology FRPs from different cyanobacteria with Synechocystis OCP, Biochim. Biophys. Acta - Bioenerg. 1859 (2018) 382–393. https://doi.org/10.1016/j.bbabio.2018.03.001.

[153] M. Gwizdala, A. Wilson, A. Omairi-Nasser, D. Kirilovsky, Characterization of the Synechocystis PCC 6803 Fluorescence Recovery Protein involved in photoprotection, Biochim. Biophys. Acta - Bioenerg. 1827 (2013) 348–354. https://doi.org/10.1016/j.bbabio.2012.11.001.

[154] I. Domonkos, M. Kis, Z. Gombos, B. Ughy, Carotenoids, versatile components of oxygenic photosynthesis, Prog. Lipid Res. 52 (2013) 539–561. https://doi.org/10.1016/j.plipres.2013.07.001.

[155] P.D. Fraser, P.M. Bramley, The biosynthesis and nutritional uses of carotenoids, Prog. Lipid Res. 43 (2004) 228–265. https://doi.org/10.1016/j.plipres.2003.10.002.

[156] R.W. Ye, K.J. Stead, H. Yao, H. He, Mutational and functional analysis of the β-carotene ketolase involved in the production of canthaxanthin and astaxanthin, Appl. Environ. Microbiol. 72 (2006) 5829–5837. https://doi.org/10.1128/AEM.00918-06.

[157] E. Aziz, R. Batool, W. Akhtar, S. Rehman, T. Shahzad, A. Malik, M.A. Shariati, A. Laishevtcev, S. Plygun, M. Heydari, A. Rauf, S. Ahmed Arif, Xanthophyll: Health benefits and therapeutic insights, Life Sci. 240 (2020) 117104. https://doi.org/https://doi.org/10.1016/j.lfs.2019.117104.

[158] S. Takaichi, Carotenoids in algae: Distributions, biosyntheses and functions, Mar. Drugs. 9 (2011) 1101–1118. https://doi.org/10.3390/md9061101.

[159] R.M. Clark, H.C. Furr, Absorption of canthaxanthin by the rat is influenced by total lipid in the intestinal lumen, Lipids. 36 (2001) 473–475. https://doi.org/10.1007/s11745-001-0745-1.

[160] P. Palozza, N. Maggiano, G. Calviello, P. Lanza, E. Piccioni, F.O. Ranelletti, G.M. Bartoli, Canthaxanthin induces apoptosis in human cancer cell lines, Carcinogenesis. 19 (1998) 373–376. https://doi.org/10.1093/carcin/19.2.373.

[161] H. Bin Li, K.W. Fan, F. Chen, Isolation and purification of canthaxanthin from the microalga Chlorella zofingiensis by high-speed counter-current chromatography, J. Sep. Sci. 29 (2006) 699–703. https://doi.org/10.1002/jssc.200500365.

[162] C. Sen Chang, C.L. Chang, G.H. Lai, Reactive oxygen species scavenging activities in a chemiluminescence model and neuroprotection in rat pheochromocytoma cells by

astaxanthin, beta-carotene, and canthaxanthin, Kaohsiung J. Med. Sci. 29 (2013) 412–421. https://doi.org/10.1016/j.kjms.2012.12.002.

[163] N. Wada, T. Sakamoto, S. Matsugo, Multiple roles of photosynthetic and sunscreen pigments in cyanobacteria focusing on the oxidative stress, Metabolites. 3 (2013) 463–483. https://doi.org/10.3390/metabo3020463.

[164] B. Fernández-González, G. Sandmann, A. Vioque, A new type of asymmetrically acting β-carotene ketolase is required for the synthesis of echinenone in the cyanobacterium Synechocystis sp. PCC 6803, J. Biol. Chem. 272 (1997) 9728–9733. https://doi.org/10.1074/jbc.272.15.9728.

[165] S. Gupta, M. Sutter, S.G. Remesh, M.A. Dominguez-Martin, H. Bao, X.A. Feng, L.J.G. Chan, C.J. Petzold, C.A. Kerfeld, C.Y. Ralston, X-ray radiolytic labeling reveals the molecular basis of orange carotenoid protein photoprotection and its interactions with fluorescence recovery protein, J. Biol. Chem. 294 (2019) 8848–8860. https://doi.org/10.1074/jbc.RA119.007592.

[166] P.E. Konold, I.H.M. Van Stokkum, F. Muzzopappa, A. Wilson, M.L. Groot, D. Kirilovsky, J.T.M. Kennis, Photoactivation Mechanism, Timing of Protein Secondary Structure Dynamics and Carotenoid Translocation in the Orange Carotenoid Protein, J. Am. Chem. Soc. 141 (2019) 520–530. https://doi.org/10.1021/jacs.8b11373.

[167] E.G. Maksimov, N.N. Sluchanko, Y.B. Slonimskiy, E.A. Slutskaya, A. V. Stepanov, A.M. Argentova-Stevens, E.A. Shirshin, G. V. Tsoraev, K.E. Klementiev, O. V. Slatinskaya, E.P. Lukashev, T. Friedrich, V.Z. Paschenko, A.B. Rubin, The photocycle of orange carotenoid protein conceals distinct intermediates and asynchronous changes in the carotenoid and protein components, Sci. Rep. 7 (2017) 1–12. https://doi.org/10.1038/s41598-017-15520-4.

[168] A. Andreoni, S. Lin, H. Liu, R.E. Blankenship, H. Yan, N.W. Woodbury, Orange Carotenoid Protein as a Control Element in an Antenna System Based on a DNA Nanostructure, Nano Lett. 17 (2017) 1174–1180. https://doi.org/10.1021/acs.nanolett.6b04846.

[169] E.G. Maksimov, I.A. Yaroshevich, G. V. Tsoraev, N.N. Sluchanko, E.A. Slutskaya, O.G. Shamborant, T. V. Bobik, T. Friedrich, A. V. Stepanov, A genetically encoded fluorescent temperature sensor derived from the photoactive Orange Carotenoid Protein, Sci. Rep. 9 (2019) 1–9. https://doi.org/10.1038/s41598-019-45421-7.

[170] L. Piccinini, S. Cazzaniga, S. Iacopino, M. Ballottari, B. Giuntoli, F. Licausi, Title: A synthetic switch based on orange carotenoid protein to control blue light responses in 2 chloroplasts 3, (n.d.). https://doi.org/10.1101/2021.01.27.428448.

[171] B. Ru, C. Ru, C1 C1, (2006) 1–7.

[172] T. Sensing, U. Red, G.F. Protein, P. Reveals, C1, (2020) 1–13.

[173] S. Lechno-Yossef, M.R. Melnicki, H. Bao, B.L. Montgomery, C.A. Kerfeld, Synthetic OCP heterodimers are photoactive and recapitulate the fusion of two primitive carotenoproteins in the evolution of cyanobacterial photoprotection, Plant J. 91 (2017) 646–656. https://doi.org/10.1111/TPJ.13593.

[174] F. Muzzopappa, A. Wilson, D. Kirilovsky, Interdomain interactions reveal the molecular evolution of the orange carotenoid protein, Nat. Plants. 5 (2019) 1076–1086. https://doi.org/10.1038/s41477-019-0514-9.

[175] R. López-Igual, A. Wilson, R.L. Leverenz, M.R. Melnicki, C.B. de Carbon, M. Sutter, A. Turmo, F. Perreau, C.A. Kerfeld, D. Kirilovsky, Different functions of the paralogs

to the N-terminal domain of the orange carotenoid protein in the cyanobacterium Anabaena sp. PCC 7120, Plant Physiol. 171 (2016) 1852–1866. https://doi.org/10.1104/pp.16.00502.

[176] M.A. Dominguez-Martin, T. Polívka, M. Sutter, B. Ferlez, S. Lechno-Yossef, B.L. Montgomery, C.A. Kerfeld, Structural and spectroscopic characterization of HCP2, Biochim. Biophys. Acta - Bioenerg. 1860 (2019) 414–424. https://doi.org/10.1016/j.bbabio.2019.03.004.

[177] F. Muzzopappa, F. Muzzopappa, P. Minard, Carotenoid translocation and protein evolution in cyanobacterial photoprotection To cite this version : Carotenoid translocation and protein evolution in cyanobacterial photoprotection, (2020).

[178] M. Moldenhauer, N.N. Sluchanko, D. Buhrke, D. V. Zlenko, N.N. Tavraz, F.J. Schmitt, P. Hildebrandt, E.G. Maksimov, T. Friedrich, Assembly of photoactive orange carotenoid protein from its domains unravels a carotenoid shuttle mechanism, Photosynth. Res. 133 (2017) 327–341. https://doi.org/10.1007/s11120-017-0353-3.

[179] E.G. Maksimov, N.N. Sluchanko, Y.B. Slonimskiy, K.S. Mironov, K.E. Klementiev, M. Moldenhauer, T. Friedrich, D.A. Los, V.Z. Paschenko, A.B. Rubin, The Unique Protein-to-Protein Carotenoid Transfer Mechanism, Biophys. J. 113 (2017) 402–414. https://doi.org/10.1016/j.bpj.2017.06.002.

[180] D. Harris, S. Bar-Zvi, A. Lahav, I. Goldshmid, N. Adir, The Structural Basis for the Extraordinary Energy-Transfer Capabilities of the Phycobilisome BT - Membrane Protein Complexes: Structure and Function, in: J.R. Harris, E.J. Boekema (Eds.), Springer Singapore, Singapore, 2018: pp. 57–82. https://doi.org/10.1007/978-981-10-7757-9_3.

[181] Y.B. Slonimskiy, F. Muzzopappa, E.G. Maksimov, A. Wilson, T. Friedrich, D. Kirilovsky, N.N. Sluchanko, Light-controlled carotenoid transfer between water-soluble proteins related to cyanobacterial photoprotection, FEBS J. 286 (2019) 1908–1924. https://doi.org/10.1111/febs.14803.

[182] D. Harris, F. Muzzopappa, F. Glaser, A. Wilson, D. Kirilovsky, N. Adir, Structural dynamics in the C terminal domain homolog of orange carotenoid Protein reveals residues critical for carotenoid uptake, Biochim. Biophys. Acta - Bioenerg. 1861 (2020) 148214. https://doi.org/10.1016/j.bbabio.2020.148214.

[183] E.G. Maksimov, A. V. Zamaraev, E.Y. Parshina, Y.B. Slonimskiy, T.A. Slastnikova, A.A. Abdrakhmanov, P.A. Babaev, S.S. Efimova, O.S. Ostroumova, A. V. Stepanov, E.A. Slutskaya, A. V. Ryabova, T. Friedrich, N.N. Sluchanko, Soluble cyanobacterial carotenoprotein as a robust antioxidant nanocarrier and delivery module, Antioxidants. 9 (2020) 1–23. https://doi.org/10.3390/antiox9090869.

[184] A.W. Williams, T.W.-M. Boileau, S.K. Clinton, J.W. Erdman, β-Carotene Stability and Uptake by Prostate Cancer Cells Are Dependent on Delivery Vehicle, Nutr. Cancer. 36 (2000) 185–190. https://doi.org/10.1207/S15327914NC3602_7.

[185] C. Tan, J. Xue, X. Lou, S. Abbas, Y. Guan, B. Feng, X. Zhang, S. Xia, Liposomes as delivery systems for carotenoids: Comparative studies of loading ability, storage stability and in vitro release, Food Funct. 5 (2014) 1232–1240. https://doi.org/10.1039/c3fo60498e.

[186] E. Hood, E. Simone, P. Wattamwar, T. Dziubla, V. Muzykantov, Nanocarriers for vascular delivery of antioxidants, Nanomedicine. 6 (2011) 1257–1272. https://doi.org/10.2217/nnm.11.92.

[187] D. Harris, F. Muzzopappa, F. Glaser, A. Wilson, D. Kirilovsky, N. Adir, Structural dynamics in the C terminal domain homolog of orange carotenoid Protein reveals residues critical for carotenoid uptake, Biochim. Biophys. Acta - Bioenerg. 1861 (2020) 148214. https://doi.org/10.1016/j.bbabio.2020.148214.

[188] M.A. Dominguez-Martin, C.A. Kerfeld, Engineering the orange carotenoid protein for applications in synthetic biology, Curr. Opin. Struct. Biol. 57 (2019) 110–117. https://doi.org/10.1016/j.sbi.2019.01.023.

1.5 Supplementary Information

1.5.1 Method: molecular biology for OCP expression

The production of OCP(CAN) in *E.coli* is taken as example to clarify the molecular biology protocol used. The process takes 5 days, preceded by a step of *E.coli* cells transformation, including steps of protein and carotenoid induction, purification on column and dialysis. It is hereafter illustrated.

- Competent cells transformation:

A volume (1µL) of β-mercaptoethanol is added to a mix (50µL) of XL10 Gold Supercompetents cells in sterile Eppendorf and incubated for 10 minutes at 0°C. Then, 3 plasmids are added: 3µL of *crtW* (for CAN expression or *crtO* for ECN), 3 µL of *cdf-OCP*, 5 µL of *ac-BETA* (for β-carotene). After incubation for 20 minutes at 0°C, a thermic shock for 1 minute at 42°C in termoblock is performed to allow esogene DNA to enter the cellular membrane. Incubation for 2 min at 0°C follows and then 250 µL of NZY^+ (growth medium made up of LB/$MgCl_2$ – $MgSO_4$/Glucose) are added. The system is incubated for 1 hour at 37°C, then spread on a petri dish with Agar and antibiotics (Ampicillin / Streptomycin / Chloramphenicol) and incubated overnight at 37°C.

- Day 1 - Cell growth in mini-culture:

After the incubation overnight, colonies of cells appear on petri dish. Each colony is suspended into 2 mL of LB growth medium plus a half volume (in µL) of each antibiotic and let to incubate overnight at 37°C. It is also possible to do a "fast growth" skipping the overnight incubation, suspending the colonies in 5 mL of LB medium plus a half volume (in µL) of each antibiotic, incubating 5h at 37°C and then moving to the procedure of Day 2.

- Day 2 – Carotenoid induction with Arabinose:

A mini culture (the most orange coloured among all) is transferred into 100 mL of TB growth medium and the 3 antibiotics (half the volume of each one, in µL) are added. After incubation at 37°C for few hours, it is necessary to measure the OD (Optical Density) at 600 nm transferring 1 mL of the culture inside a cuvette. When the OD is between 0.6 – 0.8, 0.03% of Arabinose is to add (necessary to induct the expression of Canthaxanthin from β-carotene). Incubation overnight at 37°C follows.

- Day 3 - Protein induction with IPTG:

The culture is transferred into 1 L of TB growth medium and the 3 antibiotics (half the volume of each one, in µL) plus Arabinose 0.03% (1.2 mL over 1 L) are added. After incubation at 37°C for few hours, when the OD is between 0.8 – 1, 200 µM of IPTG (starting from a stock solution of 1 M) and EtOH (100% pure) at 2% (20 mL over 1 L) are added. They are necessary to induce the expression of the protein. Incubation can be driven overnight at 28°C, or at 37°C not more than 4 hours.

- Day 4 - Purification on column:

For cells grown in 1 L of TB, it's necessary to re-suspend them in 40 mL of BB (Binding Buffer: 100 mL TRIS + 100 mL Glycerol + 75 mL NaCl, complete with H_2O till 1 L) and add 3 anti-protease to avoid the protein degradation (1 mM of each, starting from stock solutions 100 mM, so 400 µL of each), EDTA as chelate agent (1 mM of each, starting from stock solutions 100 mM) and ADNase enzyme to break up the ADN (20 µL of solution 15000 units/mL). This solution is passed inside the press to break up the cells and free the OCP. The pressed solution is centrifuged at 16000 rpm for 30 min to isolate the supernatant (containing OCP) from the pellet (containing residues of membranes and carotenoid).

The purification column could be of 20- or 40-mL volume. It is prepared using a resin enriched with Ni, necessary to bind the OCP-His-Tag and to trap it on the column. The resin is stocked in ethanol, and it is necessary to wash it (4 - 5 times) with water before using it. The column is filled with the resin in water while a pomp is activated to allow the elution of water. Resin must not remain dry. Later, 5 mL of solution of $NiSO_4$ are added to enrich the resin in Ni and then 100 mL of BB are added. When the column is ready, it is filled with the supernatant (coming from the press) and then washed with 2 different buffers: first, a solution of Imidazol 15 mM in 100 mL of BB, then with a solution of Imidazol 50 mM in 100 mL BB. After the second washing, it could be useful to measure the visible spectrum of the eluted just to know if the OCP is already being eluted. At this moment it is necessary to add on column the elution solution, made up of Imidazol 250 mM in 200 mL of BB. If there is already a signal coming from the protein in the spectra recorded, it is possible to start collecting the "Head" of the solution. Then the "Core" (containing the majority of OCP) is collected, followed by the "Tail." At the end of the elution, the "core" is kept, and it is ready for the dialysis. The resin is washed in water 4 / 5 times and stocked in EtOH 20%.

If the solution has not high purity (ratio 2 between OCP and proteins absorbance is required), a second purification on column is required. This time, a hydrophobic column of 5 mL is used, washed with 30 mL of H_2O, equilibrated with 30 mL of solution TRIS 40mM/NaCl 2M,

charged with aliquots of 5 mL OCP solution plus 5 mL NaCl 4M and eluted with NaCl 0.5 M (in H_2O). The eluted is collected in different Eppendorfs and the OD is measured to collect the purest fractions.

For the following dialysis, a solution of TRIS 40 mM in 2 L of H_2O is necessary. A membrane of nanopores with suitable dimension is required: for OCP dialysis the size is 12-14 kDa (quite the half of the protein size) to dialyze everything but the protein. The membrane is washed in water, knotted at one side, filled with the "Core" eluted and then closed and knotted on the other side, paying attention to leave some volume free because during the dialysis the imidazole molecules will be replaced by TRIS molecules, and this will increase the total volume. The membrane, once filled, is placed inside the 2 L of TRIS solution, and stored overnight in the dark inside a cold chamber, under stirring.

- Day 5 – Centrifugation:

The solution dialyzed is transferred into a beaker. The optical density is measured, using TRIS 40 mM for the baseline. If the OD is not the one required, it is necessary to centrifuge the solution until the right OD. For this centrifugation, special tubes are required: they have a double tube with a membrane to separate TRIS solvent from the OCP. Centrifuge with rotor 14, at 4500 rpm for 20 min, but it depends on the degree of centrifuged required.

The protein can be stored with NaCl (in 10mL of OCP: 62.5µL of NaCl 4M) at -80°C.

2. OCP mechanism of photoactivation investigated by UV-Visible and FT-IR difference spectroscopy

2.1 Introduction

2.1.1 FT-IR Difference Spectroscopy

Infrared (IR) difference spectroscopy is a well-established technique in the study of the molecular mechanism of reactions taking place in proteins, as it can provide information at atomic level[1]. Vibrations responsible of IR bands are in fact determined by structure and by inter (and intra-) molecular interactions. Furthermore, basically almost any molecular group absorbs in the infrared, and therefore information on almost all the constituents of the protein can be obtained, notably protein backbone, amino acid side chains, pigments/cofactors, or internal water molecules.

In absolute IR spectroscopy it is often difficult to pinpoint spectral changes induced by a given process or reaction. These changes are too tiny to be detected. Therefore, a difference approach is often used: an IR spectrum recorded before the process (or reaction) under study is subtracted from an IR spectrum recorded after the process (or reaction) has taken place. In this way, all the components of the absolute spectrum that do not change because of the process (or reaction), is eliminated and the resulting difference spectrum shows only positive and negative bands reflecting changes in molecular groups that are (directly or indirectly) related to the process under study.

In most cases, the size of this difference spectrum is so small that it becomes inconvenient to subtract spectra from two different samples. The experimental errors and the small differences (in hydration, pH and temperature) existing between two different samples give often higher spectral differences than those due to the reaction under study. For this reason, it is highly preferable (and in most cases, mandatory) to induce the reaction inside the spectrometer, so that measurements “before” and “after” the reaction, are recorded on the same sample (see **Figure 2.1**).

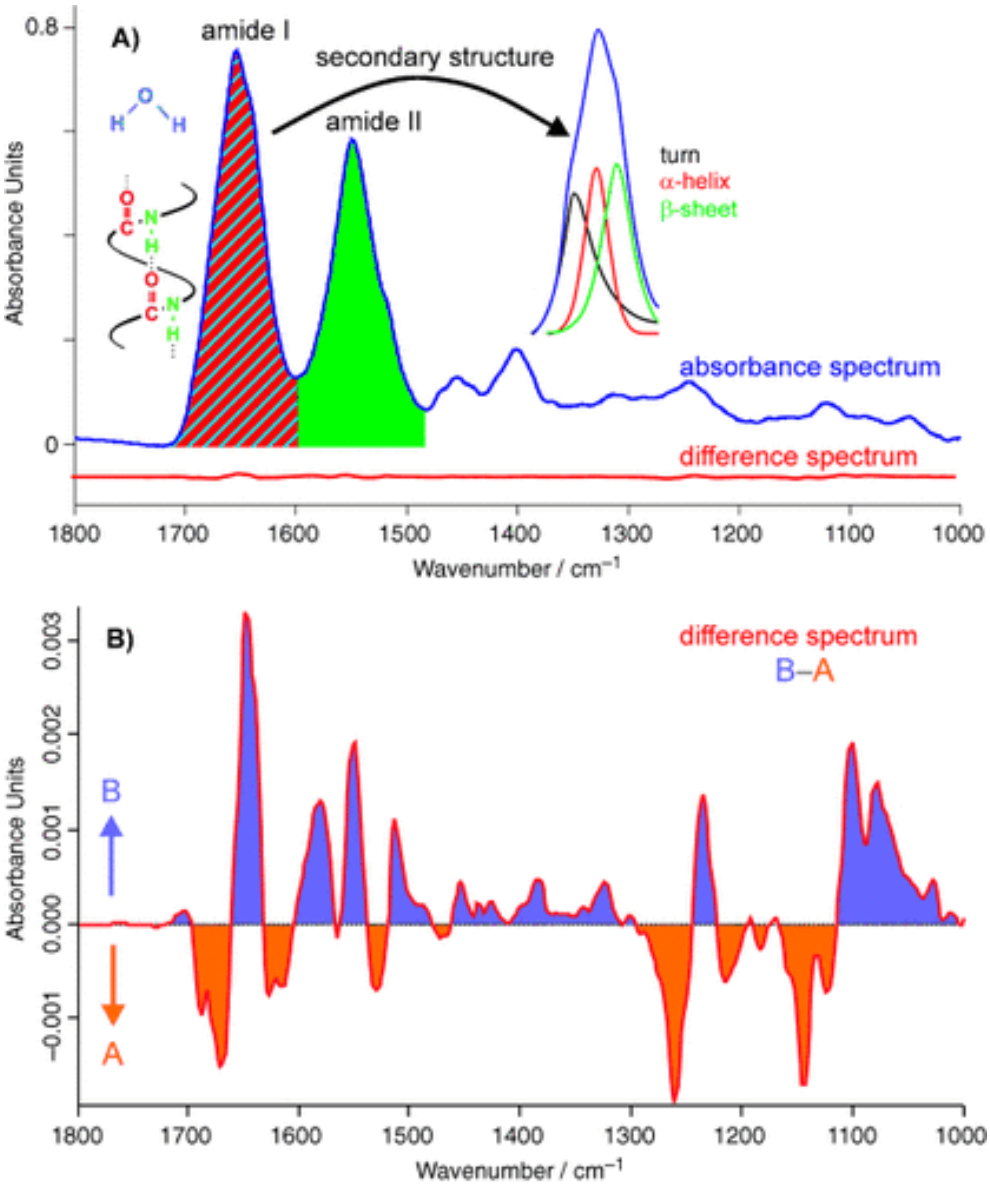

Figure 2.1 (Top) Typical IR absorbance spectrum of a protein, showing the main components, notably amide I, amide II and water (blue); in a secondary structure analysis, the components of amide I are separated: α-helix, β-sheet and coil are shown; the red spectrum in the bottom of the upper part is an IR difference spectrum of the same protein, recorded before and after a reaction took place. (Bottom) Principle of FTIR difference spectroscopy shown by the same IR difference spectrum, on an enlarged scale. Adapted with permission from Kotting and Gerwert[2]**.**

Sample preparation is minimal, and experiments under different conditions (D_2O, pH, temperature or hydration level) are possible and relatively easy to perform. Fourier Transform (FT) IR difference spectroscopy allows a large spectral range to be explored simultaneously, so that different events can be followed (localized conformational changes, pigment/cofactor displacement or redox changes, H^+ transfer, etc).

In the case of photoactive proteins, the reaction is triggered by light, and this represent an important advantage, as the process can be easily induced by a light source inside the sample compartment of a FTIR spectrometer. In fact FTIR difference spectroscopy has been widely applied to photoreceptors[3] and to photosynthetic reactions[4], including the OCP photocycle[5–8] (OCP, being a photoreceptor involved in the photoprotection of the photosynthetic apparatus, is at the interface of the two research domains).

Recording FTIR difference spectra at different times after the start of a reaction increases tremendously the amount of information that can be obtained[9]. In fact, intermediate states and/or parallel reactions can be detected. Furthermore, it can help in the difficult task of band assignment (see below). However, time-resolved experiments have some requirements. Given that in FTIR an interferogram (and therefore a spectrum) is acquired only when the movable mirror of the Michelson interferometer has performed a complete movement (see **Figure 2.2**), the most straightforward approach is to move the mirror as fast as possible (~2 - 10 cm/sec). This is not feasible with normal FTIR spectrometers but only with instruments equipped with the so-called "rapid-scan" mode. Furthermore, the instrument must be equipped with a fast response detector - usually a photoconductive HgCdTe (MCT) detector, as in this thesis - and with an Analog-to-Digital Convertor fast enough to correctly digitize the interferogram. Other instrumental approaches exist, but they were not used in this thesis because it is difficult to apply them to OCP photoactivation. It should be mentioned that the use of a MCT detector has the additional advantage of its very high detectivity in the mid infrared, and this represents an asset in FTIR difference spectroscopy. The drawback is that MCT detector needs to be cooled at low temperature through a liquid N_2 cooling system.

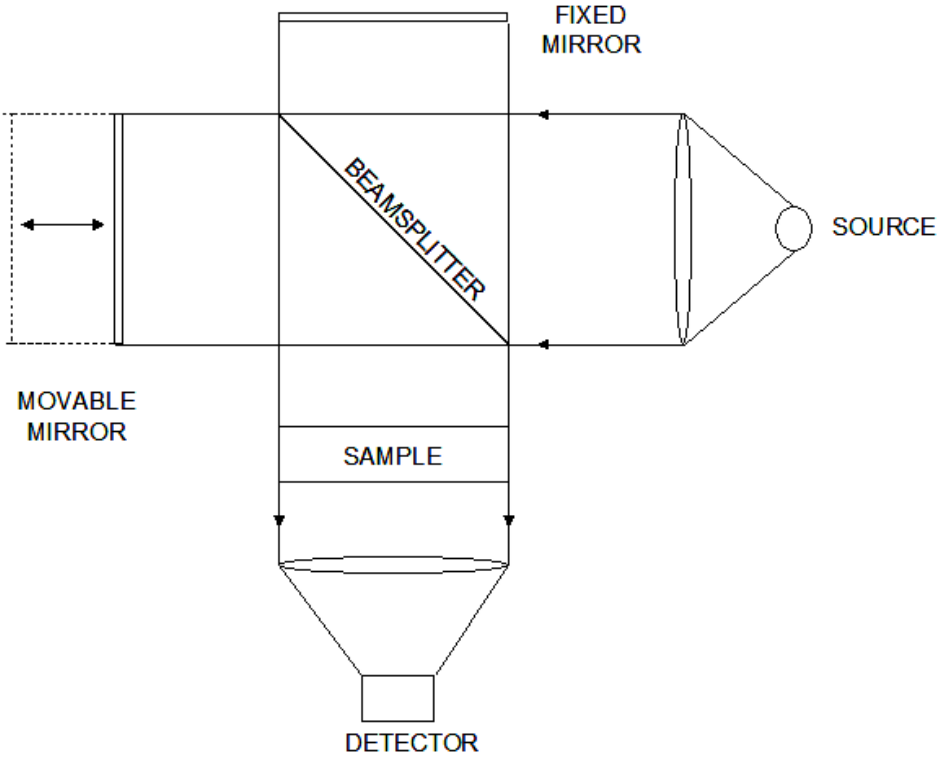

Figure 2.2 Scheme of a Michelson interferometer-based FTIR spectrometer.

2.1.2 Band assignment

Despite the first use of FTIR difference spectroscopy to study OCP photocycles dates back to 2008[7], up till now no report have focused on the assignment of the carotenoid IR bands. This step is crucial in FTIR difference spectroscopy, because IR bands in a difference spectrum are meaningful only if a robust attribution is made, at least for some of them. Pigment/cofactor bands are in principle less difficult to assign than bands arising from protein components, as several strategies are possible. First, a comparison with IR bands of the isolated pigment/cofactor can be made. Even though the exact position of the peaks might be different, due to peculiar conformations or interactions with the protein binding pocket, a first rough idea of the spectral regions of interest can be deduced. A second, more precise strategy is particularly useful for pigments/cofactors without exchangeable protons. For FTIR difference spectra recorded in H_2O and D_2O, bands belonging to the pigment/cofactor do not show any shift. It should be mentioned that the ideal situation would be the opposite, notably to record (in H_2O) FTIR difference spectra on proteins with isotopically labelled pigment/ cofactor (e.g., marked with ^{13}C) and to compare it with the FTIR difference spectrum obtained on the "normal" protein

(with non-labelled pigment/cofactor). In this case only the bands arising from the pigment/cofactor would show a shift. However, implementing this strategy is not an easy task (it requires often specific synthesis of isotopically labelled compounds, and the possibility of inserting them in the binding pockets) and it has been seldom used.

Other strategies rely on the comparison with data from other vibrational spectroscopy techniques (e.g., Raman) and on theoretical calculations. But in these cases, problems may arise for pigment/cofactors with high molecular weight (e.g., high number of molecular vibrations, which overcomplicates the analysis) and in case of conformational distortions of the pigment/cofactor induced by the intermolecular interactions with the protein binding pocket.

In the case of OCP, to our knowledge, no easy strategy to insert labelled carotenoids into the apo-protein exist. Furthermore, both in the orange and in the red form, the conformation of the carotenoid is distorted by interaction with the binding pocket, and this makes precise comparison with FTIR spectra of isolated carotenoid not very meaningful. Similarly, normal DFT calculations on isolated carotenoids in vacuum or in solvent of known dielectric constant are not very useful, as the equilibrium conformation in vacuum or in solvents is not the one assumed by the carotenoid in the binding pockets (both in OCP^O and OCP^R). More detailed calculations (considering the effect of the binding pocket) are much more difficult and time-consuming.

For the above-explained reasons, in the present thesis the step of band assignment was limited to the comparison of FTIR difference spectra of OCP recorded in H_2O and D_2O, and to the comparison of kinetic evolution under illumination of the different bands (carotenoids bands should grow with the very same kinetics). IR spectra of isolated carotenoids (notably echinenone) were used to confirm band assignment and to get a first hint on the identity of the molecular vibration responsible of a given band.

2.2 Materials and Methods

2.2.1 Sample preparation

OCP solution was prepared as described in Chapter 1 and detailed in S.I. at the end of the same chapter, following the protocol of Bourcier de Carbon[10], except for the OCP containing 3-hydroxyechinenone, which was provided by Dr. A.Wilson (CEA-Saclay).

In FTIR difference spectroscopy the first aspect to be considered is the fact that molar extinction coefficients of vibrational modes are much smaller than those of electronic transitions.

Consequently, very concentrated samples must be used (in the mM range). The normal rule of thumb is to obtain a 0.6–0.9 maximal absorbance in the amide I region (1600–1700 cm^{-1}). In addition, given that the bending band of water (~1640 cm^{-1}) largely superimposes with the amide I band, there is the need of getting rid of as much water as possible, provided that the working mechanism of the protein under study is not altered. The problem is particularly severe for water-soluble proteins like OCP. A compromise has therefore to be found between the need of minimizing the water signal and the need of keeping the protein in an environment as similar as possible to the natural conditions. In the present work, this compromise was found by checking the intensity of the amide II band versus the intensity of the so-called combination band of water at (~5150 cm^{-1})[11]. No precise protocol to perform experiments at a fixed hydration level could be established (as, for instance, for bacterial photosynthetic Reaction Centres[12]), as these protocols works only for membrane proteins which can strongly adhere to CaF_2 windows (used as support for sample preparation).

Therefore, 30 µL of OCP solution 70 µM have been placed on a CaF_2 window and dried under gentle N_2 flow to get the desired absorbance value of the combination band of water (as previously motivated). Once the desired concentration reached, the sample has been closed between two CaF_2 windows and sealed with grease to prevent sample leakage during the measurements. The windows were fixed inside the sample holder and placed inside the analysis chamber of the spectrometer (see picture in **Figure 2.4**).

2.2.2 Hydrogen/Deuterium isotopic exchange

To perform Hydrogen/Deuterium (hereafter referred to as H/D) exchange, the protocol proposed by Malferrari *et al.* [13] has been followed. In details, 30 µL of OCP 70 µM have been placed on CaF_2 window and placed under a sealed petri dish, in the vicinity of a saturated solution of LiCl in D_2O (LiCl saturated solution ensures a relative humidity of 11 %) for 3 hours. This ensures strong (but not complete) dehydration of the sample. The second step (re-hydration with D_2O) was carried out placing the sample in the vicinity of a saturated solution of NaCl in D_2O (always under a sealed petri dish) for 4 hours, ensuring a relative humidity of 75 %. Then, a second CaF_2 window was used to close the sample cell, that was then sealed with grease and analysed with FTIR spectrometer. A simple scheme of the experimental set-up for H/D exchange is shown in **Figure SI 1. 2-1**.

2.2.3 Experimental methods

2.2.3.1 UV-Visible spectroscopy

Ultraviolet-visible spectroscopy is a technique based on the principle of electronic transition in molecules or atoms, caused by absorption of light in the UV-Visible segment of the electromagnetic spectrum. It is a characterization method to evaluate the absorbance spectrum of samples.

The chromophore of the OCP is the carotenoid, whose absorbance is in the visible part of the electromagnetic spectrum. In a polar solvent, the maximum of the electronic transition for echinenone and canthaxanthin occurs at 476 nm and 490 nm, respectively[15,16]. The red shift observed between absorbance maximum of echinenone and canthaxanthin is related to the increasing number of conjugated double bounds (involving two carbonyl groups in canthaxanthin and one carbonyl group in echinenone, **Figure 2.5**)[17,18].

Absorption spectra in liquid phase were recorded on Biochrom Libra S60 spectrophotometer, between 350 and 700 nm with a resolution of 0.5 nm and an acquisition time of 0.1 s per point. A 1 cm path length cuvette in glass was used to record spectra in solution.

2.2.3.1 FT-IR difference spectroscopy

The rapid-scan FTIR difference spectroscopy approach has been applied during continuous illumination from a blue light emitting diode (LED) with $\lambda_{em,max}$ = 475 nm, monitoring the progressive conversion of OCP from the orange to the red state ($OCP^O \rightarrow OCP^R$). The very low quantum yield of photoconversion of OCP (see Chapter 1) makes unfeasible recording time-resolved spectra after a laser flash. Spectra were therefore recorded during continuous illumination. FTIR difference spectra were recorded at increasing times after the onset of blue light with a time resolution in the second time scale. The advantage of the rapid-scan mode is that in, around 10 seconds, approximately 200 spectra can be averaged, leading to a very good signal-to-noise ratio (S/N). Similarly, rapid-scan FTIR difference spectra were recorded at increasing times after switching off the light. This made it possible to follow the "relaxation" of the sample (see **Figure 2.3**).

FTIR spectra were recorded in the rapid-scan mode (mirror speed 7 cm/s) on a Bruker Vertex 80 FTIR spectrometer equipped with OPUS software, except for OCP binding 3-hydroxyechinenone, which was recorded on a Bruker IFS 88 spectrometer (Opus software, MCT detector) operating in the rapid-scan mode.

Time-resolved FTIR experiments were performed as follows: after background recording in the dark, the blue light LED was switched on and 500 interferograms were recorded (corresponding to a time interval of ~25 s). Different recordings were performed every 15 seconds during about 5 min. Then the LED was switched off and spectra were recorded during the relaxation period ($OCP^R \rightarrow OCP^O$ back-conversion). Time-resolved FTIR difference spectra were obtained after Fourier transform and after subtraction of the background, following equation (1) as described in [14].

$$\Delta A(\nu) = -\log \frac{S(t)}{S(background)} \quad (1)$$

In equation (1), S(t) represents the single beam spectrum (obtained through Fourier transform of the corresponding interferogram) at time t; S(background) represents the single beam spectrum recorded in the dark (obtained through Fourier transform of the corresponding interferogram in the dark).

FTIR difference spectra are hereafter referred to as "light-minus-dark difference spectra", meaning that the final spectrum is the difference between the one recorded before the illumination and the one recorded after the illumination.

To perform these experiments, the blue LED was placed inside the sample chamber of the spectrometer, but it was adjustable from the outside. The chamber was sealed to avoid changes in the temperature and humidity level of the environment. A picture of the experimental set-up is reported in the lower part of **Figure 2.4**.

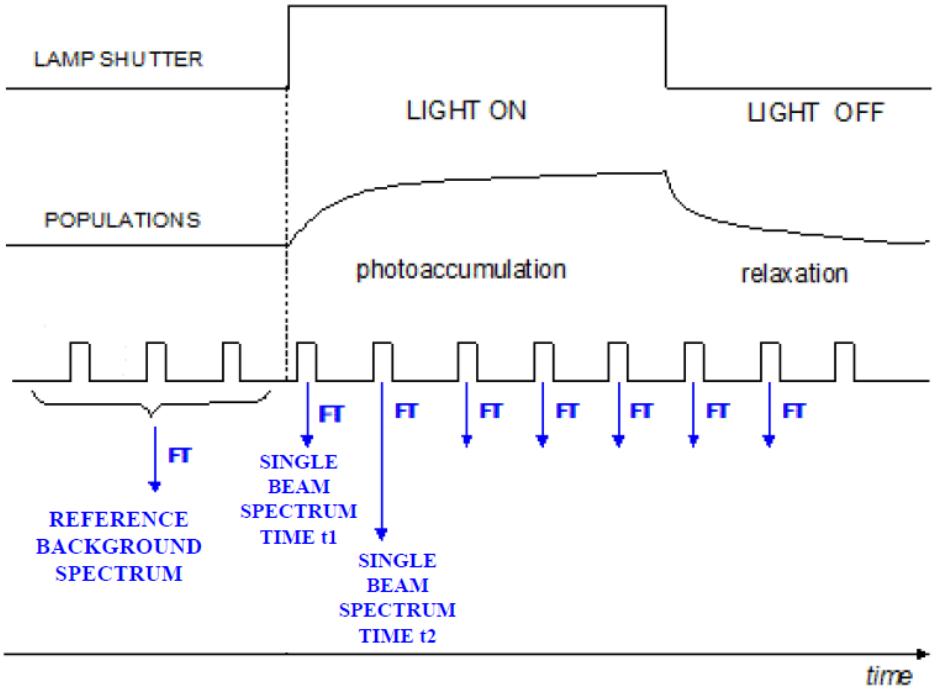

Figure 2.3 Scheme of a time-resolved FTIR experiment before, under and after illumination.

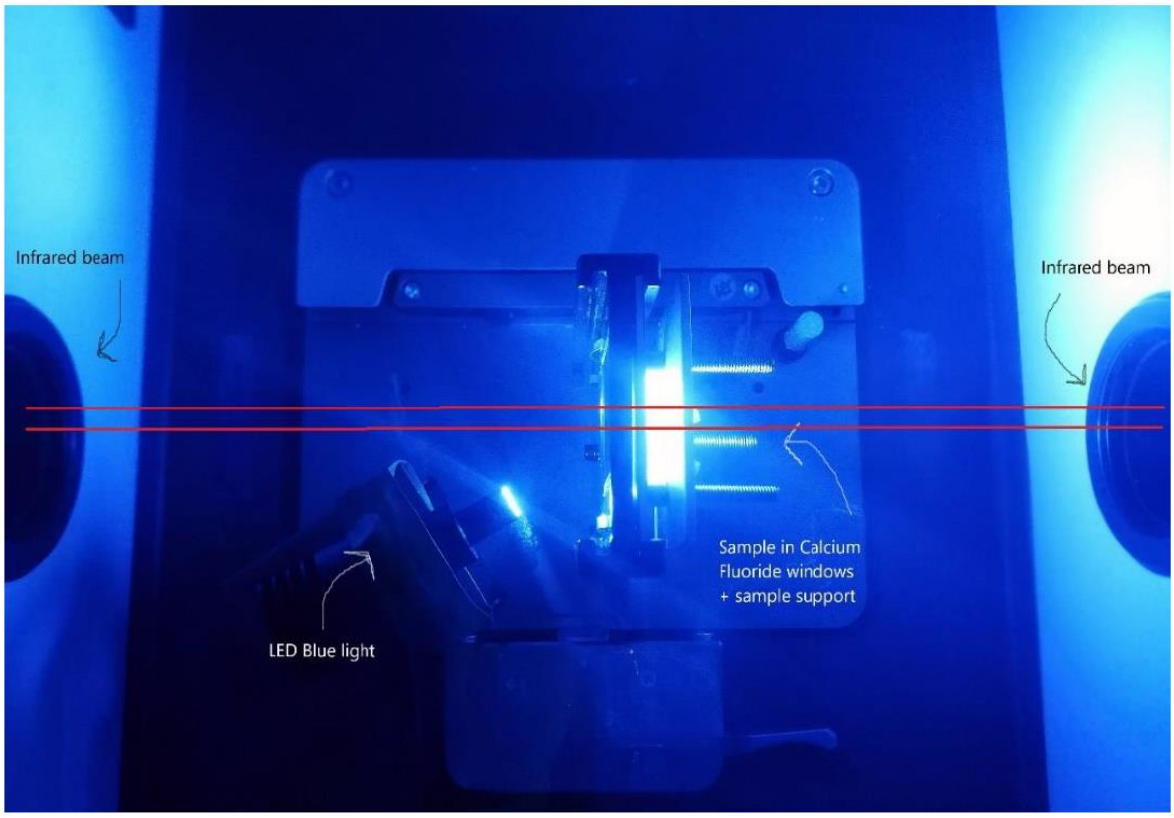

Figure 2.4 Picture of the experimental set-up used; in details, the infrared beam, the blue light LED and the sample holder made by a metallic support holding CaF_2 windows, where the sample solution is placed.

2.3 Results and discussion

2.3.1 Echinenone vs Canthaxanthin

UV-Visible spectra of OCP(ECN) and OCP(CAN) 0.5 mg/mL in water are shown (**Figure 2.5**). In darkness, both protein solutions are orange coloured. OCP(ECN) presents a vibrational structure with two maxima at 474 and 496 nm, while OCP(CAN) presents two maxima at 474 and 500 nm. Absorption of blue-green light converts, with a ~0.2% yield[19], the orange form (OCP^O) to a metastable red form (OCP^R) whose spectrum loses the vibrational band resolution observed for OCP^O, undergoes an intensity decrease with a broader spectral shape and exhibits a redshift with a unique maximum at 511 nm for OCP(ECN) and a maximum at 515 nm for OCP(CAN). The absorbance spectra in the visible range allows to unambiguously distinguish between carotenoid bound to OCP^O, to OCP^R and isolated carotenoid in solution, which appears yellow in the case of echinenone (λ_{max} = 476 nm) and orange in the case of canthaxanthin (λ_{max} = 490 nm).

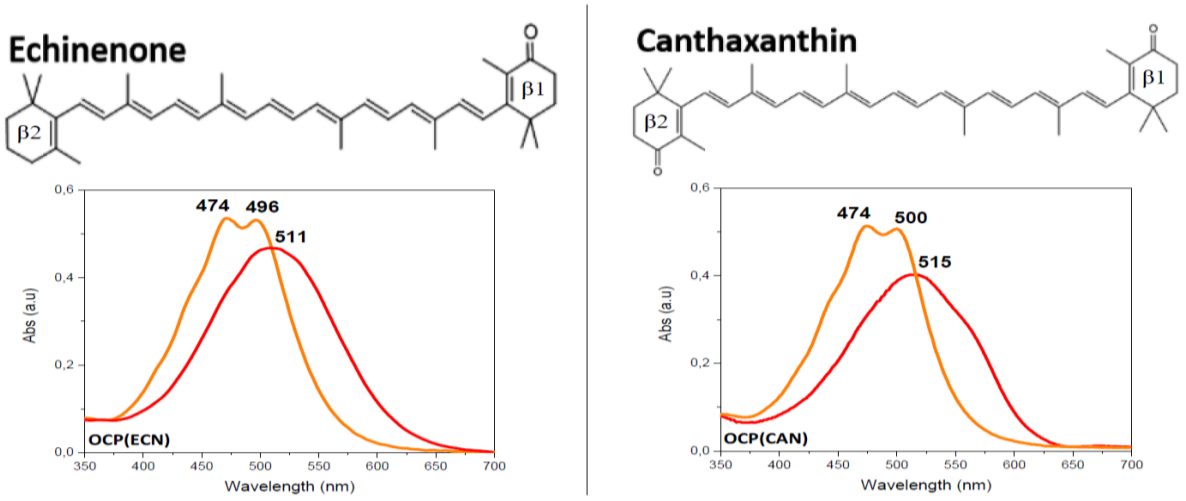

Figure 2.5 (Top) Molecular structure of echinenone (left) and canthaxanthin (right) highlighting the central double bonds chain spanning the two β rings: β1 belonging to the CTD and β2 to the NTD. (Bottom) Visible spectra recorded in solution for OCP(ECN) and OCP(CAN) 0.5 mg/mL, before (orange line) and after (red line) photoactivation with blue light LED (emission maximum at 475 nm).

2.3.2 FT-IR difference spectra recorded on OCP containing different carotenoids

At least three different kinds of OCPs (each one endowed with a different keto-carotenoid, notably 3-hydroxy echinenone, echinenone and canthaxanthin) have been studied in the

literature. Their light-minus-dark FTIR difference spectra are strikingly similar, indicating that very similar photoactivation mechanisms occur in the three cases (see **Figure 2.6**).

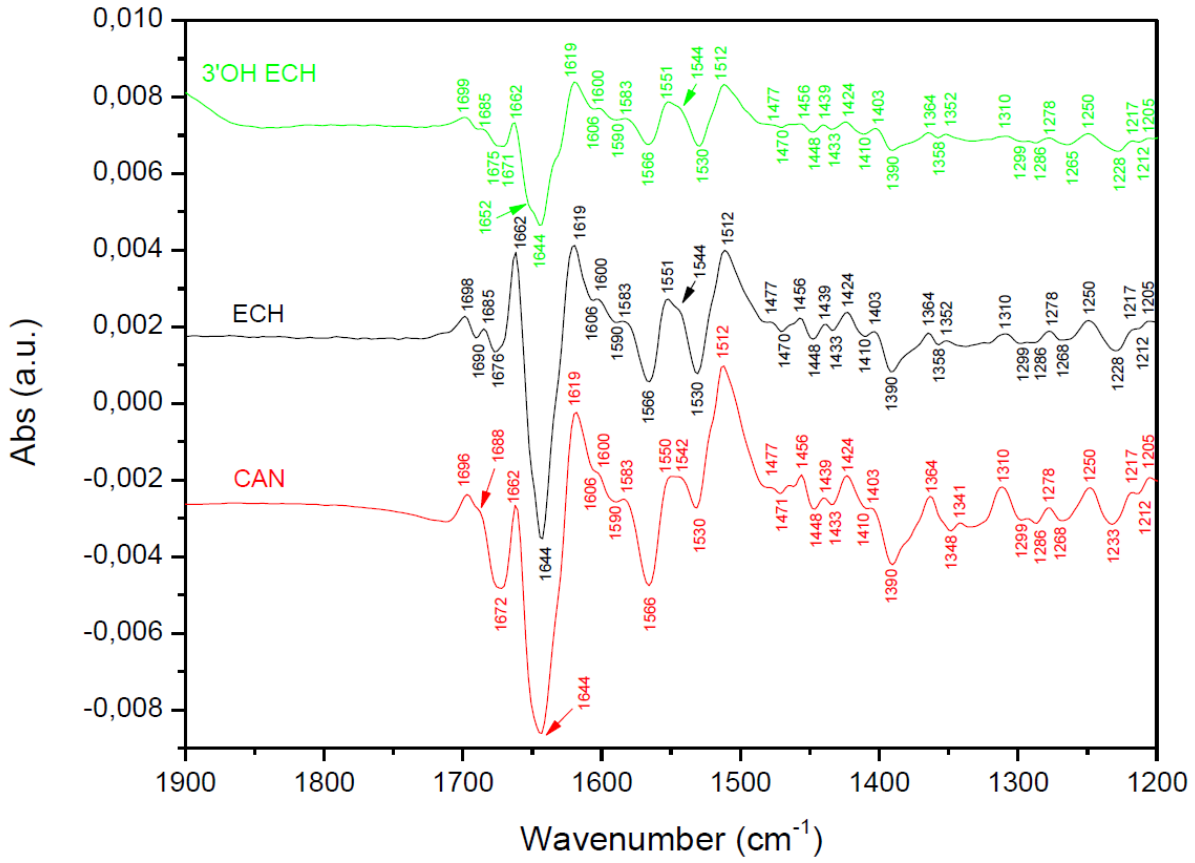

Figure 2.6 Light-minus-dark FTIR difference spectra of OCP containing 3-hydroxy echinenone (green), echinenone (black) and canthaxanthin (red).

The most prominent features are in the amide I region (1690 – 1610 cm^{-1}). As previously reported[5], the negative bands at 1644 and 1651 cm^{-1} can be attributed to disappearance of one (or more) non-solvent exposed α-helices (1651 cm^{-1} band, still unidentified) and of one (or more) solvent exposed α-helices (1644 cm^{-1} band, most likely the NTE helix and/or the CTT helix). A previous study[5], has shown that in the 1700-1580 cm^{-1} region several superposing spectral contributions are present and, on the basis of current FTIR data, no other assignments can be safely made.

2.3.3 Echinenone and Canthaxanthin bands

As stated above, identification of vibrational bands belonging to the chromophore is a mandatory step. In **Figure 2.7**, light-minus-dark FTIR difference spectra of OCP (binding

echinenone) recorded in H_2O and D_2O are shown. Bands that do not shift after H/D exchange and, furthermore, that absorb in the same regions of isolated echinenone[20], are indicated in blue. From high to low wavenumbers, bands assigned to echinenone were identified at 1583 (+), 1566 (-), 1510 (+), 1391 (-), 1364 (+), 1310 (+), 1157 (+) cm^{-1} (the (+) symbols indicates positive bands, whereas (-) indicates negative bands).The kinetics of growth and decay of the bands below 1500 cm^{-1} (outside of the amide II region where protein contribution are probably dominant) are, within experimental errors, the same (not shown). Based on DFT calculations on isolated echinenone (performed by Dr. R. Spezia, Laboratoire de Chimie Théorique, Sorbonne Université; personal communication), some tentative assignments can be made (see **Figure SI 1. 2-2**). For the time being, it is very difficult to deduce details on the molecular mechanism of the displacement of echinenone carotenoid during OCP photoactivation. Detailed quantum chemistry calculations considering the effect of the protein binding pocket in both OCP^O and OCP^R will be required to solve this issue. Nevertheless, the accomplished identification of these bands is a mandatory step for future IR experiments, especially in the time-resolved mode.

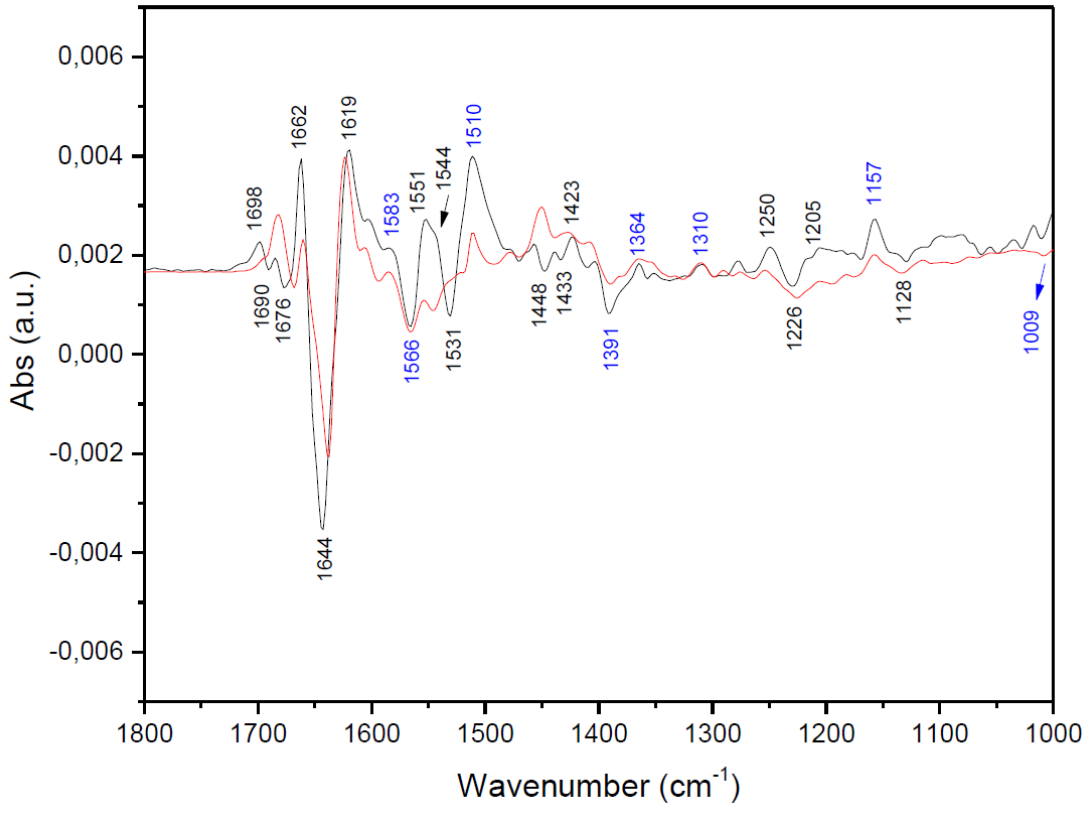

Figure 2.7 Light-minus-dark FTIR difference spectrum of OCP binding echinenone in H_2O (black) and D_2O (red).

In **Figure 2.8**, light-minus-dark FTIR difference spectra of OCP (binding canthaxanthin) recorded in H_2O and D_2O are shown. Bands that do not shift after H/D exchange and, furthermore, that absorb in the same regions of isolated canthaxanthin (see **Figure SI 1. 2-3**), are indicated in blue. From high to low wavenumbers, putative canthaxanthin bands were identified at 1512 (+), 1424 (+), 1391 (-), 1363 (+), 1311 (+), 1156 (+) cm^{-1}. Also in this case, bands below 1500 cm^{-1}grows and decay with the same kinetics (not shown). It is also interesting to remark how the FTIR difference spectrum (especially in H_2O) differs from the one of OCP containing echinenone in the 1700-1670 cm^{-1}region. It is likely that the presence of a second C=O in canthaxanthin, which probably change its conformation and/or its hydrogen bonding status when passing from the orange to the red form of OCP, gives spectral contributions in this region. However, it should be kept in mind that the observed positive and negative bands are likely to be the results of superposing spectral contributions. More detailed analysis, involving site directed mutagenesis or comparison with other spectra (e.g., a FTIR difference spectrum reflecting canthaxanthin oxidation in OCP) will be necessary to better study this issue.

Also in this case, detailed quantum chemistry calculations considering the effect of the protein binding pocket in both OCP^O and OCP^R will be particularly helpful to assign the identified band to specific vibrational modes. It finally is interesting to point out that, besides being a mandatory step for future IR experiments, identification of canthaxanthin band turned out to be useful to study an unexpected phenomenon, described in the following paragraph.

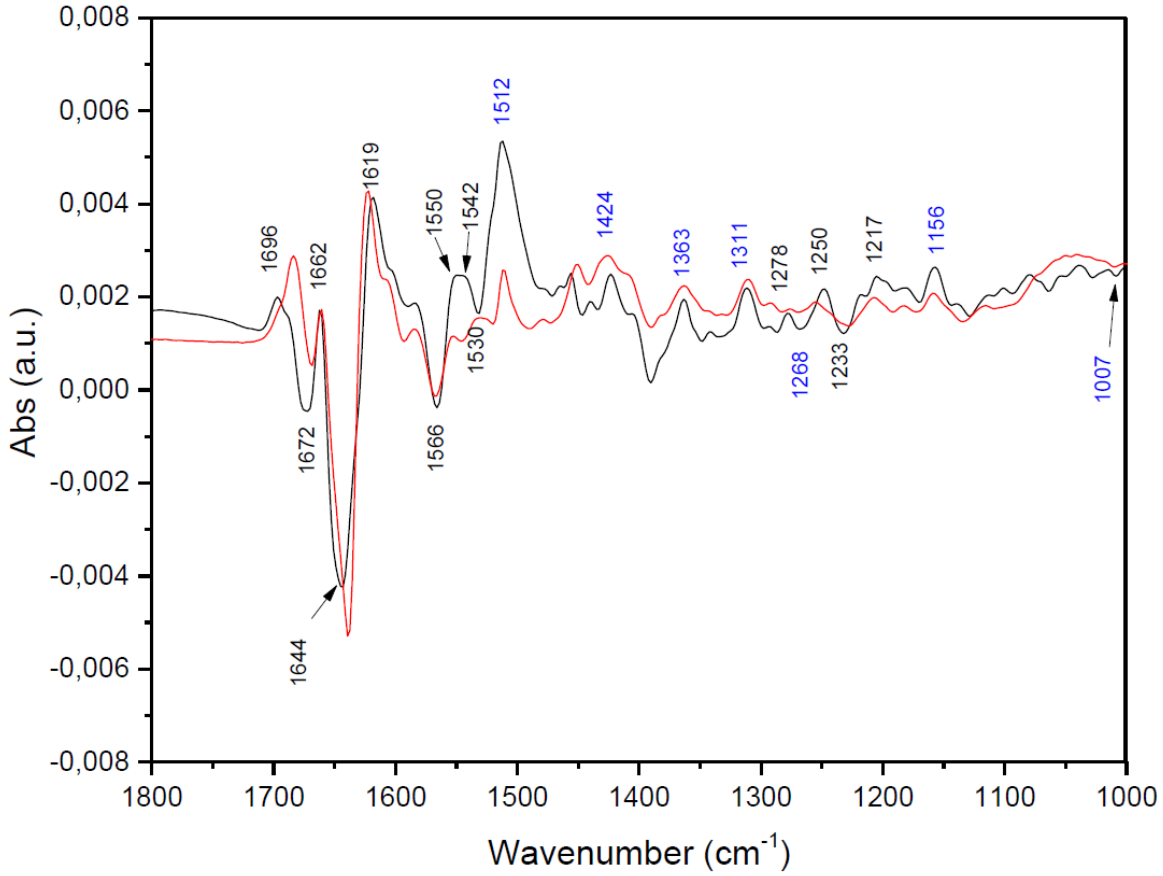

Figure 2.8 Light-minus-dark FTIR difference spectrum of OCP binding canthaxanthin in H_2O (black) and D_2O (red).

2.3.4 OCP self-activation

Following a previously reported approach on photosynthetic bacterial Reaction Centres [12], we decided to investigate the effect of the hydration state on the photo-activation of OCP by light-induced FTIR difference spectroscopy. Because of the low adhesion to the CaF_2 windows, the isopiestic method of Malferrari *et al.*[12] could not be applied. However, the hydration state of the sample can be semi-quantitatively assessed through the combination band of water at ~5150 cm^{-1}[11].

A preliminary step in light-minus-dark FTIR difference spectroscopy is to wait for sample stabilization inside the spectrometer. During this time, an unexpected process was discovered. In fact, OCP(CAN) was found, under highly dehydrated conditions, to undergo activation to the red form in the dark. The process was followed also by time resolved FTIR difference spectroscopy, in the limitations imposed by the technique in term of baseline stability and signal

size. Very interestingly, several bands are found at the same position as in normal light-minus-dark FTIR difference spectra (see **Figure 2.9**).

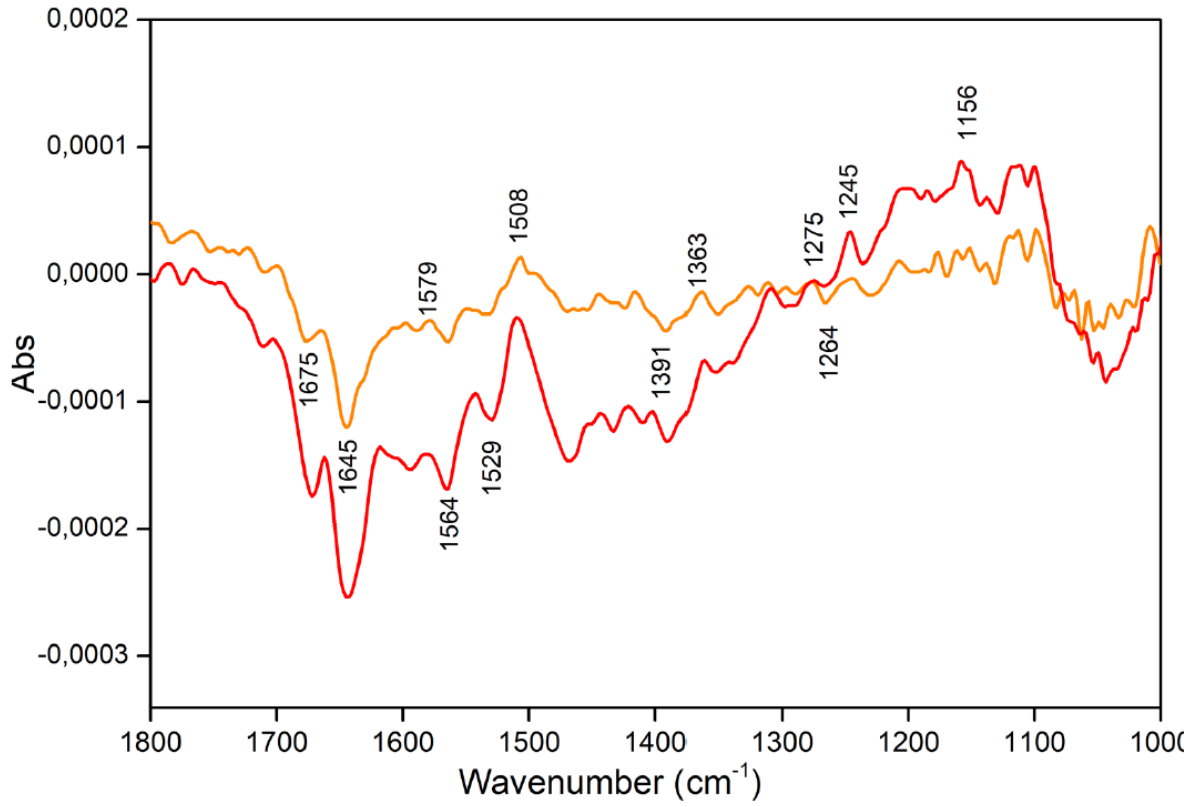

Figure 2.9 Time-resolved FTIR difference spectra in the dark on de-hydrated OCP binding canthaxanthin, recorded in the dark after 30 seconds (orange line) and after 5 min (red line).

Of peculiar relevance are the bands which can be tentatively assigned to canthaxanthin 1508 (+), 1391 (-), 1363 (+),1156 (+) cm^{-1} (in the case of the intense 1508 cm^{-1} band, a slight shift compared to the light-minus dark difference spectrum described in the previous paragraph can be due to dehydration or to dehydration-induced changes from the protein in the same spectral region). The process could be followed by time-resolved FTIR only for ~5 minutes, due to the very low intensity of the FTIR differential signal and to the intrinsic baseline shift due to thermal stabilization of the sample and to slight variation in IR intensity from the source.

The process of "self-activation" was also followed by UV-Visible spectroscopy in samples at three different hydration levels. The level of hydration was determined by Near-IR absorbance spectroscopy, with reference to the combination band of water at 5150 cm^{-1} (see **Figure SI 1. 2-3**)[11]. This made it possible to have a more precise idea of the sensitivity of the process to the exact hydration state and made it possible to follow the kinetics of the process. Results are shown in **Figure 2.10**.

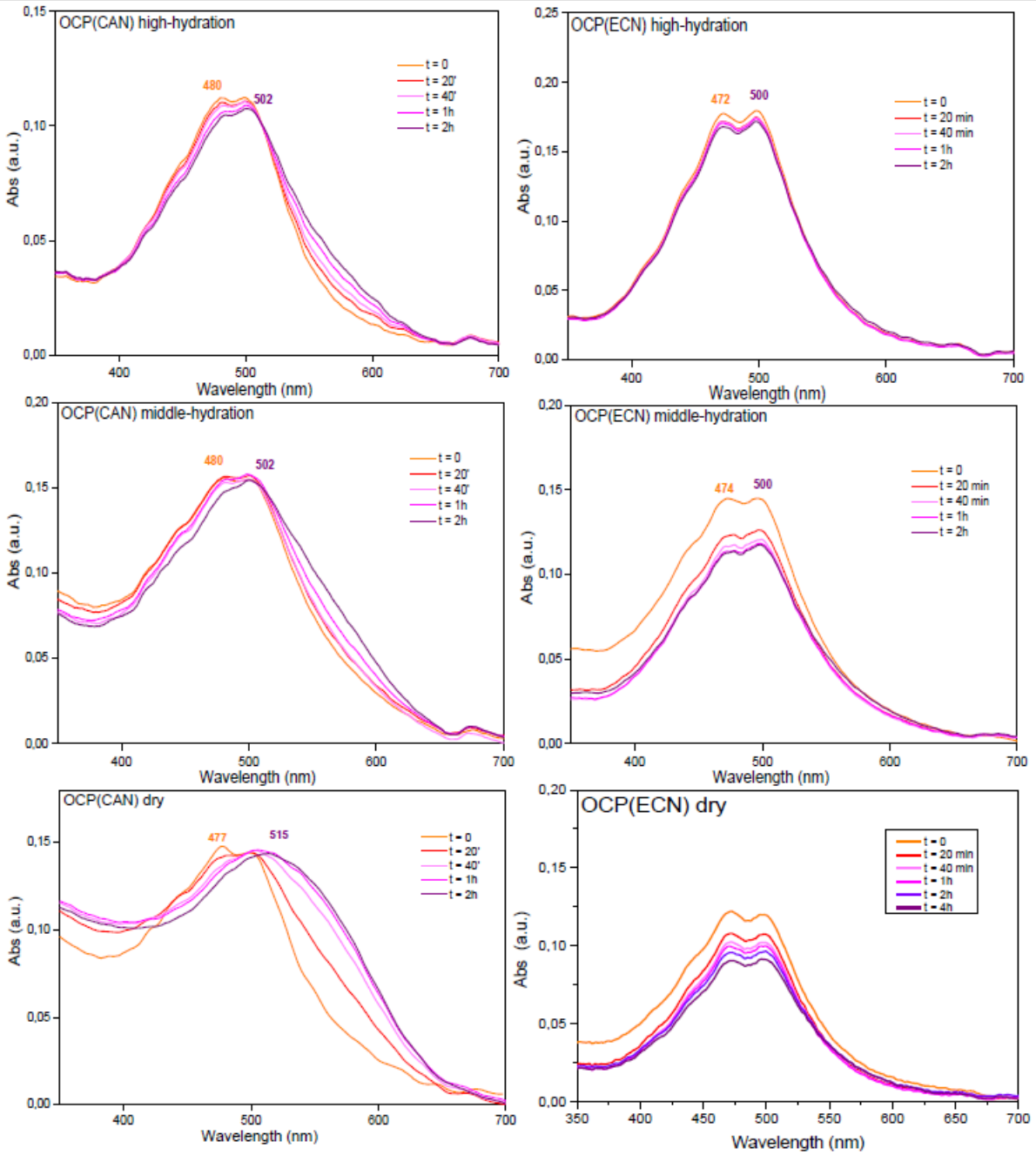

Figure 2.10 UV-Visible spectra recorded in the dark, at different times and at different level of hydration of OCP containing canthaxanthin (left) and echinenone (right). From top to bottom, samples at high, middle, and low level of hydration (referred as "dry") are shown. Spectra recorded at t=0, after 20, 40, 60, 120 min. Only for OCP(ECN) dry sample, a supplement spectrum was recorded after 4 hours.

In strongly de-hydrated OCP(CAN) samples, a band at 515 nm is progressively formed and reaches its maximum after 2 hours. Conversely, in well hydrated samples, OCP(CAN) remain stable in its orange form. An intermediate situation is found for middle hydration samples, where a small modification in the Vis spectra (notably in the 500-600 nm region) is observed.

However, the most interesting results were found for OCP(ECN). For this sample, no dark "self-activation" was observed, even on strongly dehydrated samples. Indeed, the spectrum recorded over time, is the same for all hydration levels. This shows that specific differences exist among OCP(CAN) and OCP(ECN). Most likely, the presence of a second C=O moiety in CAN stabilizes the red state of OCP.

This assumption has been confirmed by experiments carried out in parallel on OCP(CAN) and OCP(ECN), in the framework of denaturation tests of the protein made by Urea. It has been discovered that, placed in contact with a solution of Urea 6 M, the OCP(CAN) was converted into the red form (within a period of 2 hours), while the OCP(ECN) kept the orange conformation, suggesting that the second carbonyl moiety of CAN stabilizes the OCP^R form (see **Figure SI 1. 2-5**).

2.4 Conclusions

In this chapter, spectroscopic studies were carried out to investigate the mechanism of photoactivation of OCP, with a focus on OCP binding echinenone or canthaxanthin as carotenoid. The exact mechanism of photoactivation and photoconversion of the protein is still to be clarified and several studies from different groups are under revision. The aim of our study was to characterize the mechanism of photoactivation by spectroscopic investigation, notably UV-Visible spectroscopy and especially by FTIR difference spectroscopy. Several pieces of information were obtained. 1) FTIR difference spectra of three different carotenoid-binding OCPs, showed a very similar photoactivation mechanisms, because the position of the bands was almost the same. 2) Hydrogen/Deuterium isotopic exchange allowed to identify putative bands belonging to the carotenoid. 3) It has been discovered that OCP(CAN) in strongly de-hydration conditions has a tendence to self-convert to the red form, suggesting a better stability reached in the red conformation. This was, in principle, supported by the red conversion of OCP(CAN) when in contact with a denaturation agent (urea). 4) Conversely, OCP(ECN) showed a higher stability of the orange form. Indeed, it did not self-activate at low hydration level and, furthermore, it preserved the orange conformation in presence of the denaturation agent. For future studies, it will be of great interest and practical utility the assignment of the vibrational bands, to deeply investigate and clarify the mechanism of photoactivation. Therefore, calculations of spectra for echinenone and canthaxanthin in their binding pockets (both in the orange and in the red forms) will be necessary. In addition, investigation of the 4000-2000 cm^{-1} spectral region will probably be very useful, given that in this region the stretching bands of several key molecular groups (OH, NH, SH, CH) absorb.

2.5 References

[1] V.A. Lorenz-Fonfria, Infrared Difference Spectroscopy of Proteins: From Bands to Bonds, Chem. Rev. 120 (2020) 3466–3576. https://doi.org/10.1021/acs.chemrev.9b00449.

[2] C. Kötting, K. Gerwert, Proteins in action monitored by time-resolved FTIR spectroscopy, ChemPhysChem. 6 (2005) 881–888. https://doi.org/10.1002/cphc.200400504.

[3] T. Kottke, V.A. Lórenz-Fonfría, J. Heberle, The grateful infrared: Sequential protein structural changes resolved by infrared difference spectroscopy, J. Phys. Chem. A. 121 (2017) 335–350. https://doi.org/10.1021/acs.jpcb.6b09222.

[4] C. Berthomieu, R. Hienerwadel, Fourier transform infrared (FTIR) spectroscopy, Photosynth. Res. 101 (2009) 157–170. https://doi.org/10.1007/s11120-009-9439-x.

[5] A. Mezzetti, M. Alexandre, A. Thurotte, A. Wilson, M. Gwizdala, D. Kirilovsky, Two-Step Structural Changes in Orange Carotenoid Protein Photoactivation Revealed by Time-Resolved Fourier Transform Infrared Spectroscopy, J. Phys. Chem. B. 123 (2019) 3259–3266. https://doi.org/10.1021/acs.jpcb.9b01242.

[6] P.E. Konold, I.H.M. Van Stokkum, F. Muzzopappa, A. Wilson, M.L. Groot, D. Kirilovsky, J.T.M. Kennis, Photoactivation Mechanism, Timing of Protein Secondary Structure Dynamics and Carotenoid Translocation in the Orange Carotenoid Protein, J. Am. Chem. Soc. 141 (2019) 520–530. https://doi.org/10.1021/jacs.8b11373.

[7] A. Wilson, C. Punginelli, A. Gall, C. Bonetti, M. Alexandre, J.M. Routaboul, C.A. Kerfeld, R. Van Grondelle, B. Robert, J.T.M. Kennis, D. Kirilovsky, A photoactive carotenoid protein acting as light intensity sensor, Proc. Natl. Acad. Sci. U. S. A. 105 (2008) 12075–12080. https://doi.org/10.1073/pnas.0804636105.

[8] A. Wilson, M. Gwizdala, A. Mezzetti, M. Alexandre, C.A. Kerfeld, D. Kirilovsky, The essential role of the N-terminal domain of the orange carotenoid protein in cyanobacterial photoprotection: Importance of a positive charge for phycobilisome binding, Plant Cell. 24 (2012) 1972–1983. https://doi.org/10.1105/tpc.112.096909.

[9] A. Mezzetti, J. Schnee, A. Lapini, M. Di Donato, Time-resolved infrared absorption spectroscopy applied to photoinduced reactions: how and why, Photochem. Photobiol. Sci. 21 (2022) 557–584. https://doi.org/10.1007/s43630-022-00180-9.

[10] C.B. De Carbon, A. Thurotte, A. Wilson, F. Perreau, Biosynthesis of soluble carotenoid holoproteins in Escherichia coli In Anabaena PCC 7120 In Synechocystis PCC 6803 In OCP producing E . coli, (n.d.) 1–11.

[11] M. Malferrari, F. Francia, G. Venturoli, Coupling between electron transfer and protein-solvent dynamics: FTIR and laser-flash spectroscopy studies in photosynthetic reaction center films at different hydration levels, J. Phys. Chem. B. 115 (2011) 14732–14750. https://doi.org/10.1021/jp2057767.

[12] M. Malferrari, A. Mezzetti, F. Francia, G. Venturoli, Effects of dehydration on light-induced conformational changes in bacterial photosynthetic reaction centers probed by optical and differential FTIR spectroscopy, Biochim. Biophys. Acta - Bioenerg. 1827 (2013) 328–339. https://doi.org/10.1016/j.bbabio.2012.10.009.

[13] M. Malferrari, G. Venturoli, F. Francia, A. Mezzetti, A new method for D2O/H2O exchange in infrared spectroscopy of proteins, Spectrosc. (New York). 27 (2012) 337–342. https://doi.org/10.1155/2012/791342.

[14] A. Mezzetti, W. Leibl, J. Breton, E. Nabedryk, Photoreduction of the quinone pool in the bacterial photosynthetic membrane: Identification of infrared marker bands for quinol formation, FEBS Lett. 537 (2003) 161–165. https://doi.org/10.1016/S0014-5793(03)00118-2.

[15] B. Fernández-González, G. Sandmann, A. Vioque, A new type of asymmetrically acting β-carotene ketolase is required for the synthesis of echinenone in the cyanobacterium Synechocystis sp. PCC 6803, J. Biol. Chem. 272 (1997) 9728–9733. https://doi.org/10.1074/jbc.272.15.9728.

[16] P. Chábera, M. Fuciman, P. Híbek, T. Polívka, Effect of carotenoid structure on excited-state dynamics of carbonyl carotenoids, Phys. Chem. Chem. Phys. 11 (2009) 8795–8803. https://doi.org/10.1039/b909924g.

[17] E. Kish, M.M.M. Pinto, D. Kirilovsky, R. Spezia, B. Robert, Echinenone vibrational properties: From solvents to the orange carotenoid protein, Biochim. Biophys. Acta - Bioenerg. 1847 (2015) 1044–1054. https://doi.org/10.1016/j.bbabio.2015.05.010.

[18] V. Šlouf, V. Kuznetsova, M. Fuciman, C.B. de Carbon, A. Wilson, D. Kirilovsky, T. Polívka, Ultrafast spectroscopy tracks carotenoid configurations in the orange and red carotenoid proteins from cyanobacteria, Photosynth. Res. 131 (2017) 105–117. https://doi.org/10.1007/s11120-016-0302-6.

[19] F. Muzzopappa, D. Kirilovsky, Changing Color for Photoprotection: The Orange Carotenoid Protein, Trends Plant Sci. 25 (2020) 92–104. https://doi.org/10.1016/j.tplants.2019.09.013.

[20] A.J. Aasen, S.L. Jensen, Carotenoids of flexibacteria. 3. The structures of flexixanthin and deoxy-flexixanthin., Acta Chem. Scand. 20 (1966) 1970–1988. https://doi.org/10.3891/acta.chem.scand.20-1970.

2.6 Supplementary Informations

2.6.1 Hydrogen/Deuterium isotopic exchange: protocol development

H/D isotopic exchange has been carried out as described in section Materials and Methods and schematically represented in **Figure SI 1. 2-1**. The exchange has been followed by IR spectroscopy, with reference to the downshift of the O-H stretching band, converted into the O-D stretching band (see **Figure SI 1. 2-1**). With the outlined protocol, a H/D exchange of about 60% has been reached.

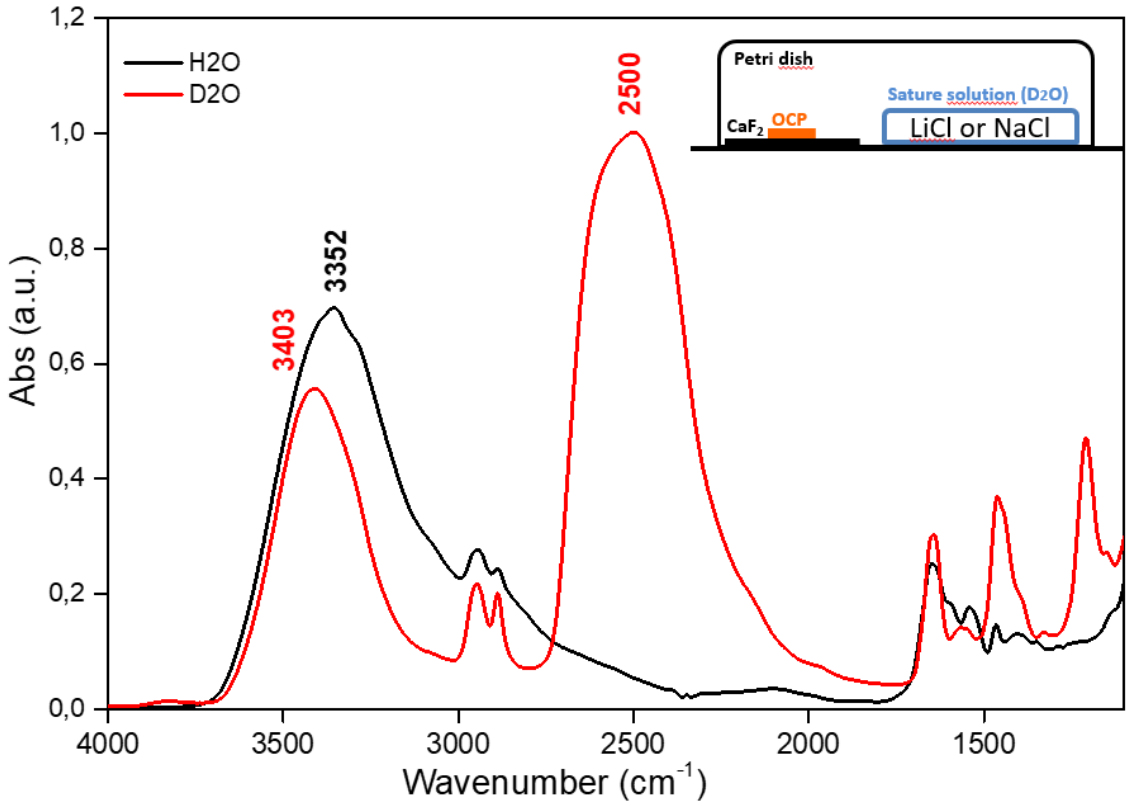

Figure SI 1. 2-1 IR absorbance spectra of OCP(CAN) in H_2O (black line) and in D_2O (red line). In the right, top, there is a simple scheme of the set-up used to perform the isotopic exchange.

2.6.2 Tentative band assignment of Echinenone

Tentative assignments based on DFT calculations on isolated echinenone (performed by Dr. R. Spezia, Laboratoire de Chimie Théorique, Sorbonne Université on a personal communication) is shown in **Figure SI 1. 2-2**

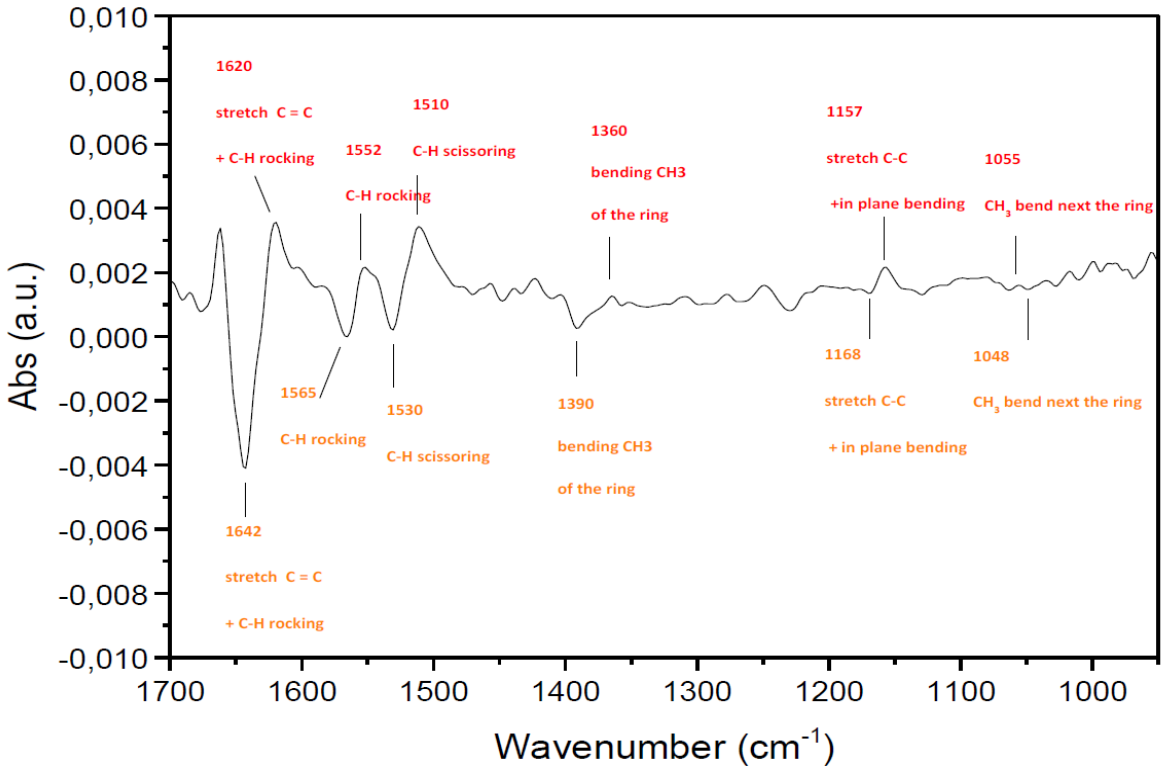

Figure SI 1. 2-2 Tentative band assignment for echinenone vibrations in light-minus-dark FTIR difference spectrum.

2.6.3 FT-IR spectrum of isolated Canthaxanthin

In the aim to perform the band assignment of OCP(CAN), the spectrum of isolated Canthaxanthin powder (purchased by Sigma Aldrich, >95%) was analysed to compare the absorbance bands (reported in **Figure SI 1. 2-3**) with the bands of the difference spectrum (see **Figure 2.8**).

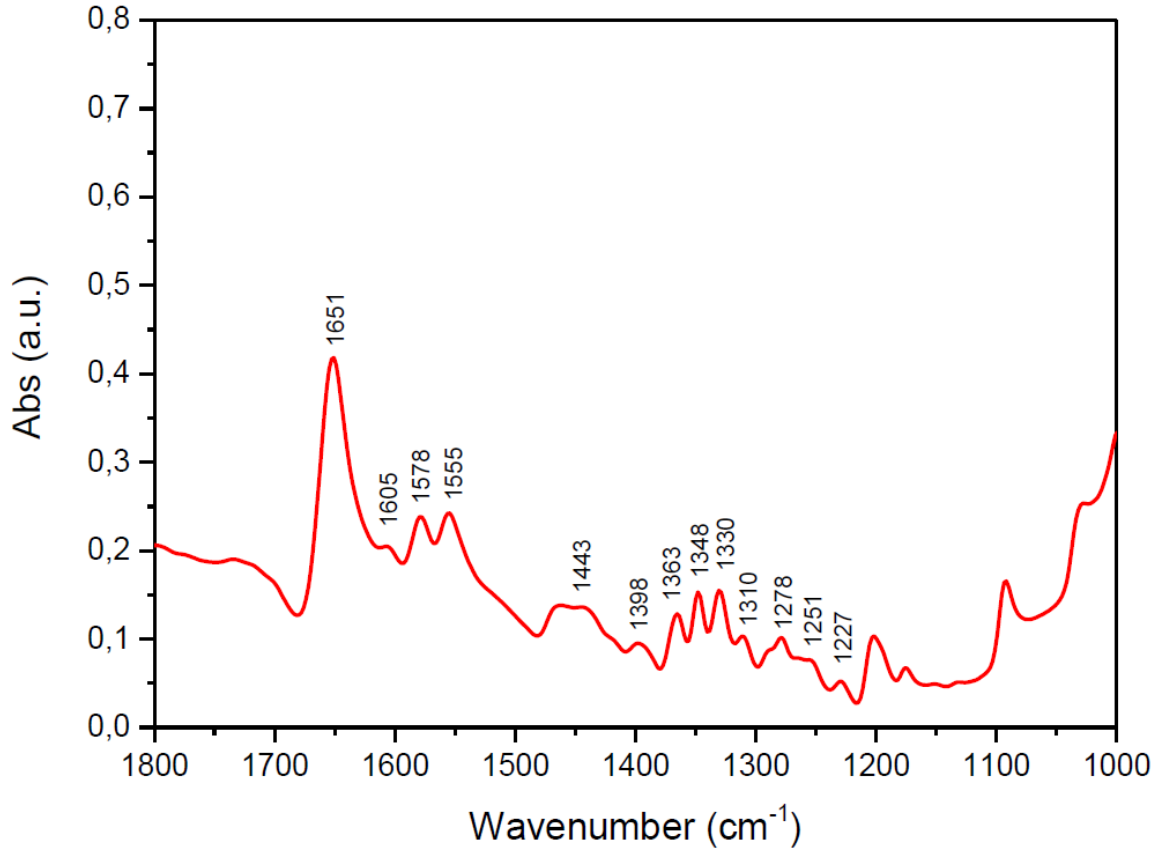

Figure SI 1. 2-3 FTIR absorbance spectrum of canthaxanthin in solid state.

2.6.4 Determination of OCP(CAN) hydration level by FT-IR absorbance spectroscopy

An aliquot of 30 µL of OCP(CAN) 70 µM has been dried on CaF_2 windows, under gentle N_2 flow, reaching different hydration levels. In the absence of a suitable protocol for the determination of the hydration level, FTIR spectroscopy has been used to measure the amount of water of the samples, with reference to the combination band of water (~ 5150 cm^{-1}). The increased hydration corresponded to an increased intensity of the combination band of water as like as an increase of the O-H stretching band in the region 3600-3400 cm^{-1}. Spectra are shown in **Figure SI 1. 2-4**.

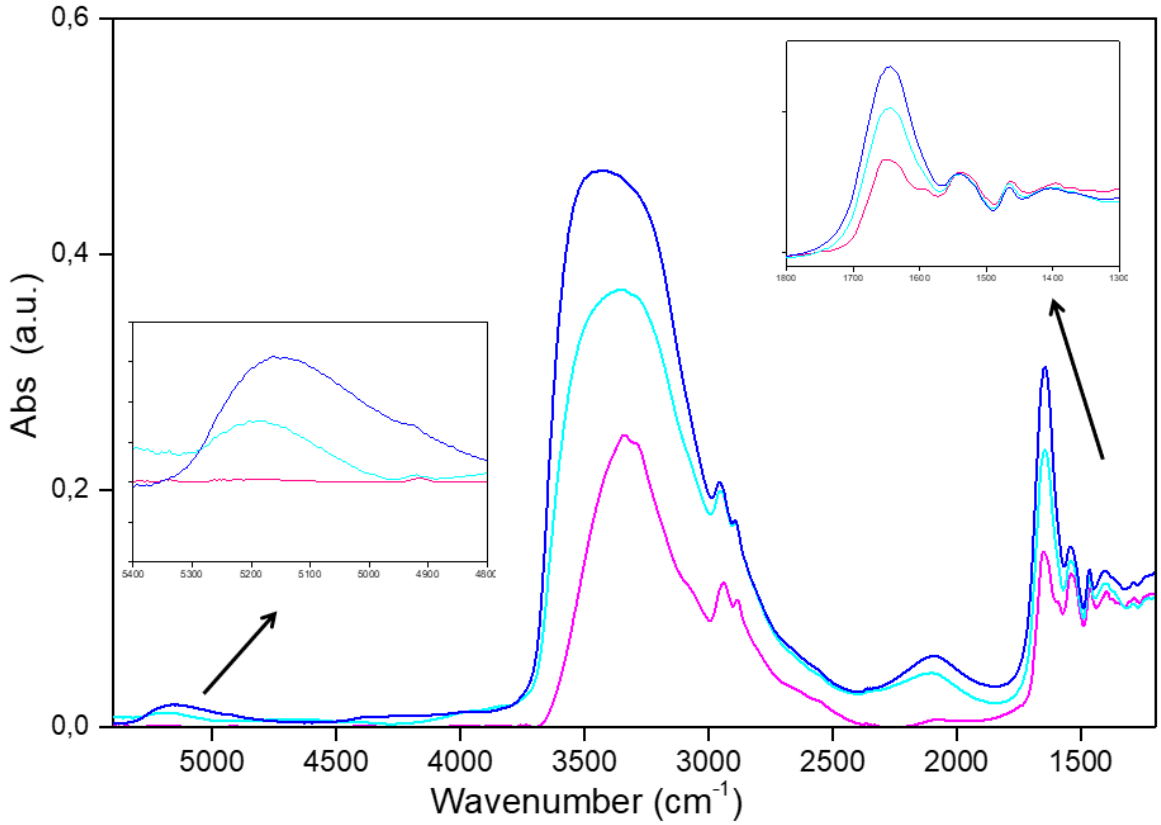

Figure SI 1. 2-4 FTIR absorbance spectra of OCP(CAN) solution at different level of hydration: (blue) high hydration, (cyan) middle hydration and (magenta) low hydration (dry sample). In the left box there is a zoom-in of the combination band region, while in the right box there is a zoom-in of the amide region of the spectrum.

2.6.5 Protein denaturation with Urea: Echinenone vs Canthaxanthin

In the framework of collateral experiments, tests of OCP denaturation by Urea have been carried out. As shown in **Figure SI 1. 2-5**, both OCP(ECN) and OCP(CAN) were not denatured by Urea 6 M. Furthermore, some differences between the two types of OCP were observed. Indeed, if OCP(ECN) kept the orange conformation once in contact with Urea, within 6 hours of observation, OCP(CAN) was converted in the red form after only 2 hours. This could support the thesis that the second carbonyl moiety of canthaxanthin, compared to echinenone, makes OCP(CAN) more stable in the red form.

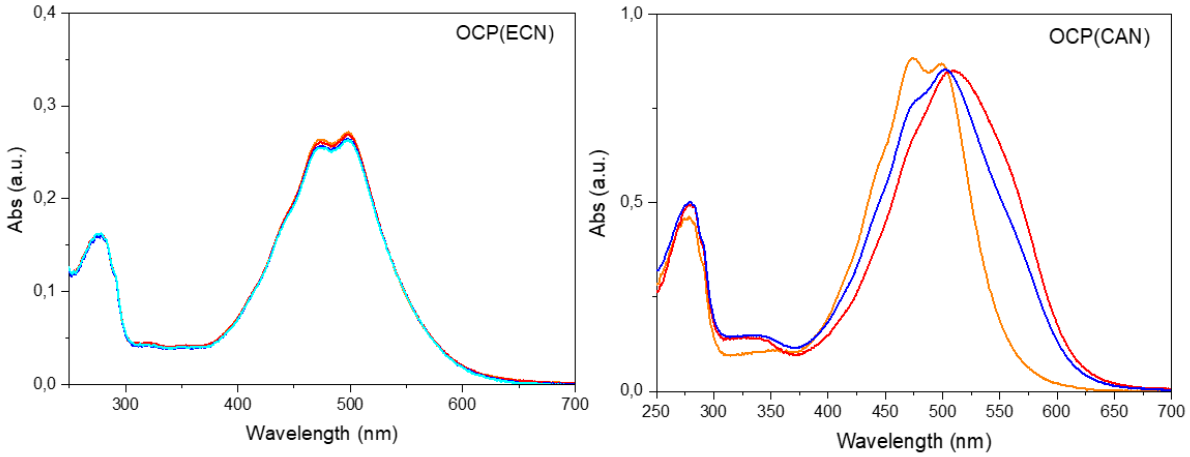

Figure SI 1. 2-5 UV-Visible spectra of OCP(ECN) 0.2 mg/mL (left, orange line) and OCP(CAN) 0.8 mg/mL (right, orange line) in water. Same solutions were reproduced in Urea 6 M. Samples kept inside the cuvette, in the dark, and spectra recorded after 30 min (blue line), 2h (red line) and (only in case of OCP(ECN)) after 6h (cyan line).

3. OCP immobilization on mesoporous silica SBA-15

3.1 Introduction

Structured mesoporous materials have always been considered of great interest for their advantageous properties such as highly reproducible structure with narrow pore size distribution, wide pore diameter range, high surface area and pore volume[1,2]. These structural and textural peculiarities let Ordered Mesoporous Materials (OMMs) be considered for applications involving proteins and enzymes because they promise to be solid supports able to preserve the stability of these biological systems[3,4]. The immobilization of proteins together with the stabilization of their native conformation after the interaction with mesostructured surfaces is increasingly considered for a wide range of nanobiotechnological applications such as biocatalysis, sensoring, nanomedicine and tissue engineering[3,5–7]. These applications depend on protein adsorption, whose uptake capacity is shown to be strongly correlated with the protein size, mesopore diameter and pore volume[1,8–10].

Among the numerous mesoporous materials described in the literature for their ability to immobilize proteins[11], SBA-15 (Santa Barbara Amorphous) was chosen as inorganic support for OCP. This nano-porous material, synthesized for the first time in 1998[12], is an ordered mesoporous silica material with hexagonal pores whose size can be tuned from 2 and 50 nm wide and from 200 nm up to a few μm long. Smaller micropores connect mesopores with each other[13]. It is characterized by highly uniform porosity, good mechanical stiffness, thermal stability, a high pore volume and a large specific surface area. The structural parameters of SBA-15, such as diameter of pores and micro-porosity can be modified by tuning parameters of its synthesis[14]. Besides to the possibility to adjust the pore size, the ability to modify the surface properties of these materials to match the targeted biomolecules can provide higher protein immobilization capacity[11,15]. Numerous biomedical applications in small molecules or protein delivery, including drug targeting strategies have consequently gained attention[16–18].

In OCP a keto-carotenoid (3-hydroxyechinenone, echinenone (ECN) or canthaxanthin (CAN)) is embedded but non-covalently linked between two structural domains of OCP (called N-terminal domain – NTD and C-terminal domain – CTD) and is therefore only sparingly solvent accessible. Carotenoids thus play a key role in the mechanism of photoprotection of cyanobacteria. Because OCP is a water-soluble protein, it could be a suitable delivery vector of carotenoids. One suitable option to protect OCP (e.g., from enzymatic degradation of harsh pH conditions) and to modulate the carotenoid delivery conditions would be to encapsulate OCP into a mesoporous inorganic material. It should be mentioned that beside its use as antioxidant,

several applications of OCP have been recently proposed, ranging from its use as optical switch and photoprotective element[19] to regulator of fluorescence in biosensors[20,21]. Furthermore, not only different kind of OCP (with different properties) have been identified[22], but also several homologs of NTD and CTD domains exist[23], so that artificial OCP-like protein can be constructed[24]. This, along with genetic engineering techniques[21,25] can make it possible to develop photoactivable and photochromic caroteno-proteins with tailored properties[26].

The aim of this study (graphically explained in **Figure 3.1**) is thus to immobilize OCP on a mesoporous SBA-15 to study the influence of structural and textural features of SBA-15 on the chemical properties of OCP and to assess the photochromic behaviour of the immobilized protein and its stability in time, aiming to the development of photo-sensitive nano-devices. SBA-15 with two different pore sizes, namely SBA-15-80 and SBA-15-120, is used to assess a possible effect of the confinement of OCP inside the pores in terms of protein loading but also the influence of surface interactions on protein structure and dynamics. To modulate the interaction between SBA-15 and the protein, the material has been functionalized with covalently bound aminopropyl groups (SBA-15-NH_2) which are likely to influence the electrostatic interactions between the solid and the protein, and consequently the OCP immobilization yield by adsorption. In addition, a modified surface may also interfere with the photoactivation process of the protein. The result is a photochromic nanomaterial that would be exploited as optical sensor (see OCP in SBA-15 as optical sensor, in this Chapter) or as photo-switch for nanoparticles with tuneable fluorescence (see Chapter 4).

This chapter, that takes origin from an article submitted to the journal Microporous Mesoporous Materials (and accepted on May 19, 2022), demonstrates that the OCP@SBA-15 system can be used as a photochromic material and as a possible optical device for nanoscale applications. Finally, this work is a first step towards the development of caroteno-protein and carotenoid release-strategies from silica matrix to be applied in the field of antioxidant drug delivery.

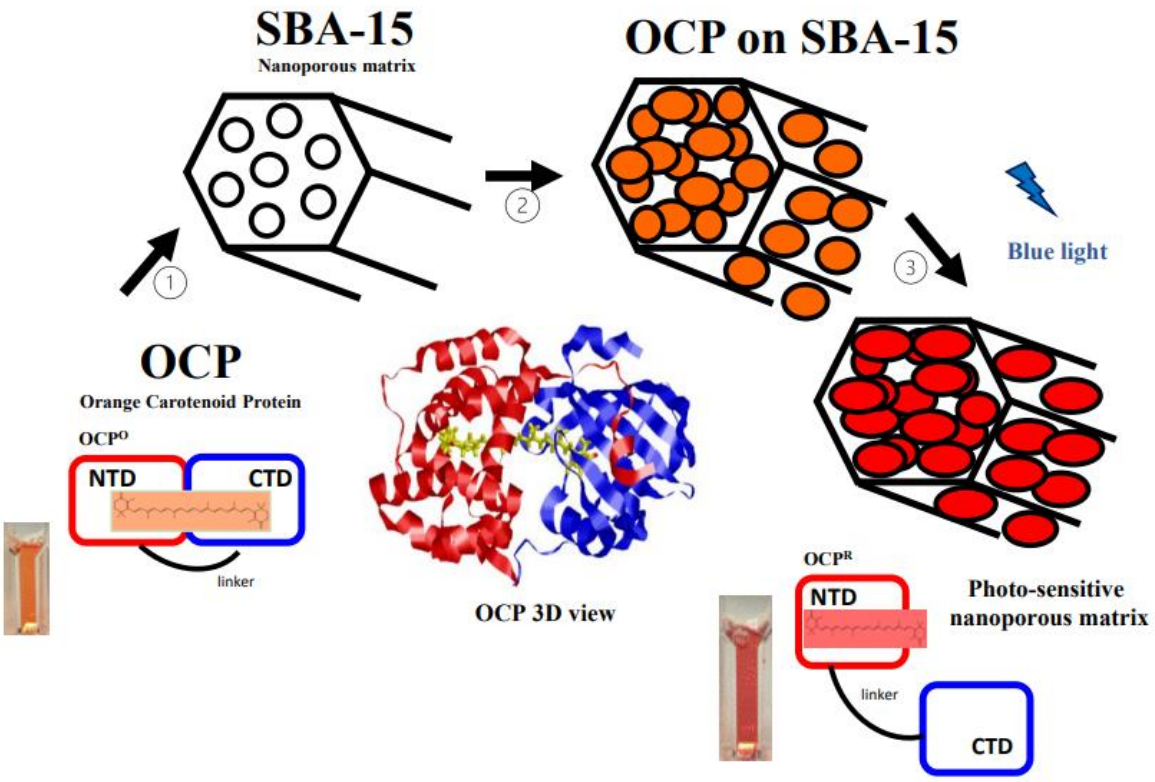

Figure 3.1 Schematic representation of OCP immobilization on SBA-15. 1-2) OCP immobilization on nano-porous matrix SB-15; 3) Photoactivation of the OCP upon blue light and development of photo-sensitive nano-porous matrix.

3.2 Synthesis and functionalization of SBA-15 matrices

3.2.1 Materials

SBA-15 was synthesized as reported in the literature using a triblock copolymer, Pluronic P123 ($(EO)_{20}(PO)_{70}(EO)_{20}$ from Aldrich) as structure directing agent[12]. In a typical synthesis 8.02 g of P123 and 16.80 g of tetraethyl-orthosilicate (TEOS; Aldrich; 98%) as silica precursor were used, so that around 4 g of SBA-15 material was obtained after the final calcination step at 550°C. Amino-functionalization of SBA-15 was performed as reported[27] and detailed in the 3.2.2.1 using aminopropyltriethoxysilane (ATPES; Aldrich; 99%) as organic reagent.

3.2.2 Methods

3.2.2.1 SBA-15-80 and SBA-15-120 synthesis procedure

SBA-15 was synthesized as reported in the literature using a triblock copolymer, Pluronic P123 ($(EO)_{20}(PO)_{70}(EO)_{20}$ from Aldrich) as a structure directing agent[200]. In a typical synthesis 8.02 g of P123 were mixed under stirring (750 rpm) with 280 mL of 0.1 mol/L HCl for 2 hours at 40°C until complete dissolution of P123 and the creation of a mesostructured phase of micelles. Then 16.80 g of tetraethyl-orthosilicate (TEOS; Aldrich; 98%) as silica precursor was added drop by drop to the solution under slower stirring (ca. 500 rpm). The resulting suspension has been let under stirring for 24 hours to allow the formation of a mesostructured silica sol-gel. The sol-gel suspension has then been transferred into a 1 L glass bottle and hydrothermally treated for 24 hours at 80°C or 120°C. The temperature of the hydrothermal synthesis identifies the nano-porosity of the matrix and is used to distinguish the two matrices (SBA-15-80 for silica synthesized at 80°C and SBA-15-120 for silica synthesized at 120°C). Finally, the obtained solid was filtrated and thoroughly washed with distilled water (approx. 4 L) to remove the P123 polymer. The resulting powder has been dried at 80°C or 120°C overnight and calcined at 550°C (heating ramp: 0.4°C/min) for 6 hours under air to remove the template. Finally, around 4 g of SBA-15 material was obtained.

3.2.2.1 Amino-functionalization of SBA-15 matrices

Prior to the functionalization, 1g of SBA-15 has been placed in a reactor and activated at 350°C (heating ramp: 5°C/min) for 3 hours under 50 mL/min air flow (Air Liquide). Silica has been then transferred into a dried balloon equipped with a septum. 50 mL of commercial anhydrous toluene (VWR, 99.9%) have been added to silica. The balloon has been then flushed with argon for few minutes and then let for 5 minutes in ultrasonic bath to get a perfect silica suspension. The balloon has been finally connected to a refrigerator and placed under argon flow. To start the functionalization reaction, 1 mL of 3-aminopropyltriethoxysilane (ATPES; Aldrich; 99%) has been added to the suspension drop by drop. Then, Argon flow stopped, the suspension has been stirred for 1 hour at room temperature and then for 24 hours refluxing (120°C). Finally, the mixture has been filtrated on Büchner and filter paper and washed with 30 mL of anhydrous toluene (VWR, 99.9%), 30 mL of acetonitrile (VWR; HPLC grade) and 30 mL of absolute ethanol (Aldrich; 99.9%). The resulting solid has been dried at 60°C over-night. The excess of

APTES has been extracted with Soxhlet apparatus, introducing 50 mL of CH_2Cl_2 (Carlo Erba Reagents; 99.9%) in a balloon and refluxing the system at 45°C for 24 hours. Finally, the functionalized silica has been dried at 60°C over-night.

3.3 Surface characterization

3.3.1 Methods

3.3.1.1 X-Ray Diffraction

The X-ray diffraction has been used to identify crystalline structure of the pure and functionalized SBA-15. Analysis have been performed from 0.4° to 5° (2θ) in steps of 0.01° with a count time of 90 s for each point. The Cu K_α (λ = 1.5418 Å) was the source of X-ray radiation. The XRD analysis have been performed using a Shimadzu XRD-6000 (Japan) X-ray diffractometer.

3.3.1.2 Electron microscopy

The morphology of the solids was investigated with a high-resolution SEM-FEG Hitachi SU-70 operating at an acceleration voltage of 1.0 kV and at a working distance of 3 mm. Transmission electron microscopy (HRTEM) was performed on a JEOL JEM 1011 (W) microscope operating at 100 kV and equipped with an ORIUS Gatan Camera. For TEM observations, the sample powders were deposited on a 3 mm copper grid coated with an amorphous carbon film. The samples were prepared by dispersion in pure alcohol using ultrasonic cleaner and putting a drop of this suspension on carbon films on copper grids.

3.3.1.3 N_2 physisorption

The specific surface area, pore size distribution and total pore volume of SBA-15 and SBA-15-NH_2 before and after adsorption of OCP were determined by recording nitrogen adsorption isotherms. Prior to the experiment, a degassing pre-treatment has been applied to the samples: empty SBA-15 was dehydrated at 120°C overnight while SBA-15-NH_2 and OCP loaded SBA-15 were dehydrated at 40°C for 30 minutes then at 60°C for other 30 minutes under vacuum. Such low temperature pre-treatment has been chosen to prevent thermal degradation of the grafted aminopropyl group or/and adsorbed protein. As a control, the same degassing pre-treatment at low temperature was used with OCP immobilized on SBA-15 and on SBA-15 treated with water but in absence of OCP, to allow the comparison between samples with or

without protein. Indeed, pre-treatment at low temperature does not completely remove water from micropores and this could affect the comparison. Nitrogen adsorption isotherms at -196°C were measured on BELSORP max apparatus. The specific surface area was obtained by using the Brunauer – Emmett – Teller equation from adsorption values at six relative pressures (P/P_0) ranging from 0.04 to 0.25. The total pore volume was determined from the amount of N_2 adsorbed at P/P_0= 0.975. The diameter of mesopores was obtained from the pore size distribution calculated using the Barrett – Joyner – Halenda (BJH) equation applied to the desorption branch of the isotherm.

3.3.1.4 Thermogravimetric analysis

The TGA has been used to characterize the weight loss due to absorption/desorption of OCP but also to estimate the amount of aminopropyl group grafted during the SBA-15 functionalization. TGA analysis have been performed on STD Q600 thermobalance (TA Instrument). The weight loss has been measured while heating from 30 to 700°C (heating rate 5°C/min) under air flow (100 mL/min).

3.3.2 Results and discussion

3.3.2.1 SBA-15-80 vs SBA-15-120

Two SBA-15 type solids were synthesized by tuning the aging temperature at 80 and 120°C. Consequently, these materials are denoted as SBA-15-80 and SBA-15-120, respectively, hereafter in the text. Their structural and textural properties are summarized in **Table 3.1**. The XRD pattern (**Figure 3.2**, a) confirmed that SBA-15 with well-ordered 2D hexagonal pores was obtained in both cases: for SBA-15-80 a single high-intensity peak at $2\Theta = 0.89°$ and two additional smaller peaks, at $2\Theta = 1.53°$ and 1.76° can be attributed to (100), (110) and (200) diffraction planes of a hexagonal lattice of p6mm symmetry. For SBA-15-120, the peaks are slightly shifted to $2\Theta = 0.97°$; 1.60° and 1.84° and an increase of the SBA-15 cell parameter (a_0) was observed (**Table 3.1**). Such an influence of aging temperature on crystal parameters was already reported in the literature[28–31] and interpreted as a result of the shrinking of the SBA-15 structure during the calcination step after an aging step at lower temperature[30]. The length of the hexagonal cell unit a_0 was calculated using the XRD (100) interplanar spacing value, namely d_{100}. A large pore wall thickness W larger than 4 nm, according to the formula $W= a_0-D_{BJH}$ is thus observed for both solids (**Table 3.1**).

To complete XRD analysis, SBA-15 type materials have been studied by Scanning Electron Microscopy (SEM) and Transmission Electron Microscopy (TEM). According to the SEM images (**Figure 3.2**, b), SBA-15 particles present a worm shape morphology with a width of about 0.2 to 0.4 µm and a length of 1 to 2 µm. In addition, TEM images of SBA-15 (**Figure 3.2**, d) clearly show a well-ordered material with perfectly aligned silica walls and pores.

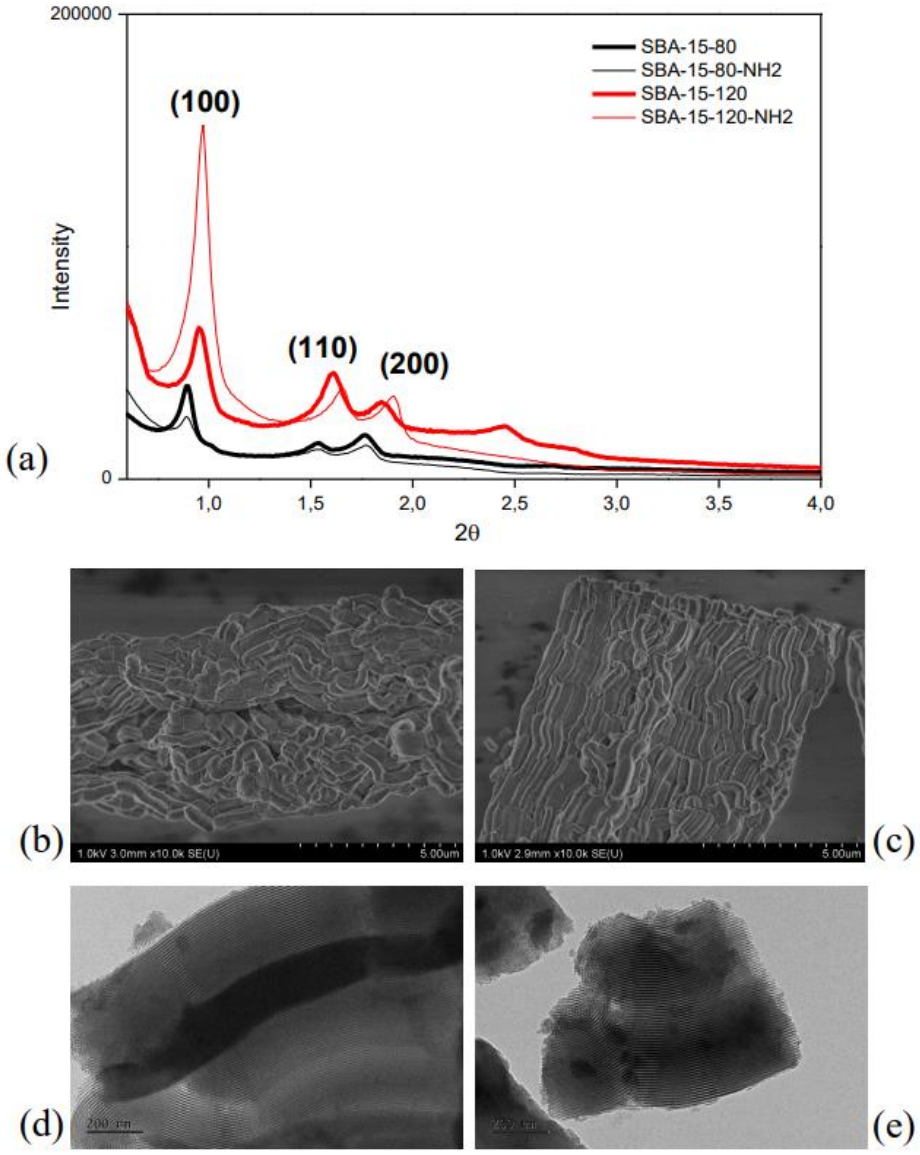

Figure 3.2 (a) XRD powder pattern of SBA-15 and SBA-15-NH_2 materials prepared at 80°C or 120°C as aging temperature; (b) and (c) SEM images of SBA-15-80 and SBA-15-80-NH_2; (d) and (e) TEM images of SBA-15-80 and SBA-15-80-NH_2.

The nitrogen adsorption-desorption isotherms at 77 K (**Figure 3.3**) are of type IV according to the IUPAC classification and exhibited a H1-type hysteresis loop with parallel adsorption and

desorption branches which is typical of mesoporous materials with cylindrical channels in a hexagonal arrangement[32,33].

For relative pressure (P/P_0) in the range from 0.7 to 0.8, isotherms exhibit a steep slope characteristic of capillary condensation of nitrogen within uniform mesopores, where the P/P_0 position of the inflection point is correlated to the diameter of the mesopores.

Depending on the aging temperature during the synthesis, materials pore size increased from 5.8 nm to 7.7 nm when aging at 80 and 120°C respectively (the textural properties for SBA-15 samples are summarized in **Table 3.1**). The effect of increasing the aging temperature thus led to an increase of the pore diameter, as extensively reported in the literature[12,32,34,35]. The rise of temperature during hydrothermal synthesis indeed induces an increase of the aggregation number of the surfactant (P123), and consequently of the volume of the formed micelles, leading to an increase of pore size[1]. In their pioneer work dealing with SBA-15 synthesis, Zhao *et al* obtained a solid with an 8.9 nm mean pore diameter after aging at 100°C for 48 hours while very similar TEOS hydrolysis and gel ripening conditions were used in the present work. A shorter aging duration, e.g., 24 hours used in the present work could explain the difference in the pore diameter. The BET surface areas of SBA-15-80 and SBA-15-120 were found to be 759 and 576 m^2/g, respectively, in good agreement with the literature[2,34,36–40]. Such an inverse correlation between the pore size and the material surface is indeed as a consequence of the cylindrical shape of the mesopores[2].

Adsorbent Name	**Aging temperature (°C)**	**d_{100} (nm)**	**a_0 (nm)**	**D_{BJH} (nm)**	**SA_{BET} (m^2/g)**	**PV (cm^3/g)**
SBA-15-80	80	9.92	11.5	5.8	759	0.90
SBA-15-80-NH_2	80	9.92	11.5	5.4	344	0.52
SBA-15-120	120	10.51	12.1	7.7	576	1.22
SBA-15-120-NH_2	120	10.64	12.3	6.7	312	0.69

Table 3.1 Properties of SBA-15 used for OPC adsorption studies. Where d_{100} is the interplanar spacing; a_0 the unit cell parameter ($a_0 = 2\times d_{100}/\sqrt{3}$); SA_{BET} is the BET surface area; PV the pore volume calculated at $P/P_0 = 0.975$.

3.3.2.1 SBA-15-80-NH_2 vs SBA-15-120-NH_2

To modify the physio-chemical properties of the solid surface to influence the subsequent protein immobilization efficiency, which is the main objective of this study, SBA-15 was grafted with 3-aminopropyltriethoxysilane (APTES) by a post-synthesis modification of the

SBA-15 silanol groups. XRD pattern of SBA-15-NH_2 was very similar to the one of SBA-15 prior to its functionalization, thus evidencing that the functionalization of the SBA-15 surfaces with –NH_2 groups did not affect the crystalline structure of the mesoporous material (**Figure 3.2**, a). This is confirmed by SEM and TEM images. Indeed, the functionalized SBA-15 particles (**Figure 3.2**, c) present the same size and morphology as the bare SBA-15 (**Figure 3.2**, b). In addition, comparison of TEM images of bare SBA-15 (**Figure 3.2**, d) and SBA-15-NH_2 (**Figure 3.2**, e) clearly evidenced that the functionalization step does not induce any modification of the meso-structuration of silica support.

Furthermore, the nitrogen sorption isotherms of organo-functionalized SBA-15-NH_2 samples (**Figure 3.3**, a-b) show the same type IV isotherms and type H1 hysteresis loop as the un-grafted SBA-15 ones. Functionalization unequivocally results in reduced pore sizes compared to the un-functionalized materials, as indicated by the pore size distribution curves (**Figure 3.3**, c-d). The mean pore size varies from 7.7 to 6.7 for SBA-15-120-NH_2, and from 5.8 to 5.4 form SBA-15-80 in line with literature results[41]. The decrease of the pore diameter is likely to be a consequence of the presence of the space filling grafted 3-aminopropyl groups, which is corroborated by the decrease of the total pore volume after APTES grafting (**Table 3.1**) [38,42]. The quantification of the number of organic moieties grafted on SBA-15 was performed by thermogravimetric analysis (TGA). For SBA-15-80 one major weight loss event (around 10 %) was observed in the temperature range between 300 and 700°C (**Figure 3.3**, e) which can be ascribed to the loss of aminopropyl groups[39,40] and allowed to estimate the density of NH_2 groups grafted on SBA-15-80-NH_2 to 1.72 mmol/g (or 1.36 –NH_2 groups/nm^2). For SBA-15-120 one major weight loss (around 18 %) event was observed in the temperature range between 300 and 700°C (**Figure 3.3**, f) which allowed estimating the density of NH_2 groups grafted on SBA-15-120-NH_2 to 3.1 mmol/g (or 3.2 –NH_2 groups/nm^2).

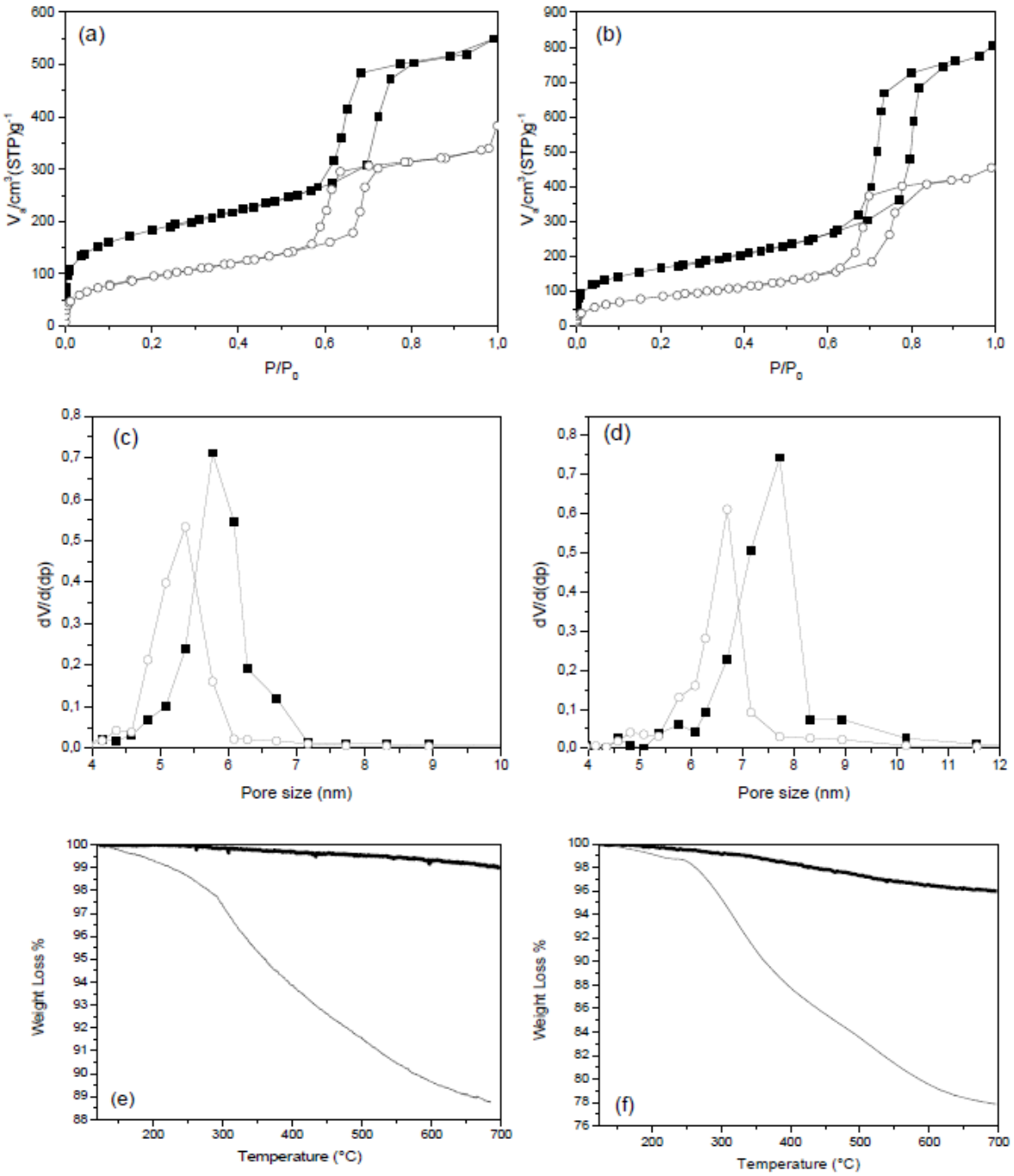

Figure 3.3 (a) N_2 adsorption isotherm of the bare SBA-15-80 (full square) and the functionalized SBA-15-NH_2 (open circle); (b) N_2 adsorption isotherm of the bare SBA-15-120 (full square) and the functionalized SBA-15-NH_2 (open circle). (c) Pore size distribution calculated on SBA-15-80 (full square) and functionalized SBA-15-NH_2 (open circle); (d) Pore size distribution calculated on SBA-15-120 (full square) and functionalized SBA-15-NH_2 (open circle). (e) TGA analysis of SBA-15-80 and (f) SBA-15-120 before (thick) and after (thin) –NH_2 functionalization.

3.4 OCP immobilization on SBA-15 surface

3.4.1 Methods

3.4.1.1 Z potential

Measures of ζ potential at different pH were performed to work out the best condition for OCP adsorption. Tests concerns SBA-15-80, SBA-15-120, SBA-15-80-NH_2 and OCP(CAN) in solution or immobilized on SBA-15-80-NH_2. As shown in **Figure 3.4** and reported in **Table 3.2**, SBA-15-80 and SBA-15-120 hovers round zero at pH 6, while SBA-15-80-NH_2 is positively charged at pH lower than 8. OCP(CAN) in solution hovers round zero at pH 6 and the influence of the matrix at this pH value has been tested resulting in a ζ potential slightly negative for OCP(CAN) in SBA-15-80-NH_2. From these tests we deduce that the best condition to work out the interaction OCP–SBA-15 is at pH 6.

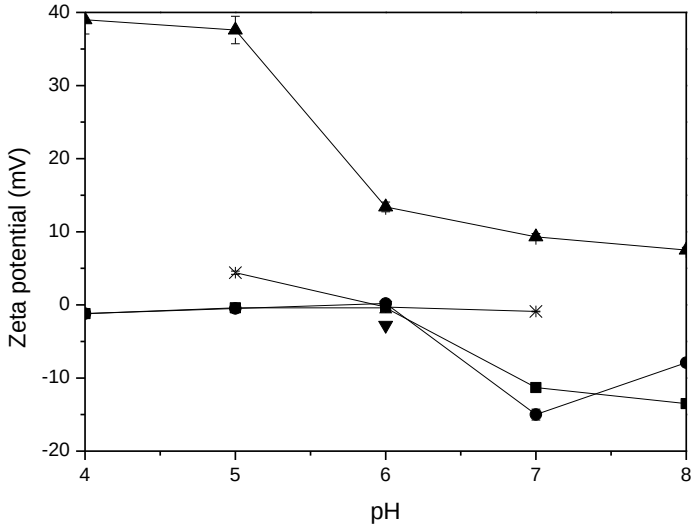

Figure 3.4 Determination of ζ potential of SBA-15-80 (solid square), SBA-15-120 (solid circle), SBA-15-80-NH_2 (solid up triangle), OCP(CAN) 0.2 mg/mL in solution (cross), OCP in SBA-15-80-NH_2 (solid down triangle).

ζ potential (mV)	**SBA-15-80**	**SBA-15-80-NH_2**	**SBA-15-120**	**OCP(CAN) 0.2mg/mL**	**OCP in SBA-15-80-NH_2**
pH = 4	-1,2	39	-1,2		
pH = 5	-0,4	37,6	-0,5	4,4	
pH = 6	-0,4	13,4	0,2	-0,3	-2,8
pH = 7	-11,3	9,3	-15	-0,9	
pH = 8	-13,5	7,5	-7,9		

Table 3.2 Values of ζ potential (mV) reported at different pH for each sample.

3.4.1.2 OCP immobilization protocol

Typically, 1 mL of a 0.2 mg/mL OCP solution in water was mixed with 10 mg silica powder. The mixture (pH 8.5) was incubated under gentle stirring for 4 hours (except for time course experiments) at room temperature in the dark, to avoid the photo-activation of the protein. The initial concentration of OCP or the stirring duration of the suspension varied for the adsorption isotherm and kinetics experiments. IE (immobilization efficiency) of OCP has been calculated by measuring the supernatant absorbance Abs_{supnat} at 474 nm and subtracting this value from the initial OCP absorbance, as shown in (2):

(2) $$IE\ \% = \frac{Abs_{OCP} - Abs_{supnat}}{Abs_{OCP}} \times 100$$

3.4.1.3 Leaching extent of OCP(CAN) from SBA-15-80 and SBA-15-80-NH_2

To study the release of OCP from silica matrices, two different procedures were used. Firstly, the ionic strength effect was tested: OCP (1 mg/mL) immobilized on 10 mg of silica was suspended in 5 mL of NaCl solution 1 M, the mixture (pH 6.9 for SBA-15-80 sample and pH 8.4 for SBA-15-80-NH_2) was gently stirred at room temperature in the dark. Leaching extent has been calculated by measuring the supernatant absorbance at 474 nm each 24h, for 1 week. Furthermore, pH effect was tested: OCP (1 mg/mL) immobilized on 10 mg of SBA-15-80-NH_2 was suspended in 5 mL of Acetic acid/Acetate buffer 50 mM (pH 4.3) to have either OCP or SBA-15-NH_2 positively charged; the mixture (pH 4.2) was gently stirred at room temperature in the dark. In parallel, OCP immobilized on 10 mg of SBA-15-80 was suspended in 5 mL of Phosphate buffer 50 mM (pH 7.3) to have either OCP or SBA-15 negatively charged; the mixture (pH 6.9) was gently stirred at room temperature in the dark. Leaching extent has been calculated by measuring the supernatant absorbance at 474 nm each 24h, for 1 week.

3.4.1.4 UV-visible spectroscopy in liquid and solid phase

Absorption spectra of solids were recorded on a Varian 2300 UV Vis spectrophotometer equipped with an integrating sphere between 350 and 750 nm with a resolution of 1 nm and an acquisition time of 0.1 s per point. Absorption spectra in liquid phase were recorded on Biochrom Libra S60 spectrophotometer, between 350 and 750 nm with a resolution of 0.5 nm and an acquisition time of 0.1 s per point.

3.4.2 Results and discussion

3.4.2.1 OCP on SBA-15 equilibration time

OCP was adsorbed on four different mesoporous silica matrices: SBA-15-80, SBA-15-120 and their derivatives functionalized with amino groups. Two OCPs were studied, which contained two different carotenoids, namely echinenone (ECN) and canthaxanthin (CAN). Only these ketocaroteno-proteins (in addition to 3-hydroxyechinenone, 3h-ECN) make OCP photoactive[43,44].

OCP was immobilized on SBA-15 by adsorption on the solid support. The kinetics of the adsorption process was studied with OCP(CAN) and showed that the amount of immobilized OCP on both SBA-15-80 and SBA-15-80-NH_2 silica materials increased with time from 0 to 4 hours (**Figure 3.5**). Then, a plateau was reached for SBA-15-80 as well as for SBA-15-80-NH_2 although a slight decrease of the protein uptake was observed for the latter solid after a 24h long experiment. However, it could be concluded that the equilibrium was almost reached after around 4 hours for both materials.

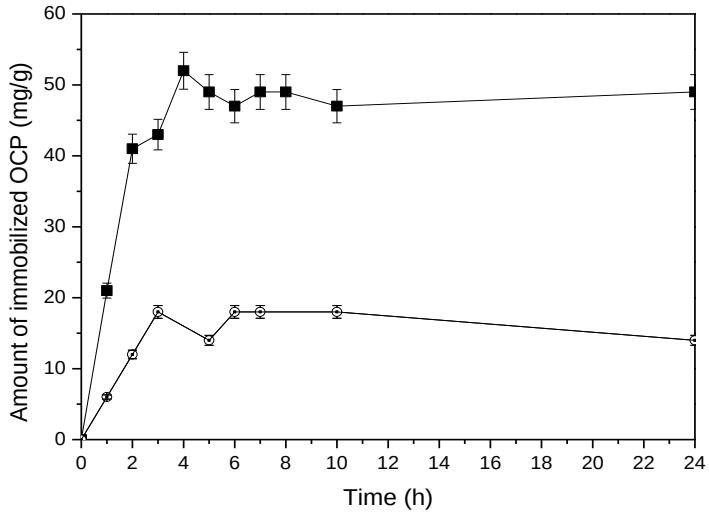

Figure 3.5 OCP(CAN) adsorption on SBA-15-80 (full square) and SBA-15-80-NH_2 (open circle) followed-up in time. Initial OCP(CAN) concentration 2 mg/mL (50µM).

3.4.2.2 OCP adsorption isotherms on SBA-15

The loading efficiencies of OCP(CAN) and OCP(ECN) are shown in **Figure 3.6** and **Table 3.3**. The OCP adsorption behaviour on SBA-15-80 as a function of the initial protein concentration

(**Figure 3.6**) follows a typical isotherm adsorption profile on solids, with an increase of the amount of immobilized protein when increasing the initial protein concentration. At the maximum tested initial OCP(CAN) concentration, namely 2 mg/mL, the protein loading reached 52 mg/g of solid. As an attempt to provide an alternative measurement of the protein uptake, thermogravimetric analysis has been also performed, showing a weight loss of 88 mg/g between 120 and 700 °C (**Figure SI 1. 3-1** at the end of this chapter). The overestimation of the protein loading from thermogravimetry analysis compared to absorbance measurements of the solution could arise from the presence of water bound to the protein and released from the support at higher temperatures than free water, thus increasing the overall weight loss. Thermogravimetric analysis was consequently not further used for OCP uptake quantification. In the whole range of protein initial concentration tested, as the slope of the adsorption isotherm remains positive, it is expected that maximum loading capacity of SBA-15-80 was not reached, in line with results reported in the literature for several other proteins such as lysozyme, bovine serum albumin, glucose oxidase, cytochrome c or myoglobin whose loading capacity was shown to reach several hundreds of mg/g of SBA-15 or SBA-15-type mesoporous silicas[1,2,34,36,38,41,45,46].

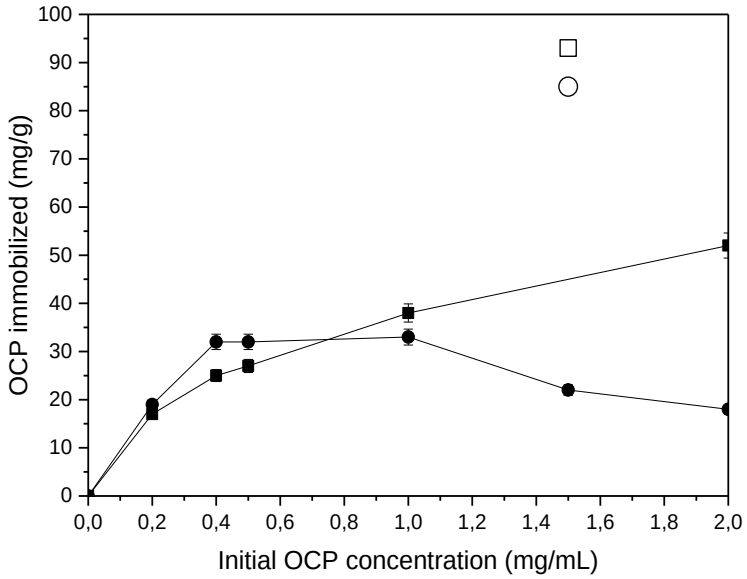

Figure 3.6 OCP(CAN) adsorption isotherms on SBA-15-80 (solid square) and SBA-15-80-NH_2 (solid circle). OCP(CAN) adsorption isotherms on SBA-15-80 under blue light LED (open square) and SBA-15-80-NH_2 (open circle).

Size of the protein relative to the one of the SBA-15 pores as well as electrostatic interactions with the solid surface being two main parameters governing the adsorption efficiency, it is

worth taking account of the latter parameters with the ones of OCP for a more accurate comparison. Indeed, lysozyme (molecular weight 15 kDa) was found to adsorb in larger amount on SBA-15 (450 mg/g of solid) than bovine serum albumin (molecular weight 66.5 kDa) whose maximum uptake capacity on the same support was limited to 58 mg/g[47]. OCP has a molecular weight around 35 kDa, so that its maximum binding capacity on SBA-15-80 is expected to be lower than the one of lysozyme, a smaller protein, but higher than the one of bovine serum albumin, a larger protein. The large SBA-15-80 uptake capacity of lysozyme reported in the work of Sang *et al.*[47] also originates in favourable electrostatic interactions between the silica surface and the protein since the pH of the solution was chosen to be equal to the isoelectric point of lysozyme (pH 11) in order to minimize repulsion between protein molecules and consequently this favours a close packing of the protein inside the mesopores[1,41,48,49]. In the present work, the pH of the protein solution was around 8.5 (storage pH of OCP after its purification process). In such conditions, OCP, whose isoelectric point (pI) value is around 5.4, is negatively charged. The unfavourable interactions with the silica surface, whose zeta potential is negative for pH >2 due to the deprotonation of the silanol groups[37], are thus likely to limit the protein uptake. The amount of absorbed protein varied in these conditions from around 16 mg/g of SBA-15 for OCP(CAN) to 19 mg/g for OCP(ECN). Overall, the obtained protein loading on SBA-15 was suitable for the further photosensitivity analysis, which are the main objectives of the study, even at the lowest OCP initial concentration tested, e.g., 0.2 mg/mL.

Immobilization Efficiency	**SBA-15-120**	**SBA-15-120-NH_2**	**SBA-15-80**	**SBA-15-80-NH_2**
OCP(ECN)	93%	95%	71.7 ± 2.8 %	84.1 ± 6.5 %
OCP(CAN)	80%	85%	83.0 ± 1.1 %	94.9 ± 5.4 %

Table 3.3 Immobilization efficiency % of OCP(ECN) and OCP(CAN) in SBA-15120 and SBA-15-80 and the corresponding functionalized SBA-15-NH2. OCP initial concentration: 0.2 mg/mL. The experimental error has been calculated only on SBA-15-80 samples.

According to **Table 3.3**, another parameter that influences OCP(ECN) immobilization efficiency is the pore size of the silica mesoporous materials. Indeed, it was observed that the protein adsorption was favoured on SBA-15 with larger pore size, which could result from a better diffusion of OCP inside channels of mean 7.7 nm diameter than inside smaller ones (mean 5.7 nm pore diameter for SBA-15-80), knowing the dimensions of an OCP monomer are around 4*4*7.5 nm[50]. Such a conclusion however does not apply to OCP(CAN), whose dimensions

are yet the same as the OCP(ECN) ones and differs from the latter only by the presence of ECN instead of CAN, both carotenoids being buried in the protein pocket, with no influence on the surface electrostatic properties of the protein. Further investigations at higher OCP initial concentration could provide additional information to explain the effect of the pore size upon OCP adsorption.

To modulate the electrostatic interactions that govern the adsorption of OCP on the mesoporous solid, SBA-15 was functionalized by grafting of aminopropyl groups. As shown from zeta potential measurements (**Figure 3.4**), SBA-15-NH_2 surface remains positive in the pH range between 4 and 8. As OCP isoelectric point is around 5.4, as calculated from its primary sequence (3MG1 PDB file), the protein is overall negatively charged at pH 8.5 where the adsorption process takes place. In such conditions, electrostatic interactions are thus expected to favour OCP adsorption compared to immobilization on bare SBA-15. However, as shown in **Table 3.3**, at low OCP initial concentration (0.2 mg/mL), SBA-15-120-NH_2 led to unchanged (within the experimental error) OCP immobilization efficiencies compared to SBA-15-120 while for SBA-15-80, only a slight, although significant, increase of the protein loading was observed from 71.7 ± 2.8 % to 84.1 ± 6.5 % for OCP(ECN) and 83.0 ± 1.1 % to 94.9 ± 5.4 % for OCP(CAN). This latter expected result could thus arise from local favourable electrostatic interactions between the positively charged aminopropyl groups and deprotonated carboxylic groups (pKa around 5) on OCP. Such a favourable effect however was not observed for SBA-15-120-NH_2. One explanation for this behaviour could result from the ability of both OCP^O and OCP^R to dimerize at high solution concentration[51,52]. OCP dimers are thus likely to be adsorbed inside the meso-porosity of SBA-15-120, whose pores are large enough to accommodate the dimer. However, the dimer surface charge distribution could be modified compared to the monomer one, thus inducing less favourable electrostatic interactions with the silica support. Finally, a lower OCP uptake capacity on SBA-15-80-NH_2 compared to SBA-15-80 was observed for high initial OCP concentrations: 18 and 52 mg/g, respectively for 2 mg/mL OCP initial concentration (**Figure 3.6**). A maximum immobilization amount of 33 mg/g was reached on SBA-15-80-NH_2 for 1 mg/mL OCP initial concentration. When the latter was further increased, a decrease of the amount of immobilized OCP was found, opposite to what was observed with SBA-15-80. Such a saturation effect could be related to the support properties: protein/support interactions could be too strong to allow any diffusion of the protein inside the pores, so that OCP is located only at the pores entrance and may block pores upon adsorption hindering further protein uptake[34].

3.4.2.3 Effect of blue light on OCP adsorption

As an additional experiment, adsorption of OCP(CAN) was performed while a blue light LED (λ = 475nm) illuminated the protein. For both SBA-15-80 and SBA-15-80-NH_2, OCP(CAN) adsorption was substantially enhanced: from 52 to 93 mg/g on SBA-15-80 and from 18 to 85 mg/g on SBA-15-80-NH_2 (**Figure 3.6**). Such an improvement of the uptake capacity could result from the conformational modifications of OCP upon activation of the protein by light. These conformational changes are critical for OCP function since OCP^R is able to bind the purified phycobilisomes *in vitro*, whereas OCP^O does not[53]. The active OCP^R form appears to have a more open conformation and an increased surface exposure of the interface between the N- and C-terminal domains[54]. Dynamic X-ray crystallography (OCP(ECN) and OCP(CAN) from *Synechocystis* PCC6803) has identified some structural intermediates of OCP photo-conversion process, showing that H-bonds between the ketolated β-ring of carotenoid and both Tyr-201 and Trp-288 are broken, allowing a 12 Å long translocation of the carotenoid towards the N-terminal domain whose α-helices move away from C-terminal domain leading to solvent exposure of both carotenoids β rings[54–57]. As a consequence, the conformational changes associated with OCP activation are therefore significant with an OCP^R molecule with a more elongated shape compared to OCP^O [56]. Furthermore, it was shown that while at high concentration OCP^O dimerizes in a globular shape, OCP^R forms dimers with a more elongated shape[58]. Such significant structural modifications of OCP^O upon illumination which lead to reduced dimensions of OCP, could therefore explain the enhanced amount of immobilized OCP since the OCP^R, having a reduced steric hindrance, could more easily diffuse into the mesopores.

An argument corroborating the hypothesis of a possible adsorption of OCP inside the SBA-15 porosity is that OCP adsorption led to the modification of the meso-porous volume and pore size distribution of the material, determined from the desorption branch of the isotherm using the BJH model, as depicted in **Figure 3.7**. N_2 physisorption analysis was conducted on samples with the maximum loading of OCP(CAN) on bare and organo-functionalized SBA-15-80. As a control, the pore size distribution was calculated for an SBA-15 sample whose nitrogen sorption pre-treatment was the same as the one performed for OCP loaded on solid, i.e., at 30°C for 36 hours to avoid any OCP degradation. The meso-porous volume of SBA-15-80 was reduced from 0.64 cm^3/g to 0.57 cm^3/g after OCP loading (93 mg/g), while the meso-porous volume of SBA-15-80-NH_2 from 0.45 cm^3/g to 0.27 cm^3/g after OCP loading (85 mg/g). No reduction of pore size distribution is shown for SBA-15-80 after OCP loading. However, for SBA-15-80-

NH_2, the pore size distribution was significantly shifted towards lower pore sizes. Instead of the maximal pore size at 5.4 nm before OCP adsorption, two maxima were observed for SBA-15-80-NH_2 after OCP immobilization at around 4.8 nm and 4 nm. Such a smaller pore size could result from the adsorption of OCP inside the meso-porosity of SBA-15-80-NH_2. The combination of these two results, notably the reduction of meso-porous volume and pore size distribution, suggests the idea that nanopores are partially occupied by OCP molecules (the volume occupied by 20 mg of OCP molecules/g of SBA-15 is around 0.02 cm^3/g if considering its shape comparable to an ellipsoid) even if OCP could lock pores entrance preventing further loading.

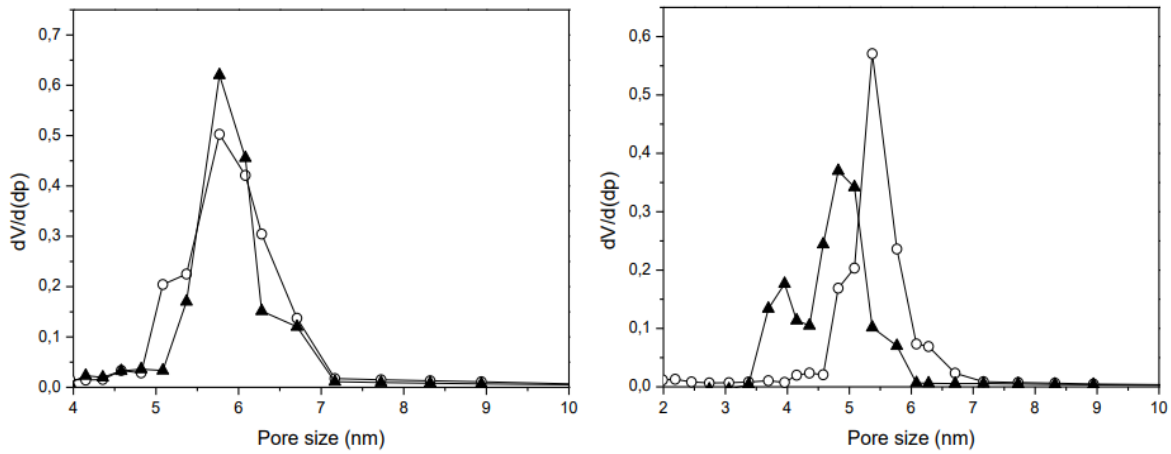

Figure 3.7 (Left) BJH pore size distribution of SBA-15-80 soaked into water (open circle) and OCP(CAN) 93 mg/g immobilized on SBA-15-80 under blue light (full triangle). (Right) BJH pore size distribution of SBA-15-80-NH_2 soaked into water (open circle) and OCP(CAN) 85 mg/g immobilized on SBA-15-80-NH_2 under blue light (full triangle).

As a conclusion, the tested SBA-15 materials are suitable supports for the immobilization of both OCP(ECN) and OCP(CAN) by adsorption. With an initial OCP concentration in solution of 2 mg/mL, the protein loading in the dark reached 52 mg/g on native SBA-15-80 while an 18 mg/g maximal loading was measured on the corresponding functionalized mesoporous material with aminopropyl groups. The immobilization yield could be significantly enhanced when the immobilization experiments were performed in the presence of light, which was interpreted as a clue of the OCP(CAN) uptake into the meso-porosity of silica. To our knowledge, this is the first report on successful use of a photo-activation process to enhance protein immobilization.

3.4.3 Photosensitivity of immobilized OCP

Furthermore, photo-properties of OCP(ECN) and OCP(CAN) have been evaluated after protein immobilization on silica matrices, notably its photo-activation, to assess the influence of the

surrounding environment on OCP photocycle, aiming to the development of nano-optical devices.

UV-Visible spectra of OCP(ECN) and OCP(CAN) solubilized in water are shown (**Figure 3.8**, I and II, respectively). In darkness, both protein solutions are orange coloured. OCP(ECN) presents a vibrational structure with two maxima at 474 and 495 nm, while OCP(CAN) presents two maxima at 474 and 500 nm. Absorption of blue-green light converts, with a low yield [23], the orange form (OCP^O) to a metastable red form OCP^R whose spectrum loses the vibrational band resolution observed for OCP^O, undergoes an intensity decrease with a broader spectral shape and exhibits a redshift with a unique maximum at 511 nm for both OCP(CAN) and OCP(ECN).

The spectra of the echinenone and canthaxanthin alone in water have a similar shape to the one of OCP. In a polar solvent, the maximum of the electronic transition occurs at 476 nm for echinenone and 490 nm canthaxanthin[59,60]. The red shift observed between absorbance maximum of echinenone and canthaxanthin is related to the increasing number of conjugated double bounds (involving two carbonyl groups in canthaxanthin and one carbonyl group in echinenone). However, the absorbance behaviour in the visible range allows to unambiguously decipher between OCP-bond carotenoid and carotenoid alone.

Suspensions of SBA-15 with immobilized OCP(CAN) and OCP(ECN) have been analysed by UV-Visible spectroscopy before and after photo-activation with a blue light LED (**Figure 3.8**).

In case of OCP(ECN), the UV-visible spectra recorded in the dark of SBA-15-80 after protein adsorption are like the ones recorded for $OCP(ECN)^O$ in solution, with two local maxima at 474 et 495 nm (**Figure 3.8**, left part). It is thus likely that the immobilization process has no influence on the conformation of the OCP(ECN). However, photosensitivity of OCP(ECN) clearly differs between SBA-15-80 and SBA-15-120. While OCP(ECN) remains photoactive on SBA-15-80 with a unique local maximum observed at 508 nm, no significant shift of the maximum was observed after illumination for OCP(ECN) immobilized on SBA-15-120 (**Figure 3.8**, IA-IB). The properties of OCP(ECN) were however completely different when immobilized on functionalized SBA-15-NH_2 (**Figure 3.8**, IC-ID). Indeed, OCP(ECN) retains its orange form after immobilization and was able to shift to its red form after photoactivation: a unique local maximum was observed at 508 nm on SBA-15-80-NH_2 and 507 nm on SBA-15-120-NH_2, close to the maximum observed for OCP^R in solution. OCP(ECN) thus remained photoactive when immobilized on SBA-15-NH_2, whatever the pore size.

In case of OCP(CAN) immobilized on native SBA-15, the UV-visible spectra recorded in the dark are very similar to the ones of the OCP^R form of the protein in solution whatever the pore

size of the mesoporous silica (**Figure 3.8**, IIA-IIB). After photoactivation, no significant modification of the spectra was observed. It can therefore be concluded that OCP(CAN) was immobilized under its red form and consequently is inactive towards illumination when immobilized. Again, the properties of OCP(CAN) were however completely different when immobilized on functionalized SBA-15-NH_2 (**Figure 3.8**, IIC-IID). In the latter case, it was observed that OCP(CAN) retains its orange form after immobilization and that it was able to shift to its red form after photoactivation: a unique local maximum was observed at 508 nm on SBA-15-80-NH_2 and 510 nm on SBA-15-120-NH_2, very close to the maximum observed for OCP^R in solution.

To summarize, the results above showed that both OCP(ECN) and OCP(CAN) remain photoactive when immobilized on organo-functionalized SBA-15-NH_2 whatever the pore size of the functionalized material, allowing to consider the use of immobilized OCP for applications involving a photoactivation process.

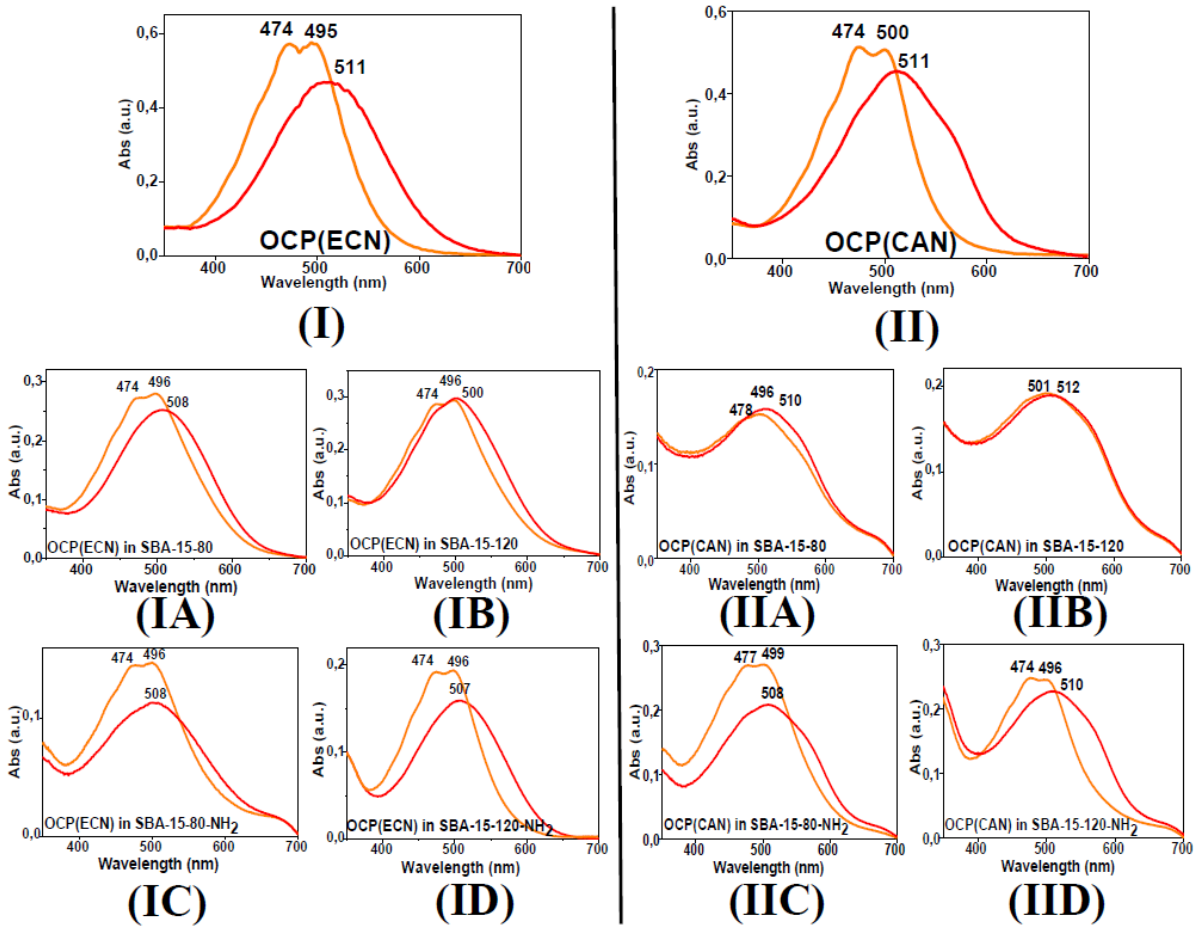

Figure 3.8 Visible spectra recorded in 350-700 nm range. Spectra before (orange) and after photoactivation with blue light LED (red). (I) OCP(ECN) in solution; (II) OCP(CAN) in solution. OCP(ECN) in SBA-15-80 (IA), SBA-15-120 (IB), SBA-15-80-NH_2 (IC), SBA-15-120-NH_2 (ID). OCP(CAN) in SBA-15-80 (IIA), SBA-15-120 (IIB), SBA-15-80-NH_2 (IIC), SBA-15-120-NH_2 (IID).

3.4.4 Stability in time

Stability of OCP(CAN) in solution and immobilized on SBA-15-80-NH_2 has been assessed. Samples have been stored at room temperature for 1 month in the dark and analysed with UV-Visible spectroscopy in liquid and solid phase, before and after photoactivation with Blue light LED after one week and after one-month storage (**Figure 3.9**). After 1 week at RT in the dark, OCP(CAN) spectra in solution and immobilized on SBA-15-80-NH_2 are representative of the one of their orange conformations in solution. In addition, the protein converted into the red form in both cases, showing it keeps its photoactivation properties. After one-month storage at RT in the dark, OCP(CAN) in solution undergoes a partial conversion to the red form as demonstrated by the slight redshift of the spectrum and by the decrease of spectral intensity at 474 nm (**Figure 3.9**, left); despite this, the protein is still completely photoactive. On the contrary, when immobilized, OCP(CAN) is not photoactive. Indeed, before or after blue light exposition, spectral properties do not change: its spectrum blue-shifts and loses its vibrational structure, suggesting a modification of the interactions between canthaxanthin and its binding pocket.

To summarize, if the storage of solution at RT does not affect the photoactivation properties of the protein, once immobilized on SBA-15-80-NH_2, the photo-activity is preserved for 1 week but not for 1 month.

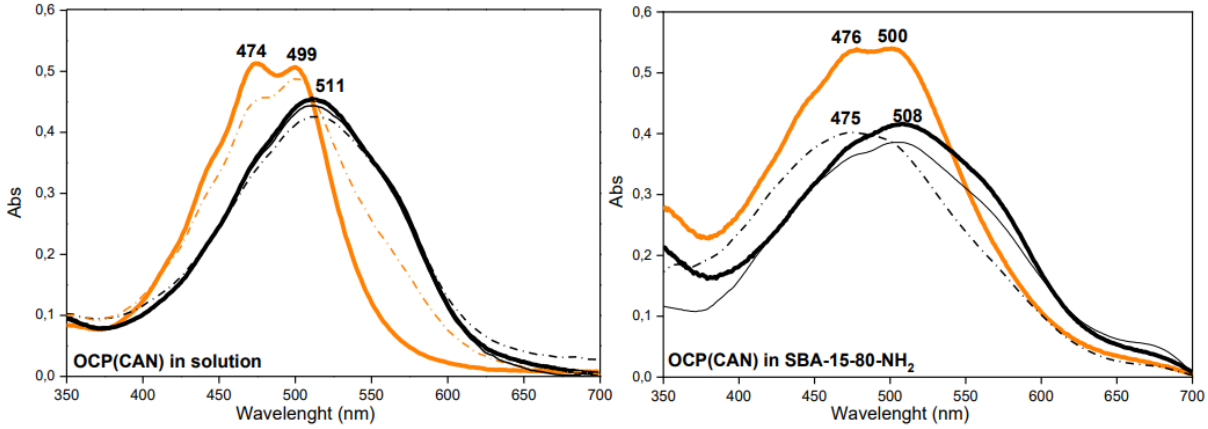

Figure 3.9 (Left) Visible spectra of OCP(CAN) 0.4 mg/mL in solution, before (orange) and after (thick black) exposition to blue light LED at t=0 (day of immobilization); after blue light LED at t=1week (thin black); before and after blue light LED at t=1 month (thin dash-dot-dash orange and black, respectively). (Right) Visible spectra of OCP(CAN) in SBA-15-80-NH_2, before (orange) and after (thick black) exposition to blue light LED at t=0; after blue light LED at t=1week (thin black); before and after blue light LED at t=1 month (thin dash-dot-dash black).

3.4.5 Kinetic of OCP back-conversion

The sample of OCP(CAN) immobilized on SBA-15-120-NH_2 has been used to study the back-conversion of the protein on silica solid support and to compare it with the fast back-conversion occurring in solution. The sample, placed on UV-Vis solid phase sample holder, has been photo-activated with Blue light LED for 30 minutes. Then, spectra have been collected at different time intervals from time 0 up to 2h (**Figure 3.10**). Gradual back-conversion $OCP^R \rightarrow OCP^O$ was observed, with a slower different kinetic compared to the faster one occurring in solution (few seconds), attributable to the presence of matrix constrain. No back-conversion has been recorded for OCP(ECN) in any type of SBA-15. As a conclusion, the external constraint of SBA-15-NH_2 results in a slower back-conversion kinetic of OCP(CAN) after photoactivation.

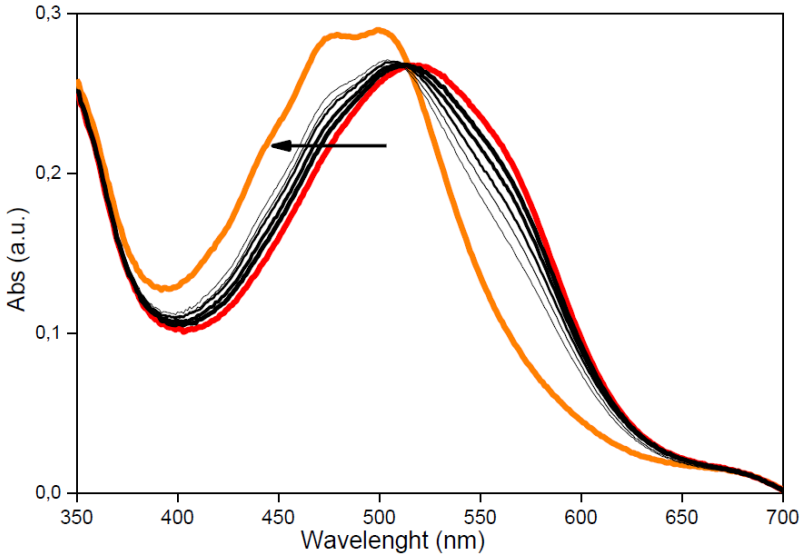

Figure 3.10 Visible spectra of OCP(CAN) in SBA-15-120-NH_2 following the photo-activation and relaxation of the protein. Before (orange), after blue light LED exposition (red), relaxation after 10, 20, 40, 60, 120 min in the dark (black lines from the thickest to the thinner following the arrow).

3.4.6 OCP leaching extent from SBA-15 matrices

The release of OCP(CAN) adsorbed on SBA-15-80 or SBA-15-80-NH_2 (quantity of adsorbed OCP 38 and 33 mg/g of solid, respectively) was assayed in different conditions (

Table 3.4) keeping the samples in the dark. Adsorption of OCP is likely to be driven by electrostatic interactions between the support and the protein. At pH around 7, SBA-15-80 surface is negatively charged due to the deprotonation of free silanol groups while it is positively charged for SBA-15-80-NH_2 due to the grafting of aminopropyl groups. This was

confirmed by zeta potential measurements (**Figure 3.4**). On the other hand, OCP is overall negatively charged at pH 7 since its isoelectric point is around 5.4, as calculated from its primary sequence. Consequently, electrostatic interactions between OCP and SBA-15-80-NH_2 are favoured at pH 7. The opposite is observed concerning OCP and SBA-15-80. To screen the positive interactions with SBA-15-NH_2 and favour OCP desorption, the ionic strength of the solution was increased with NaCl 1M. Up to 12.5 % of OCP leaching from SBA-15-80-NH_2 was observed after 24 hours. Surprisingly, the leaching extent decreased after one week. Lower leaching (around 2 %) was observed from SBA-15-80. These results, together with the fact that very similar amounts of OCP could be adsorbed on SBA-15-80 and SBA-15-80-NH_2 at pH 8.5 while electrostatic interactions between OCP and the support are opposite, could corroborate the hypothesis that electrostatic interactions are not the main driving force of OCP adsorption. To help to clarify this point, leaching of OCP from SBA-15-80-NH_2 was assessed in unfavourable electrostatic conditions, e.g., at pH 4.2 where OCP overall charge and the surface charge are both positive. In such conditions, the OCP leaching reached 18.5 % after 24 hours and 7 % after one week. Such conditions are thus more efficient, which is compatible with a contribution of electrostatic forces in the OCP adsorption process. In anyway light-induced leaching was tested but no effect has been detected suggesting that photo-conversion of OCP and its structural rearrangement do not help the release of the protein.

Interestingly, the leaching extent of OCP(CAN) from SBA-15-80 could be discussed in relationship with the photoactivity of immobilized OCP, which was irreversibly converted to its red form after its adsorption. Together with the very low leaching observed, it could be concluded that its adsorption induces an irreversible conformational change into the red form of the protein (and an irreversible adsorption), probably related to strong interactions between specific moieties of the red form of the protein and silanol groups. On the contrary, the preserved photoactivity of OCP(CAN) on SBA-15-80-NH_2 is somehow consistent with a partly reversible adsorption of the protein.

The leaching extent was also tested under blue light LED illumination to evaluate if the photo-conversion of the protein could help its detachment from the silica surface, but no effect of release was detected.

OCP(CAN) leaching extent (%)	**NaCl 1 M**		**pH**		
	24h	1 week		24h	1 week
SBA-15-80	2.5 %	2 %	7.3	2 %	2 %
SBA-15-80-NH_2	12.5 %	5 %	4.2	18.5 %	7 %

Table 3.4 Leaching extent of OCP(CAN) from SBA-15-80 and SBA-15-80-NH_2 in NaCl 1 M or under pH effect (pH 7.3 for SBA-15-80 and pH 4.3 for SBA-15-80NH_2).

3.5 OCP in SBA-15 as optical sensor

Among the numerous applications of protein-loaded mesostructured silica surfaces[4,6], the optical sensing is one of the most interesting. OCP-loaded NPs were tested as possible optical indicators for pH and temperature changes. In fact, the high yield of immobilization of OCP on mesoporous silica, its weak leaching, and the resistance of the protein to ageing suggest its suitability as optical sensor. Temperature and pH effect were evaluated on OCP-loaded silica NPs using Visible spectroscopy in solid phase to measure the optical response.

3.5.1 Effect of temperature on OCP (ECN or CAN) in SBA-15 matrices

Recently OCP, bound to fluorescent proteins, has been used as a sensor for temperature inside biological cells[21]. In this framework, temperature effect on OCP in SBA-15 matrices has been tested with UV-Visible spectroscopy in solid phase. Protein 0.2 mg/mL as starting concentration, immobilized on 10 mg of silica as described before (see OCP immobilization protocol), have been treated at 40°C and 60°C in a water-bath for 40 minutes in the dark and then spectra recorded.

OCP(ECN) and OCP(CAN) in water solution keep their structure and spectroscopical properties at 40°C but they are denatured at 60°C as confirmed by the loss of the vibronic structure of the Vis spectrum and by the appearance of yellow colour, typical of the free carotenoid (**Figure 3.11**). OCP(ECN) in SBA-15-120 at 40°C is thermally activated and turns to the red form, losing the vibrational structure of the orange form, with a single maximum at 504 nm, while at 60°C the protein is denatured and a single maximum at 457 nm is shown, more similar to the spectrum of echinenone in solution (476 nm), suggesting a denaturation of the protein (**Figure 3.12**, IB). OCP(ECN) in SBA-15-80, at 40°C shows a decrease in absorbance intensity but no redshift is recorded, while at 60°C the protein is denatured and a single maximum at 438 nm is shown (**Figure 3.12**, IA). OCP(ECN) in SBA-15-NH_2 (both types) does not show a clear redshift at 40°C and seems to preserve a partial orange form before being denatured at 60°C (**Figure 3.12**, IC-ID).

In parallel, temperature response of OCP(CAN) has been tested after protein loading and thermal exposition as described before. OCP(CAN) in SBA-15-80 and SBA-15-120 is not able to preserve the orange form (as already described in **Figure 3.8**, IIA-IIB) indeed there is no observable red shift at 40°C but a small decrease of absorbance intensity. This decrease could be explained as red conversion of a part of the protein population inside the NPs. At 60°C the

spectral maximum shifts to 450 nm, which is relatively close to the CAN Vis spectrum in solution (maximum at 490 nm), suggesting the denaturation of the protein (**Figure 3.12**, IIA-IIB). On the contrary, OCP(CAN) in SBA-15-NH_2 (both types) preserves the orange form, at 40°C the spectral intensity is decreased but not red-shifted, suggesting a partial thermal-activation, while at 60°C the spectrum of free CAN is observed, again suggesting denaturation of the protein (**Figure 3.12**, IIC-IID).

To summarize, comparing the samples of OCP(ECN) and OCP(CAN) in solution with those immobilized on bare and functionalised SBA-15 (both type of pore dimension), the OCP response to temperature variation, is the same. At 40°C the protein keeps its orange form in all conditions, while at 60°C the protein is denatured, and the spectrum of the free carotenoid is observed. Therefore, it is possible to deduce that the system of OCP-loaded silica nanoparticles can be exploited as two-colour optical sensor in the range 40°C - 60°C changing its colour from orange to yellow when exposed to a local temperature of 60°C. These results were reproduced on 1 week-aged samples, stored at 4°C (see **Figure SI 1. 3-2**), suggesting a good stability in time of the photochromic properties of the system.

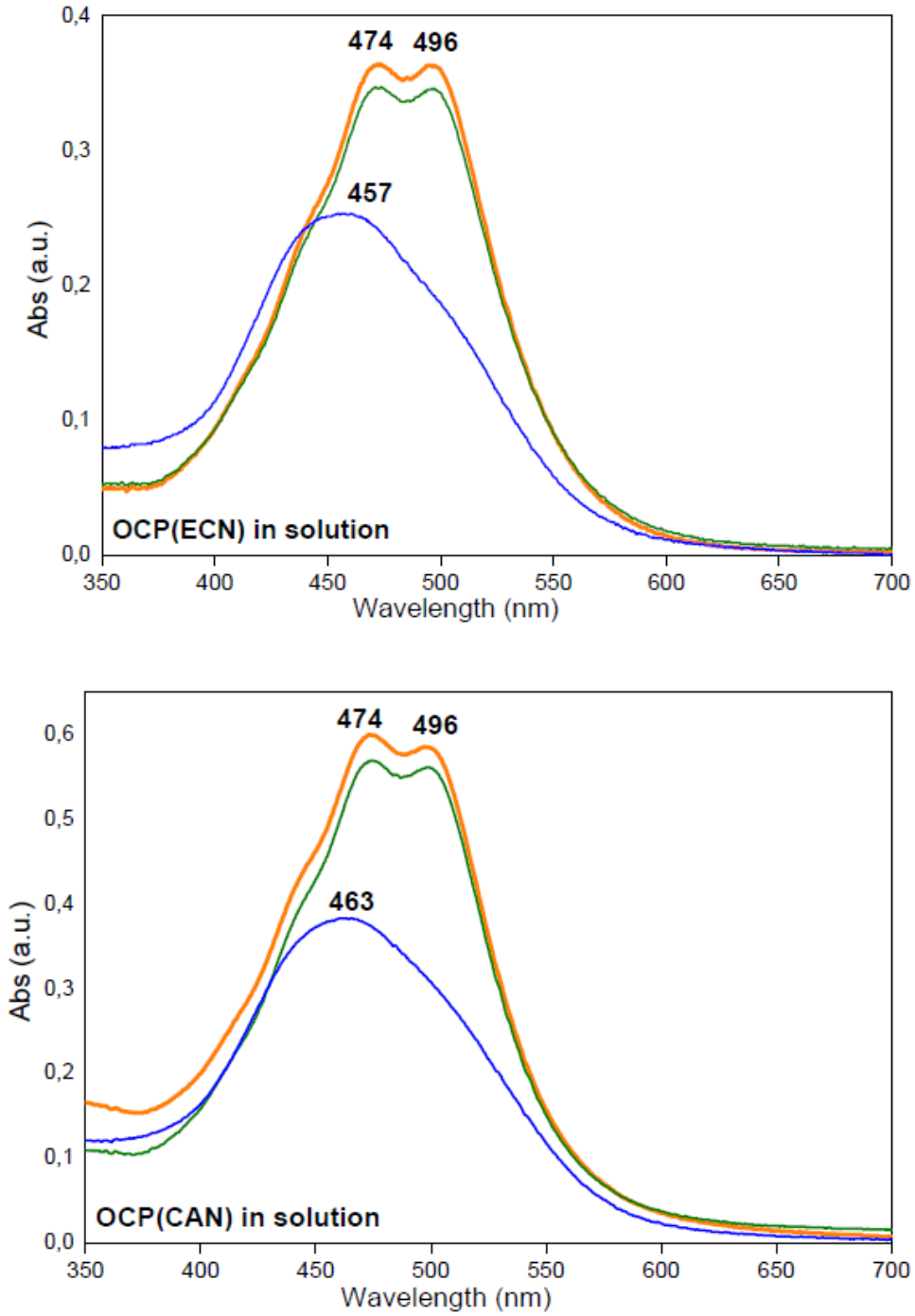

Figure 3.11 (Top) OCP(ECN) in solution; (bottom) OCP(CAN) in solution. Visible spectra recorded in 350-700 nm range. (Orange) Spectra before thermal treatment (RT); (Green) spectra of samples treated at 40°C; (Blue) spectra of samples treated at 60°C.

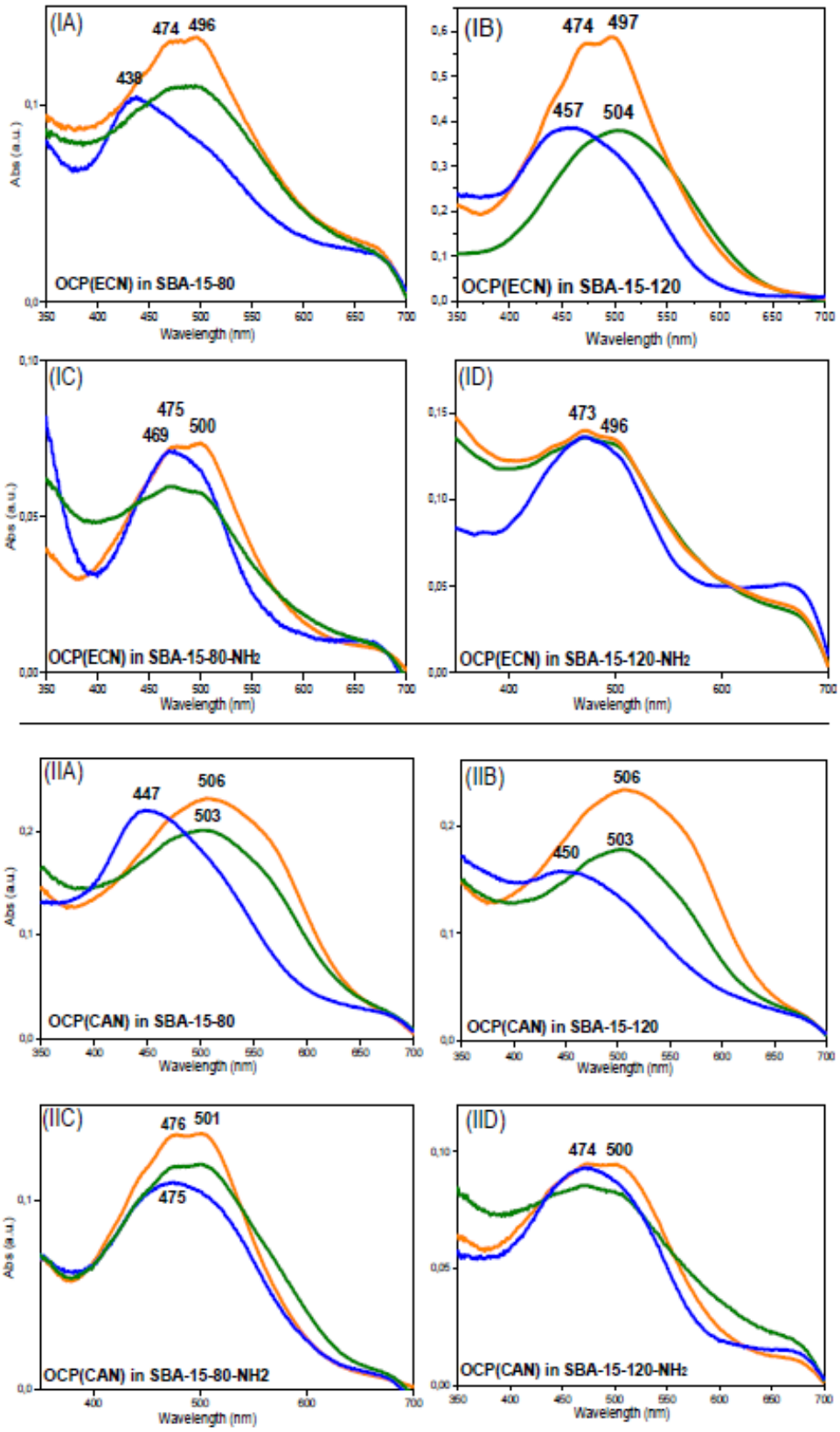

Figure 3.12 OCP(ECN) in SBA-15-80 (IA), SBA-15-120 (IB), SBA-15-80-NH_2 (IC), SBA-15-120-NH_2 (ID). OCP(CAN) in SBA-15-80 (IIA), SBA-15-120 (IIB), SBA-15-80-NH_2 (IIC), SBA-15-120-NH_2 (IID). Visible spectra recorded in 350-700 nm range. (Orange) Spectra before thermal treatment (RT); (Green) spectra of samples treated at 40°C; (Blue) spectra of samples treated at 60°C. Spectral intensity variability depends on sample preparation before the analysis.

3.5.2 Effect of pH on OCP (ECN or CAN) in SBA-15-NH_2 matrices

The effect of pH on OCP(ECN) and OCP(CAN) encapsulated in SBA-15 matrices has been tested to study the influence of pH on the system OCP@SBA-15 in comparison to the effect of pH on OCP in solution and to suggest its use for applications as pH-optical sensors. For experiments in solution, samples obtained mixing OCP stock solution (pH = 8.7) with water solutions at different pH (concentration of protein 0.2 mg/mL) were analysed with UV-Visible spectrometer in 350-700 nm range. OCP(ECN) shows that at strong acidic pH (e.g., pH 1) the protein is in the red form (λ_{max} 510 nm) while in the pH 3 - 11 range it is in the orange form. At pH 13 the Vis spectrum of the free carotenoid appears (λ_{max} 446 nm), indicating probable denaturation of the protein as shown in **Figure 3.13**. In line with the previous, OCP(CAN) in solution shows that at strong acidic pH (e.g., pH 1) the protein is in the red form (λ_{max} 520 nm) while in the pH 3 - 11range it is in the orange form. At pH 13 the spectrum of free carotenoid appears (λ_{max} 450 nm) suggesting denaturation of the protein (**Figure 3.13**).

In parallel, the effect of silica environment has been tested. Differences in terms of absorbance intensity are due to the preparation of the UV-Vis solid phase samples. SBA-15-80-NH_2 (hereafter referred to as SBA-15-NH_2) matrices were taken as examples for these experiments because, as already demonstrated, OCP keeps its orange form after being immobilised on silica surface. OCP(ECN) inside SBA-15-NH_2 was tested (**Figure 3.13**) and it is shown that at strong acidic pH (e.g., 1) the protein, even inside the matrix, is red and the vibrational structure is lost (λ_{max} 500 nm); for pH 3 up to 11 it is in the orange form; while at pH 13 the free carotenoid spectrum is observed (indicating probable denaturation of the protein) (λ_{max} 464 nm). For OCP(CAN) in SBA-15-NH_2 the situation is reproduced (**Figure 3.13**). At strong acidic pH (e.g., 1) the protein is red (λ_{max} 510 nm); in the pH 3 - 11 range the Vis spectrum characteristic of OCP in the orange form is observed, while at pH 13 the spectrum of the free carotenoid appears (λ_{max} 468 nm) indicating probable protein denaturation. As previously stated, testing temperature effect, the presence of the constraint of the silica matrix partially prevents the denaturation or the red-conversion of the protein, as deduced by the fact that Visible spectra are less blue- or red- shifted compared to those in solution.

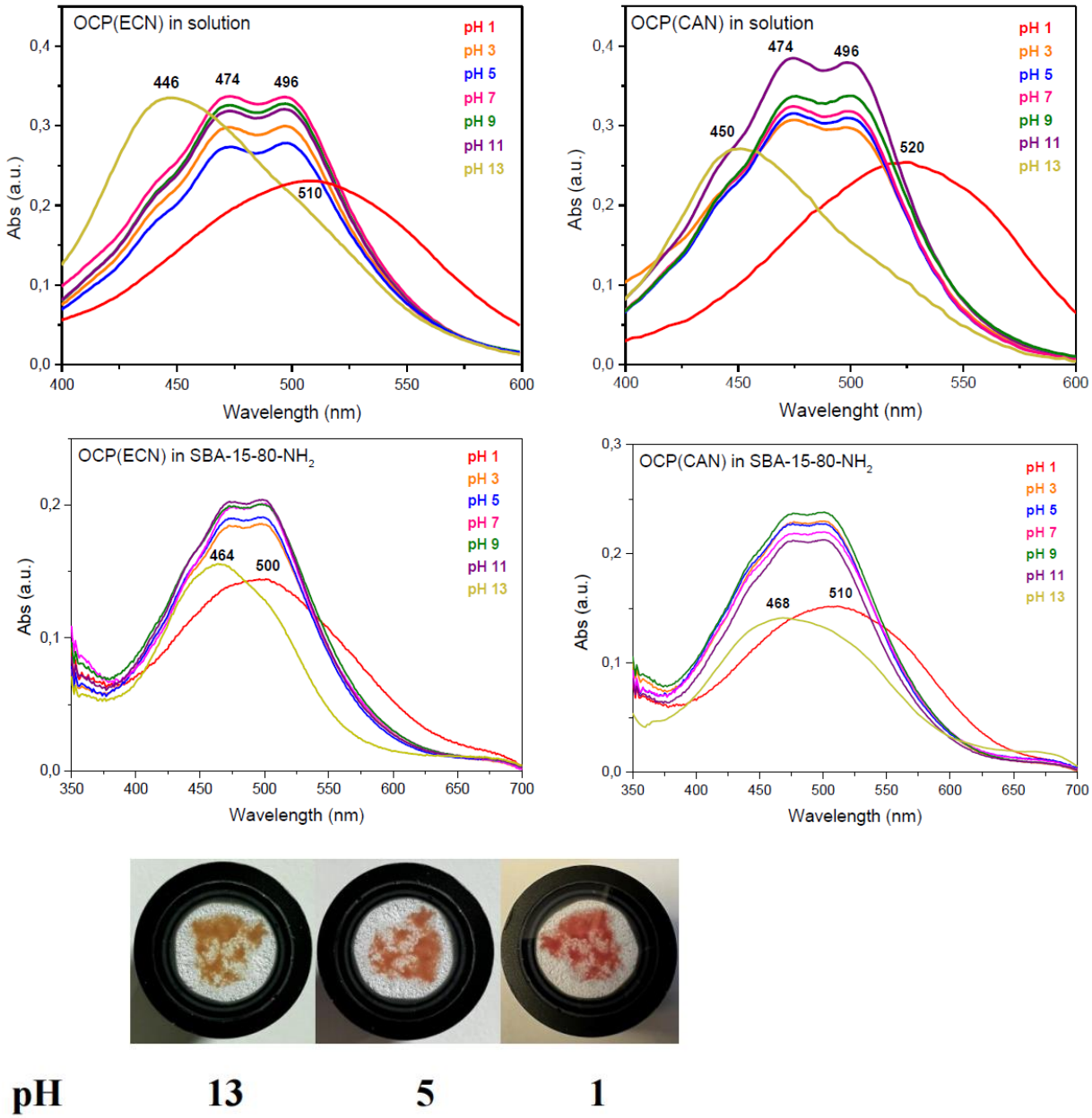

Figure 3.13 Visible spectra of OCP(ECN) (left) and OCP(CAN) (right) in solution (top) and in SBA-15-80-NH_2 (bottom) at different pH (1, 3, 5, 7, 9, 11, 13). Samples kept in the dark during the experiment. At the bottom pictures of sample-holders are shown, corresponding to samples of OCP(CAN)@SBA-15-NH_2 treated at pH 13, 5 and 1 (from left to right).

To summarize, comparing the samples of OCP(ECN) and OCP(CAN) in solution with those immobilized in SBA-15-80-NH_2, the OCP response to pH variation, is the same. Therefore, it is possible to deduce that the system of OCP-loaded silica nanoparticles can be exploited as *tri*-functional pH optical sensor (see pictures in **Figure 3.13**), being orange in the pH range 3-11, turning to the red colour at strong acidic pH and yellow at strong basic pH.

Furthermore, after having tested separately the samples under the effect of different pH values, pH tests were performed "*in situ*" by titration of the same sample firstly at pH 1, then at pH 3 and eventually at pH 13, that correspond to the protein colour change values. Data are reported in **Figure SI 1. 3-4** and it was observed that the sample treated at pH 1 (and red coloured, consistently with previously shown data) was not able to restore the orange colour and spectrum when treated at pH 3, but it turned to the yellow colour after treatment at pH 13, due to the denaturation of the protein.

Nevertheless, these tests were also performed on bare SBA-15 even if this matrix does not allow the OCP to keep the orange conformation (as shown in **Figure SI 1. 3-3**). Indeed, as reported in **Figure SI 1. 3-3**, the OCP shows a red conformation in the pH range 5-11 while at strong pH conditions (either acidic or basic), it is denatured and spectrum (and yellow colour) of the carotenoid is shown.

3.6 Conclusion

In conclusion, considering the wide range of nanobiotechnological applications involving the immobilization of proteins, this work has achieved several goals. 1) SBA-15 meso-porous materials synthesized at different aging temperature, bare and organo-functionalized, have shown a worm shape morphology with well-ordered crystalline structure which is not affected by the functionalization with amino groups. 2) SBA-15 materials with two different pore sizes are suitable and promising supports for the immobilization of both OCP(ECN) and OCP(CAN) by adsorption. The equilibrium of immobilization, driven by electrostatic interactions, is reached after 4 hours on both types of SBA-15, bare and organo-functionalized, and the maximum loading yield is achieved for an initial OCP concentration of 0.2 mg/mL. At higher initial OCP concentration, the amount of immobilized OCP was enhanced up to more than 30 mg of protein per g of material. 3) Illumination by blue light increases immobilization efficiency on both SBA-15-80 and SBA-15-80-NH_2 nanoparticles leading to around four-fold more immobilized OCP and suggesting that the conformation of OCP (ellipsoidal for OCP^O and more elongated for OCP^R) plays a key-role in entering the mesopores thereby increasing protein loading. 4) Protein photo-activity is completely preserved after immobilization on SBA-15-NH_2 if compared with SBA-15 which, on the contrary, tends to dark-activate the protein converting it into OCP^R. 5) OCP@SBA-15-NH_2 looks a promising photo-active system, still stable after 1 week at room temperature, able to slow down the kinetic of back conversion $OCP^R \rightarrow OCP^O$. This property can, in principle, be exploited in several domains: from biocompatible photochromic nanoparticles to the development of nano-scaled support for caroteno-proteins and carotenoid delivery and release. In the latter case, further studies should be undertaken to improve the release extend of OCP, for example by varying the functionalized groups grafted on the solid, thus modulating the interactions between the protein and the surface. 6) The OCP@SBA-15-NH_2 system demonstrated to be, *in vitro*, a suitable biocompatible material to be exploited in the domain of optical sensing, such as a *bi*-functional optical sensor for temperature changes between 40°C and 60°C or as a *tri*-functional pH optical sensor spanning the whole pH range.

3.7 References

[1] L.C. Sang, A. Vinu, M.O. Coppens, General description of the adsorption of proteins at their iso-electric point in nanoporous materials, Langmuir. 27 (2011) 13828–13837. https://doi.org/10.1021/la202907f.

[2] P.R.A.F. Garcia, R.N. Bicev, C.L.P. Oliveira, O.A. Sant'Anna, M.C.A. Fantini, Protein encapsulation in SBA-15 with expanded pores, Microporous Mesoporous Mater. 235 (2016) 59–68. https://doi.org/10.1016/j.micromeso.2016.07.033.

[3] J. Siefker, R. Biehl, M. Kruteva, A. Feoktystov, M.O. Coppens, Confinement Facilitated Protein Stabilization As Investigated by Small-Angle Neutron Scattering, J. Am. Chem. Soc. 140 (2018) 12720–12723. https://doi.org/10.1021/jacs.8b08454.

[4] M. De, P.S. Ghosh, V.M. Rotello, Applications of nanoparticles in biology, Adv. Mater. 20 (2008) 4225–4241. https://doi.org/10.1002/adma.200703183.

[5] M. Hartmann, Ordered mesoporous materials for bioadsorption and biocatalysis, Chem. Mater. 17 (2005) 4577–4593. https://doi.org/10.1021/cm0485658.

[6] M.C. Daniel, D. Astruc, Gold Nanoparticles: Assembly, Supramolecular Chemistry, Quantum-Size-Related Properties, and Applications Toward Biology, Catalysis, and Nanotechnology, Chem. Rev. 104 (2004) 293–346. https://doi.org/10.1021/cr030698+.

[7] J.J. Storhoff, A.D. Lucas, V. Garimella, Y.P. Bao, U.R. Müller, Homogeneous detection of unamplified genomic DNA sequences based on colorimetric scatter of gold nanoparticle probes, Nat. Biotechnol. 22 (2004) 883–887. https://doi.org/10.1038/nbt977.

[8] J. Fan, C. Yu, F. Gao, J. Lei, B. Tian, L. Wang, Q. Luo, B. Tu, W. Zhou, D. Zhao, Cubic mesoporous silica with large controllable entrance sizes and advanced adsorption properties, Angew. Chemie - Int. Ed. 42 (2003) 3146–3150. https://doi.org/10.1002/anie.200351027.

[9] J. Zhao, F. Gao, Y. Fu, W. Jin, P. Yang, D. Zhao, Biomolecule separation using large pore mesoporous SBA-15 as a substrate in high performance liquid chromatography, Downloaded by Sorbonne. (2001). https://doi.org/10.1039/b110637f.

[10] R. Tian, J. Sun, H. Zhang, M. Ye, C. Xie, J. Dong, J. Hu, D. Ma, X. Bao, H. Zou, Large-pore mesoporous SBA-15 silica particles with submicrometer size as stationary phases for high-speed CEC separation, Electrophoresis. 27 (2006) 742–748. https://doi.org/10.1002/elps.200500630.

[11] M. Hartmann, X. Kostrov, Immobilization of enzymes on porous silicas – benefits and challenges, Chem. Soc. Rev. 42 (2013) 6277–6289. https://doi.org/10.1039/c3cs60021a.

[12] D. Zhao, J. Feng, Q. Huo, N. Melosh, G.H. Fredrickson, B.F. Chmelka, G.D. Stucky, Triblock copolymer syntheses of mesoporous silica with periodic 50 to 300 angstrom pores, Science (80-.). 279 (1998) 548–552. https://doi.org/10.1126/science.279.5350.548.

[13] Ł. Laskowski, M. Laskowska, N. Vila, M. Schabikowski, A. Walcarius, Mesoporous silica-based materials for electronics-oriented applications, Molecules. 24 (2019) 1–31. https://doi.org/10.3390/molecules24132395.

[14] M. Imperor-Clerc, P. Davidson, A. Davidson, Existence of a microporous corona around the mesopores of silica-based SBA-15 materials templated by triblock

copolymers, J. Am. Chem. Soc. 122 (2000) 11925–11933. https://doi.org/10.1021/ja002245h.

[15] F. Sevimli, A. Yilmaz, Surface functionalization of SBA-15 particles for amoxicillin delivery, Microporous Mesoporous Mater. 158 (2012) 281–291. https://doi.org/10.1016/j.micromeso.2012.02.037.

[16] M. Martínez-Carmona, A. Baeza, M.A. Rodriguez-Milla, J. García-Castro, M. Vallet-Regí, Mesoporous silica nanoparticles grafted with a light-responsive protein shell for highly cytotoxic antitumoral therapy, J. Mater. Chem. B. 3 (2015) 5746–5752. https://doi.org/10.1039/c5tb00304k.

[17] E. Ahmadi, N. Dehghannejad, S. Hashemikia, M. Ghasemnejad, H. Tabebordbar, Synthesis and surface modification of mesoporous silica nanoparticles and its application as carriers for sustained drug delivery, Drug Deliv. 21 (2014) 164–172. https://doi.org/10.3109/10717544.2013.838715.

[18] K. Scaramuzzi, G.D. Tanaka, F.M. Neto, P.R.A.F. Garcia, J.J.M. Gabrili, D.C.A. Oliveira, D. V. Tambourgi, J.S. Mussalem, D. Paixão-Cavalcante, M.T. D'Azeredo Orlando, V.F. Botosso, C.L.P. Oliveira, M.C.A. Fantini, O.A. Sant'Anna, Nanostructured SBA-15 silica: An effective protective vehicle to oral hepatitis B vaccine immunization, Nanomedicine Nanotechnology, Biol. Med. 12 (2016) 2241–2250. https://doi.org/10.1016/j.nano.2016.06.003.

[19] A. Andreoni, S. Lin, H. Liu, R.E. Blankenship, H. Yan, N.W. Woodbury, Orange Carotenoid Protein as a Control Element in an Antenna System Based on a DNA Nanostructure, Nano Lett. 17 (2017) 1174–1180. https://doi.org/10.1021/acs.nanolett.6b04846.

[20] E.G. Maksimov, W.J. Li, E.A. Protasova, T. Friedrich, B. Ge, S. Qin, N.N. Sluchanko, Hybrid coupling of R-phycoerythrin and the orange carotenoid protein supports the FRET-based mechanism of cyanobacterial photoprotection, Biochem. Biophys. Res. Commun. 516 (2019) 699–704. https://doi.org/10.1016/j.bbrc.2019.06.098.

[21] E.G. Maksimov, I.A. Yaroshevich, G. V. Tsoraev, N.N. Sluchanko, E.A. Slutskaya, O.G. Shamborant, T. V. Bobik, T. Friedrich, A. V. Stepanov, A genetically encoded fluorescent temperature sensor derived from the photoactive Orange Carotenoid Protein, Sci. Rep. 9 (2019) 1–9. https://doi.org/10.1038/s41598-019-45421-7.

[22] F. Muzzopappa, A. Wilson, D. Kirilovsky, Interdomain interactions reveal the molecular evolution of the orange carotenoid protein, Nat. Plants. 5 (2019) 1076–1086. https://doi.org/10.1038/s41477-019-0514-9.

[23] F. Muzzopappa, D. Kirilovsky, Changing Color for Photoprotection: The Orange Carotenoid Protein, Trends Plant Sci. 25 (2020) 92–104. https://doi.org/10.1016/j.tplants.2019.09.013.

[24] M.A. Dominguez-Martin, C.A. Kerfeld, Engineering the orange carotenoid protein for applications in synthetic biology, Curr. Opin. Struct. Biol. 57 (2019) 110–117. https://doi.org/10.1016/j.sbi.2019.01.023.

[25] Y.B. Slonimskiy, E.G. Maksimov, E.P. Lukashev, M. Moldenhauer, T. Friedrich, N.N. Sluchanko, Engineering the photoactive orange carotenoid protein with redox-controllable structural dynamics and photoprotective function, Biochim. Biophys. Acta - Bioenerg. 1861 (2020) 148174. https://doi.org/10.1016/j.bbabio.2020.148174.

[26] M. Moldenhauer, N.N. Sluchanko, D. Buhrke, D. V. Zlenko, N.N. Tavraz, F.J. Schmitt, P. Hildebrandt, E.G. Maksimov, T. Friedrich, Assembly of photoactive orange

carotenoid protein from its domains unravels a carotenoid shuttle mechanism, Photosynth. Res. 133 (2017) 327–341. https://doi.org/10.1007/s11120-017-0353-3.

[27] L. Wang, R.T. Yang, Increasing selective CO2 adsorption on amine-grafted SBA-15 by increasing silanol density, J. Phys. Chem. C. 115 (2011) 21264–21272. https://doi.org/10.1021/jp206976d.

[28] A. Vinu, C. Streb, V. Murugesan, M. Hartmann, Adsorption of cytochrome c on new mesoporous carbon molecular sieves, J. Phys. Chem. B. 107 (2003) 8297–8299. https://doi.org/10.1021/jp035246f.

[29] A. Galarneau, H. Cambon, F. Di Renzo, F. Fajula, True microporosity and surface area of mesoporous SBA-15 silicas as a function of synthesis temperature, Langmuir. 17 (2001) 8328–8335. https://doi.org/10.1021/la0105477.

[30] A. Galarneau, H. Ne Cambon, F. Di Renzo, R. Ryoo, M. Choi, F. Fajula, Microporosity and connections between pores in SBA-15 mesostructured silicas as a function of the temperature of synthesis, (n.d.). https://doi.org/10.1039/b207378c.

[31] A.B. Fuertes, Synthesis of ordered nanoporous carbons of tunable mesopore size by templating SBA-15 silica materials, Microporous Mesoporous Mater. 67 (2004) 273–281. https://doi.org/10.1016/j.micromeso.2003.11.012.

[32] T. Benamor, L. Vidal, B. Lebeau, C. Marichal, Influence of synthesis parameters on the physico-chemical characteristics of SBA-15 type ordered mesoporous silica, Microporous Mesoporous Mater. 153 (2012) 100–114. https://doi.org/10.1016/j.micromeso.2011.12.016.

[33] S.M.L. Santos, J.A. Cecilia, E. Vilarrasa-García, I.J. Silva Junior, E. Rodríguez-Castellón, D.C.S. Azevedo, The effect of structure modifying agents in the SBA-15 for its application in the biomolecules adsorption, Microporous Mesoporous Mater. 232 (2016) 53–64. https://doi.org/10.1016/j.micromeso.2016.06.004.

[34] A. Katiyar, S. Yadav, P.G. Smirniotis, N.G. Pinto, Synthesis of ordered large pore SBA-15 spherical particles for adsorption of biomolecules, J. Chromatogr. A. 1122 (2006) 13–20. https://doi.org/10.1016/j.chroma.2006.04.055.

[35] D. Jung, C. Streb, M. Hartmann, Oxidation of indole using chloroperoxidase and glucose oxidase immobilized on SBA-15 as tandem biocatalyst, Microporous Mesoporous Mater. 113 (2008) 523–529. https://doi.org/10.1016/j.micromeso.2007.12.009.

[36] N.H. Abdallah, M. Schlumpberger, D.A. Gaffney, J.P. Hanrahan, J.M. Tobin, E. Magner, Comparison of mesoporous silicate supports for the immobilisation and activity of cytochrome c and lipase, J. Mol. Catal. B Enzym. 108 (2014) 82–88. https://doi.org/10.1016/j.molcatb.2014.06.007.

[37] Q. Tao, Z. Xu, J. Wang, F. Liu, H. Wan, S. Zheng, Adsorption of humic acid to aminopropyl functionalized SBA-15, Microporous Mesoporous Mater. 131 (2010) 177–185. https://doi.org/10.1016/j.micromeso.2009.12.018.

[38] J. Meissner, A. Prause, C. Di Tommaso, B. Bharti, G.H. Findenegg, Protein immobilization in surface-functionalized SBA-15: Predicting the uptake capacity from the pore structure, J. Phys. Chem. C. 119 (2015) 2438–2446. https://doi.org/10.1021/jp5096745.

[39] A.S. Maria Chong, X.S. Zhao, Functionalization of SBA-15 with APTES and Characterization of Functionalized Materials, J. Phys. Chem. B. 107 (2003) 12650–12657. https://doi.org/10.1021/jp035877+.

[40] N. Balistreri, D. Gaboriau, C. Jolivalt, F. Launay, Covalent immobilization of glucose oxidase on mesocellular silica foams: Characterization and stability towards temperature and organic solvents, J. Mol. Catal. B Enzym. 127 (2016) 26–33. https://doi.org/10.1016/j.molcatb.2016.02.003.

[41] D. Jung, C. Streb, M. Hartmann, Covalent anchoring of chloroperoxidase and glucose oxidase on the mesoporous Molecular Sieve SBA-15, Int. J. Mol. Sci. 11 (2010) 762–778. https://doi.org/10.3390/ijms11020762.

[42] B.-H. Min, E.-Y. Jeong, M. Thommes, S.-E. Park, Direct synthesis of plugged SBA-15 type mesoporous silica using alcoholaminesw ChemComm, Chem. Commun. 47 (2011) 4673–4675. https://doi.org/10.1039/c1cc10420a.

[43] C. Punginelli, A. Wilson, J.M. Routaboul, D. Kirilovsky, Influence of zeaxanthin and echinenone binding on the activity of the Orange Carotenoid Protein, Biochim. Biophys. Acta - Bioenerg. 1787 (2009) 280–288. https://doi.org/10.1016/j.bbabio.2009.01.011.

[44] C.B. De Carbon, A. Thurotte, A. Wilson, F. Perreau, D. Kirilovsky, Biosynthesis of soluble carotenoid holoproteins in Escherichia coli, Sci. Rep. 5 (2015) 1–8. https://doi.org/10.1038/srep09085.

[45] K.C. Kao, T.S. Lin, C.Y. Mou, Enhanced activity and stability of lysozyme by immobilization in the matching nanochannels of mesoporous silica nanoparticles, J. Phys. Chem. C. 118 (2014) 6734–6743. https://doi.org/10.1021/jp4112684.

[46] J. Kijima, Y. Shibuya, K. Katayama, T. Itoh, H. Iwase, Y. Fukushima, M. Kubo, A. Yamaguchi, Structural Characterization of Myoglobin Molecules Adsorbed within Mesoporous Silicas, J. Phys. Chem. C. 122 (2018) 15567–15574. https://doi.org/10.1021/acs.jpcc.8b04356.

[47] L.C. Sang, A. Vinu, M.O. Coppens, General description of the adsorption of proteins at their iso-electric point in nanoporous materials, Langmuir. 27 (2011) 13828–13837. https://doi.org/10.1021/la202907f.

[48] J. Meissner, A. Prause, B. Bharti, G.H. Findenegg, Characterization of protein adsorption onto silica nanoparticles: influence of pH and ionic strength, Colloid Polym. Sci. 293 (2015) 3381–3391. https://doi.org/10.1007/s00396-015-3754-x.

[49] Z. Wu, D. Zhao, Ordered mesoporous materials as adsorbents, Chem. Commun. 47 (2011) 3332–3338. https://doi.org/10.1039/c0cc04909c.

[50] A. Wilson, J.N. Kinney, P.H. Zwart, C. Punginelli, S. D'Haene, F. Perreau, M.G. Klein, D. Kirilovsky, C.A. Kerfeld, Structural determinants underlying photoprotection in the photoactive orange carotenoid protein of cyanobacteria, J. Biol. Chem. 285 (2010) 18364–18375. https://doi.org/10.1074/jbc.M110.115709.

[51] E.G. Maksimov, N.N. Sluchanko, Y.B. Slonimskiy, E.A. Slutskaya, A. V. Stepanov, A.M. Argentova-Stevens, E.A. Shirshin, G. V. Tsoraev, K.E. Klementiev, O. V. Slatinskaya, E.P. Lukashev, T. Friedrich, V.Z. Paschenko, A.B. Rubin, The photocycle of orange carotenoid protein conceals distinct intermediates and asynchronous changes in the carotenoid and protein components, Sci. Rep. 7 (2017) 1–12. https://doi.org/10.1038/s41598-017-15520-4.

[52] Y.B. Slonimskiy, F. Muzzopappa, E.G. Maksimov, A. Wilson, T. Friedrich, D. Kirilovsky, N.N. Sluchanko, Light-controlled carotenoid transfer between water-soluble proteins related to cyanobacterial photoprotection, FEBS J. 286 (2019) 1908–1924. https://doi.org/10.1111/febs.14803.

[53] M. Gwizdala, A. Wilson, D. Kirilovsky, In vitro reconstitution of the cyanobacterial photoprotective mechanism mediated by the orange carotenoid protein in synechocystis PCC 6803, Plant Cell. 23 (2011) 2631–2643. https://doi.org/10.1105/tpc.111.086884.

[54] S. Gupta, M. Guttman, R.L. Leverenz, K. Zhumadilova, E.G. Pawlowski, C.J. Petzold, K.K. Lee, C.Y. Ralston, C.A. Kerfeld, Local and global structural drivers for the photoactivation of the orange carotenoid protein, Proc. Natl. Acad. Sci. U. S. A. 112 (2015) E5567–E5574. https://doi.org/10.1073/pnas.1512240112.

[55] R.L. Leverenz, M. Sutter, A. Wilson, S. Gupta, A. Thurotte, C.B. De Carbon, C.J. Petzold, C. Ralston, F. Perreau, D. Kirilovsky, C.A. Kerfeld, A 12 Å carotenoid translocation in a photoswitch associated with cyanobacterial photoprotection, Science (80-.). 348 (2015) 1463–1466. https://doi.org/10.1126/science.aaa7234.

[56] E.G. Maksimov, N.N. Sluchanko, Y.B. Slonimskiy, K.S. Mironov, K.E. Klementiev, M. Moldenhauer, T. Friedrich, D.A. Los, V.Z. Paschenko, A.B. Rubin, The Unique Protein-to-Protein Carotenoid Transfer Mechanism, Biophys. J. 113 (2017) 402–414. https://doi.org/10.1016/j.bpj.2017.06.002.

[57] S. Bandara, Z. Ren, L. Lu, X. Zeng, H. Shin, K.H. Zhao, X. Yang, Photoactivation mechanism of a carotenoidbased photoreceptor, Proc. Natl. Acad. Sci. U. S. A. 114 (2017) 6286–6291. https://doi.org/10.1073/pnas.1700956114.

[58] M. Golub, M. Moldenhauer, F.J. Schmitt, W. Lohstroh, E.G. Maksimov, T. Friedrich, J. Pieper, Solution Structure and Conformational Flexibility in the Active State of the Orange Carotenoid Protein. Part II: Quasielastic Neutron Scattering, J. Phys. Chem. B. 123 (2019) 9536–9545. https://doi.org/10.1021/acs.jpcb.9b05073.

[59] P. Chábera, M. Fuciman, P. Híbek, T. Polívka, Effect of carotenoid structure on excited-state dynamics of carbonyl carotenoids, Phys. Chem. Chem. Phys. 11 (2009) 8795–8803. https://doi.org/10.1039/b909924g.

[60] B. Fernández-González, G. Sandmann, A. Vioque, A new type of asymmetrically acting β-carotene ketolase is required for the synthesis of echinenone in the cyanobacterium Synechocystis sp. PCC 6803, J. Biol. Chem. 272 (1997) 9728–9733. https://doi.org/10.1074/jbc.272.15.9728.

3.8 Supplementary Information

3.8.1 Quantification of OCP(CAN) loaded on SBA-15-80 by TGA

Sample of OCP(CAN) in SBA-15-80 has been chosen to perform thermo-gravimetric analysis. Data of TGA have been normalized around 100°C to not visualize the loss caused by water. As a blank, a sample of SBA-15-80 treated with water following the same procedure of protein loading has been used. The greatest evidence is that for sample of OCP in SBA-15-80, there is an inflection point around 300°C that could be attributed to the loss of the protein because of its lack in sample of empty SBA-15. The amount of OCP loaded was 52 mg/g while a weight loss of 88 mg/g has been recorded by TGA.

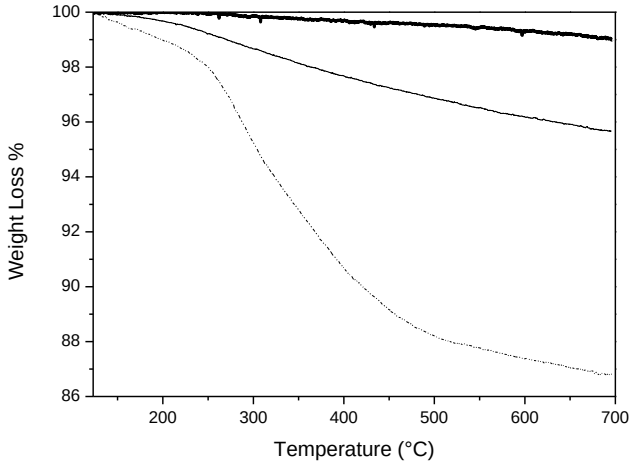

Figure SI 1. 3-1 TGA on SBA-15-80 (thick), SBA-15-80 water blank (thin) and OCP(CAN) 52mg/g on SBA-15-80 (thin dash-dot).

3.8.2 Effect of temperature on 1 week-aged samples

The aging effect was tested on temperature-sensors based on OCP immobilized on SBA-15. OCP(ECN), OCP(CAN), SBA-15-80 and SBA-15-80-NH_2 were chosen to perform these tests. Solutions of OCP(ECN) and OCP(CAN) as well as samples of the two types of proteins immobilized on SBA-15 and SBA-15-NH_2 were prepared as previously described and stored in the fridge at 4°C for 1 week, in the dark. Then, they have been tested and analysed as already described in 3.5.1. OCP(ECN) and OCP(CAN) in water solution keep their structure and spectroscopical properties at 40°C but they are denatured at 60°C and this is confirmed by the loss of the vibrational structure and by the yellow colour, typical of the free carotenoid (**Figure**

SI 1. 3-2, IA-IIA). OCP(ECN) in SBA-15 at 40°C is not thermally activated as for the fresh sample, while at 60°C the protein is denatured and a single maximum is shown, more similar to the spectrum of echinenone in solution (476 nm), suggesting a denaturation of the protein (**Figure SI 1. 3-2**, IB). OCP(ECN) in SBA-15-NH_2 does not show a clear redshift at 40°C and preserves a partial orange form before being denatured at 60°C (**Figure SI 1. 3-2**, IC). In parallel, temperature response of OCP(CAN) has been tested after protein loading and thermal treatment as described before. OCP(CAN) in SBA-15 is not able to preserve the orange form (as already described in **Figure 3.8**, IIA-IIB) indeed there is no red shift at 40°C, while at 60°C the protein is denatured and the spectral maximum down-shifts suggesting the denaturation of the protein (**Figure SI 1. 3-2**, IIB). OCP(CAN) in SBA-15-NH_2 preserves the orange form, at 40°C is not thermal activated, while at 60°C it is denatured (**Figure SI 1. 3-2**, IIC).

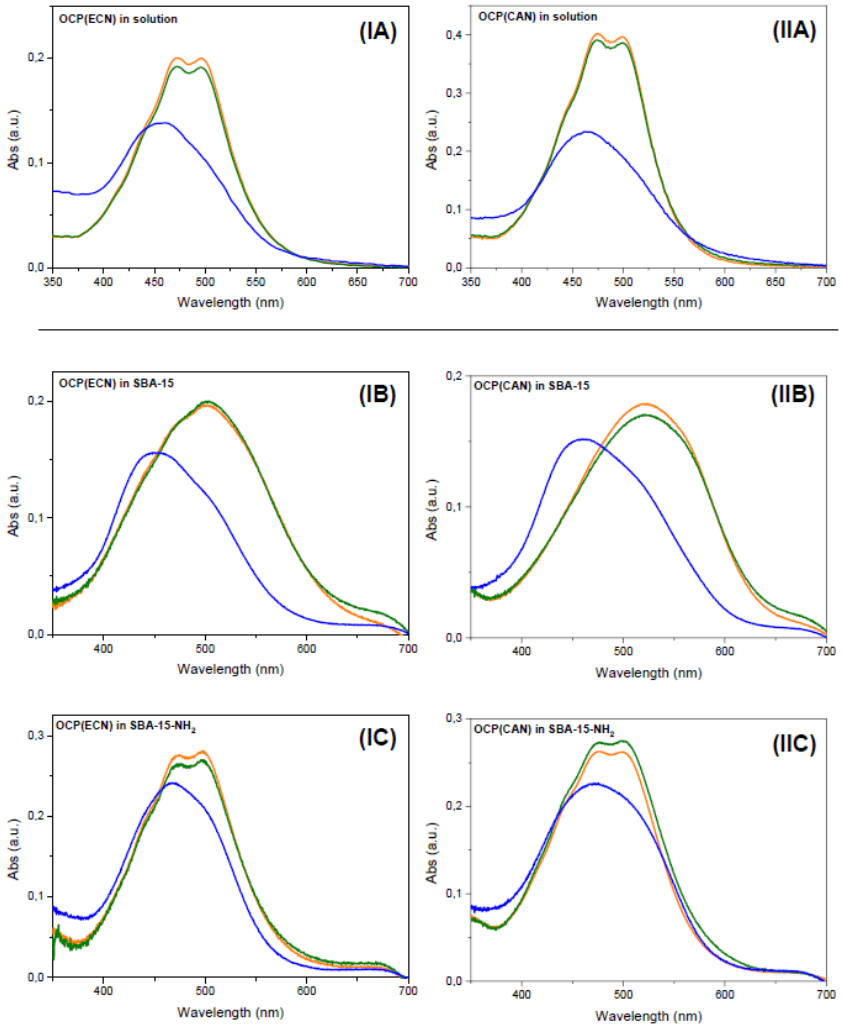

Figure SI 1. 3-2 Visible spectra recorded in 350-700 nm range. (Orange) Spectra before thermal treatment; (Green) spectra of samples treated at 40°C; (Blue) spectra of samples treated at 60°C. OCP(ECN) in solution (IA), OCP(CAN) in solution (IIA), OCP(ECN) in SBA-15-80 (IB), OCP(ECN) in SBA-15-80-NH_2 (IC), OCP(CAN) in SBA-15-80 (IIB), OCP(CAN) in SBA-15-80-NH_2 (IIC). Spectral intensity variability depends on sample preparation before the analysis.

3.8.3 Effect of pH on OCP (ECN or CAN) in SBA-15 matrices

SBA-15 bare matrices were initially dismissed because the bare surface is not able to keep OCP orange form (see **Figure 3.8**). However, we decided to test the effect of pH even on this matrix. SBA-15-120 matrix was chosen for these experiments. For OCP(ECN) immobilized on SBA-15-120, at strong acidic pH (e.g., 1 and 3) the protein is denatured, and the spectrum of the carotenoid is shown (λ_{max} 446 nm); almost a similar situation is reproduced at strong basic pH (e.g., 13) even if OCP seems to be less denatured as stated by the peak at λ_{max} 468 nm (**Figure SI 1. 3-3**). In the range of pH 5 to 11 the protein is red, as shown by the λ_{max} of the peak at 500 nm and by the pictures of the sample-holders (bottom of **Figure SI 1. 3-3**). For OCP(CAN) immobilized on SBA-15-120 at strong acidic pH (e.g., 1) the protein is denatured (λ_{max} 455 nm), while for pH from 3 up to 11 OCP is in the red form (λ_{max} 506 nm). At pH 13 the protein is orange, as shown by the vibronic structure of the spectrum (**Figure SI 1. 3-3**).

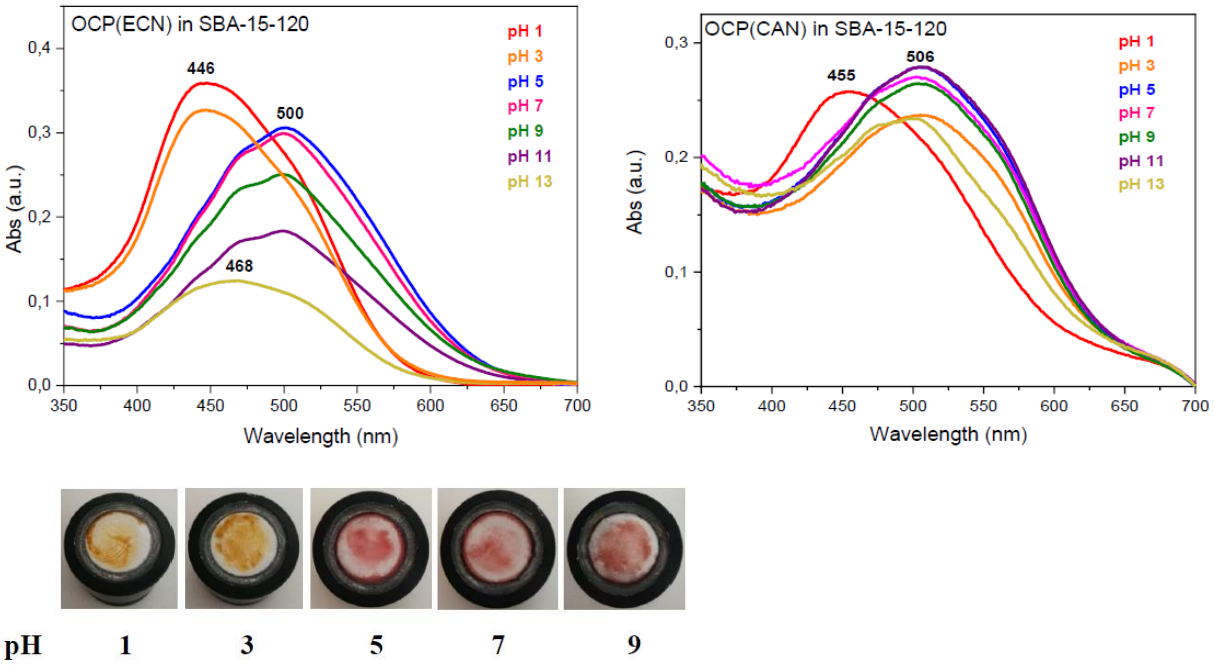

Figure SI 1. 3-3 (Top) Visible spectra of OCP(ECN) (left) and OCP(CAN) (right) immobilized on SBA-15-120 at different pH. Samples kept in the dark during the experiment. (Bottom) Pictures of sample-holder of samples of OCP(CAN) in SBA-15-120 treated at different pH: 1, 3, 5, 7 and 9 (left to right).

3.8.4 Effect of “in situ” titration on OCP in SBA-15-NH_2 matrix

An “*in situ*” titration of the same sample was performed by titration of the same sample at pH 1, 3 and 13 which correspond to the protein colour change values. Experiments were performed on OCP(CAN)-loaded SBA-15-80-NH_2. The sample was firstly placed in contact with 1 mL of solution at pH 1, stirred for 30 min, centrifuged, and then analysed with Visible solid phase spectroscopy. The same sample was then titrated with 1 mL of solution at pH 3 and analysed in the same way. Eventually, the sample was treated at pH 13 and analysed.

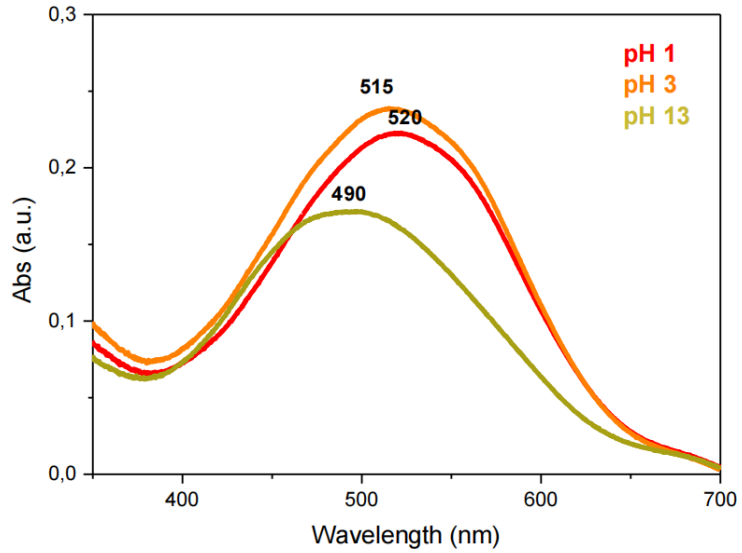

Figure SI 1. 3-4 Visible spectra of OCP(CAN) immobilized on SBA-15-80-NH_2 titrated at different pH (1, 3 and 13). Samples kept in the dark during the experiment.

4. OCP on SBA-15 for the development of photoactivable nanodevices

4.1 Introduction

The work described in this chapter takes inspiration from a work published by Andreoni *et al.*[1] and focused on the development of a light-dependent tuneable energy-transfer between two dyes, using the spectral shift of the Vis absorption spectrum of OCP upon photoconversion. The authors developed a three-strand DNA junction, incorporating OCP, aiming to the construction of photonic systems to be applied in artificial photosynthesis or as starting point for the development of complex photonic networks[1].

The idea of tuning the energy-transfer between fluorescent dyes, inspired us for the development of photoactivable nanodevices with tuneable fluorescence based on OCP- and dye-loaded nanoparticles of SBA-15. The photoconversion of OCP^O into OCP^R creates an overlap between the emission spectra of the fluorophores and the absorption spectrum of OCP^R, which is therefore able to partially quench the fluorescence of the fluorophores (see the scheme in **Figure 4.1**). The main application of this system could be in fluorescence imaging, a technique widely used in several fields, including biology. However, the performance of these nanodevices depends on OCP and dye loading, stability over time, photostability and possible dye and OCP leakages. On the other hand, the possibility of modifying SBA-15 internal surfaces by chemical functionalization and the appropriate choice of dyes have a high potential for the tailoring of these properties[2]. Furthermore, the possibility of size and surface properties tuning makes these mesoporous silica nanoparticles suitable supports[3]. Furthermore, mesoporous silica NPs are also a suitable vehicle for fluorescent molecules because of their optical transparency[4]. Finally, the hydrophilic surface of these NPs make it possible to use hydrophobic or poor water-soluble dyes[5].

Fluorescent NPs have been mostly used in biomedical research for diagnosis and treatment of solid tumours for their ability to penetrate the tumour tissues[6,7]. Indeed, mesoporous silica NPs have been used to increase the levels of anticancer drugs in cancerous tissues, increasing the efficacy and reducing the side effects of the loaded anticancer drugs[8,9]. Furthermore, these systems have been used as fluorescent biosensors to detect biomolecules[10,11] or ions in aqueous media[12,13], for quantitative or qualitative analysis[14,15], to study the conformational dynamics of folding and unfolding of proteins immobilized on silica NPs[16].

Among the several groups of organic fluorophores, cyanine molecules were chosen, as they are widely-used synthetic organic fluorescent dyes. Furthermore, the attention was also focused on some naturally occurring fluorescent flavonols (a sub-class of flavonoids). Beside their interesting emitting properties, they are also powerful antioxidants.

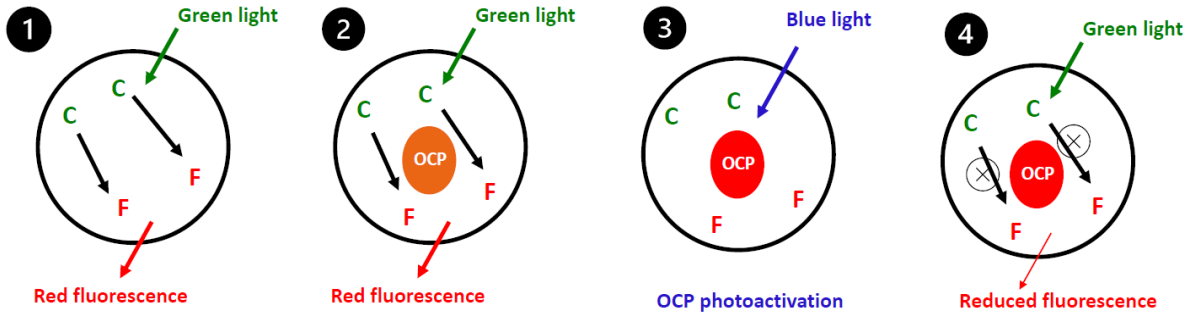

Figure 4.1 Scheme of energy-transfer between a chromophore (C) and a fluorophore (F) immobilized on silica NPs (black circle). (1) Green light absorbed by C is transferred to F which emits fluorescence in the red range. (2) OCP immobilized on the NPs allows the same energy-transfer between C and F. (3) Photoactivation of OCP by blue light converts the protein into the red form. (4) In presence of OCP^R the fluorescence of the system is partially quenched, and the intensity of the emission is reduced.

4.1.1 Cyanine Cy3 and cyanine Cy5

Cyanine molecules are dyes classified into two main types, naturally occurring cyanine dyes (vegetable source) and pure synthetic cyanine dyes (chemical source) with a general formula ($R_2N[CH=CH]_nCH=N^+R_2$) in which the nitrogen and part of the conjugated chain usually form part of a heterocyclic system, such as imidazole, pyridine, pyrrole, quinoline and thiazole[17]. Cyanine dyes were synthetised over a century ago and they were originally used in film-based photography to increase the wavelength range forming an image on the film. Nevertheless, it was accidentally discovered that cyanine dyes are present as colourants in natural products as the toadstool *Amanita muscaria*[18].

Cyanine dyes generally have two nitrogen heterocyclic rings joined by a conjugation chain of carbon atoms. The real structure of the cyanine is a resonance hybrid between two resonance forms that have the responsibility for the intensity of the colour of cyanine dyes where they produce a delocalized positive charge over the conjugated structure system of cyanine dyes. These dyes have tuneable wavelengths across the visible spectrum and exhibit high molar extinction coefficients (values in the order of 2.5×10^4 M^{-1} cm^{-1})[19] permitting the use of low concentrations. Cyanine dyes are classified according to the number of methine (-CH=) groups in the chain between the two ring systems and the nature of the ring moiety present[20].

Nowadays cyanine dyes are widely used in several fields as biotechnology industry, material engineering, medicine and pharmacology[21–23]. There is a growing number of applications

of modified biomolecules including clinical immunoassay, DNA hybridization tests, gene fusion detection tests, etc[24,25].

A study was published by Song *et al.*[26] about the synthesis of mesoporous silica-coated Au NPs loaded with a NIR fluorescent cyanine dye (adsorbed on the surface by electrostatic interactions) for *in vivo* computed tomography and fluorescence imaging. Indeed, fluorescence imaging is a non-invasive, and sensitive imaging technique; it can provide, in real time, information at cellular and molecular level.

4.1.2 Flavonols

Flavonoids are natural polyphenolic compounds, widely distributed among the plants. Indeed, more than 5000 varieties of flavonoids are known[27]. Flavonoids exist as aglycones, glycosides and methylated derivatives and they occur in huge variety of structures[28]. Flavonoids aglycones contain fifteen carbon atoms in their basic nucleus, that consist of two six-membered rings linked with a three carbon unit which may be a part of a third ring (the rings are labelled A, B, and C)[29]. A and C rings are numbered with ordinary numerals while "primed" numerals are used for B ring (structure of Flavone is shown in **Figure 4.2**).

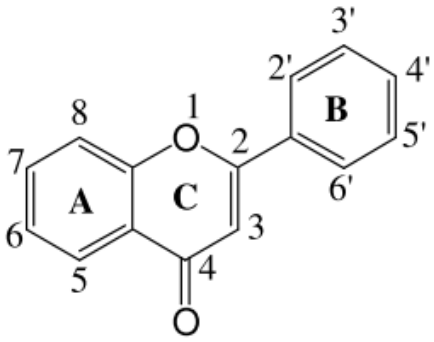

Figure 4.2 Chemical structure of Flavone[30].

Flavonoids are commonly found in fruit, vegetables, onions, olives, tea and red wine[31]. They have shown potential beneficial effects: antioxidants, anti-inflammatory, antiallergic, hepatoprotective, antithrombotic, antiviral, antibacterial and anticarcinogenic activities[32–38]. Immobilization of flavonoids on mesoporous silica NPs gained attention over the past years. Organo-functionalized silica NPs were used as topical carrier of antioxidant flavonoids increasing their stability, epidermal delivery and topical efficiency[39,40]. Indeed, these compounds are sensitive to several environmental factors such as light, oxygen and pH[41].

Silica NPs have demonstrated to be a suitable vehicle for the antioxidant flavonoids, resulting to be good radical scavengers and $^1O_2$ quenchers[42]. Furthermore, flavonoid-doped mesoporous silica NPs were found to interact with model cell membranes aiming to the development of innovative markers and delivery systems of bioactive molecules with the purpose of monitoring drug-induced effects at the cellular level[43].

To the best of our knowledge, no studies have been reported regarding the use of flavonoid-doped mesoporous silica NPs in fluorescence imaging. This work takes origin from a previous study on flavonoid immobilization on MCM-41 mesoporous silica matrices which has shown that 3-hydroxyflavone and 7-hydroxyflavone-based fluorescent silica NPs can be easily obtained by a post-doping procedure[44,45]. The present work aims to develop photo-modulable fluorescent NPs which are not only biocompatible, but also endowed with antioxidant properties. Indeed, both the fluorophore (flavonoid) and the photo-modulation element - OCP - are strong antioxidants.

The "flavonol" sub-group was chosen for this study. Flavonols are abundant in a variety of fruits and vegetables but also in tea and red wine. They have a hydroxyl group in position 3 of the C ring (see **Figure 4.2**). The intramolecular hydrogen bond between the 3-hydroxyl group and the carbonyl moiety (position 4 of the C ring), plays a key role in the photo-physics of these molecules. When irradiated, two emissions are in competition: fluorescence can originate from the photoexcited state of the neutral form N*, or from the photo-tautomer T*, or from the Excited-State Intramolecular Proton Transfer (ESIPT) from the 3-OH group to the C=O. (**Figure 4.3**). Therefore, excitation of the flavonol results in a dual emission: a first around 400 nm (from N* state) and a second in the 510–540 nm range (from T*). In the case of the ESIPT pathway, the obtained ground state tautomer (T) finally undergoes a thermal back proton transfer to the N ground state[46]. In apolar solvents, ESIPT is the only occurring process. However, emission properties depend on the interaction with the surrounding environment and as a result the N* emission is often observed. Furthermore, specific interactions with the surrounding molecular environment induce ground state deprotonation of the 3-OH group to give anionic form (A). The emission from A* takes place in the 460–500 nm range and is therefore separated from N* and T* fluorescence bands[47]. Situation can be even more complicated in flavonols possessing other OH groups on the A or B rings.

After the test on the combined use of two cyanine dyes, we tried to use one single fluorescent molecule (a flavonol) which, thanks to its ESIPT based photo-physics, absorbs light in the UV and emits fluorescence mainly in the green.

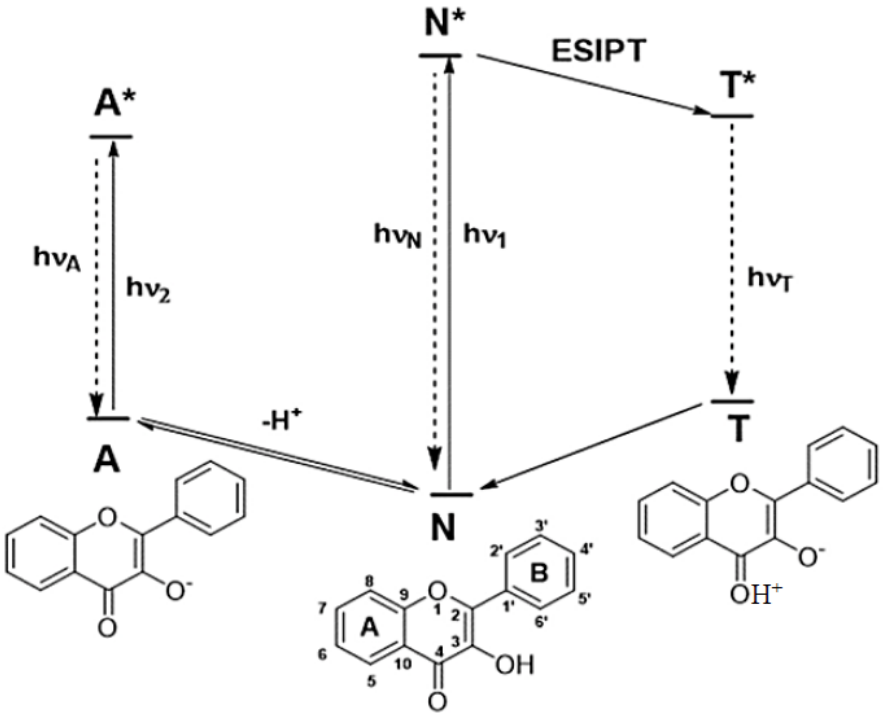

Figure 4.3 Pathway of excitation from the ground state and emission from the excited states of 3HF (3-hydroxy flavone) : (left) anionic form A, (middle) neutral form N, (right) tautomeric form (T)[46].

4.2 Materials

4.2.1 Cyanine Cy3 and cyanine Cy5

The two organic dyes, Cyanine Cy3 carboxylic acid and Cyanine Cy5 carboxylic acid respectively, were purchased by Lumiprobe - Life science solutions. Their structure and spectroscopical features are shown in **Figure 4.4**. The two dyes differ in the number of conjugated C–C double bonds: Cy5 has one more double bond compared to Cy3 and this difference is reflected in the red-shift of the spectroscopical properties of Cy5. Cy3 appears as a red powder in solid phase and gives a magenta solution in water. Its excitation/absorption maximum is at 555 nm while the emission maximum is at 570 nm. Cy5 appears as a dark blue powder in solid phase and gives a light blue solution in water. Its excitation/absorption maximum is at 646 nm while the emission maximum is at 670 nm. The two fluorophores undergo a FRET (Forster Resonance Energy Transfer) phenomenon, a non-radiative energy-transfer occurring between a donor and an acceptor. Indeed, there is a spectral overlap between the emission spectrum of Cy3 and the excitation spectrum of Cy5 so that, if the two cyanine dyes are close enough to each other (FRET efficiency is inversely proportional to the distance

between donor and acceptor), the energy absorbed by Cy3 and then emitted during its relaxation, is directly absorbed by Cy5 which will relax emitting at a red-shifted wavelength[1]

.

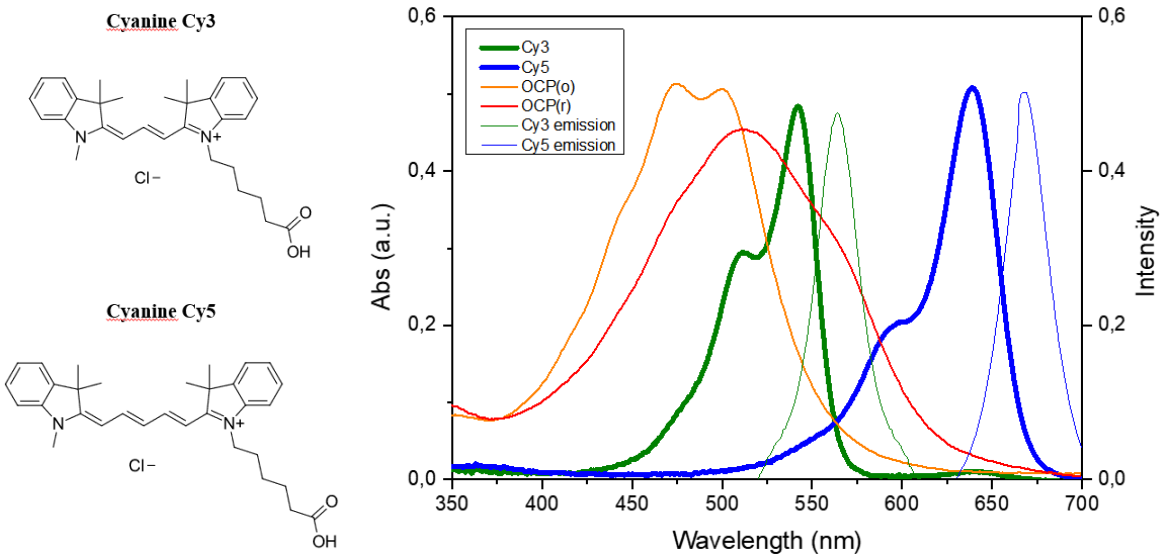

Figure 4.4 (Left) Chemical structure of cyanine Cy3 (top) and cyanine Cy5 (bottom). (Right) Absorption (thick lines) and emission (thin lines) spectra of Cy3 (green lines) and Cy5 (blue lines); absorption spectra of OCP^O (orange line) and OCP^R (red line).

4.2.1 Flavonols

The flavonols used to carry out the experiments are: 3-hydroxyflavone (3HF) (Aldrich, > 90%), Morin (Aldrich, > 90%) and Fisetin (Aldrich, > 90%). Flavonol solutions were prepared in absolute ethanol (Aldrich; 99.9%) at a concentration of 50 µM. The 3HF has shown to be the most suitable flavonol to perform the fluorescence tuning in presence of the photoactive OCP. Data of Morin and Fisetin (more affected by photo-decomposition problems) are shown in S.I. at the end of this chapter.

The chemical structure and the absorbance-emission spectra of the 3HF are shown in **Figure 4.5**. The absorbance maximum was used as maximum wavelength of excitation for photoluminescence experiments, notably 350 nm for 3HF.

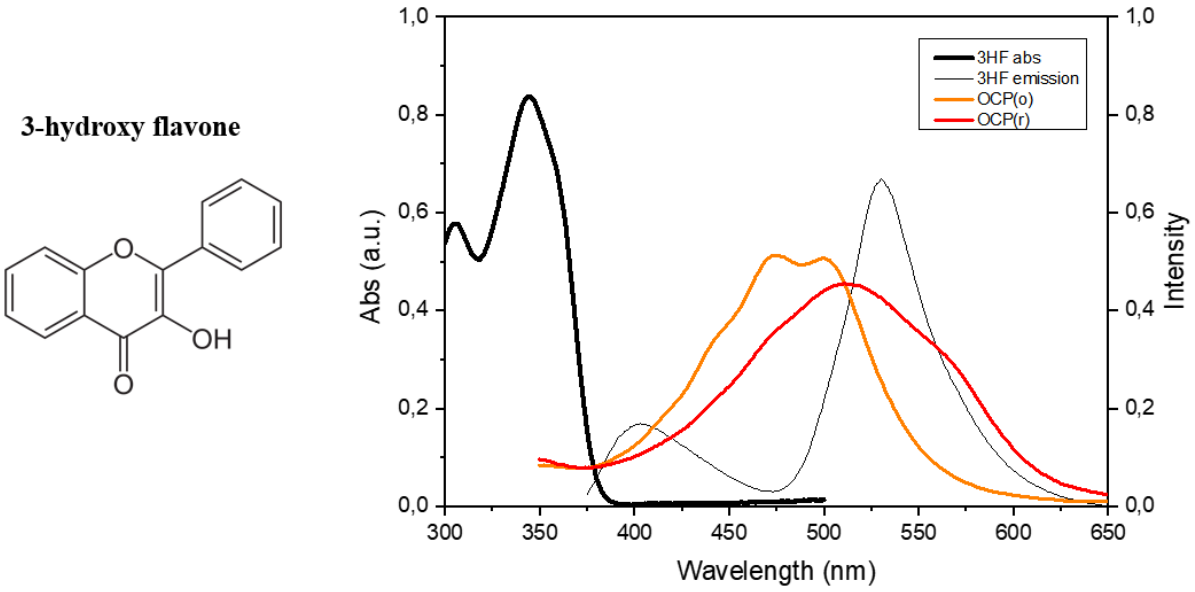

Figure 4.5 (Left) Chemical structure of 3-hydroxy flavone (3HF). (Right) Absorbance and emission spectra of 3HF (thick and thin black lines, respectively) and absorbance spectra of OCP^O (orange line) and OCP^R (red line).

4.3 Methods

4.3.1 Sample preparation

Experiments were carried out with SBA-15-80-NH_2 (hereafter referred to as SBA-15-NH_2) as mesoporous solid support and OCP(CAN) solution at 0.2 mg/mL concentration which corresponds to the maximum immobilization efficiency recorded (see Chapter 3). The choice of the matrix and the type of OCP was motivated by the efficiency of the system OCP(CAN)@SBA-15-NH_2 in terms of better immobilization efficiency, preservation of photo-properties of OCP, stability in time, back-conversion of the system (with a slower kinetic), as detailed in Chapter 3.

4.3.1.1 Cyanine Cy3 and Cyanine Cy5

Experiments were carried out using 4 µM stock solutions of Cy3 and Cy5 in Milli-Q water (pH 7 for Cy3 and pH 6.5 for Cy5). First, immobilization of cyanine on SBA-15-NH_2 was performed adding 1 mL of cyanine stock solution to 10 mg of SBA-15-NH_2 powder in an Eppendorf. The sample was gently stirred for 1 hour on a moving plate and then centrifuged for 30 min at 8000 rpm. Cyanine dyes were first immobilized on silica separately and, in parallel, solution of the

two cyanine dyes at different ratio (Cy3:Cy5 = 1:1, 1:4 and 1:10) were immobilized following the same procedure.

To carry out the following immobilization of OCP, 1 mL of OCP(CAN) 0.2 mg/mL was added to the dye-loaded SBA-15-NH_2 pellet and gently stirred for 4 hours (time required to reach the OCP maximum loading, see Chapter 3) on a moving plate, in the dark, to avoid the photo-activation of the protein. Then the sample was centrifuged for 30 min at 8000 rpm and the solvent removed. A blank sample was prepared adding 1 mL of aqueous buffer (Tris/NaCl) to the cyanine-doped SBA-15-NH_2 (10 mg), gently stirring for 4 hours on moving plate and then centrifuging for 30 min at 8000 rpm. The supernatant collected was used to carry out UV-Visible spectroscopy analysis in liquid phase, while the pellet was used to carry out UV-Visible spectroscopy analysis in solid phase and photoluminescence tests.

4.3.1.2 Flavonols

Several types of flavonols have been tested. Among them, best results were obtained with 3-hydroxy flavone (3HF), and they are shown in this chapter, while data obtained with morin and fisetin are shown in S.I. at the end of the chapter. Other flavonols, notably quercetin, kaempferol and galangin were tested but they did not produce satisfactory results because of their low photo-stability.

The 3HF loading on SBA-15-NH_2 was carried out adding 1 mL of flavonoid solution 50 µM in ethanol (pH = 7.5) to 10 mg of SBA-15-NH_2 powder, gently stirring for 30 min on moving plate and drying for 2 hours at 30°C under vacuum to remove the solvent. The following loading of OCP was carried out adding 1 mL of OCP(CAN) solution 0.2 mg/mL to the flavonoid-doped SBA-15-NH_2 dry powder (10 mg), gently stirring for 4 hours (following the protocol of protein immobilization outlined in Chapter 3) and then centrifuging for 30 min at 8000 rpm. A blank sample was prepared adding 1 mL of aqueous buffer (Tris/NaCl) to the flavonoid-doped SBA-15-NH_2 (10 mg), gently stirring for 4 hours on moving plate and then centrifuging for 30 min at 8000 rpm. The supernatant collected was used to carry out UV-Visible spectroscopy analysis in liquid phase, while the pellet was used to carry out UV-Visible spectroscopy analysis in solid phase and photoluminescence tests.

4.3.2 Detection

Fluorescence was measured on HORIBA Scientific Fluorolog 3 apparatus. The instrument is composed by a Xenon lamp at 450 W, equipped with a dual array monochromator (Grating 1200 gr/mm) to select the incident wavelength, with a dual array monochromator (Grating 1200 gr/mm) to analyse the emission and with a photomultiplier-type detector (PM R928).
Absorption spectra of solids were recorded on a Varian 2300 UV Vis spectrophotometer equipped with an integrating sphere between 350 and 750 nm with a resolution of 1 nm and an acquisition time of 0.1 s per point. Absorption spectra in liquid phase were recorded on Biochrom Libra S60 spectrophotometer, between 250 and 700 nm with a resolution of 0.5 nm and an acquisition time of 0.1 s per point. A 1 cm path quartz cuvette was used.

4.4 Results and discussion

4.4.1 Cy3-Cy5 and OCP on SBA-15-NH_2 as photo-modulable fluorescent device

4.4.1.1 Immobilization of Cy3 and Cy5 on SBA-15-NH_2

Cy3 and Cy5 were separately immobilized on silica to test the effect of the constraint of the matrix on the absorbance and emission of the dyes. UV-Visible solid phase and photoluminescence analysis have shown that the external environment did not affect the spectroscopical properties of Cy3 and Cy5 (left side of **Figure 4.6**). The actinic light used for fluorescence experiments did not induce significant photodegradation of Cy3 and Cy5, indeed the absorbance spectra of the two cyanine dyes after photoluminescence measurements were the same as before (**Figure SI 1. 4-1**).
Later, immobilization of the dyes on SBA-15-NH_2 was carried out following the protocol over illustrated, exploring different Cy3:Cy5 ratio (notably 1:1, 1:4 and 1:10 to a global concentration of 4 µM). Experiments of Visible spectroscopy in liquid phase (carried out on the supernatant after the immobilization on silica) have shown that, for the three ratios, the maximum immobilization efficiency (IE %) reached, hovers around 70%. For each ratio, analysis of Visible spectroscopy and photoluminescence spectroscopy were performed (right side of **Figure 4.6**). Visible spectroscopy demonstrated that the absorbance intensity of Cy3 and Cy5 was proportional to the ratio of the solution. In parallel, photoluminescence was carried out exciting the system with the maximum λ_{ex} of Cy3 (550 nm) and detecting the fluorescence of Cy5 in the range 620-700 nm. The highest intensity of emission was detected for the ratio

Cy3:Cy5=1:10, with the maximum at 672 nm (**Figure 4.6**). Aiming to detect the maximum quenching of the fluorescence caused by OCP photo-activation, the sample of dyes at ratio 1:10 was chosen for further experiments because of the maximum intensity of emission and therefore the maximum OCP-photoconversion-induced fluorescence quenching.

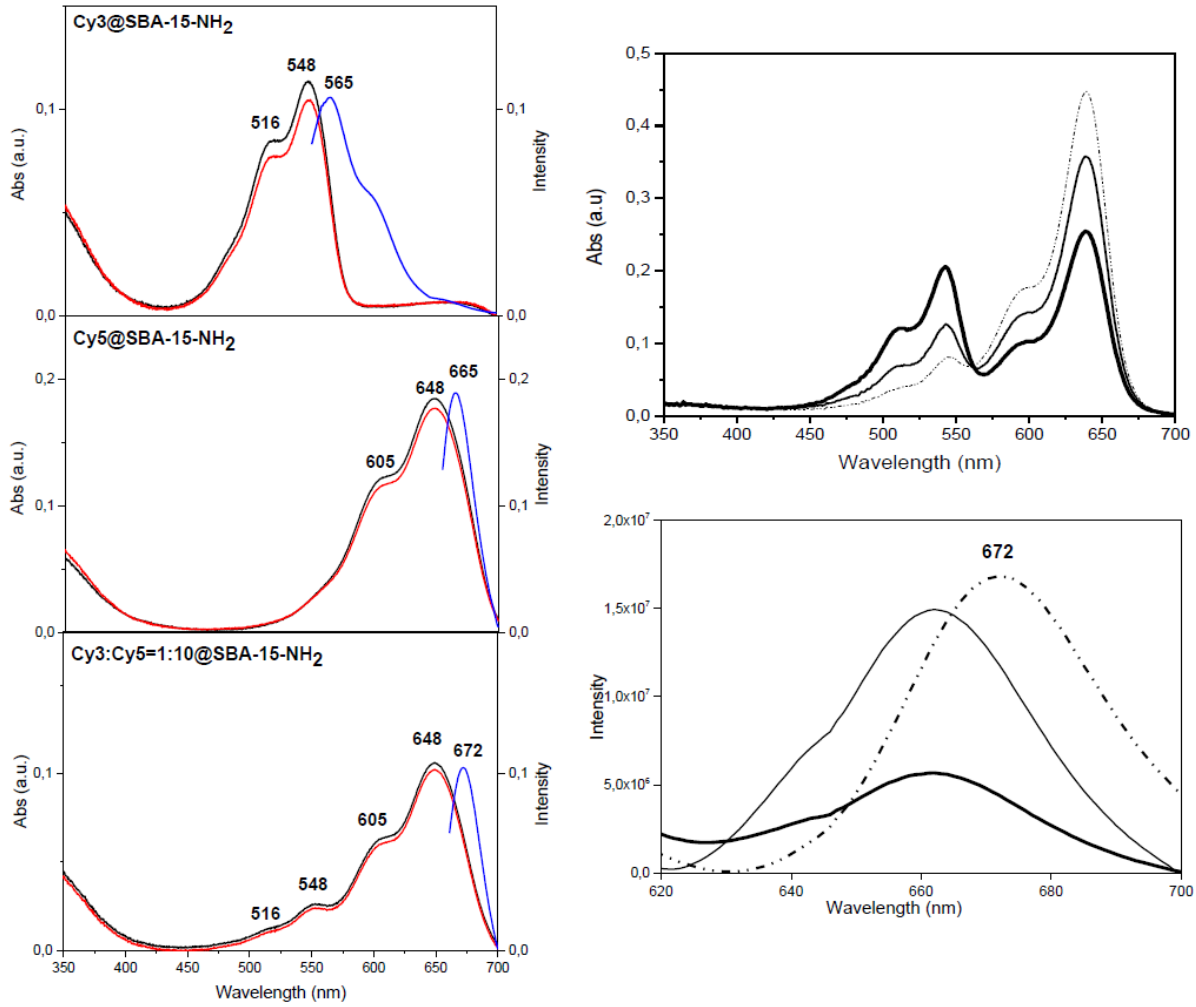

Figure 4.6 (Left) Visible solid phase spectra of Cy3, Cy5 and Cy3:Cy5=1:10 before (black line) and after (red line) illumination under blue light and emission spectra (blue line) recorded after cyanine dyes immobilization on SBA-15-NH_2. (Right) Visible absorbance spectra in solution (top) and emission spectra (bottom) of Cy3:Cy5 solutions 4 µM in H_2O at ratio 1:1 (thick line), 1:4 (thin line) and 1:10 (dash-dot-dash line).

The photostability of the system Cy3:Cy5=1:10 on SBA-15-NH_2 was tested. Dry samples prepared as described in the Methods section were placed in a thin quartz tube inside the photoluminescence analysis chamber. A blue light LED was also placed inside the chamber, 2 cm far away from the sample (see schematic representation in **Figure 4.7**). Once the LED lighted on, the fluorescence emission was measured at different times, notably after 10 min, 30 min and 1 hour (switching off the LED during the fluorescence measurement) and the experiment

showed that the system keeps its photo-stability because no difference in emission intensity was detected (**Figure SI 1. 4-1**).

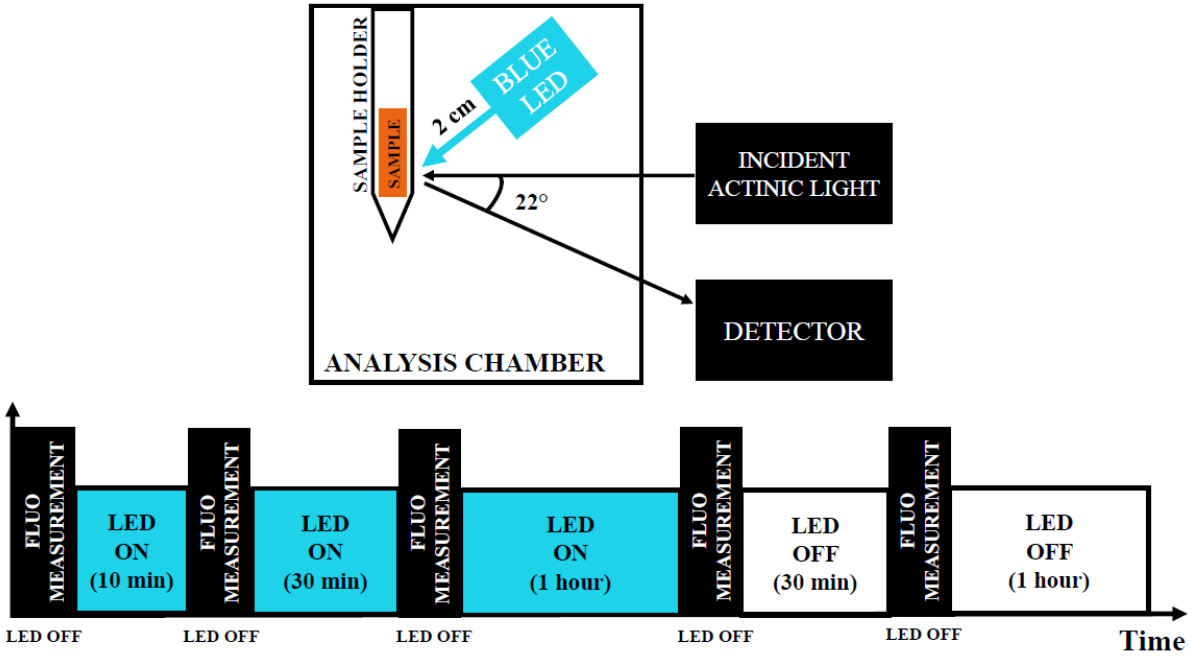

Figure 4.7 (Top) Schematic representation of experimental set up : blue light LED is placed inside the analysis chamber 2 cm far away from the sport of the sample (placed inside the sample holder); excitation comes from the incident actinic light and emission is detected with a 22 degrees angle. (Bottom) Time scheme of the experiment: LED is off during fluorescence measurement at t = 0; LED is switched on during different periods of time to photoactivate OCP and quench the fluorescence and after each period the LED is switched off to measure fluorescence; the recovery of OCP^O and the recovery of initial fluorescence is followed up keeping the analysis chamber in the dark, with the LED switched off.

4.4.1.2 Immobilization of OCP on Cy3:Cy5-loaded SBA-15-NH_2

OCP(CAN) was chosen for further experiments because it keeps the photo-activity and back-conversion properties once immobilized on SBA-15-NH_2 (see Chapter 3). Visible experiments in solid phase have shown that the presence of Cy3 and Cy5 on SBA-15-NH_2 does not affect the spectroscopical properties of OCP and its photoactivity. Indeed, the protein is photo-converted into the OCP red form after exposition to blue light LED and the spectrum is redshifted (**Figure 4.8**). The peak around 650 nm is attributed to Cy5 while absorbance of Cy3 (expected at 555 nm) is hidden under the spectra of OCP.

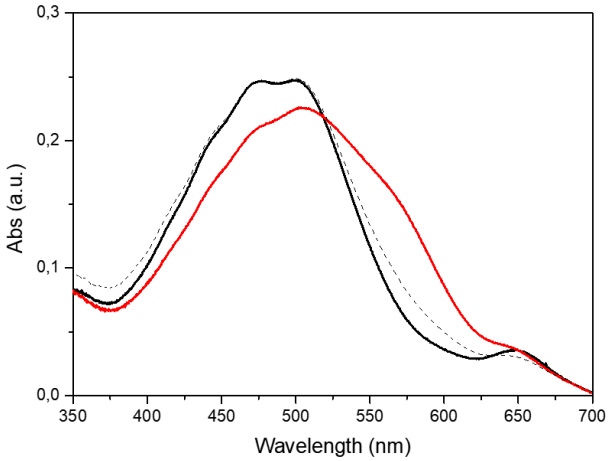

Figure 4.8 Visible solid phase spectra of OCP(CAN) 0.2 mg/mL immobilized on Cy3:Cy5=1:10-loaded SBA-15-NH_2 recorded before (black solid line), after 30 min (red line) of blue light LED illumination and after 12 hours dark-recovery (black dash line).

4.4.1.3 Fluorescence quenching and recovery

Photoluminescence experiments after different time of exposure to blue LED light were performed aiming to assess if the OCP^O - OCP^R photo-conversion (and the spectral overlap that this photo-conversion induces) can induce quenching of Cy5 fluorescence (**Figure 4.4**). The sample where OCP is immobilized on Cy3:Cy5-loaded SBA-15-NH_2, prepared as described above, was placed in photoluminescence sample-holder, inside the analysis chamber, and kept in the dark for 1 hour before performing the measure. At t = 0 an emission spectrum was collected, exciting the system at 555 nm (Cy3 (λ_{ex} max) and collecting the emission in the range 620 – 700 nm, where Cy5 emits. Later, the system was exposed to blue light from a LED placed 2 cm far away from the sample-holder (see picture in **Figure 4.9**). LED exposure times were 5, 10, 20 and 30 minutes. After each exposure a new emission spectrum was collected (the LED was switched off during the measurement). As shown in **Figure 4.9**, at t = 0 a peak at 672 nm appears, corresponding to Cy5 emission (already shown in **Figure 4.6**). Exposure to blue light, which triggers the photo-activation of OCP and the spectral red-shift of its Vis absorption spectrum, entails partial quenching of Cy5 fluorescence as observed by the decrease in intensity of the emission peak at ~665 nm (cyan lines, **Figure 4.9**). A 19 % quenching of fluorescence intensity is observed after 5 min of LED illumination. The percentage of fluorescence quenching rises to 27 % after 10 min of LED illumination, to 33 % after 20 min of LED illumination, and to 37 % after 30 min of LED illumination, reaching a plateau (see the left box

in **Figure 4.9**). Further exposure to LED blue light was avoided to prevent cyanine dyes photo-degradation.

The sample was kept in the dark and emission spectra (λ_{ex} = 555 nm) were collected after 30 minutes, 1 hour, 2 hours and 12 hours (overnight). The fluorescence intensity was almost completely restored after 2 hours in the dark and completely restored after 12 hours (black lines, **Figure 4.9**). Experiments were reproduced twice (**Figure SI 1. 4-2**). Furthermore, a blank-control sample without OCP (but in presence of its Tris-NaCl buffer solution) was analysed. No decrease in fluorescence intensity was observed after exposition to blue LED, suggesting that the quenching of Cy5 fluorescence was exclusively due to the OCP photo-conversion and consequent energy transfer from Cy3 to the carotenoid inside the protein (**Figure SI 1. 4-3**).

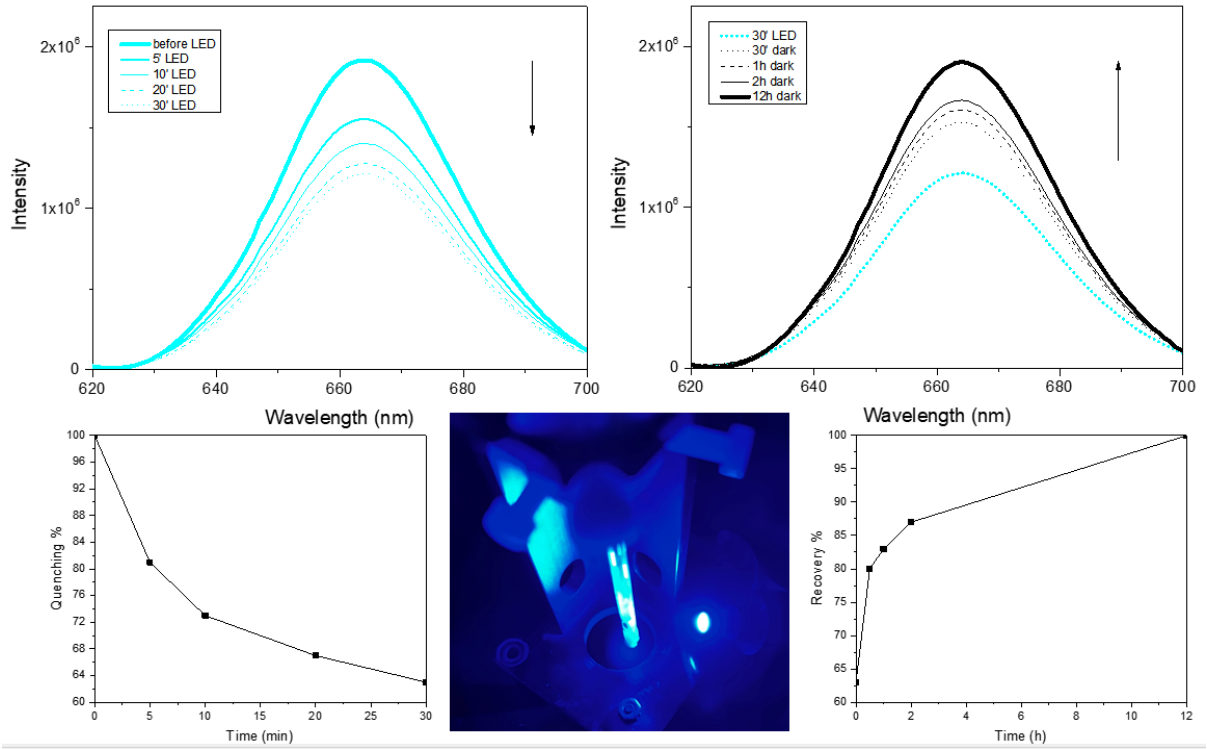

Figure 4.9 (Top) Emission spectra of Cy3:Cy5=1:10 immobilized on SBA-15-NH_2 in presence of OCP(CAN) 0.3 mg/mL. Spectra recorded exciting the system at 555 nm (Cy3 λ_{ex}) and detecting the fluorescence of Cy5 in the range 620-700 nm (Cy5 max λ_{em} at 672 nm) with a detector slit of 5 nm. (Left, top) Spectra recorded at t = 0 (before LED illumination), after 5, 10, 20 and 30 min of blue light LED illumination (LED was switched off during the emission measurements). (Left, bottom) Time (min)-resolved quenching % of Cy5 fluorescence under blue light LED exposition. (Right, top) Relaxation of the system and recovery of fluorescence were recorded after 30 min, 1 h, 2 h and 12 h in the dark. (Right, bottom) Time (h)-resolved recovery % of Cy5 fluorescence in the dark. (Bottom, in the middle) Picture of the inside of the analysis chamber, with the quartz thin tube holding the sample and the blue LED placed at 2 cm distance from the sample spot.

A second cycle of OCP photo-activation and fluorescence quenching was tested on the same sample and experiments have shown that Cy5 fluorescence is still able to be quenched as for the first cycle. Moreover, keeping the sample in the dark for 12 hours, fluorescence intensity was almost completely restored. Visible solid phase spectra confirmed that a 2nd cycle of photo-activation and back-conversion of OCP immobilised on Cy3:Cy5-loaded SBA-15-NH_2 NPs is possible (**Figure 4.10**).

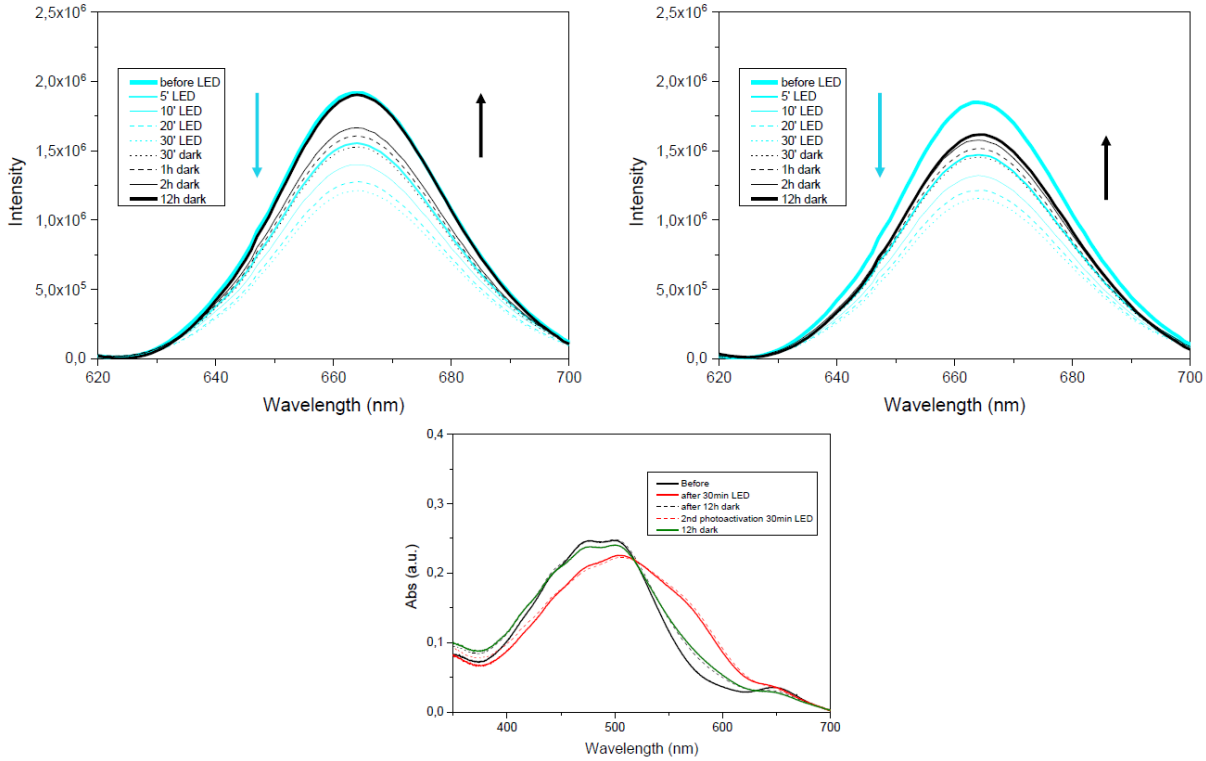

Figure 4.10 (Top) First cycle (left) and second cycle (right) of Cy5 fluorescence quenching. Emission spectra of Cy3:Cy5=1:10 immobilized on SBA-15-NH_2 in presence of OCP(CAN) 0.3 mg/mL. Spectra recorded exciting the system at 555 nm (Cy3 λ_{ex}) and detecting the fluorescence of Cy5 in the range 620-700 nm (Cy5 max λ_{em} at 672 nm) with a detector slit of 5 nm. (Cyan lines)) Spectra recorded at t = 0 (before LED illumination), after 5, 10, 20 and 30 min of blue light LED illumination (LED was switched off during the emission measurements). (Black lines) Relaxation of the system and recovery of fluorescence were recorded after 30 min, 1 h, 2 h and 12 h in the dark. (Bottom) Visible solid phase spectra of OCP(CAN) immobilized on Cy3:Cy5=1:10-loaded SBA-15-NH_2 recorded before (black solid line), after 30 min (red solid line) of blue light LED illumination and after 12 hours dark-recovery (black dash line); 2nd cycle of photoactivation was performed (red dash line) and 2nd back-conversion was observed (green line).

In parallel, a 5-day-old sample kept in the dark at 4°C, showed to keep the photo-properties of the system. Indeed, after exposition to LED illumination, fluorescence was quenched (25 % after 30 min of illumination) and almost completely restored after 12 hours in the dark (**Figure SI 1. 4-4**).

Based on data reported on Chapter 3 about the effect of pH on OCP immobilised on SBA-15-NH_2 showing that at pH = 1 OCP turns to the red form (even without blue light effect), we decided to test the chemically induced red conversion of OCP, so that a pH-drop induced Cy5 fluorescence quenching is obtained. Preliminary photoluminescence experiments were performed on a sample of Cy3:Cy5=1:10 and OCP(CAN) 0.3 mg/mL immobilised on SBA-15-NH_2 (as previously described). The sample was placed inside the sample-holder in the dark analysis chamber, emission spectrum was recorded and then a drop of HCl 1 M (pH = 1) was added inside the sample holder. Emission spectra, recorded after the addition of HCl, show a quenching of 80% of Cy5 fluorescence (**Figure 4.11**). This intensity decrease is only partially attributable to a degradation of Cy5, because the experiment performed on a blank sample of cyanine-loaded SBA-15-NH_2 (without OCP), shows that after addition of HCl drop, the intensity of Cy5 emission has only a 10% decrease (**Figure 4.11**). Data were repeated twice.

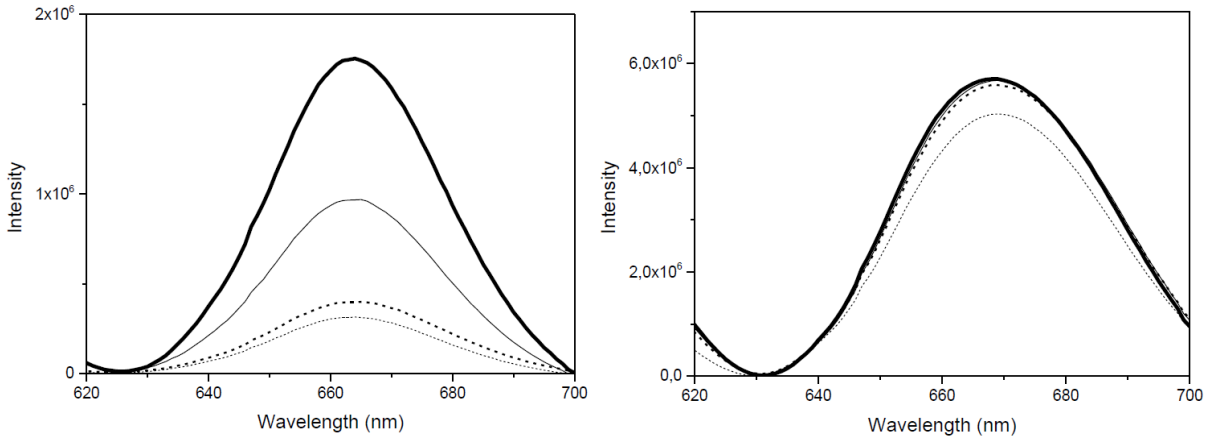

Figure 4.11 Emission spectra of (left) Cy3:Cy5=1:10 immobilized on SBA-15-NH_2 in presence of OCP(CAN) 0.3 mg/mL and (right) Cy3:Cy5=1:10 immobilized on SBA-15-NH_2 in absence of OCP. Spectra recorded exciting the system at 555 nm (Cy3 λ_{ex}) and detecting the fluorescence of Cy5 in the range 620-700 nm (Cy5 max λ_{em} at 672 nm) with a detector slit of 5 nm. Spectra recorded before (thick line) and after addition of a drop of HCl solution at pH=1, at t=0 from the addition (thin solid line), after 5 min (dash line) and after 30 min (dot line).

4.4.2 Flavonols and OCP on SBA-15-NH_2 as photo-modulable fluorescent device

Several types of flavonoids have been tested. Among them, results obtained on 3-hydroxy flavone (3HF) are shown in the chapter, while data obtained on morin and fisetin are shown in S.I. at the end of this chapter.

After having tested the system of the two molecules Cy3-Cy5 in relation to OCP, the 3HF was chosen as single-molecule to test, for several reasons. First, it allows to obtain a shift of around 180 (or 170) nm between the λ_{ex} (350 nm) and the λ_{em} (~530 nm) while the system Cy3-Cy5 has a shift of around 100 nm ($\lambda_{ex\text{-}Cy3}$ = 555 nm, $\lambda_{em\text{-}Cy5}$ = 665 nm). As shown in **Figure 4.5**, the spectral overlap between 3HF emission and OCP^O absorption, is increased when the protein is in the red form, suggesting the idea that OCP-photoconversion-induced quenching of the fluorescence of 3HF is possible. Second, the system is now composed by only two components, an absorber/emitter with high Stokes shift, and the photochromic switch (OCP). This should facilitate the OCP-photoactivation-induced fluorescence quenching, as only a suitable average distance between 3HF and OCP must be obtained. Finally, compared to cyanine dyes, 3HF is endowed with high antioxidant properties[31]. However, 3HF has shown a worse photo-stability compared to cyanine dyes. For this reason, exposure to blue light from the LED was shorter in time compared to the sample possessingCy3-Cy5 as the absorbing-emitting system.

4.4.2.1 Immobilization of 3HF on SBA-15-NH_2

The sample of 3HF immobilised on SBA-15-NH_2 prepared as previously described, and it was analysed with Visible solid phase spectroscopy before and after 20 min of exposition to blue light LED (**Figure 4.12**). In this condition, the 3HF is partially present as anion (see scheme in **Figure 4.3**). Indeed, the absorbance peak at around 400 nm is characteristic of the anionic form of 3HF and after illumination with LED, it was observed a light decrease of intensity of the absorbance maximum, suggesting a partial photo-degradation of the molecule. This assumption was then confirmed by photoluminescence experiments (**Figure 4.12**). The emission spectrum of 3HF showed the emission peak of the anionic form (~ 480 nm) and the emission peak of the tautomer T* (~ 530 nm). After blue light illumination, the emission spectrum changes shape and decreases its intensity (**Figure 4.12**).

To reduce the amount of 3HF anion and to increase the emission of the tautomer, the pH of 3HF solution was lowered from 7.5 to 5. Sample was prepared adding 1 mL of 3HF solution (at pH = 5) to 10 mg of SBA-15-NH_2 and same analysis described before were performed.

Visible solid phase spectroscopy revealed that the amount of neutral form (absorption maximum ~ 350 nm) was increased, even if the anion was still present (**Figure 4.122**). Photoluminescence experiments have shown that also the emission of the anion was decreased, compared to the tautomer emission. Furthermore, the system turns out to be more photo-stable: the illumination with blue light LED only slightly modifies the intensity of the emission, suggesting a higher stability of the molecule (**Figure 4.12**).

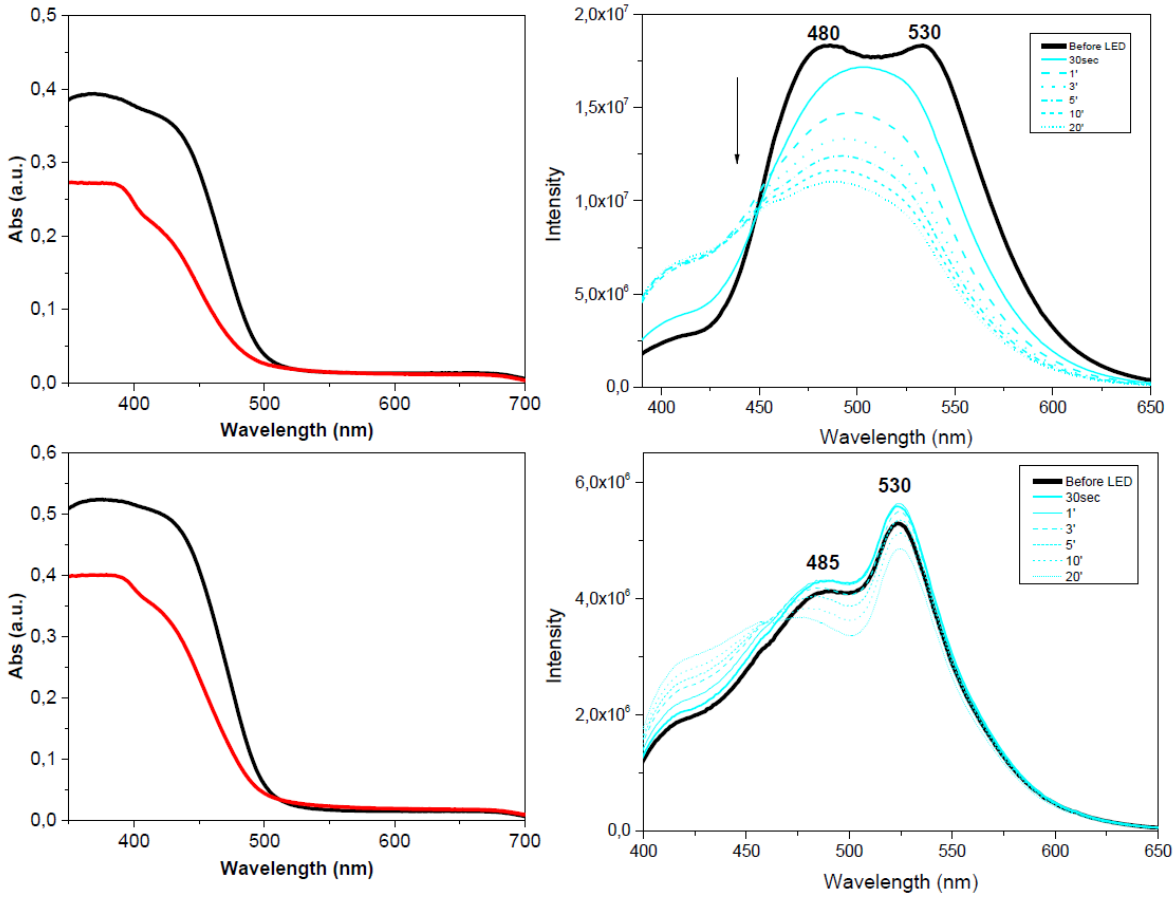

Figure 4.12 (Left, top) Visible absorbance spectra of 3HF (pH=7.5) immobilized on SBA-15-NH_2; spectra recorded before (black line) and after (red line) blue light LED exposition for 20 min. (Right, top) Emission spectra of 3HF (pH=7.5) immobilized on SBA-15-NH_2 excited at λ_{ex} 350 nm, with a slit of 3 nm; time-resolved emission recorded after blue light LED exposition of the sample after 30 s, 1, 3, 5, 10 and 20 min. (Left, bottom) Visible absorbance spectra of 3HF (pH=5) immobilized on SBA-15-NH_2; spectra recorded before (black line) and after (red line) blue light LED exposition for 20 min. (Right, bottom) Emission spectra of 3HF (pH=5) immobilized on SBA-15-NH_2 excited at λ_{ex} 350 nm, with a slit of 3 nm; time-resolved emission recorded after blue light LED exposition of the sample after 30 s, 1, 3, 5, 10 and 20 min.

4.4.2.2 Immobilization of OCP on 3HF-loaded SBA-15-NH_2

OCP(CAN) was immobilized on the 3HF-loaded SBA-15-NH_2. Visible experiments in solid phase have shown that the presence of 3HF on SBA-15-NH_2 does not affect the spectroscopic

properties of OCP and its photo-activity. Indeed, the protein is photo-activated into the OCP^R after exposition to blue light LED and the spectrum is red-shifted (**Figure 4.13**). An almost complete recovery to the OCP^O form was observed after 24 hours in the dark. Sample of 3HF at pH = 5 was also analysed, after immobilization of OCP (**Figure 4.13**). It was observed that even at pH = 5 the protein was photo-active and able to back-converts to the orange form after 24 hours in the dark.

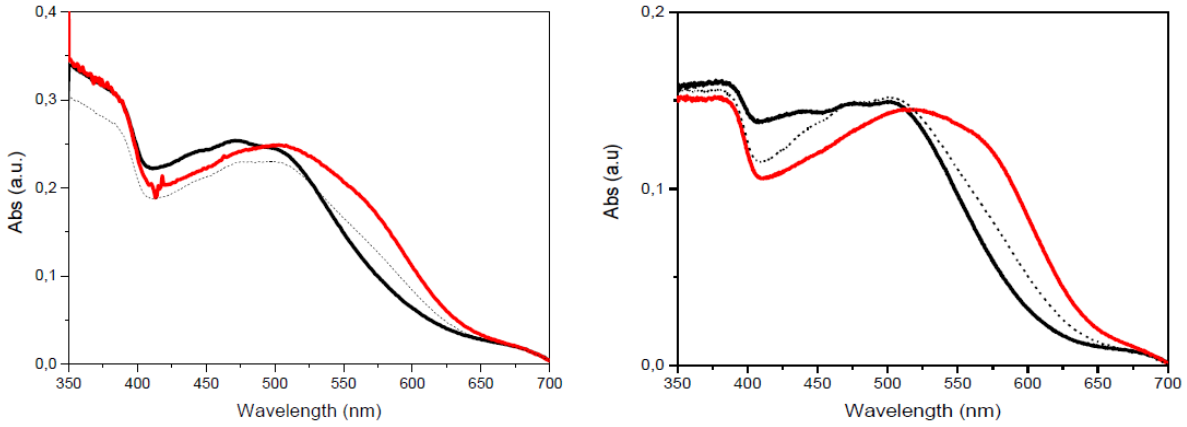

Figure 4.13 (Left) Visible solid phase spectra of OCP(CAN) immobilized on 3HF (pH=7.5) -loaded SBA-15-NH_2 recorded before (thick black line) and after 20 min (red line) of blue light LED exposition; back-conversion was recorded after 24 h in the dark (dot black line). (Right) Visible solid phase spectra of OCP(CAN) immobilized on 3HF (pH=5)-loaded SBA-15-NH_2 recorded before (thick black line) and after 20 min (red line) of blue light LED exposition; back-conversion was recorded after 12 h in the dark (dot black line).

4.4.2.3 Fluorescence quenching and recovery

Photoluminescence experiments were performed aiming to quench the tautomeric excited state of 3HF (T*) fluorescence exploiting the OCP^O - OCP^R photo-conversion and the spectral overlap that this photo-conversion induces (**Figure 4.5**). Samples of 3HF at pH = 7.5 and pH = 5 were prepared and analysed in parallel (**Figure 4.14**). The sample of OCP immobilized on 3HF-loaded SBA-15-NH_2, prepared as described above, was placed in the photoluminescence sample-holder, and kept in the dark for 1 hour before performing the measurement. At t = 0 an emission spectrum was collected, exciting the system at 350 nm (3HF (λ_{ex} max) and collecting the emission in the range between 500 – 650 nm, where the T* is supposed to emit. Later on, the system was exposed to blue light from a LED placed 2 cm far away from the sample-holder (see picture in **Figure 4.9**) for 30 seconds, 1, 3, 5, 10 and 20 minutes and after each time exposure, a new emission spectrum was collected (keeping the blue LED switched off during the measurement). As shown in **Figure 4.14**, at t = 0 a peak around 530 nm appears,

corresponding to T* emission. Exposure to blue light, which triggers the photo-activation of OCP and the spectral red-shift of its Vis spectrum, entails the partial quenching of T* fluorescence and the decrease of the intensity of the 530 nm peak. The fluorescence quenching is lower compared to cyanine dyes system: around 10% of fluorescence intensity is lost, after 20 min of blue light in the case of 3HF at pH = 7.5. However, the fluorescence quenching is higher (around 18%) in the case of 3HF at pH = 5 (**Figure 4.14**).

Keeping the sample in the dark, the fluorescence intensity was almost completely restored after 24 hours (**Figure 4.14**, black lines).

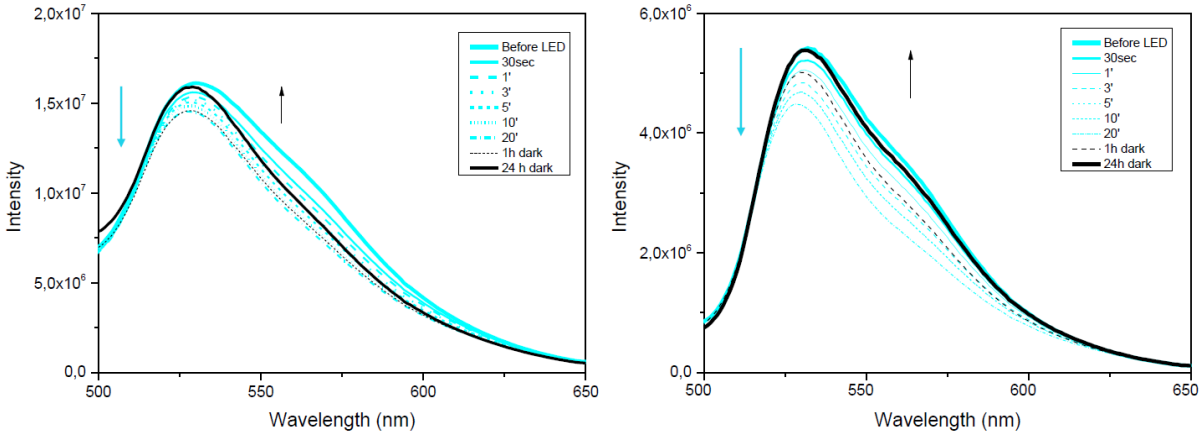

Figure 4.14 Emission spectra of (left) 3HF (pH=7.5) and (right) 3HF (pH=5) immobilized on SBA-15-NH_2 in presence of OCP(CAN) 0.2 mg/mL. Spectra recorded exciting the system at 350 nm (3HF λ_{ex}) and detecting 3HF fluorescence in the range 500-650 nm. Spectra (cyan lines) recorded at t = 0 (before LED illumination), after 1, 3, 5, 10 and 20 min of blue light LED illumination (LED was switched off during the emission measurements). Relaxation of the system and recovery of fluorescence (black lines) were recorded after 1 h and 24 h in the dark.

4.5 Conclusions

This study has achieved several goals: 1) Different fluorescent systems have been studied, notably cyanine dyes and flavonols. These molecules have been successfully immobilised on SBA-15-NH_2 and the resulting fluorescent NPs have been analysed with Visible spectroscopy and photoluminescence. Cyanine dyes have shown a better photo-stability compared to flavonols, which have a higher tendence to photo-degradation under light illumination. 2) OCP can be absorbed on dye-loaded silica NPs using the immobilisation protocol described in Chapter 3 and allowing to have a simple and rapid way of production of these photo-modulable fluorescent NPs. 3) As far as the cyanine dye pair Cy3-Cy5 in SBA-15-NH2 system is concerned, OCP can be used as a photochromic fluorescence modulator component. Indeed, the high spectral overlap between the emission of the cyanine Cy3 dye and the absorption of OCP when the OCP is in the red form, makes OCP^R a good fluorescence quencher: a 37% fluorescence intensity decrease is observed after 30 min exposure to blue light. The back-conversion to the OCP orange form in the dark allows to recover the initial fluorescence intensity, even after a second cycle of photo-activation. Samples stored at 4°C for 5 days show the same photo-properties of freshly prepared samples. 4) Preliminary data have shown that the fluorescence quenching of cyanine dyes is also possible under the effect of acidic pH (e.g., pH = 1) and in absence of light illumination. Further analyses are necessary to explore this domain of applications. 5) Concerning 3HF-doped NPs, OCP turned out to be a good fluorescence quencher of the tautomeric excited state (T*) of 3HF when photo-converted into OCP^R form. The system was reversible, and the fluorescence intensity was restored after incubation in the dark. However, the OCP photoconversion-induced fluorescence quenching was lower than the one obtained with Cy3-Cy5 doped NPs.

In conclusion, these results pave the way for the development of nano-scaled OCP-based photoactive switch with tuneable fluorescence with possible applications in imaging. Moreover, this system can be involved as light-regulator into an artificial antenna system, able to regulate energy-transfer pathways in response to light variations. Further experiments are necessary to improve the quenching yield of the cyanine dyes and to minimize the photo-degradation of the flavonoids improving their quenching and recovery.

4.6 References

[1] A. Andreoni, S. Lin, H. Liu, R.E. Blankenship, H. Yan, N.W. Woodbury, Orange Carotenoid Protein as a Control Element in an Antenna System Based on a DNA Nanostructure, Nano Lett. 17 (2017) 1174–1180. https://doi.org/10.1021/acs.nanolett.6b04846.

[2] H. Cabral, K. Miyata, A. Kishimura, Nanodevices for studying nano-pathophysiology, Adv. Drug Deliv. Rev. 74 (2014) 35–52. https://doi.org/10.1016/j.addr.2014.06.003.

[3] I.I. Slowing, J.L. Vivero-Escoto, C.-W. Wu, V.S.-Y. Lin, Mesoporous silica nanoparticles as controlled release drug delivery and gene transfection carriers, Adv. Drug Deliv. Rev. 60 (2008) 1278–1288. https://doi.org/https://doi.org/10.1016/j.addr.2008.03.012.

[4] G.H. Koenderink, S. Sacanna, C. Pathmamanoharan, M. Raşa, A.P. Philipse, Preparation and properties of optically transparent aqueous dispersions of monodisperse fluorinated colloids, Langmuir. 17 (2001) 6086–6093. https://doi.org/10.1021/la010181y.

[5] Y. Wang, Q. Zhao, N. Han, L. Bai, J. Li, J. Liu, E. Che, L. Hu, Q. Zhang, T. Jiang, S. Wang, Mesoporous silica nanoparticles in drug delivery and biomedical applications, Nanomedicine Nanotechnology, Biol. Med. 11 (2015) 313–327. https://doi.org/10.1016/j.nano.2014.09.014.

[6] R. Duncan, Polymer therapeutics as nanomedicines: new perspectives, Curr. Opin. Biotechnol. 22 (2011) 492–501.

[7] M.R. Kano, Y. Bae, C. Iwata, Y. Morishita, M. Yashiro, M. Oka, T. Fujii, A. Komuro, K. Kiyono, M. Kaminishi, K. Hirakawa, Y. Ouchi, N. Nishiyama, K. Kataoka, K. Miyazono, Improvement of cancer-targeting therapy, using nanocarriers for intractable solid tumors by inhibition of TGF-β signaling, Proc. Natl. Acad. Sci. U. S. A. 104 (2007) 3460–3465. https://doi.org/10.1073/pnas.0611660104.

[8] J. Lu, M. Liong, Z. Li, J.I. Zink, F. Tamanoi, Biocompatibility, biodistribution, and drug-delivery efficiency of mesoporous silica nanoparticles for cancer therapy in animals, Small. 6 (2010) 1794–1805. https://doi.org/10.1002/smll.201000538.

[9] H. Meng, M. Xue, T. Xia, Z. Ji, D.Y. Tarn, J.I. Zink, A.E. Nel, Use of size and a copolymer design feature to improve the biodistribution and the enhanced permeability and retention effect of doxorubicin-loaded mesoporous silica nanoparticles in a murine xenograft tumor model, ACS Nano. 5 (2011) 4131–4144. https://doi.org/10.1021/nn200809t.

[10] P.P. Nampi, C.C. Kartha, G. Jose, A.K. P.R., T. Anilkumar, H. Varma, Sol–gel nanoporous silica as substrate for immobilization of conjugated biomolecules for application as fluorescence resonance energy transfer (FRET) based biosensor, Sensors Actuators B Chem. 185 (2013) 252–257. https://doi.org/https://doi.org/10.1016/j.snb.2013.04.067.

[11] A. Chaicham, J. Kongwutthivech, T. Tuntulani, B. Tomapatanaget, Couple of Histamine blue fluorescence chemosensor and surface charge selector of FC-modified silica nanoporous for highly specific histamine detection via FRET-process, Sensors Actuators, B Chem. 258 (2018) 621–627. https://doi.org/10.1016/j.snb.2017.11.101.

[12] G. Mohammadi Ziarani, Z. Ebrahimi, F. Mohajer, A. Badiei, A Fluorescent

Chemosensor Based on Functionalized Nanoporous Silica (SBA-15 SBA-IC-MN) for Detection of Hg2+ in Aqueous Media, Arab. J. Sci. Eng. 47 (2022) 397–406. https://doi.org/10.1007/s13369-021-05518-6.

[13] M. Karimi, A. Badieia, G.M. Ziarani, Fluorescence-enhanced optical sensor for detection of Al3+ in water based on functionalised nanoporous silica type SBA-15, Chem. Pap. 70 (2016) 1431–1438. https://doi.org/doi:10.1515/chempap-2016-0079.

[14] C.-C. Chen, D. Pestov, J.D. Nelson, J.E. Anderson, G. Tepper, Uranyl Soil Extraction and Fluorescence Enhancement by Nanoporous Silica Gel: pH effects, J. Fluoresc. 21 (2011) 119–124. https://doi.org/10.1007/s10895-010-0695-0.

[15] S.A.M.A. Peerzade, N. Makarova, I. Sokolov, Ultrabright fluorescent silica nanoparticles for multiplexed detection, Nanomaterials. 10 (2020). https://doi.org/10.3390/nano10050905.

[16] B. Campanini, S. Bologna, F. Cannone, G. Chirico, A. Mozzarelli, S. Bettati, Unfolding of Green Fluorescent Protein mut2 in wet nanoporous silica gels, Protein Sci. 14 (2005) 1125–1133. https://doi.org/10.1110/ps.041190805.

[17] G.P. Moss, P.A.S. Smith, D. Tavernier, Glossary of class names of organic compounds and reactivity intermediates based on structure (IUPAC Recommendations 1995), Pure Appl. Chem. 67 (1995) 1307–1375. https://doi.org/doi:10.1351/pac199567081307.

[18] H. Musso, The pigments of fly agaric, Amanita muscaria, Tetrahedron. 35 (1979) 2843–2853. https://doi.org/10.1016/S0040-4020(01)99498-0.

[19] K. Licha, U. Resch-Genger, Fluorescent reporters and optical probes, in: A. Brahme (Ed.), Compr. Biomed. Phys., Elsevier, Bundesanstalt fuer Materialforschung und -pruefung (BAM), Berlin, Germany, 2014: p. Chapter 4.08, 85-109. https://opus4.kobv.de/opus4-bam/frontdoor/index/index/docId/31635.

[20] H.A. Shindy, Fundamentals in the chemistry of cyanine dyes: A review, Dye. Pigment. 145 (2017) 505–513. https://doi.org/10.1016/j.dyepig.2017.06.029.

[21] A. Waggoner, Fluorescent labels for proteomics and genomics, Curr. Opin. Chem. Biol. 10 (2006) 62–66. https://doi.org/https://doi.org/10.1016/j.cbpa.2006.01.005.

[22] M.Y. Berezin, K. Guo, W. Akers, J. Livingston, M. Solomon, H. Lee, K. Liang, A. Agee, S. Achilefu, Rational approach to select small peptide molecular probes labeled with fluorescent cyanine dyes for in vivo optical imaging, Biochemistry. 50 (2011) 2691–2700. https://doi.org/10.1021/bi2000966.

[23] B.G. Moreira, Y. You, R. Owczarzy, Cy3 and Cy5 dyes attached to oligonucleotide terminus stabilize DNA duplexes: Predictive thermodynamic model, Biophys. Chem. 198 (2015) 36–44. https://doi.org/10.1016/j.bpc.2015.01.001.

[24] D. Komljenovic, M. Wiessler, W. Waldeck, V. Ehemann, R. Pipkorn, H.-H. Schrenk, J. Debus, K. Braun, NIR-Cyanine Dye Linker: a Promising Candidate for Isochronic Fluorescence Imaging in Molecular Cancer Diagnostics and Therapy Monitoring, Theranostics. 6 (2016) 131–141. https://doi.org/10.7150/thno.11460.

[25] H.A. Shindy, M.A. El-Maghraby, M.M. Goma, N.A. Harb, Dicarbocyanine and tricarbocyanine dyes: Novel synthetic approaches, photosensitization evaluation and antimicrobial screening, Chem. Int. 6 (2020) 30–41. https://doi.org/10.5281/zenodo.2631739.

[26] J.T. Song, X.Q. Yang, X.S. Zhang, D.M. Yan, Z.Y. Wang, Y. Di Zhao, Facile Synthesis of Gold Nanospheres Modified by Positively Charged Mesoporous Silica,

Loaded with Near-Infrared Fluorescent Dye, for in Vivo X-ray Computed Tomography and Fluorescence Dual Mode Imaging, ACS Appl. Mater. Interfaces. 7 (2015) 17287–17297. https://doi.org/10.1021/acsami.5b04359.

[27] A.N. Panche, A.D. Diwan, S.R. Chandra, Flavonoids: An overview, J. Nutr. Sci. 5 (2016). https://doi.org/10.1017/jns.2016.41.

[28] J.B. Harborne, The flavonoids: advances in research since 1980, (2013).

[29] E. Middleton, Trends Pbarmacol, Sci. 5 (1984) 335.

[30] J.K. Lin, M.S. Weng, Flavonoids as nutraceuticals, Sci. Flavonoids. 7 (2006) 213–238. https://doi.org/10.1007/978-0-387-28822-2_8.

[31] A.D. Agrawal, Pharmacological Activities of Flavonoids: A Review, Int. J. Pharm. Sci. Nanotechnol. 4 (2011) 1394–1398. https://doi.org/10.37285/ijpsn.2011.4.2.3.

[32] Y. Arai, S. Watanabe, M. Kimira, K. Shimoi, R. Mochizuki, N. Kinae, Dietary intakes of flavonols, flavones and isoflavones by Japanese women and the inverse correlation between quercetin intake and plasma LDL cholesterol concentration, J. Nutr. 130 (2000) 2243–2250. https://doi.org/10.1093/jn/130.9.2243.

[33] M. Tordera, M.L. Ferrándiz, M.J. Alcaraz, Influence of Anti-Inflammatory Flavonoids on Degranulation and Arachidonic Acid Release in Rat Neutrophils, Zeitschrift Für Naturforsch. C. 49 (1994) 235–240. https://doi.org/doi:10.1515/znc-1994-3-412.

[34] J.R.S. Hoult, M.A. Moroney, M.B.T.-M. in E. Payá, [44] Actions of flavonoids and coumarins on lipoxygenase and cyclooxygenase, in: Oxyg. Radicals Biol. Syst. Part D, Academic Press, 1994: pp. 443–454. https://doi.org/https://doi.org/10.1016/0076-6879(94)34115-X.

[35] E. De Stefani, P. Boffetta, H. Deneo-Pellegrini, M. Mendilaharsu, J.C. Carzoglio, A. Ronco, L. Olivera, Dietary Antioxidants and Lung Cancer Risk: A Case-Control Study in Uruguay, Nutr. Cancer. 34 (1999) 100–110. https://doi.org/10.1207/S15327914NC340114.

[36] T. Fotsis, M.S. Pepper, E. Aktas, S. Breit, S. Rasku, H. Adlercreutz, K. Wähälä, R. Montesano, L. Schweigerer, Flavonoids, dietary-derived inhibitors of cell proliferation and in vitro angiogenesis, Cancer Res. 57 (1997) 2916–2921.

[37] H.-K. Wang, Y. Xia, Z.-Y. Yang, S.L. Morris Natschke, K.-H. Lee, Recent Advances in the Discovery and Development of Flavonoids and their Analogues as Antitumor and Anti-HIV Agents BT - Flavonoids in the Living System, in: J.A. Manthey, B.S. Buslig (Eds.), Springer US, Boston, MA, 1998: pp. 191–225. https://doi.org/10.1007/978-1-4615-5335-9_15.

[38] R.J. Gryglewski, R. Korbut, J. Robak, J. Święs, On the mechanism of antithrombotic action of flavonoids, Biochem. Pharmacol. 36 (1987) 317–322. https://doi.org/https://doi.org/10.1016/0006-2952(87)90288-7.

[39] S. Sapino, E. Ugazio, L. Gastaldi, I. Miletto, G. Berlier, D. Zonari, S. Oliaro-Bosso, Mesoporous silica as topical nanocarriers for quercetin: characterization and in vitro studies, Eur. J. Pharm. Biopharm. 89 (2015) 116–125. https://doi.org/https://doi.org/10.1016/j.ejpb.2014.11.022.

[40] G. Berlier, L. Gastaldi, E. Ugazio, I. Miletto, P. Iliade, S. Sapino, Stabilization of quercetin flavonoid in MCM-41 mesoporous silica: positive effect of surface functionalization, J. Colloid Interface Sci. 393 (2013) 109–118. https://doi.org/https://doi.org/10.1016/j.jcis.2012.10.073.

[41] O.I. Parisi, F. Puoci, D. Restuccia, G. Farina, F. Iemma, N. Picci, Chapter 4 - Polyphenols and Their Formulations: Different Strategies to Overcome the Drawbacks Associated with Their Poor Stability and Bioavailability, in: R.R. Watson, V.R. Preedy, S.B.T.-P. in H.H. and D. Zibadi (Eds.), Academic Press, San Diego, 2014: pp. 29–45. https://doi.org/https://doi.org/10.1016/B978-0-12-398456-2.00004-9.

[42] F. Arriagada, O. Correa, G. Günther, S. Nonell, F. Mura, C. Olea-Azar, J. Morales, Morin flavonoid adsorbed on mesoporous silica, a novel antioxidant nanomaterial, PLoS One. 11 (2016) 1–22. https://doi.org/10.1371/journal.pone.0164507.

[43] L. Mandić, A. Sadžak, V. Strasser, G. Baranović, D.D. Jurašin, M.D. Sikirić, S. Šegota, Enhanced protection of biological membranes during lipid peroxidation: Study of the interactions between flavonoid loaded mesoporous silica nanoparticles and model cell membranes, Int. J. Mol. Sci. 20 (2019). https://doi.org/10.3390/ijms20112709.

[44] A. Landström, S. Leccese, H. Abadian, J.F. Lambert, I. Concina, S. Protti, A.P. Seitsonen, A. Mezzetti, Fluorescent silica MCM-41 nanoparticles based on flavonoids: Direct post-doping encapsulation and spectral characterization, Dye. Pigment. 185 (2021). https://doi.org/10.1016/j.dyepig.2020.108870.

[45] A. Landström, A.P. Seitsonen, S. Leccese, H. Abadian, J.-F. Lambert, S. Protti, I. Concina, A. Mezzetti, Electron spectroscopies of 3-hydroxyflavone and 7-hydroxyflavone in MCM-41 silica nanoparticles and in acetonitrile solutions. Experimental data and DFT/TD-DFT calculations, Data Br. 34 (2021) 106630. https://doi.org/10.1016/j.dib.2020.106630.

[46] S. Lazzaroni, D. Dondi, A. Mezzetti, S. Protti, Role of solute-solvent hydrogen bonds on the ground state and the excited state proton transfer in 3-hydroxyflavone. A systematic spectrophotometric study, Photochem. Photobiol. Sci. 17 (2018) 923–933. https://doi.org/10.1039/c8pp00053k.

[47] S. Protti, A. Mezzetti, J.-P. Cornard, C. Lapouge, M. Fagnoni, Hydrogen bonding properties of DMSO in ground-state formation and optical spectra of 3-hydroxyflavone anion, Chem. Phys. Lett. 467 (2008) 88–93.

4.7 Supplementary Information

4.7.1 Effect of SBA-15-NH_2 matrix on Cy3 and Cy5

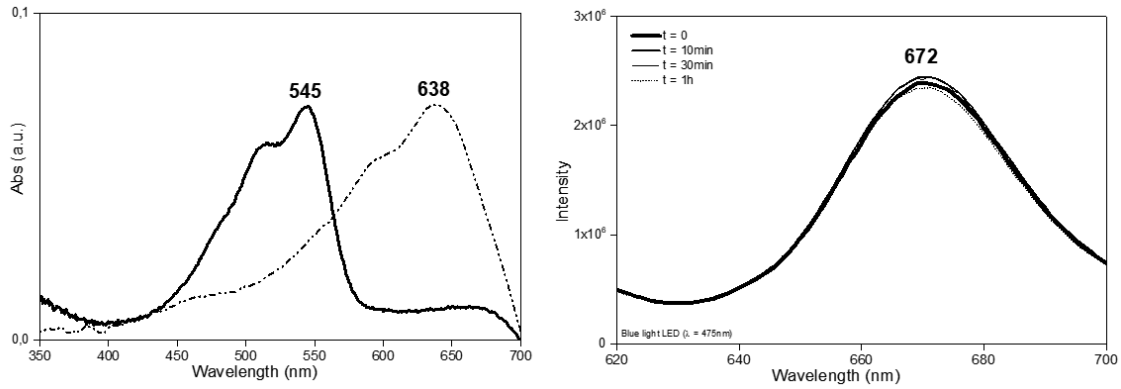

Figure SI 1. 4-1 (Left) Visible solid phase spectra of Cy3 (solid line) and Cy5 (dash-dot-dash line) immobilized on SBA-15-NH_2 recorded after photoluminescence experiments. (Right) Emission spectra of Cy3:Cy5=1:10 on SBA-15-NH_2 after exposition to blue light LED placed at 2 cm far from the sample. Spectra recorded before the LED exposition (t = 0), after 10 min, 30 min and 1 hour (LED switched off during measures).

4.7.2 Cy3-Cy5 fluorescence quenching and recovery

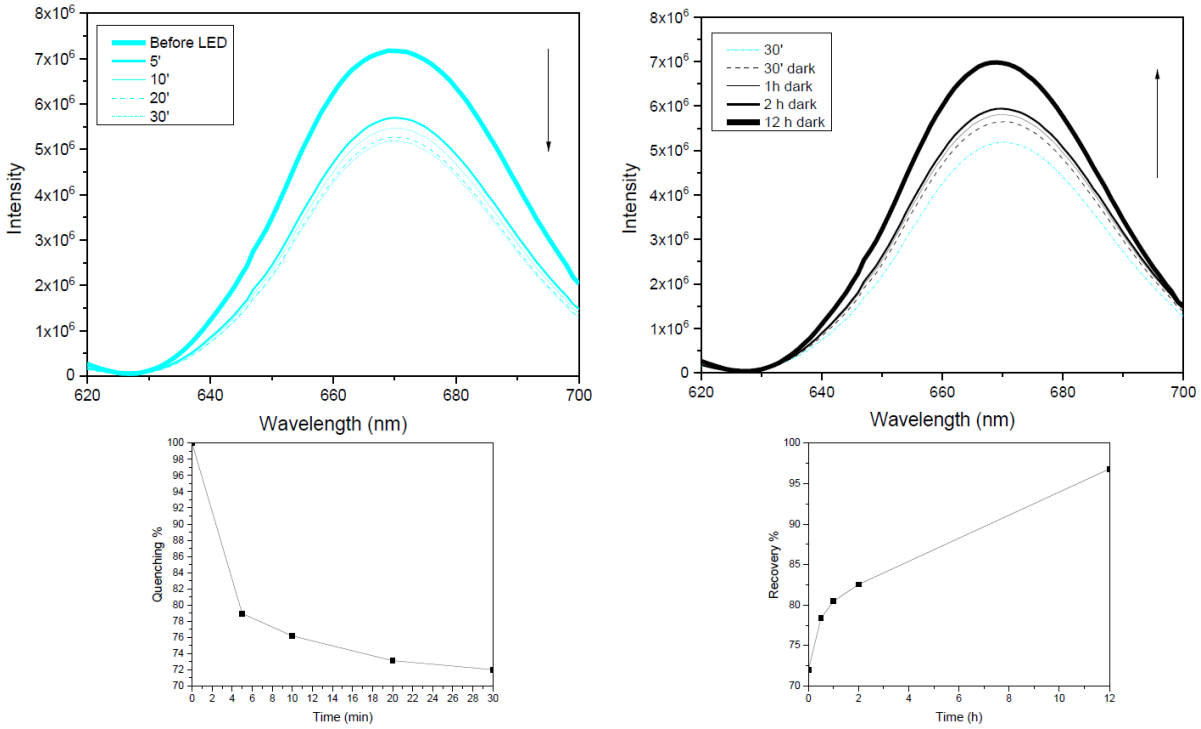

Figure SI 1. 4-2 Duplicate sample of the one shown in Figure 4.9. Emission spectra of Cy3:Cy5=1:10 immobilized on SBA-15-NH_2 in presence of OCP(CAN) 0.2 mg/mL. Spectra recorded exiting the system at 555 nm (Cy3 λ_{ex}) and detecting the fluorescence of Cy5 in the range 620-700 nm (Cy5 max λ_{em} at 672 nm) with a slit of 5 nm. (Left, top) Spectra recorded at t = 0 (before LED illumination), after

5, 10, 20 and 30 min of blue light LED illumination (LED was switched off during the emission measurements). (Left, bottom) Time (min)-resolved quenching % of Cy5 fluorescence under blue light LED exposition. (Right, top) Relaxation of the system and recovery of fluorescence were recorded after 30 min, 1 h, 2 h and 12 h in the dark. (Right, bottom) Time (h)-resolved recovery % of Cy5 fluorescence in the dark.

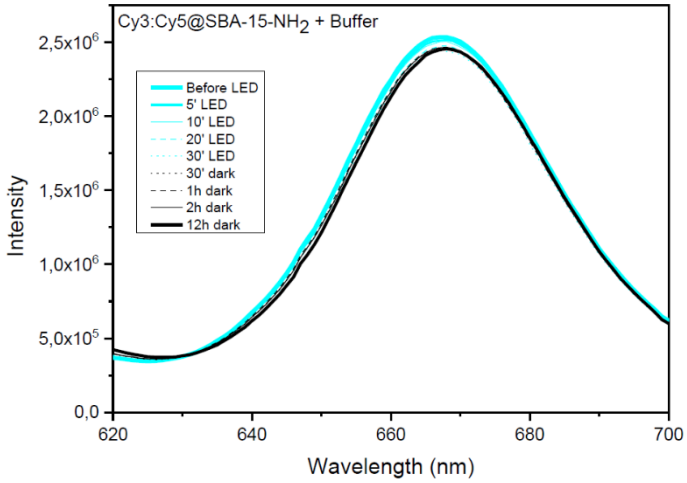

Figure SI 1. 4-3 Emission spectra of Cy3:Cy5=1:10 immobilized on SBA-15-NH_2 in presence of OCP-buffer (TRIS-NaCl). Spectra recorded exiting the system at 555 nm (Cy3 λ_{ex}) and detecting the fluorescence of Cy5 in the range 620-700 nm (Cy5 max λ_{em} at 672 nm) with a slit of 5 nm. (Cyan lines) Spectra recorded at t = 0 (before LED illumination), after 5, 10, 20 and 30 min of blue light LED illumination (LED was switched off during the emission measurements). (Black lines) Relaxation of the system and recovery of fluorescence were recorded after 30 min, 1 h, 2 h and 12 h in the dark.

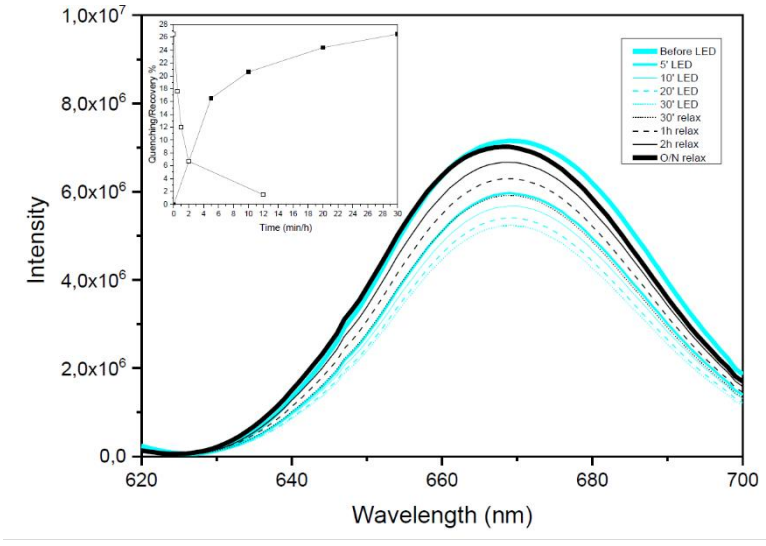

Figure SI 1. 4-4 5-days-old sample stored in the dark at 4°C. Emission spectra of Cy3:Cy5=1:10 immobilized on SBA-15-NH_2 in presence of OCP(CAN) 0.2 mg/mL. Spectra recorded exiting the system at 555 nm (Cy3 λ_{ex}) and detecting the fluorescence of Cy5 in the range 620-700 nm (Cy5 max λ_{em} at 672 nm) with a slit of 5 nm. (Cyan lines) Spectra recorded at t = 0 (before LED illumination), after 5, 10, 20 and 30 min of blue light LED illumination (LED was switched off during the emission measurements). (Black lines) Relaxation of the system and recovery of fluorescence were recorded after

30 min, 1 h, 2 h and 12 h in the dark. (Box on the left, top) Time (min/h)-resolved quenching/recovery % of Cy5 fluorescence.

4.7.3 Flavonols

4.7.3.1 Morin and OCP on SBA-15-NH_2

The flavonol morin was a suitable molecule to perform the OCP-induced tuneable quenching. The chemical structure of morin and its spectroscopical features are summarized in **Figure SI 1. 4-5**. As 3HF, the excited state of morin ((λ_{ex} = 365 nm) undergoes an ESIPT to the tautomeric excited state (T*), which emits at ~ 530 nm. As shown in **Figure SI 1. 4-5**, the spectral overlap between Morin (T*) emission and OCP^O absorption, is strongly increased when the protein is in the red form, suggesting the idea of using OCP photoconversion to quench the fluorescence of the T* form.

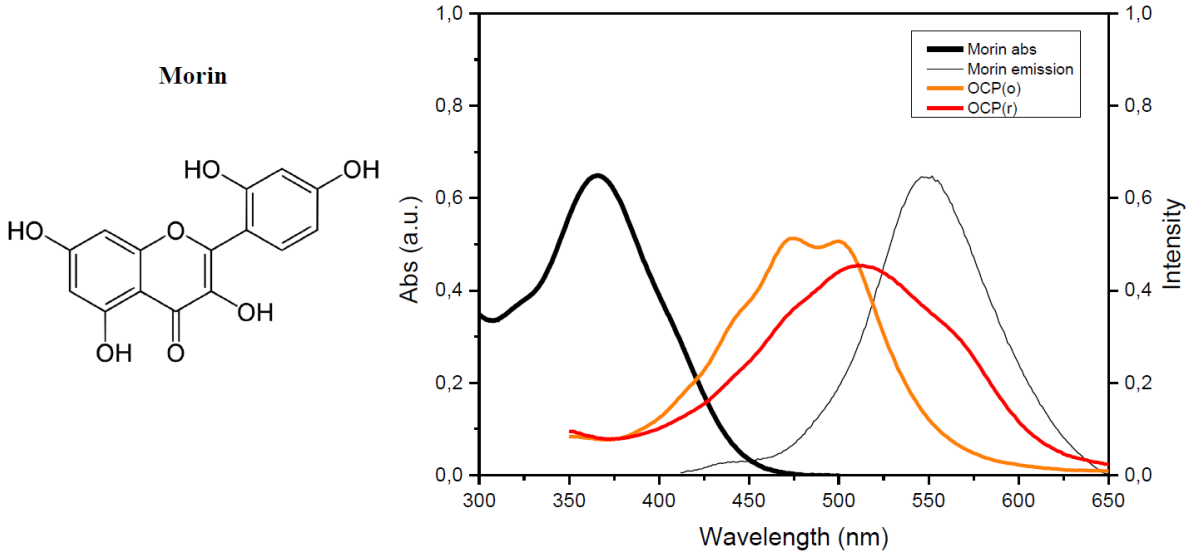

Figure SI 1. 4-5 (Left) Chemical structure of Morin. (Right) Absorbance spectrum (thick black line) and emission spectrum (thin black line) of morin, absorbance spectra of OCP^O (orange line) and OCP^R (red line).

The sample of morin immobilised on SBA-15-NH_2 prepared as described for 3HF, was analysed with Visible solid phase spectroscopy before and after 20 min of exposition to blue light LED (**Figure SI 1. 4-6**). The absorbance peak at around 400 nm is characteristic of the anionic form of morin and after 20 min of illumination with blue LED, it was observed a decrease of intensity of the absorbance maximum of the anion and the increase of the peak of the neutral form, suggesting a partial photo-degradation of the molecule and its conversion to

the neutral form. This assumption was then confirmed by photoluminescence experiments (**Figure SI 1. 4-6**). Indeed, the intensity of the emission spectrum of morin after illumination, was decreased (**Figure SI 1. 4-6**).

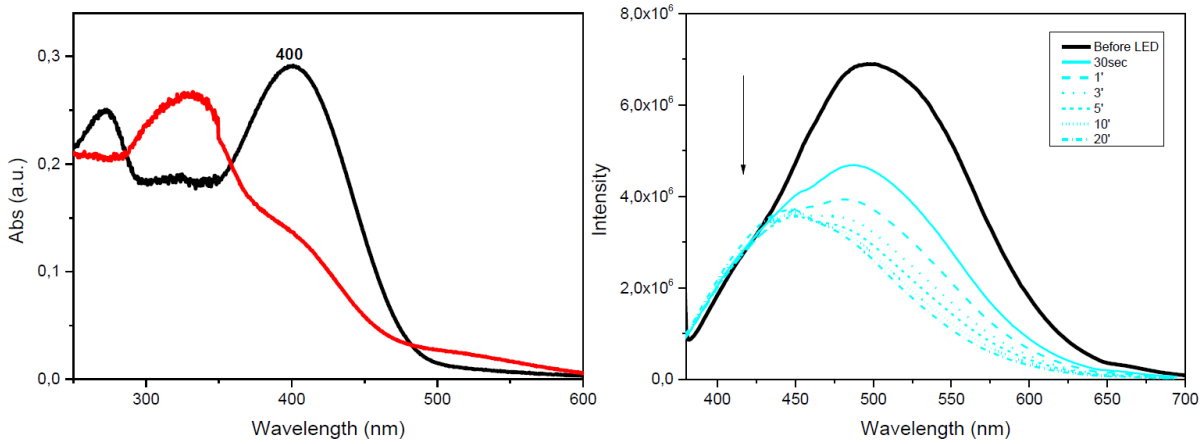

Figure SI 1. 4-6 (Left) Visible solid phase spectra of morin immobilized on SBA-15-NH_2; spectra recorded before (black line) and after (red line) blue light LED exposition for 20 min. (Right) Emission spectra of morin immobilized on SBA-15-NH_2 excited at λ_{ex} 365 nm; time-resolved emission recorded before and after blue light LED exposition of the sample for 30 s, 1, 3, 5, 10 and 20 min.

OCP(CAN) was immobilized on morin-loaded SBA-15-NH_2. Visible solid phase showed that OCP was still photo-active because a red shift was observed after blue LED illumination, but it was not able to back-convert to the OCP^O form (**Figure SI 1. 4-7**). Photoluminescence experiments revealed an intense decrease of fluorescence, but the emission intensity was not restored after 24 hours in the dark, suggesting a partial photodecomposition of morin. (**Figure SI 1. 4-7**).

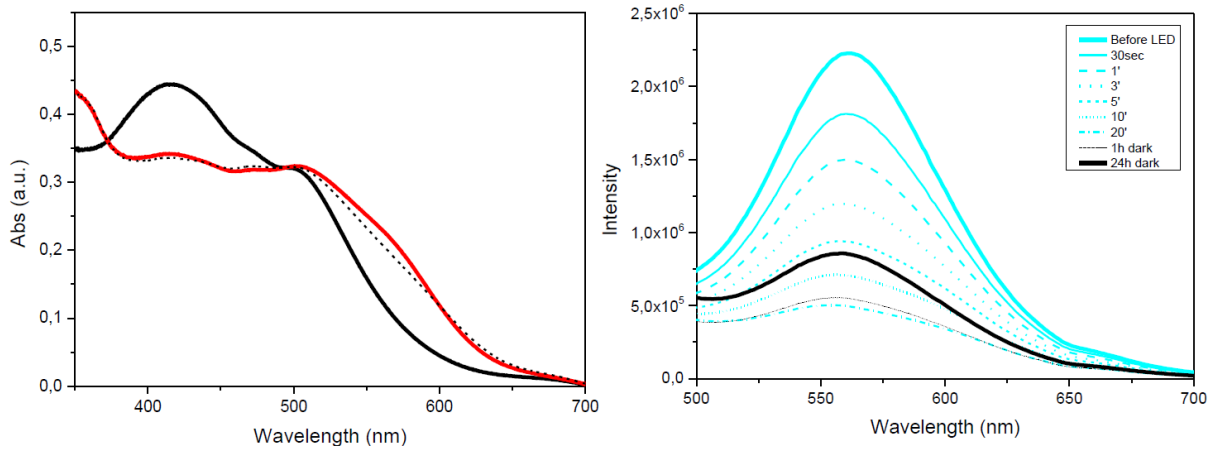

Figure SI 1. 4-7 (Left) Visible solid phase spectra of OCP(CAN) immobilized on morin-loaded SBA-15-NH_2 recorded before (thick black line) and after 20 min (red line) of blue light LED exposition; back-conversion was recorded after 24 h in the dark (dot black line). (Right) Emission spectra of morin immobilized on SBA-15-NH_2 in presence of OCP(CAN) 0.2 mg/mL. Spectra recorded exciting the system at 365 nm (morin λ_{ex}) and detecting fluorescence in the range 500-700 nm. Spectra (cyan lines) recorded at t = 0 (before LED illumination), after 1, 3, 5, 10 and 20 min of blue light LED illumination

(LED was switched off during the emission measurements). Relaxation of the system and recovery of fluorescence (black lines) were recorded after 1 h and 24 h in the dark.

4.7.3.1 Fisetin fluorescence quenching and recovery

Fisetin was the last flavonol tested that gave results of fluorescence quenching and recovery due to OCP photo-conversion (and back-conversion) even though, as in the case of morin, it is photo-instable. Fisetin solution was immobilized on SBA-15-NH_2 following the protocol described for the other flavonoids. OCP(CAN) was immobilized on fisetin-loaded SBA-15-NH_2. Samples were analysed with photoluminescence (**Figure SI 1. 4-8**). For fisetin-loaded SBA-15-NH_2 it was observed a fluorescence decrease after exposition to blue light LED, suggesting a partial photo-degradation of fisetin. Indeed, in presence of OCP, a quenching of fluorescence was observed after time-resolved illumination, but only a slight recovery of fluorescence was detected after 24 hours in the dark, confirming the previous assumption (**Figure SI 1. 4-8**).

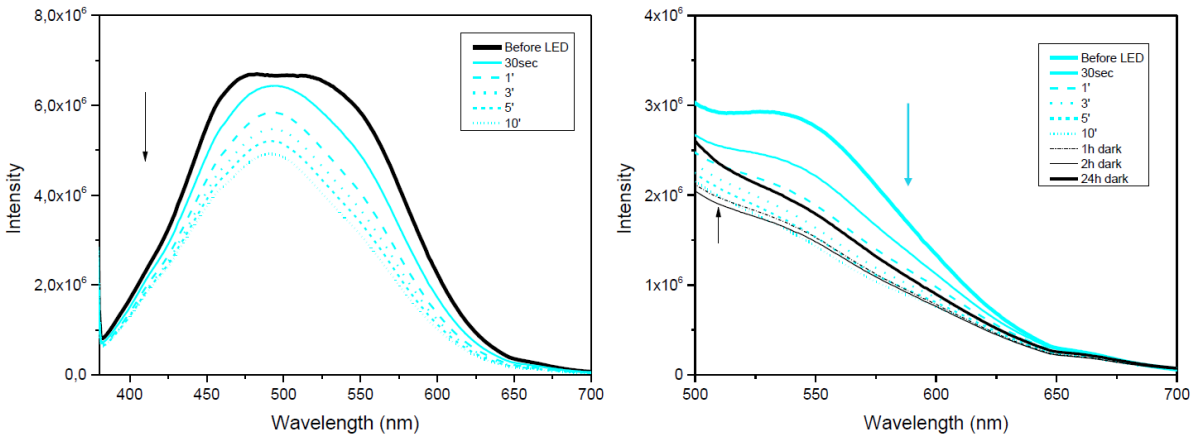

Figure SI 1. 4-8 Emission spectra of fisetin immobilized on SBA-15-NH_2 (left) and fisetin immobilized on SBA-15-NH_2 in presence of OCP(CAN) 0.2 mg/mL (right). Spectra recorded exciting the system at 365 nm (fisetin (λ_{ex}). Spectra (cyan lines) recorded at t = 0 (before LED illumination), after 1, 3, 5, 10 and 20 min of blue light LED illumination (LED was switched off during the emission measurements). (Right) Relaxation of the system and recovery of fluorescence (black lines) were recorded after 1 h, 2 h and 24 h in the dark.

General Conclusions

This thesis has different objectives. On the one hand, spectroscopic investigation studies regarding the mechanism of photoactivation of Orange Carotenoid Protein were performed. On the other hand, more applied research topics aiming to the development of mesoporous silica-based photoactive nano-devices were also carried out.

In the first literature review chapter, a general overview on photoreceptors and photoactive proteins has been highlighted. Furthermore, a focus on the main applications based on photoreceptors or photoactive proteins immobilised on mesoporous silica has been shortly presented. Hence, the second part of this review chapter comprehensively covered the introduction to the OCP. Since its first isolation and biological identification, the mechanism of photoactivation of the OCP has been deeply analysed and many of its aspects are known nowadays. Nevertheless, important questions remain opened. The fluorescence quenching mechanism is unclear, as well as the exact mechanism of photo-activation. The sequential steps occurring after the absorption of blue photons is still to be defined. Similarly, the mechanism of back conversion needs to be elucidated. In addition, the crystalline structure of OCP^R has yet to be solved, even though very recently the structure of the quenched OCP-phycobilisome complex has been solved. Probably the lower stability of OCP^R makes the crystallization process difficult. Structural details of OCP^R conformation would be extremely useful in the understanding of the photoactivation mechanism and in the interpretation of experimental spectroscopic data.

In the following chapters the experimental work was described, starting from fundamental spectroscopic investigations on the OCP in solution, through its immobilization on mesoporous silica SBA-15 and aiming to the development of photoactive nanodevices with tuneable fluorescence.

In the second chapter spectroscopic investigations in solution were carried out, aiming to clarify the mechanism of photoactivation and photoconversion of OCP. We focused the attention on OCP binding echinenone, canthaxanthin and 3-hydroxyechinenone as chromophore. From UV-Visible and FTIR difference spectroscopy, several pieces of information were obtained. Indeed, from the analysis of FTIR difference spectra it has been deduced that the mechanism of photoactivation is very similar in all the studied OCPs (binding different carotenoids), because the position and shape of the IR bands was almost the same. Then, isotopic exchange

(hydrogen/deuterium) made it possible to identify the bands belonging to the carotenoid, distinguishing them from bands arising from chemical moieties of the protein, sensitive to H/D exchange. Furthermore, it has been discovered that OCP(CAN) in de-hydration conditions has a tendance to self-convert to the OCP red form, while OCP(ECN) showed a higher stability of the orange form in the same conditions. This suggested the idea that the second carbonyl moiety of canthaxanthin stabilizes the OCP red conformation. Nevertheless, this result also suggests the idea that water plays a key role in the photoconversion mechanism. However, further calculations of spectra for the two carotenoids will be necessary for the assignment of vibrational bands, as well as investigation of the spectral region (4000-2000 cm^{-1}) in which key molecular groups absorb (notably OH, NH, SH, CH stretching bands).

In the third chapter we present the results obtained studying the interaction between different types of SBA-15 and OCP. SBA-15 mesoporous materials synthesized at different temperatures, raw and surface-functionalized, have shown a worm shape morphology with well-ordered crystalline structure which is not affected by the functionalization with amino groups. Indeed, SBA-15 materials with two different pore sizes are suitable and promising supports for the immobilization of both OCP(ECN) and OCP(CAN) by adsorption. The equilibrium of immobilization, driven by electrostatic interactions, is reached after 4 hours on both types of SBA-15, bare and organo-functionalized, and the maximum loading yield is achieved for an initial OCP concentration of 0.2 mg/mL. At higher initial OCP concentration, the amount of immobilized OCP was enhanced up to more than 30 mg of protein per g of material. Illumination by blue light increases immobilization efficiency on both SBA-15-80 and SBA-15-80-NH_2 nanoparticles leading to around four-fold more immobilized OCP and suggesting that the conformation of OCP plays a key role in entering the mesopores. Protein photo-activity is completely preserved after immobilization on SBA-15-NH_2 if compared with raw SBA-15 which, conversely, tends to dark-activate the protein converting it into OCP^R. OCP@SBA-15-NH_2 seems to be a promising photo-active system, still stable after 1 week at room temperature and able to slow down the kinetic of back conversion $OCP^R \rightarrow OCP^O$. This property can, in principle, be exploited in several domains: from biocompatible photochromic nanoparticles to the development of nano-scaled support for caroteno-proteins and carotenoid delivery and release. In the latter case, further studies should be undertaken to improve the release extend of OCP, for example by varying the functionalized groups grafted on the solid, thus modulating the interactions between the protein and the surface. Nevertheless, the OCP@SBA-15-NH_2 system demonstrated to be, *in vitro*, a suitable biocompatible material to

be exploited in the domain of optical sensing, such as a *bi*-functional optical sensor for temperature changes between 40°C and 60°C or as a *tri*-functional pH optical sensor spanning the whole pH range.

In the last chapter we focused the attention on the development of photoactive nanoparticles with tuneable fluorescence. Several goals were achieved. Different fluorescence systems have been studied, notably cyanine dyes and flavonols (derivatives of 3-hydroxyflavone – 3HF). These molecules have been successfully immobilised on SBA-15-NH_2 and the resulting fluorescent NPs have been analysed with Visible spectroscopy and photoluminescence. Cyanine dyes have shown a better photo-stability compared to flavonols, which have a higher tendence to photo-degradation under light illumination. OCP can be absorbed on dye-loaded silica NPs ensuring a simple and rapid way of production of these photo-modulable fluorescent NPs. As far as the cyanine dye pair Cy3-Cy5 in SBA-15-NH_2 system is concerned, OCP can be used as a photochromic fluorescence modulator component. Indeed, the high spectral overlap between the emission of the cyanine Cy3 dye and the absorption of OCP when the OCP is in the red form, makes OCP^R a good fluorescence quencher. The back-conversion to the OCP orange form in the dark allows to recover the initial fluorescence intensity, even after a second cycle of photo-activation. Samples stored at 4°C for 5 days show the same photo-properties of freshly prepared samples. Concerning 3HF-doped NPs, OCP turned out to be a good fluorescence quencher of the tautomeric excited state (T*) of 3HF when photo-converted into OCP^R form. The system was reversible, and the fluorescence intensity was restored after incubation in the dark. However, the OCP photoconversion-induced fluorescence quenching was lower than the one obtained with Cy3-Cy5 doped NPs. In conclusion, these results pave the way for the development of nano-scaled OCP-based photoactive switches with tuneable fluorescence with possible applications in imaging. Moreover, this system can be involved as light-regulator into an artificial antenna system, able to regulate energy-transfer pathways in response to light variations. Further experiments are necessary to improve the quenching yield of the cyanine dyes and to minimize the photo-degradation of the flavonoids improving their quenching and recovery.

Appendixes

1. Publications

S. Leccese, T. Onfroy, A. Wilson, D. Kirilovsky, S. Guira, M. Selmane, C. Jolivalt, A. Mezzetti, "Immobilization of Orange Carotenoid Protein on mesoporous silica SBA-15 for the development of photoactivable nanodevices" Microporous and Mesoporous Materials (*accepted May 19, 2022*)

A. Landström, S. Leccese, H. Abadian, JF Lambert, I. Concina, S Protti, A. Paavo Seitsone, A. Mezzetti, "Fluorescent silica MCM-41 nanoparticles based on flavonoids: Direct post-doping encapsulation and spectral characterization" Dyes and Pigments 185 (2021) 108870

A. Landström, A. Paavo Seitsonen, S. Leccese, H. Abadian, J-F. Lambert, Stefano Protti, I. Concina, A. Mezzetti, "Electron spectroscopies of 3-hydroxyflavone and 7-hydroxyflavone in MCM-41 silica nanoparticles and in acetonitrile solutions. Experimental data and DFT/TD-DFT calculations" Data in Brief 34 (2021) 106630 Contents

2. Oral and poster communications

Oral communications

Silvia Leccese *et al.*, "Interactions between Orange Carotenoid Protein (OCP) and mesoporous silica (SBA-15) : from fundamental research to the development of photoactivable nanodevices" Journées de l'ED397 / 8-9 Nov **2021** / Sorbonne Université - Campus des Cordeliers, Paris

Silvia Leccese *et al.*, "Orange Carotenoid Protein: insights on its molecular mechanism and possible biomedical applications" Journées de la Société Française de Photobiologie, Nov **2019**, Sorbonne Université, Paris "

Poster communications

Silvia Leccese *et al.*, "Interactions between Orange Carotenoid Protein (OCP) and mesoporous silica (SBA-15) : from fundamental research to the development of photoactivable nanodevices" Journées de l'ED397 / 8-9 Nov **2021** / Sorbonne Université - Campus des Cordeliers, Paris

3. Thesis's synopsis (French)

Les photorécepteurs sont des protéines dont l'activité est déclenchée par la lumière. Ainsi, grâce aux photorécepteurs, l'activité biologique dans plusieurs organismes est modulée par la lumière. La Orange Carotenoid Protein (OCP), est un photorécepteur activé par la lumière bleue-verte. La OCP est soluble dans l'eau, et participe à la photoprotection de l'appareillage photosynthétique des cyanobactéries. Il induit la dissipation thermique de l'excès d'énergie solaire en empêchant le stress oxydatif photo-induit et les photo-dommages. OCP se compose de deux domaines structurels (domaine N-terminal, NTD et domaine C-terminal, CTD) qui partagent un caroténoïde antioxydant comme chromophore, placé au milieu de la poche protéique (**Fig. A**). La lumière bleue absorbée par le cofacteur, induit la photo-activation de l'OCP et enchaine des changements conformationnels qui produisent un changement de couleur de la protéine de l'orange (OCP^O) au rouge (OCP^R).

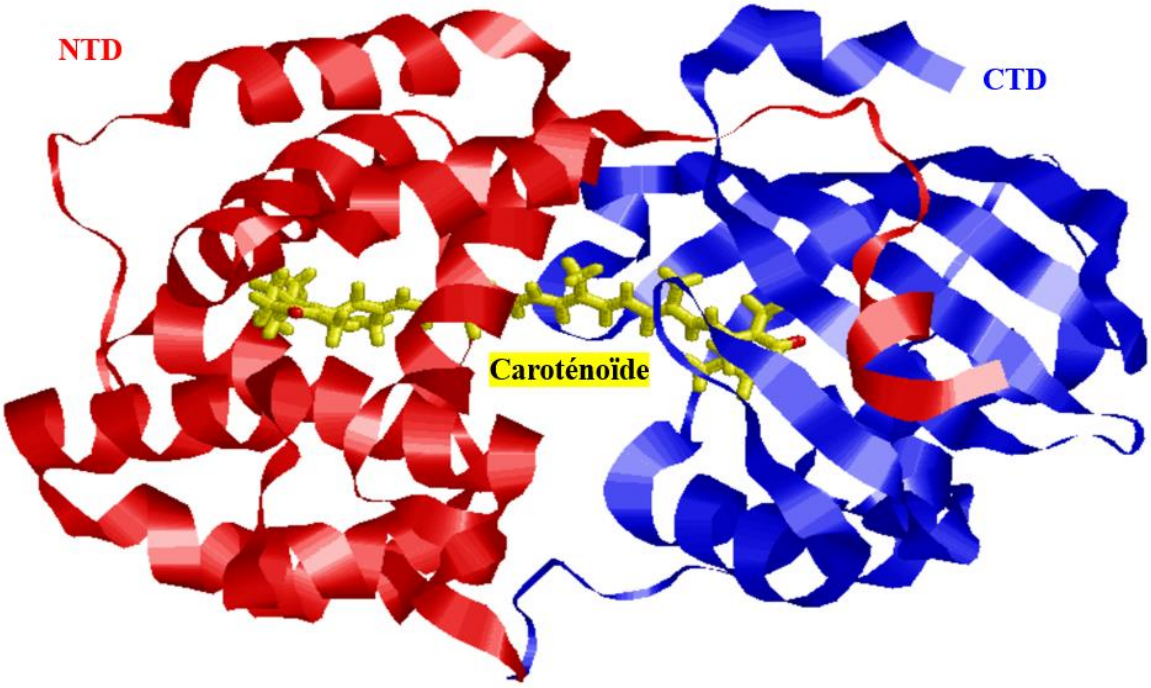

Fig. A Représentation tridimensionnelle de l'OCP. Domaine N-terminal en rouge, domaine C-terminal en bleue et le caroténoïde en jaune, au milieu de la poche protéique.

SBA-15 (Santa Barbara Amorphous) a été choisi comme support inorganique pour l'OCP, dans le but de développer des nanodispositifs photochromiques biocompatibles (voir **Fig. B**). SBA-15 est une matrice de silice mésoporeuse qui a attiré beaucoup d'attention pour l'immobilisation des enzymes ainsi que des systèmes moléculaires de vectorisation des médicaments. Les

paramètres structurels de SBA-15, tels que le diamètre des pores, peuvent être modifiés en ajustant les paramètres de sa synthèse. La capacité de modifier les propriétés des surfaces de ces matériaux permet de mieux les adapter aux protéines à encapsuler. Ainsi, une capacité d'immobilisation des protéines plus élevée peut être obtenue. Dans ce travail, nous avons immobilisé l'OCP sur différents types de nanoparticules de silice mésoporeuse SBA-15, fonctionnalisées (ou pas) en surface. Nous avons ensuite caractérisé structurellement les systèmes obtenus. Les matrices SBA-15 se sont avérées être des supports appropriés pour l'OCP, dont l'immobilisation est fortement augmentée par la pré-photo-activation de la protéine. L'OCP reste photo-active à l'intérieur de la matrice de silice mésoporeuse, produisant ainsi des nanoparticules photochromiques. Les études de spectroscopie IRTF différentielle résolues dans le temps suggèrent fortement que le mécanisme de photo-activation est le même que dans la solution. De plus, dans des conditions appropriées, l'OCP peut également être relarguée par les nanoparticules de SBA-15.

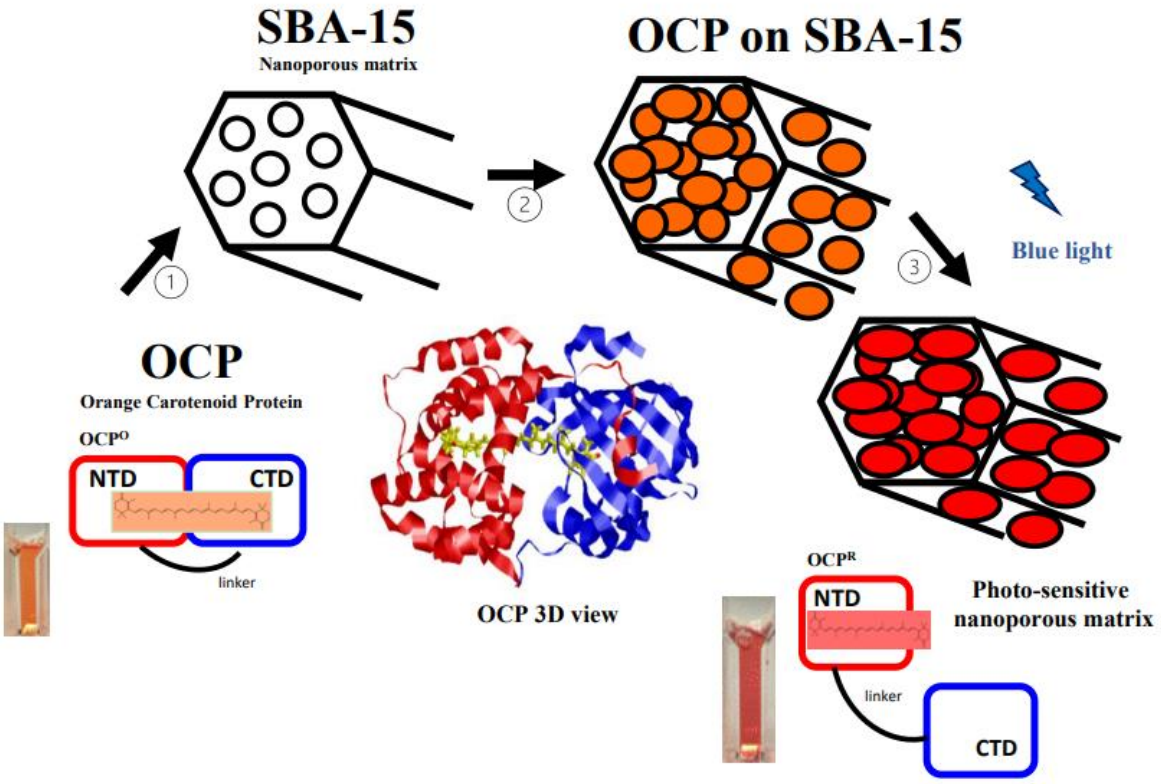

Fig. B Représentation schématique de l'immobilisation d'OCP sur SBA-15. 1-2) Immobilisation de l'OCP sur la matrice nanoporeuse SBA-15 ; 3) photo-activation de l'OCP par la lumière bleue et développement de la matrice nanoporeuse photosensible.

Nous avons aussi développé des nanodispositifs photo-activables avec une fluorescence réglable en intensité, basée sur des nanoparticules de SBA-15 chargées de colorants et d'OCP. Plus en détail, nous avons immobilisé plusieurs types de molécules fluorescents (des colorants cyanine ou des flavonols antioxydants) sur SBA-15, en présence d'OCP. L'éclairage à lumière bleue a enchainé l'extinction réversible de la fluorescence de ces colorants.

Ce manuscrit de thèse est composé par quatre chapitres.

Le premier chapitre décrit les photorécepteurs les plus importants connus en nature ; la particularité de l'OCP par rapport aux autres familles de photorécepteurs est soulignée. Dans la première partie du chapitre, des exemples de photorécepteurs et de protéines photo-actives, dont les mécanismes photochimiques sont connus, sont présentés. De plus, leur immobilisation sur des surfaces de silice mésoporeuses à des fins plus applicatives est aussi examinée. Dans la deuxième partie du chapitre, les propriétés particulières de l'OCP sont décrites. Tout d'abord, le rôle biologique de l'OCP en tant que système photo-protecteur dans les cyanobactéries est décrit. Ensuite, l'attention est tournée vers les connaissances actuelles de son mécanisme de photo-activation, en passant par sa structure et la photo-physique du caroténoïde-chromophore. La possibilité de modifier la structure de l'OCP pour moduler ses propriétés spectroscopiques, ou l'utilisation de l'OCP comme capteur de température et pH ou pour la vectorisation de caroténoïdes antioxydants est aussi décrite. Néanmoins, des questions importantes restent ouvertes. Le mécanisme de photoprotection n'a toujours pas été compris dans tous ses détails, tout comme le mécanisme de photo-activation. Les étapes séquentielles survenant après l'absorption des photons bleus restent à définir. De même, le mécanisme de rétro-conversion doit être élucidé. Pour terminer, la structure cristalline de l'OCP^R n'a pas encore été résolue. Probablement sa moindre stabilité par rapport à OCP^O rend le processus de cristallisation difficile. Les détails structurels de l'OCP^R seraient extrêmement utiles pour comprendre le mécanisme de photo-activation.

Le deuxième chapitre de cette thèse traite des études spectroscopiques sur l'OCP en solution. La spectroscopie UV-Visible et la spectroscopie de différence IRTF ont été utilisées dans l'étude du mécanisme de photo-activation de l'OCP. Cette étude est principalement axée sur l'OCP lié à l'echinenone ou la canthaxanthine en tant que chromophore, et vise à identifier leurs similitudes ou différences dans le cadre des études sur la photo-activation de la protéine. Une digression sur la spectroscopie de différence IRTF, habituellement utilisée dans l'étude des

protéines photo-actives, est présentée ; des détails sur les méthodes expérimentales ainsi que sur la préparation des échantillons sont également fournis. Les résultats des expériences spectroscopiques ont permis d'obtenir plusieurs informations. Tout d'abord, l'analyse des spectres de différence IRTF a permis de déduire que le mécanisme de photo-activation est très similaire dans les OCPs photo-actives – qui contiennent de l'echinenone, de la canthaxanthin ou de la 3-hyroxy-echinenone comme chromophores., En effet la position des bandes IR est pratiquement la même dans les trois cas. Ensuite, l'échange isotopique (hydrogène H/deutérium D) a permis d'identifier les bandes appartenant au caroténoïde et de les distinguer des bandes de la protéine sensibles à l'échange H/D. De plus, il a été découvert que OCP(CAN) dans des conditions de déshydratation a tendance à se transformer en OCP rouge, tandis que OCP(ECN) a montré une plus grande stabilité de la forme orange dans les mêmes conditions. Ceci a suggéré l'idée que le deuxième groupe carbonyle de la canthaxanthine stabilise la conformation rouge de l'OCP. Ce résultat suggère également l'idée que l'eau joue un rôle clé dans le mécanisme d'activation. Cependant, des calculs théoriques pur simuler les spectres IR seront nécessaires pour l'attribution des bandes du caroténoïde. L'étude de la région spectrale (4000-2000 cm^{-1}) dans laquelle plusieurs groupes moléculaires clés sont censés absorber est aussi très prometteuse.

Le troisième chapitre est consacré au domaine de l'interaction entre l'OCP et la silice mésoporeuse. Parmi les nombreux matériaux mésoporeux décrits dans la littérature pour leur capacité à immobiliser les protéines, la SBA-15 a été choisie comme support inorganique de l'OCP. L'objectif de cette étude était donc d'immobiliser l'OCP sur SBA-15 mésoporeuse afin d'étudier l'influence des caractéristiques structurelles et texturales de la SBA-15 sur les propriétés chimiques de l'OCP et d'évaluer le comportement photochromique de la protéine immobilisée et sa stabilité dans le temps, visant au développement de nanodispositifs photosensibles. La SBA-15 avec deux tailles de pores différentes a été synthétisée et fonctionnalisée avec des groupes NH_2, par liaison covalente. Ceci a permis de moduler l'interaction entre la surface et la protéine et augmenter le rendement d'immobilisation de l'OCP par adsorption, ainsi que les performances photochromiques de l'OCP encapsulée. Les matrices SBA-15 ont été caractérisées par la diffraction des rayons X (XRD), la microscopie électronique (SEM/TEM), la physisorption N_2 et l'analyse thermogravimétrique (TGA). L'immobilisation de l'OCP sur ces matrices et son comportement photochromique ont été suivies par spectroscopie visible en phase liquide et solide.

Plusieurs objectifs ont été atteints. Les matériaux mésoporeux SBA-15 synthétisés à différentes températures, vides et fonctionnalisés, ont montré une structure cristalline bien ordonnée qui n'est pas affectée par la fonctionnalisation avec des groupes NH_2. En effet, les nanoparticules SBA-15 avec deux tailles de pores différentes se sont avérés être des supports prometteurs pour l'immobilisation de l'OCP par adsorption. L'équilibre de l'immobilisation, induit par des interactions électrostatiques, est atteint après 4 heures sur les deux types de SBA-15, vide et fonctionnalisé, et le rendement maximal de charge est atteint pour une concentration initiale d'OCP de 0.2 mg/mL. À une concentration initiale plus élevée d'OCP, la quantité de OCP immobilisée a été augmentée jusqu'à plus de 30 mg de protéines, par g de SiO_2. L'éclairage par lumière bleue augmente d'un facteur 4 l'efficacité d'immobilisation sur les nanoparticules. Ceci suggère que la conformation de l'OCP (plus allongée dans la forme rouge) joue un rôle-clé pour faciliter l'insertion de la protéine dans les pores. La photo-activité de la protéine est complètement préservée après immobilisation sur la SBA-15-NH_2 par rapport à la SBA-15 qui, au contraire, tend à activer la protéine en la convertissant en OCP^R. OCP@SBA-15-NH_2 semble être un système photo-actif prometteur, toujours stable après 1 semaine à température ambiante et capable de ralentir la cinétique de rétro-conversion $OCP^R \rightarrow OCP^O$. Cette propriété peut, en principe, être exploitée dans plusieurs domaines. Tout d'abord, pour le développement de nanoparticules photochromiques biocompatibles. Ensuite, elle démontre que la SBA-15 peut servir comme support à l'échelle nanométrique pour les caroténo-protéines et pour une possible utilisation pour la vectorisation des caroténoïdes. Dans ce dernier cas, d'autres études devront être entreprises pour améliorer le taux de relargage d'OCP, par exemple en faisant varier les groupes fonctionnalisés greffés sur la surface, qui modulent les interactions entre la protéine et la nanoparticule. Néanmoins, le système OCP@SBA-15-NH_2 s'est avéré être, *in vitro*, un matériau biocompatible approprié à être exploité dans le domaine de la détection optique, comme un capteur optique bifonctionnel pour les changements de température entre 40 °C et 60 °C ou comme un tri-capteur optique de pH couvrant toute la gamme 1-14.

Le dernier chapitre de ce manuscrit est inspiré d'un article publié par Andreoni *et al*. (Univ. Arizona, Etats-Unis) axé sur le développement d'un système où l'OCP agit sur le transfert d'énergie entre deux colorants. Le principe s'appuie sur le décalage spectral du spectre d'absorption visible de l'OCP lors de la photo-conversion. L'idée de régler le transfert d'énergie entre les colorants fluorescents, nous a inspiré pour le développement de nanodispositifs photo-activables avec fluorescence réglable, basé sur les nanoparticules de SBA-15 chargées de colorants et OCP. La photo-conversion de l'OCP^O en OCP^R crée un chevauchement entre les

spectres d'émission des fluorophores et le spectre d'absorption de l'OCP^{R}, qui est donc capable de quencher partiellement la fluorescence des fluorophores (**Fig. C**).

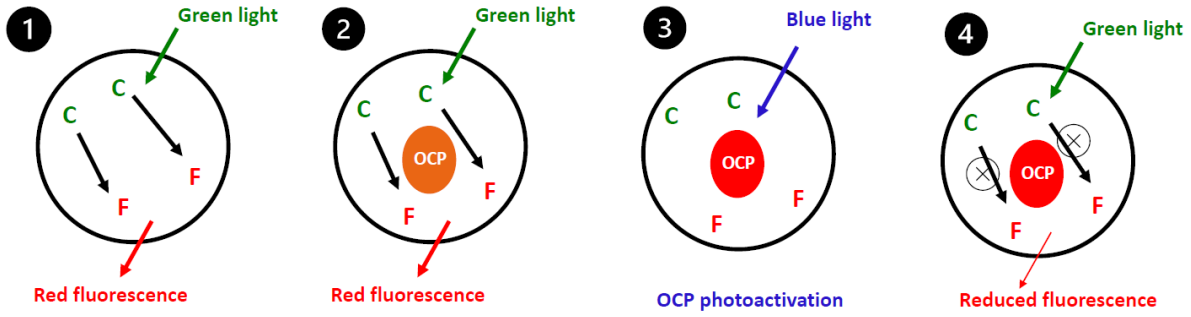

Fig. C Schéma de transfert d'énergie entre un chromophore (C) et un fluorophore (F) immobilisés sur des NPs de silice (cercle noir). (1) La lumière verte absorbée par C est transférée à F qui émet de la fluorescence dans la gamme rouge. (2) L'OCP immobilisé sur les NPs permet le même transfert d'énergie entre C et F. (3) La photo-activation de l'OCP par la lumière bleue convertit la protéine en forme rouge. (4) En présence d'OCP^{R} la fluorescence du système est partiellement quenchée, et l'intensité de l'émission est réduite.

L'application principale de ce système pourrait être dans l'imagerie par fluorescence, une technique largement utilisée dans plusieurs domaines, y compris la biologie. En effet, les nanoparticules de silice mésoporeuse sont également un véhicule approprié pour les molécules fluorescentes, et ils ont déjà été exploités dans plusieurs applications. Parmi les nombreux groupes de fluorophores organiques, des molécules de cyanine ont été choisies, car elles sont largement utilisées comme colorants fluorescents organiques synthétiques. En outre, l'attention s'est également portée sur certains flavonols (une sous-classe de flavonoïdes, molécules fluorescents naturels) (**Fig. D**). En plus de leurs propriétés émettrices intéressantes, ils sont également des antioxydants puissants. Les systèmes ont été analysés par photoluminescence et spectroscopie UV-visible.

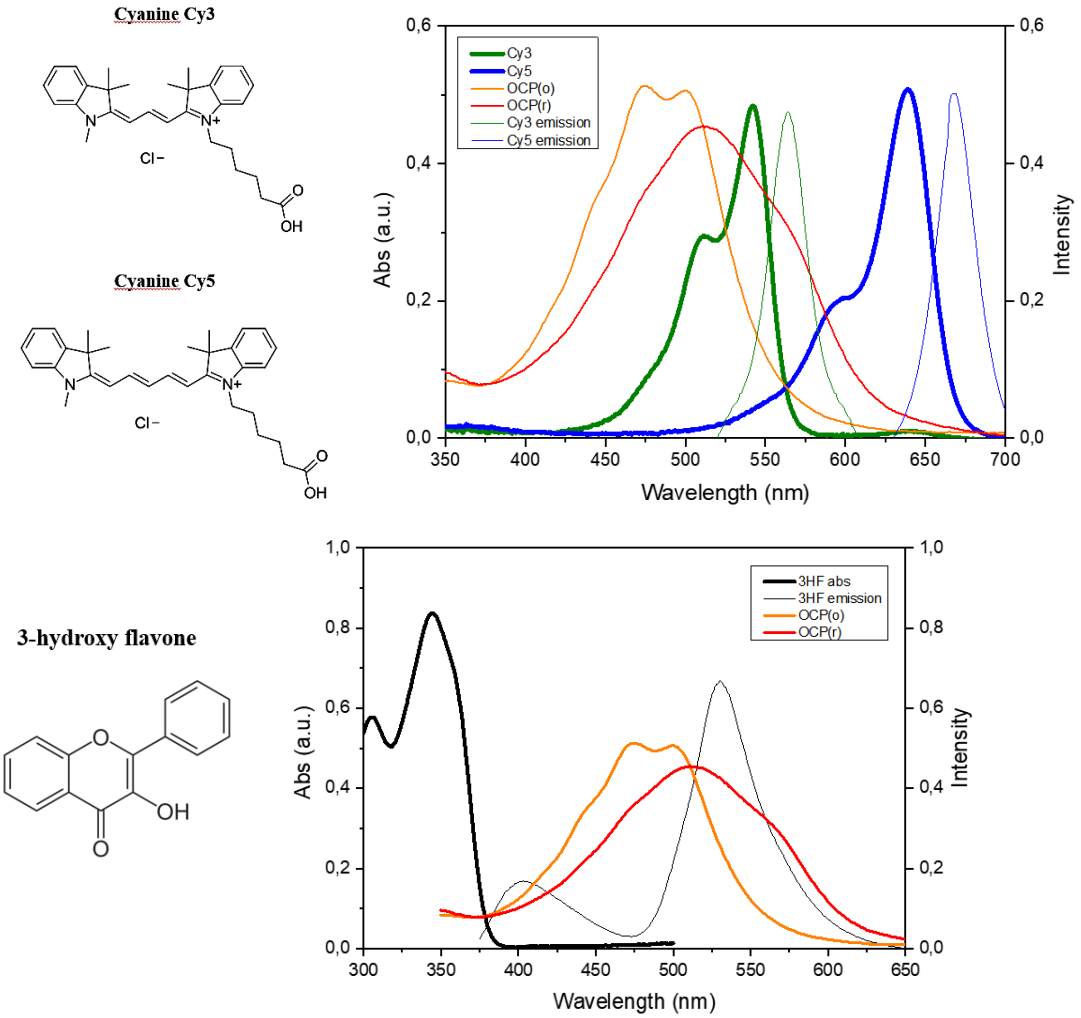

Fig. D (En haut) Structure chimique de les cyanines Cy3 et Cy5; spectres d'absorption (lignes épaisses) et d'émission (lignes minces) du Cy3 (lignes vertes) et du Cy5 (lignes bleues); spectres d'absorption de l'OCP^{O} (ligne orange) et de l'OCP^{R} (ligne rouge). (En bas) Structure chimique du flavonol 3HF ; spectres d'absorbance et d'émission du 3HF (lignes noires épaisses et minces, respectivement) et spectres d'absorbance de l'OCP^{O} (ligne orange) et de l'OCP^{R} (ligne rouge).

Ces molécules ont été immobilisées avec succès sur la SBA-15-NH_2 et les nanoparticules fluorescentes ainsi produites ont été analysées par spectroscopie visible et par photoluminescence. Les colorants cyanine ont montré une meilleure photo-stabilité par rapport aux flavonols, qui ont une tendance plus élevée à la photo-dégradation sous éclairage lumineux. L'OCP peut être absorbé sur les nanoparticules de silice chargée de colorants, ce qui assure un mode de production simple et rapide de ces nanoparticules à intensité de fluorescence photo-modulable. En ce qui concerne la paire de colorants cyanine Cy3-Cy5 dans le système SBA-15-NH_2, l'OCP peut être utilisé comme composant photochromique de modulation de fluorescence. En effet, le chevauchement spectral élevé entre l'émission du colorant cyanine Cy3 et l'absorption de l'OCP lorsque ce dernier est sous forme rouge, fait de l'OCP^{R} un bon

quencher de fluorescence. La rétro-conversion à la forme orange dans l'obscurité permet de récupérer l'intensité de fluorescence initiale, même après un deuxième cycle de photo-activation. Les échantillons stockés à 4 °C pendant 5 jours présentent les mêmes photo-propriétés que les échantillons préparés quelques heures avant. En ce qui concerne les nanoparticules dopées par le flavonol 3HF, l'OCP s'est avéré être un bon quencher de fluorescence de l'état tautomère excité du 3HF (qui émet dans le vert) lors de la photo-conversion en forme rouge. Le système était réversible, et l'intensité de fluorescence a été rétablie après incubation dans l'obscurité. Cependant, l'extinction par fluorescence induite par photo-conversion de l'OCP était inférieure à celle obtenue avec des NPs dopés aux cyanines Cy3-Cy5.

En conclusion, ces résultats ouvrent la voie au développement d'interrupteurs photo-actifs pour nanoparticules à intensité de fluorescence réglable. En outre, ces systèmes peuvent être impliqués comme régulateurs de lumière dans un système d'antenne artificielle, capable de réguler (et protéger) les voies de transfert d'énergie en réponse aux variations de lumière. D'autres expériences sont nécessaires pour améliorer le rendement de quenching des colorants cyanine et pour minimiser la photo-dégradation des flavonols.

Interaction entre la Orange Carotenoid Protein et la silice mésoporeuse : des investigations spectroscopiques aux nanodispositifs photo-actifs

Résumé

Ce projet de thèse concerne l'étude des interactions entre la Orange Carotenoid Protein (OCP) et la silice mésoporeuse SBA-15, visant à la mise au point de nanodispositifs photo-actifs. La OCP est une protéine photo-active impliquée dans la photoprotection des cyanobactéries. Il implique la dissipation thermique de l'excès d'énergie solaire en prévenant le stress oxydatif et les photo-dommages. L'OCP se compose de deux domaines structurels partageants un caroténoïde antioxydant, qui agit comme chromophore. La lumière bleue induit la photo-activation de l'OCP et son changement de couleur de l'orange au rouge. La SBA-15 a été choisie comme support inorganique pour l'OCP, visant à développer des nanodispositifs photochromiques biocompatibles. En effet la SBA-15 est largement utilisée pour l'immobilisation des protéines. Les paramètres structurels de la SBA-15, tels que le diamètre des pores, peuvent être modifiés en ajustant les paramètres de sa synthèse. Dans ce travail, nous avons immobilisé l'OCP sur différents types de nanoparticules de silice mésoporeuse SBA-15, vides ou fonctionnalisées en surface. Nous avons ensuite caractérisé structurellement les systèmes. Les matrices de SBA-15 se sont avérées être des supports appropriés pour l'OCP, dont le taux d'immobilisation est fortement renforcé par la pré-photo activation de la protéine. L'OCP reste photo-active à l'intérieur de la matrice de silice mésoporeuse, produisant ainsi des nanoparticules photochromiques. Les études de spectroscopie IRTF différentielle suggèrent que le mécanisme de photo-activation est le même qu'en solution, et très similaire pour tous les types d'OCP étudiés. En outre, dans des conditions appropriées, l'OCP peut également être relarguée à partir des nanoparticules de SBA-15. Enfin, nous avons développé des nanodispositifs photo-activables avec une fluorescence réglable en intensité, basée sur des nanoparticules de SBA-15 chargées de colorants et OCP. Plus en détail, nous avons immobilisé des molécules colorants et fluorescents (cyanine ou flavonols) sur la SBA-15, en présence d'OCP. L'éclairage à lumière bleue entraine une diminution réversible de la fluorescence. Également, la SBA-15 agit non seulement comme un échafaudage biocompatible, mais aussi comme un agent de protection contre le vieillissement des nanodispositifs développés.

Mots clés : Orange Carotenoid Protein, silice mésoporeuse, absorption de protéine, spectroscopie, photo-activité, fluorescence modulable, nanodispositifs

Interaction between Orange Carotenoid Protein and mesoporous silica: from spectroscopic investigations to photoactive nanodevices

Abstract

This thesis deals with the study of interactions between the Orange Carotenoid Protein and mesoporous silica SBA-15, aiming to the development of photoactive nano-devices. The photoactive Orange Carotenoid Protein (OCP) is a protein involved in photo-protective responses in cyanobacteria. It induces the thermal dissipation of excess solar energy counteracting oxidative stress and photodamage. OCP consists of two structural domains sharing a non-covalently linked antioxidant carotenoid as a chromophore. Blue light induces photoactivation of OCP and its colour changes from orange to red. SBA-15 (Santa Barbara Amorphous) was chosen as an inorganic support for OCP aiming at the development of photochromic bio-compatible nanodevices. SBA-15 is a mesoporous silica matrix that has attracted much attention as host for immobilization of enzymes as well as drug delivery systems. The structural parameters of SBA-15, such as the diameter of pores, can be modified by tuning parameters of its synthesis. Furthermore, the ability to modify the surface properties of SBA-15 can provide higher protein immobilization capacity. In this work we have immobilized OCP on different kinds of raw and surface-functionalized SBA-15 mesoporous silica nanoparticles, and we have structurally characterized the systems. SBA-15 matrices have demonstrated to be suitable supports for OCP, whose immobilization is strongly enhanced by the pre-photoactivation of the protein. OCP remains photoactive inside the mesoporous silica matrix, thereby producing photochromic nanoparticles. FTIR difference spectroscopy studies strongly suggest that the photoactivation mechanism is the same as in solution, and very similar for all the studied OCPs. Furthermore, under appropriate conditions, OCP can also be released from SBA-15 nanoparticles. Finally, we have developed photoactivable nanodevices with intensity-tuneable fluorescence based on OCP- and dye-loaded SBA-15 nanoparticles. More in details, we have immobilized synthetic cyanine dyes or natural fluorescent antioxidant flavonols on SBA-15, in presence of OCP. Blue light illumination was found to provide reversible quenching of red or green fluorescence under green or violet illumination, respectively. In addition, SBA-15 act not only as a biocompatible scaffold, but also as a protecting agent against aging of the developed nanodevices.

Key words: Orange Carotenoid Proteins, mesoporous silica, protein adsorption, spectroscopy, photoactivity, tuneable fluorescence, nanodevices